University of Trento

Department of Information Engineering and Computer Science

Doctoral School in

Information and Communication Technology

A Service Robot for Navigation Assistance and Physical Rehabilitations of Seniors

PhD Candidate

Stefano Divan

Advisor

Prof. Luigi Palopoli

Co-Advisor

Prof. Daniele Fontanelli

To my family

Abstract

The population of the advanced countries is ageing, with the direct consequence that an increasing number of people will have to live with sensitive, cognitive and physical disabilities. People with impaired physical ability are not confident to move alone, especially in crowded environment and for long journeys, highly reducing the quality of their life. We propose a new generation of robotic walking assistants whose mechanical and electronic components are conceived to optimize the collaboration between the robot and its users. We will apply these general ideas to investigate the interaction between older adults and a robotic walker, named *FriWalk*, exploiting it either as a navigational or as a rehabilitation aid.

For the use of the *FriWalk* as a navigation assistance, the system guides the user securing high levels of safety, a perfect compliance with the social rules and non–intrusive interaction between human and machine. To this purpose, we developed several guidance systems ranging from completely passive strategies to active solutions exploiting either the rear or the front motors mounted on the robot. The common strategy at the basis of all the algorithms is that the responsibility of the locomotion belongs always to the user, both to increase the mobility of elder users and to enhance their perception of control over the robot. This way the robot intervenes only whenever it is strictly necessary not to mitigate the user safety. Moreover, the robotic walker has been endowed with a tablet and graphical user interface (GUI) which provides the user with the visual indications about the path to follow. Since the *FriWalk* was developed to suit the needs of users with different deficits, we conducted extensive human-robot interaction (HRI) experiments with elders, complemented with direct interviews of the participants.

As concerns the use of the *FriWalk* as a rehabilitation aid, force sensing to estimate the torques applied by the user and change the user perceived inertia can be exploited by doctors to let the user feel the device heavier or lighter. Moreover, thanks to a new generation of sensors, the device can be exploited in a clinical context to track the performance of the users' rehabilitation exercises, in order to assist nurses and doctors during the hospitalization of older adults.

Acknowledgments

Foremost, I would like to express my deepest gratitude to my advisors, Prof. Luigi Palopoli and Prof. Daniele Fontanelli, who guided me during my PhD.
My sincere thanks also go to prof. Yasuhisa Hirata, who guided me with great patient during my abroad period at the Tohoku University in Japan.
My deep gratitude goes also to my family, without which this would have been impossible to realize, supporting me in all difficult times and throughout my all life. A special thanks goes to my brother Luca, who has always been a point of reference for me, both in sports and professional level. During all these years he has been so willing with me and I always sought his advice in order to take the right decision many many times.
Another special gratitude goes to Fabiano, who I met during my first year of PhD. He is my best friend and has been my deepest support during these three years. Thanks to his intelligence and his acumen we have been able to solve many difficult challenge that arose during my years. Honestly, I have to say that without him this achievement would have been impossible to obtain by myself. Thanks a lot for the amazing time spent in Madrid so many times! My appreciation also extends to my laboratory mates Marco A., with whom I did a lot of great job during my PhD and we published several works in perfect collaboration, Valerio M., Paolo B., with whom I established a good relationship that will last for the whole life. With them we spent a very good period, exchanging ideas and doing amazing jobs together. A special thanks is deserved to Bernardo, who helped me so much in the first month to understand many basic informatics things and issues over the robot. Thanks to Cristina, who was fundamental for the success of the project ACANTO, I wish you all the luck for your future in the Netherlands. Another thanks goes to Marco F. for his mathematical help and his friendship and, of course, to Roberta for her immense availability. I would never be able to complete my PhD without one of them.
Thanks to all the guys that enjoyed all the barbecues done in summer and at Fabiano's house, they are too much to be listed and of course I will forget someone.
Thanks to my friends Pietro, Aurora, Matteo and Monica, whit whom I spend many enjoyable adventures.
A special thanks goes to my girlfriend family Carlo, Daniela and Marco, who accepted me as part of their family, giving hospitality to me at their house and in their

camper. We have spent a great summer all together, doing unforgettable journeys. I left for last the most important person because it deserves a whole space for her. A special and huge thanks goes to my girlfriend Chiara with whom I fell complete and loved. She is very important for me because I shared unforgettable moments which are printed in my mind and will last forever. We spent an amazing summer, playing volleyball, swimming in the Maiorca's see, in Sardinia and with the camper. I am sure that these moments are only the first step of something bigger that will happen in our future.
Again a big thank you to everyone, even to those who I forgot to include in this list but that also should deserve a mention.

Contents

1 Introduction **11**
- 1.1 Outline of the thesis . . . 15
- 1.2 Scientific contributions . . . 16
- 1.3 Patents from the thesis . . . 18

2 State of the art **19**
- 2.1 Robotic walkers in literature . . . 19
  - 2.1.1 Cobot . . . 19
  - 2.1.2 Smart Walkers . . . 20

I The *FriWalk* prototype development **31**

3 Background **33**
- 3.1 Vehicle modelling . . . 33
  - 3.1.1 Kinematic model of the *FriWalk* . . . 34
  - 3.1.2 Dynamic model of the *FriWalk* . . . 37
- 3.2 Path following problem definition . . . 38
  - 3.2.1 Curvilinear coordinates: the Frenet Frame . . . 39
  - 3.2.2 Dynamic Frenet Frame . . . 42
  - 3.2.3 A solution for the approach angle . . . 44
  - 3.2.4 Path following with humans . . . 46

4 Smart Walker in Acanto **49**
- 4.1 The DaLi Smart Walker . . . 50
- 4.2 The *FriWalk* Smart Walker . . . 51
  - 4.2.1 Mechanical design . . . 53
  - 4.2.2 Software architecture . . . 56
  - 4.2.3 *FriWalk* node design and definition . . . 61
  - 4.2.4 Robot localization . . . 66
  - 4.2.5 Path planner . . . 68

II The *FriWalk* as a navigational aid **71**

5 Passive Guidance Solutions **77**
5.1 Problem formulation and solution overview 78
5.2 The Bang–Bang steering controller 79
5.2.1 The hybrid controller: a solution for the chattering 81
5.3 The Haptic strategy 83
5.4 Combining Haptic with Bang–Bang 84
5.5 Experimental results 85
5.5.1 Quantitative analysis 87
5.5.2 Performance analysis 90
5.5.3 Users' evaluation 92
5.6 Discussions about the guidance strategies 96
5.7 Conclusions 97

6 Active Guidance Solutions **99**
6.1 Problem formulation and solution overview 100
6.2 Simulating passivity strategy 101
6.2.1 Forward velocity selection to simulate passivity 102
6.2.2 Basic idea of the controller 104
6.2.3 Experimental results 105
6.2.4 Performance analysis 107
6.2.5 User's evaluation 107
6.2.6 Comments about the simulated passivity strategy 110
6.3 Introduction of a GUI 111
6.3.1 Experimental Design and Hypotheses 111
6.3.2 Results 114
6.4 Discussions 115
6.5 Conclusions 116

7 Front steering actuations **119**
7.1 Problem formulation 120
7.2 Solution overview 121
7.2.1 Control law 121
7.3 Experimental results 122
7.3.1 Comparison for singularity handling 122
7.3.2 Path–following performance 123
7.3.3 Considerations about the guidance 124
7.4 The variable stiffness approach (confidential) 125
7.4.1 Motor control 126
7.4.2 Solution overview 128
7.4.3 Rigid path following controller 131
7.4.4 Variable–stiffness controller 131

7.4.5 Experiments . . . 132
7.4.6 Conclusions . . . 135

8 Probabilistic controller 137
8.1 Localization issues . . . 138
8.2 Probabilistic controller idea and design . . . 139
8.3 Experiments . . . 141
8.4 Conclusions . . . 143

III The *FriWalk* as a rehabilitation device 145

9 The rehabilitation device (confidential) 147
9.1 The *FriWalk* rehabilitation platform . . . 147
9.1.1 Isometric/isotonic exercise . . . 149
9.1.2 Tip–toe stand exercise . . . 149
9.1.3 Single–leg stand exercise . . . 150
9.1.4 SPPB test . . . 150
9.2 Therapeutic activities . . . 152
9.2.1 Orthogeriatric activities . . . 152
9.2.2 Therapeutic activities . . . 152
9.3 Overview of the experimental validation . . . 153
9.4 Results and discussions . . . 154
9.4.1 Usability . . . 154
9.4.2 User experience . . . 155
9.4.3 Acceptance . . . 155
9.5 Conclusions . . . 156

10 Towards variable inertia 159
10.1 Model . . . 159
10.2 Parameter identification of the motor-wheel mechanical model . . . 161
10.2.1 Problem solution . . . 163
10.2.2 Experimental results . . . 164
10.3 Observer . . . 168
10.3.1 The observer on the *FriWalk* . . . 169
10.4 A solution to modify the *FriWalk* perceived inertia . . . 173
10.4.1 Experimental results . . . 175

11 Conclusions 177
11.1 Research evaluation . . . 177
11.2 Future work . . . 179

A The CAN bus and the CANOpen protocol 181

B ST schematic circuit **187**

References **191**

Chapter 1

Introduction

Several studies reveal that life expectancy is increasing thanks to the improvement in medical cares [48], [64]. Inevitably, due to this continuous ageing, the number of older persons in the world has increased substantially in recent years and that growth is projected to accelerate in the coming decades, as visible in Figure 1.1. Technological developments have always attempted to satisfy and overcome the possible needs of society. One of the main global societal challenge of our times is population ageing: by year 2050 the population of 60+ years will be larger than the population aged between 10–24 years (2.1 billion versus 2.0 billion), as shown in Figure 1.2. In the most developed regions of the world, such as USA, EU, Japan and Australia, the people with 65+ years will exceed the 20% of the total population [89].

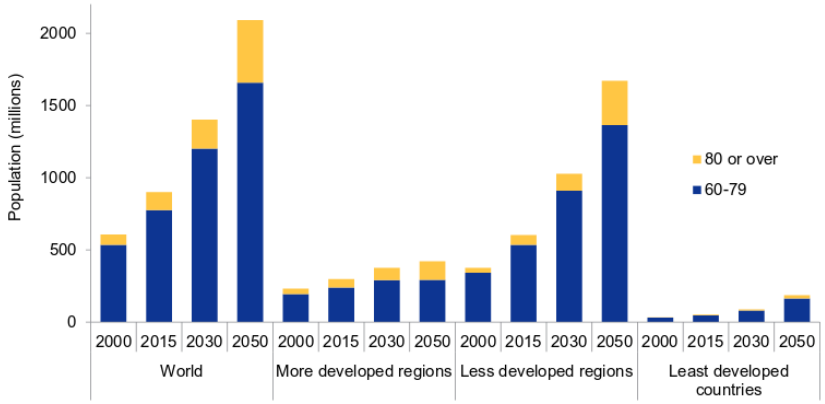

Figure 1.1: Population aged 60-79 years and aged 80 or over by development group 2000, 2015, 2030 and 2050 [89].

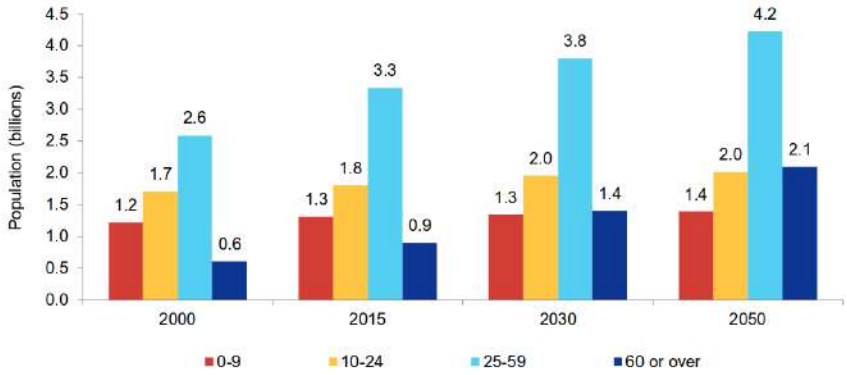

Figure 1.2: Distribution of the world population age among the years [89].

The senior citizens face changes in their physical and cognitive abilities, which are exemplified by a slowdown in reflexes [69] and an impoverishment of muscle tone [63]. One of the worst and direct effect of limited physical and cognitive capabilities, due to the continuous aging, is a reduced mobility. The reduction of mobility highly affects the life of seniors, worsening both their physical and psychological health. In fact, mobility limitation leads to an increase of the overall time spent at home by seniors, causing a dramatic penalization in their social relationship. A direct effect is loneliness, which is proved to be a cause (not only a consequence) of reduced physical activity [46]. Therefore, a self-reinforcing loop damaging physical health of the senior is automatically generated.

In this scenario, the development of new technological devices which can provide support to the elders becomes a priority in order to face the increasing assistance request of the future society. In particular, service robots are becoming increasingly popular as intelligent mobility aids to prolong mobility independence and, hence, mitigate physical decline and a series of cognitive problems of older adults [49, 65].

Several literature results focused on how to tackle specific problems related to physical deficits which can be linked to the ageing. For example, some mobility service robots were specifically developed to assist visually impaired people in walking [94, 96, 119]. However, a research conducted on 3,000 US people aged 57 and 85 years, showed that 94% of the sample had problems with at least one of the five senses (taste, smell, hearing, viewing or touch), 40% with two senses, and 28% with three or more senses [100]. Moreover, the 2015 report of the Italian Institute of Statistics on elders in Italy and in the European Union [59], highlighted an important gap between 65 and 80 years old Italians, showing an exponentially increase of percentage of older adults with severe difficulties in viewing and hearing (from 5.1% for 65 y.o., to 29.5% for 80 y.o.). The results show that physical and cognitive deficits are not uniform within the elder population. For these reasons, a priority in the the development of technological assistive devices should deal with the heterogeneity of elder individuals. Another important challenge is represented by the reluctance and

the difficult adaptation of senior uses to the use of new technologies [29]. Understanding of elders' feelings and their perception of advantages and disadvantages of new technological products is fundamental for an effective application [117]. As a consequence, the development of assistive service robots for older adults must take into due account their involvement. In this context, user-centred approaches come to rescue as they allow the developer to effectively capture the users' needs, and, in the mean time, to show and explain the potential of the proposed technologies in order to facilitate their acceptance [50]. This is a crucial point also when the development embrace other players, such as other users of the technology (both elderly and caregivers) and/or service providers (elder centres, hospital, social services, charities, etc.) [32].

A possible way to face the effects of reduced mobility is the combination of deambulation aids and modern robotic technologies. The European ACANTO project [2] aims at the design of an assistive robotic walker for seniors, named *FriWalk*, taking into account all these requirements. The *FriWalk*, reported in Figure 1.3, is similar to a standard four-wheeled rollator, but it is endowed with actuators, sensors and computing abilities in order to directly interact with the user and, most importantly, take decisions.

Figure 1.3: Rehabilitation version of the *FriWalk* prototype [6].

In fact, the *FriWalk* has been developed with several sensing and reasoning abilities, but one of the most important is the capability to act as a navigation aid to safely and comfortably guide the user through indoor environments [19, 18, 5] along a planned path that satisfies his/her requirements [38, 95]. This device is developed as a navigation support rather than an autonomous assistive vehicle, which is a big difference due to the need to directly interact with an user. Since this robot has to collaborate with the assisted person, the human–robot interaction has to be widely taken in consideration. In order to achieve this perfect synergy between the

device and its user, the robot has to predict and understand the humans' intention in order to modify its behaviour to comply with the user needs. Furthermore, since the target of the *FriWalk* are people who can suffer different kind of physical and cognitive problems, comfortability, manoeuvrability and little intrusiveness are the mandatory features that the robot has to own. The *FriWalk* was created with the intention of leaving the user a complete perception of freedom and control over the robot and the environment, reducing at the same time the impact choice that could endanger her/his safety or undermine her/his sense of confidence. Beyond the development of such a device to reduce the effect of limited mobility, the ACANTO project created a social network for seniors to underline the importance of social interaction to prevent loneliness. Thanks to such social network, users with similar profiles are linked and connected automatically in order that they can do activities (e.g., go to a museum) together. At last but not least the *FriWalk* is also endowed with sensors to adapt the robot to work as a rehabilitation device, in order to support the clinical staff during hospitalization of patients.
In order to achieve all the goals of the project, the *FriWalk* has mainly to satisfy the following requirements:

- *Flexibility and versatility*: develop a robot that can adapt to the user needs;
- *Navigational aid*: develop a robot with different guidance strategies that can adapt to the user needs;
- *Cognitive and reactive aid*: develop a robot endowed with sensors able to localize itself inside an environment and able to detect and recognize moving obstacles;
- *Rehabilitation aid*: develop a robot able to work with patients to assist doctors and physiotherapists during hospitalization.

So, this research aims to the mechanical and software design of the *FriWalk*, which definitely belongs to a new generation of robotic walking assistants. Thanks to a perfect synergy between mechanics, software and electronics the human–robot interaction is maximized, limiting as much as possible the robot authority and perceiving the user feel always in full control of the device, hence maximizing the user's comfort while using the *FriWalk*. Among all the features developed on the *FriWalk*, one of its main novelty is the clinical application, since it can be easily exploited as a rehabilitation device. The benefits of relying on such robot to enhance recovery during hospitalization has been proved thanks to a deep pilot study and the gathered results are really promising. Directly connected to such scenario the *FriWalk* ability of autonomous navigation highly increases the usability and the benefits of the device. Thanks to a new generation of low cost and high quality sensors the *FriWalk* is completely able to recognize the surrounding environment, distinguish between fixed obstacles and moving persons. Moreover, a sophisticated planner computes, in

real–time, the safest and best route to reach the target always taking into account the surrounding environment, changing the path whenever a possible dangerous situation is detected. This feature is exploited, for example, in a clinical environment to pick up the patient from his/her bed or to reach the docking station. Another big novelty of the *FriWalk* is given by advanced guidance solutions for elderly obtained with low cost sensors and actuators, maintaining an extremely high level of comfort and human–robot interaction. Obviously the comfortability depends on the user and can be very personal and, for this reason, a questionnaire and an interview has been proposed at the end of each experiments. However a common basic idea of comfort, shared by all users, can be defined. For comfort we mean the feeling perceived by the user during the use of the *FriWalk*. Whenever the control action intervenes gradually and smoothly, letting the user to feel always in control of the device, then the comfortability is maximized. Conversely, if the controller is abrupt and feels the user lose the control of the *FriWalk*, then the comfortability of the device is compromised.
At the same time the quality of construction has been maximized to increase the robustness. A simple but functional graphical interface has been entirely designed and developed to let the user communicate with the robot and make the robot usable by many different users (doctors, physiotherapists and seniors). In addition, the *FriWalk* has a high autonomy (around 6 hours) and a docking station can be easily exploited to recharge the different batteries installed on the robot.

1.1 Outline of the thesis

After an analysis covered by Chapter 2 about the evolution among the last years of the Smart Walkers, with a deep focus on their features, their potentiality and their weakness, this essay is organized and split into three parts, for readiness simplicity and convenience. These parts present the different strategies and solutions exploited to cover the requirements introduced in the previous section (flexibility and versatility, navigational aid, cognitive and reactive aid, rehabilitation aid).
In particular, Part I is focused on the topic about the prototype development to maximize the flexibility and versatility, giving with Chapter 3 the necessary information about the mathematical background at the basis of the vehicle modelling and the solution for the path–following problem, especially if the robot has to collaborate with humans to solve such task. After that, Chapter 4 introduces the robotic platforms used within this research with a special focus on the *FriWalk* evolution, starting from a previous rudimentary prototype. The strategies adopted to improve the mechanics and to increase the robustness and the quality of the software are discussed to understand all the benefits of all the choices made. Moreover, a brief description about the localization solution and about the path–planning algorithm is also provided.
This essay proceeds with Part II where the potentiality of exploiting the *FriWalk*

as a navigational, cognitive and reactive aid for elderly is deeply treated. Several guidance strategies have been developed during this project, ranging from complete passive solutions to active strategies, exploiting either the front or the rear actuation independently. In particular Chapter 5 proposes three guidance solutions based on a passive version of the *FriWalk* that rely on the rear braking system, on a haptic interface or on the combination of both solutions. Such guidances have been extensively tested with elderly and real users. Regarding the active guidance strategy, Chapter 6 presents a guidance solution based on a rear–driven version of the *FriWalk*, that simulates the passivity of the device by alternating an estimation phase with a controlling phase. Also in this case the solution has been deeply tested with real users. Chapter 7 shows the use of a front steering passive *FriWalk*, starting from a solution that solves a big singularity issue that arises whenever the thrust is provided by an user. After that a definitely novel solution that maximises the interaction and the level of comfort for the user is presented, exploiting a concept called *variable stiffness*. This Part II ends with Chapter 8 that explores an innovative guidance strategy to deal with extremely inaccurate localization of the robot, a situation that can happen anytime and has to be considered to not mitigate user safety.
After the use of the *FriWalk* as a navigational aid this essay continues with Part III where the *FriWalk* is presented as an innovative device for rehabilitation purposes. In Chapter 9 the results obtained after a pilot study lasted 6 month at the University Hospital of Getafe (Spain) to evaluate the clinical validity of the *FriWalk* is presented, reporting the overall impressions of the medical staff and of the patients. Moreover, Chapter 10 deals the problem to estimate the user thrust applied to the *FriWalk* in absence of expensive force sensors attached to the robot frame. This can be done by measuring the current absorbed by the motors and, such information, can be exploited to modify the *FriWalk* inertia to let the user feel a lighter or an heavier walker during the walk. The variable inertia can be exploited for rehabilitation purposes since the physiotherapist can decide how much effort the patient has to apply to move the robot. This thesis ends with the conclusions and with a focus on the possible future works.

1.2 Scientific contributions

This thesis collects the results obtained in 11 publications, listed in Table 1.1, during the Acanto project in the field of the *FriWalk* as a navigational aid. Beyond the overall mechanical and software architecture at the basis of the *FriWalk*, entirely developed by myself, the contributions can be summarized into two topics:

- *FriWalk* as a navigational aid:
  - *Passive guidance solutions*, where the thrust is provided only by the user, and the contribution of this work can be found in [10, 11, 5, 8]. While in

[10, 11] I contributed on the control strategy, in [5, 8] I concentrated more on the human–robot interaction aspects, performing experiments with elderly and pointing out the differences between the guidances strategies and benefits from the user point of view;

- *Rear active guidance solutions*, where the thrust is provided both by the user and by the robot. The contribution of this work can be found in the following publications [7, 9]. In such works I gave a marginal contribution from the control strategy point of view, but I worked on the implementation and on the integration on the device of the strategies. While in [37], beyond the development of the graphical interface for the experiments with elderly, I contributed with the human–robot interaction in order to compare the guidance performance with other guidance strategies;
- *Front active guidance solutions*, where the thrust is provided by the user only but the robot intervenes on the front steering system actively. In [12] I contributed on the solution of the singularity issue, while in [13] I worked on the implementation of the control strategy on a dedicated embedded board.

- *FriWalk* as a rehabilitation aid:
  - *Variable inertia*: the contribution of this work can be found in [6], where I contributed with the realization of a dedicated embedded board with which it was possible to implement the characterization of the actuators. This embedded board is also fundamental to implement the observer to estimate the user thrust by means of the absorbed currents by the motors;
  - *Clinical scenario*: the contribution of this work can be found in [102], where I contributed on the integration and on the strengthening of the algorithms on the *FriWalk* to let the device be used in a real scenario, i.e. hospital. Moreover I developed the graphical interface exploited both by the medical staff and by the patients during the pilot study.

Reference	Appearing in	Thesis main chapter
[10]	CDC	Chapter 5
[11]	IROS	Chapter 5
[5]	Robotics and Automation Letters	Chapter 5
[8]	Transaction on Haptics	Chapter 5
[7]	IROS	Chapter 6
[9]	Robotics and Automation Letters	Chapter 6
[37]	IJSR	Chapter 6
[12]	ICRA	Chapter 7
[13]	Patent pending	Chapter 7
[77]	ICRA	Chapter 8
[102]	THC	Chapter 9
[6]	RTSI	Chapter 10

Table 1.1: Scientific contributions of the thesis.

1.3 Patents from the thesis

In the thesis there are two topics that are confidential. In particular Section 7.4 covers a work under patent pending and also the solution presented in Chapter 9 has two patents, in collaboration with Siemens, University of Forth and the University Hospital of Getafe, in proceeding.

Chapter 2

State of the art

2.1 Robotic walkers in literature

When developing robotic aids for assisting people who suffer physical and cognitive disabilities, the most important concern is safety. The paradigm of *passive robotics* have been introduced for the first time by Goswami et al. [44]. The author show a set of possible control law that could be implemented through a mechanical wrist consisting of un–powered hydraulic cylinders and variable stiffness connections. During the years, several different kind of service robots have been developed, ranging from Cobots to robotic walkers and wheelchairs.
Wheelchairs represent one of the most important topics in the field of service robots. Recently, the artificial intelligence approaches adopted for devices has brought the system to estimate and predict user's intention [116], in order to increase the collaboration between the human and the machine.
Anyway, these types of devices are thought for people with a motor dysfunction that does not allow them to walk independently, hence the need to fully control the system. This control paradigm is just one of the possibility offered by the system we are aiming at, in which the control authority is in general shared with the user.

2.1.1 Cobot

The aforementioned approach has been adopted in [98] for developing a Cobot walking assistant. This has been a great improvement from the Cobot robot proposed by [14] since the idea of passive robotics has been brought to mobile robots. The architecture of the device in [98] describes the Cobot as a robot composed of a cane with a caster wheel equipped with a servo motor for actuating the steering angle. In [121] the authors propose a control law for where the user supplies the motive power, while the artificial intelligence acts on the steering angle of the device in order to let him follow a defined path. However, since these types of devices are too specific and focused on performing a well defined task, their versatility is very

limited.

2.1.2 Smart Walkers

In the last years, a high number of intelligent walking assistants have been proposed in literature and, nowadays, they are well known as *Smart Walkers*. Smart Walkers have emerged with the same structure as the conventional ones, but they include additional robotic and electronic components, that provide a better assistance to user gait, navigation and body weight support. Smart walkers are designed to work in perfect synergy with elderly and/or users who have disabilities not only in locomotion, but also have shortages at cognitive and sensory levels. Furthermore, elderly people usually present low familiarity with mechatronic and technology, making the challenge even more complicated. In summary, Martins et.al. in [82], state that Smart Walkers needs to satisfy three mandatory features, that are safety, comfort and simplicity of use of the device. The authors also report that these devices have changed a lot during the last years but, generally, they can present the following functionalities:

- Physical support;
- Sensorial assistance;
- Cognitive assistance;
- Health monitoring;
- Advanced human-machine interface.

Physical support

The most important feature that is required for a Smart Walker is to provide physical support for the user, directly improving his/her gait stability. In order to satisfy this requirement, in the last years, a high number of intelligent walking assistants have been proposed in literature, and can be basically classified into two big categories:

- Passive walkers: leave the responsibility of the locomotion to the user;
- Active walkers: the locomotion is provided by a combination of user and motor thrust.

In order to provide physical support relying on passive walkers, usually the improvements consist on the enlargement of the basis to increase the stability. Another important improvement is the replacement of the handlebars of the walker by forearm support platforms [3], which has also been clinically tested with elderly and injured. The tests showed that these supports eliminate the degree of freedom of the elbow articulation and a higher fraction of the user's weight is supported by the device.

In this way it is easier to move the robot and, at the same time, the wheel friction is increased, reducing the risk of sliding.

Anyway, considering the fact that Smart Walkers have wheels, controlling the device free motion can easily become a big problem. In fact, braking a conventional walker is a task that requires muscular strength, coordination and good reaction time, which are skills that decrease by ageing Since Smart Walkers are even heavier then standard rollators, because of batteries and electronic accessories, the risk of an excessive acceleration of the device, with consequence fall, is highly increased. A significant toward an improvement in safety have been introduced by Hirata et al. in [51]. The authors propose a standard walker (see Figure 2.1), with two caster wheels on the front and a pair of electromechanical brakes mounted on the rear wheels. Thanks to the incorporation of an inclinometer it is possible to detect

Figure 2.1: RT walker proposed in [51].

whether the surface is inclined or not, providing the gravity compensation feature. This information enables the walker to decrease the velocity depending on whether the device is going downhill.

The main advantage of the passive walkers is the lightness, with the direct consequence that they can move easily applying small forces. Nevertheless, at the same time, this feature can be a big issue since the device is very sensitive, causing movements even when forces are applied unintentionally. This happens in the falling accident of the user, which is potentially harmful and must be completely avoided. A fall prevention function based on estimation of user state has been proposed in [53]. By estimating the user state accurately, many people could utilize the system dependably and safely. The author identifies three state for the walker, i.e. walking state, stopping state and emergency state. To distinguish these state, the author

exploits the information gathered from a laser scanner, measuring the distance of the person with respect to the walker. Whenever a fall is detected, the emergency state is activated, so that the apparent dynamics of the Smart Walker is modified by controlling the brake torques of the wheel to realize the fall–prevention function. In a previous training phase, thanks to the laser finder, an ellipsoid describing the distribution of the center of the mass of the user during the walking state has been estimated. In this way, whenever the relative position of the user is out of that ellipsoid, than the user state must be transited to an emergency state, so the system has to be halted to prevent the falling of the user. This method has been improved in [54], where the authors propose a method for estimating the user's fall by detecting and tracking the human upper body in 3D using a stereovision approach. Using this data the user's state is estimated to be whether seated, standing up, falling down or walking.

In addition to the braking problems for elderly people, it is important to emphasize that both strength and coordination are necessary to push and guide the walker, especially if the Smart Walker is heavy or whenever the user goes uphill. To prevent such situations, active walkers mounting motors on the rear wheels can be exploited to compensate gravity on inclined grounds and provide the pushing energy necessary to move the device. An example of such device is proposed by [87] and is shown in Figure 2.2. Unfortunately, the presence of actuation disrupts the system

Figure 2.2: Smart Walker proposed by [87].

passivity, with potential safety problems, so that the estimation of user's intention becomes the major challenge for such devices.

Sensorial assistance

One of the main task of Smart Walkers is to act as a navigational assistance, which means providing motion control abilities to the robot. This feature is implemented

on such devices thanks to the ability to detect obstacles or dangerous situations, that have to be avoided mandatorily. In fact, early obstacle detection is extremely important for people who needs to use Smart Walkers, since sudden changes in terrain, or unexpected obstacles, can present serious challenges to balance and security to the user.

Normally the motion control ability is given by the employment of ultrasonic, vision or infrared sensors capable of detecting both static and dynamic obstacles. Whenever an obstacle is detected, the control system can act mainly in two different ways:

1. Passively: in such a case the system assists the user thanks to sound or vibration alerts. One example is given by the PAM-AID [68], a walker visible in Figure 2.3, which aims to guide blind people and is equipped with three types of sensors that continuously scan the surrounding environment: sonars for collision avoidance, proximity sensors and bumper switches. The information gathered by the sensors is transmitted to the user via voice messages, describing the emergency detected.

Figure 2.3: Smart Walker PAM–AID proposed by [68].

2. Actively: in such a case the system intervenes directly on the device's actuators, momentarily changing the path that the user was following. An example of such device is given by [51] (device visible in Figure 2.1), where a laser sensors is mounted in the front of the walker and is used to detect stairs and obstacle. This information is used by the control system, which directly acts on the brakes, in order to modify the user's direction of movement to prevent crashing or falling from stairs.

This feature is usually installed on Smart Walkers to provide sensorial assistance to users with visual problems and/or poor reaction time.

Another sensorial assistance that is necessary to install on such devices is the avoidance of the possibility that the walker may roll away from the user while walking. This is possible thanks to the use of sensors mounted backwards measuring the relative distance between the user and the device, like what done in [52] and in the ASBGo walker [80] reported in Figure 2.4. In the latter, beyond the laser sensor, a contact sensors has been mounted on the handlebars to be sure that the user is effectively guiding the walker with two hands.

Figure 2.4: ASBGo Walker [80].

Cognitive assistance

Smart Walkers can also be classified according to their ability to assist the user navigation, performing path–following control.

In the last years, a high number of intelligent walking assistants solving this specific task have been proposed in literature, ranging from steering–only controlled walkers [56], to fully actuated assistive carts [103]. In the first case, the adopted device is a walker with three wheels, where the rear tires hosts incremental encoders, while the front caster wheel an absolute encoder to measure the heading angle. The actuation is performed by two independent motors mounted on the rear, while the front wheel presents a stepper motor driven belt and a pulley system. In addition, a clutch is used to disconnect the motor from the wheel when control is not required. The control system is based on a synthesis of heuristic logic that exploit a dynamic model of the walker which can detect loss of walker stability. Moreover, thanks to the sensor information, the authors show how it is possible to predict the user's intended path, and by the collaboration between the dynamic model and the sensors information, they developed a shared navigational control and the mechanism for detecting and handling errors in the model's predictions. The fully–actuated cart proposed by [103] feature higher manoeuvrability and can actively force the assisted

person to travel along the desired path. This can be potentially harmful if the user does not comply with the planned trajectory, even if force and moment sensors are used to predict his intentions.
A significant step toward an improvement in the safety have been introduced by Hirata et al. in [51], thanks to the removal of active actuators. The authors propose a standard walker, with two caster wheels on the front and a pair of electromechanical brakes mounted on the rear wheels. The control of the device is based on a differential breaking principle, thanks to the information gathered by force and moment sensors. This method is at the basis of many stability control systems for cars [99] which, by suitably modulating the braking torque applied at each rear wheel, is able to steer the vehicle toward the desired path. While the main limitation of this solution is the difficulty in applying the right force and moment to the cart, it results in a lightweight and less expensive design thanks to the absence of motors. The same principle has been applied in [105] for improving potentiality in more complex situations. Anyway, other limitations of these solution regard expensive sensors and sophisticated algorithms, which require a powerful and expensive computer. Moreover, all these algorithms work under the hypothesis that the user pushes only without imposing any torque to the cart, which is a strong limitation.
Relying on this type of design, the authors in [34] developed a new walking assistant which takes the advantage of passive architecture in terms of safety, cost, weight and comfort. The authors propose a device which doesn't impose a strict trajectory but uses a strategy to gently guide the user toward the desired path. To this purpose, a configurable tunnel has been introduced to allow the user moving freely inside it, while the control intervenes only as soon as he/she exits from the safety region. Furthermore, in order to achieve a higher level of comfort for the user, the authors proposed a solution of an optimal control where the objective function is the braking time. This solution is really promising but has the main limitation that user's force has to be estimated with accuracy and the controller has to apply a torque to the brakes. Since electromechanical brakes are controlled in current, in order to be sure to apply the desired torque, it is necessary to know the inner model of the actuator.
Other Smart Walkers may also implement another feature to perform path following, like the iWalker [67]. This device has a navigation service that sounds the user to the user a map of the environment and the location of the user on it. Thanks to the graphical interface, the user can ask for a route to reach a desired destination, and the robot suggests the correct direction to take thanks to a moving arrow on the screen.

Health monitoring

Some Smart Walkers, depending on the operative condition, can be used to monitor some health parameter of the user. This information are gathered and used to keep a medical history about the user's health. Moreover, if the device is network connected, it is also able to inform through a wireless communication a health centre

or the medical staff in case that an emergency situation is detected. An example of such a device is given by [33], where the robot monitors the heartbeat rate of the user and, moreover, notifies him/her whenever it is scheduled to take some drugs.

Advanced human–machine interface

In the last years, Smart Walkers have become more and more complex to assist the user in performing tasks of higher level of complexity. For this reason, the human–machine interface, which is the way of dialog between robots and users, has to be as much efficient and sensitive as possible, in order to establish a perfect bridge of communication. Sensors cover one of the most relevant role in interfaces, since they scan the surrounding environment and gather the human interaction with the device. According to [82], Smart Walkers can present two kinds of interface:

- Direct interface: the commands imposed by the user are directly sent to the robot;
- Indirect interface: the user intentions are estimated with sensors mounted on the robot.

For the former, user commands/intentions are directly communicated to the device through, for instance, a joystick like in [45] (Smart Walker in Figure 2.5). In this work the joystick, beside transmitting the intentions of the user to the motors, provides a force feedback allowing the user to perceive detected obstacles. According to this repulsive force the user can know the direction and the distance of the obstacle, allowing the user to walk safely avoiding them. Other examples of direct

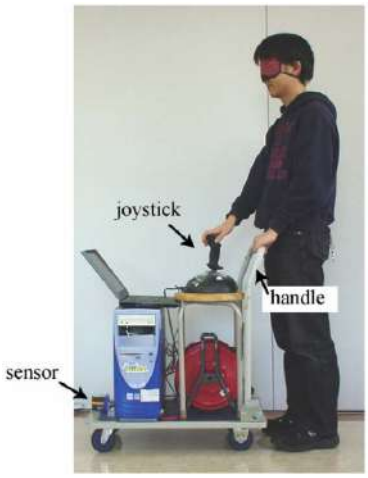

Figure 2.5: Walker with a joystick interface [45].

interface are given by the implementation of turn buttons and voice commands as

in [67]. A speech recognition algorithm is used to understand the voice command from the user and accomplish the desired manoeuvrer Moreover, whenever the robot exceeds a certain velocity, an alarm is activated to warn the user to slow down. The same method is used to inform the user about moving obstacles. Another example of direct interface is covered by force sensors, which have been widely studied and used in the literature. This type of sensors are classified as direct interfaces in [80] since they are able to detect the user's intention through a physical interaction. In the last years, many different kind of ways to mount force sensors have been proposed all over the world. The main idea is to incorporate force sensors inside the grips, so that the user can still use the robot in the most natural way, but at the same time the force applied to the device is estimated. The device visible in Figure 2.6, proposed in [76], exploits a sophisticated solution relying on multiple strip force sensors mounted inside the two handlebars. In this way, each grip have been divided into 10 sector, enabling the possibility to perfectly understand the user's intention.

Figure 2.6: Smart Walker proposed by [76].

Another way to integrate the force sensors in the handlebar is presented by [81] with the solution visible in Figure 2.7. The authors propose an interface based on two potentiometers and in order to understand the user's desired horizontal and lateral force. Relying on such handlebar, in order to increase/decrease the walking speed, the user has to turn the overall structure counter–clockwise/clockwise. At the same time, to steer the robot, the user has simply to slide laterally the handlebars according to the direction that he/she wants to take.

A possible but not economic and not practical solution, due to calibration and mounting problem, is given by the hosting on the walker handles of two six–axial force and moment sensors. [97] proposes a measurement system which mainly include a set of force sensor resistors and accelerometers to obtain, in real time, the

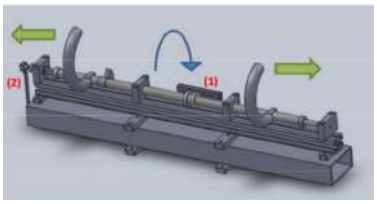

Figure 2.7: Innovative handlebar design proposed by [81].

values of related strength, acceleration and attitude of the device. The main focus of the author is the rehabilitation problem, in order to estimate, from the force on the handles, the positioning of the walker legs during gait, excessive oscillations or tilt angles of the walker device.
In [101] the information gathered by the force sensor is combined with the inertial measurement unit to reconstruct the amplitude of the acceleration along its three components. Anyway, since gravitational acceleration is not sufficient to extract the yaw angle, a magnetometer is furthermore mounted on the device to completely estimate the attitude of the device.

Many different works exploit force sensors, ranging from the complete transformation of the handlebars to the simple installation of axial–sensors inside them like [120, 110, 124].

For what concern Smart Walkers that exploit indirect interfaces, they are able to recognize user's movement and/or intent without requiring her/his input. For instance, the *JAIST* walker guesses the user's intention using laser scanned shin positions [71] (prototype visible in Figure 2.8). In this work, the authors have

Figure 2.8: Prototype of the JAST Smart Walkers [71].

preliminarily divided the base frame into six non–overlapping region. According to the measure gathered by the laser, the user's leg placement is assigned to a region. This information is then exploited to predict the user's intentions.

Another work that relies on indirect interfaces is proposed by Hirata et.al in [115] where a depth camera is used to track the user limbs.

Part I

The *FriWalk* prototype development

Chapter 3

Background

As seen in section 2.1.2, one of the most important features of Smart Walkers is the ability to provide cognitive assistance to the user [80], which means assist the user path–following navigation. The path–following problem is one of the central topic of the project ACANTO [2], and one of the main requirements as seen in the introduction. Suppose, for instance, that this device is used in a museum, and that the robot is assigned to a user who suffers limited mobility and is not confident to move in crowded environments. The user can decide, thanks to a graphical interface, which part of the museum he/she would like to visit. At this point the *FriWalk* will firstly plan the safest route to reach the desired target and, then, will gently guide him/her through the desired planned path, avoiding unexpected obstacles and dangerous situations. To solve these problems it is necessary to implement a model of the robot, either kinematic or dynamic. It is mandatory to remind that all models presented in this chapter are valid under the hypothesis of roll without slipping for the wheels.

3.1 Vehicle modelling

The *FriWalk* prototype developed and adopted in this thesis is visible in Figure 3.1. The prototype has been built on the basis of a commercial walker by mounting motors on the rear wheels, in order to control the forward velocity and the angular velocity of the device, and on the front wheels, in order to properly steer the robot. The reason of such an over–actuated choice is due to obtain the most versatile robot as possible. In fact, according to which actuation we want to exploit, it is possible to rely on two different models:

- unicycle model: the *FriWalk* can be modelled by an unicycle if it is rear actuated, while the front wheels can freely rotate (front caster wheels);
- car–like model: the *FriWalk* has to be modelled in this way if front steering wheels are actively controlled.

Figure 3.1: *FriWalk* prototype.

3.1.1 Kinematic model of the *FriWalk*

The kinematic model is implemented if the dynamic motion can be neglected, i.e. if the velocity and the inertia of the device, are not important to achieve the task.

Unicycle–like model

In the case that the *FriWalk* is rear actuated, then it is possible to exploit the differential kinematic proposed by [111]. So, relying on picture Figure 3.2, let us define the world reference frame $\{O_w, X_w, Y_w, Z_w\}$ having the axis Z_w orthogonal to the plane of motion. According to [111], it is possible to attach a mobile reference frame $\{O_m, X_m, Y_m, Z_m\}$ to the vehicle, in order that its origin O_m is located in the mid point of the wheelbase of the vehicle, having Z-axis Z_m parallel to Z_w, and X-axis X_m oriented in the direction of motion of the vehicle. In this way the vehicle position, with respect to the world frame, can be determined by two coordinates (x, y) identifying the position of O_m, and by a variable θ representing the vehicle yaw, defined as the orientation of the mobile reference frame. The main feature of the kinematic model of wheeled mobile robots is the presence of nonholonomic constraints due to the rolling without slipping conditions between wheels and ground. So, under the hypothesis of pure rolling motion of the wheels,

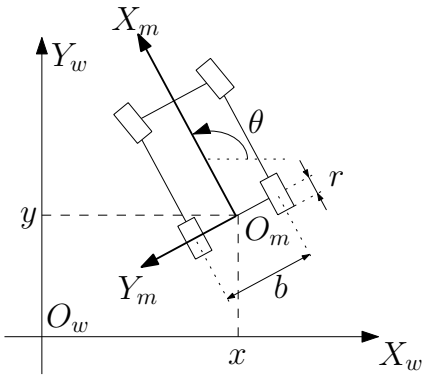

Figure 3.2: *FriWalk* unicycle modelling

the differential kinematics of a unicycle–like robot is given by

$$\begin{cases} \dot{x} = \cos(\theta)v, \\ \dot{y} = \sin(\theta)v, \\ \dot{\theta} = \omega, \end{cases} \tag{3.1}$$

where the scalar quantities v and ω represent, respectively, the forward and the angular velocity of the vehicle. The forward velocity v is positive in case of forward motion of the robot, while the angular velocity ω is positive for counter–clockwise rotations. Equation (3.1) directly links the state of the system $\chi = [x, y, \theta]^T$ with the control inputs v and ω. In a matrix form we can express equation (3.1) as

$$\begin{bmatrix} \dot{x} \\ \dot{y} \\ \dot{\theta} \end{bmatrix} = \begin{bmatrix} \cos(\theta) & 0 \\ \sin(\theta) & 0 \\ 0 & 1 \end{bmatrix} \begin{bmatrix} v \\ \omega \end{bmatrix}.$$

This means that, properly controlling v and ω it is possible to impose a desired motion to the vehicle. Usually these control inputs are expressed as a combination of the angular velocities of the wheels of the unicycle. Let ω_R and ω_L be, respectively, the angular velocity of the right and left wheels. The relationship between the control inputs and the wheel angular velocities is then

$$\begin{aligned} v &= \frac{r(\omega_R + \omega_L)}{2}, \\ \omega &= \frac{r(\omega_R - \omega_L)}{b}, \end{aligned} \tag{3.2}$$

where $b > 0$ is the axle length and $r > 0$ is the wheel radius. Moreover, since a unicycle is driven by two independent motors coupled with the wheels, it is necessary to invert equation (3.2) in order to derive the angular wheels velocity actuation from

the desired control inputs v and ω. This lead to have $\omega_L(v,\omega)$ and $\omega_R(v,\omega)$:

$$\begin{aligned} \omega_L &= \frac{1}{2}\frac{\omega b - 2v}{R}, \\ \omega_R &= \frac{1}{2}\frac{\omega b + 2v}{R}. \end{aligned} \tag{3.3}$$

Car–like model

In the case that front wheels of the *FriWalk* are equipped with motors, then it is possible to exploit them in order to properly control the motion of the robot. In such a case it is possible to rely on the rear–driven car–like model, by replacing the front steering wheels with a single virtual wheel, i.e. single track model, as visible in Figure 3.3.

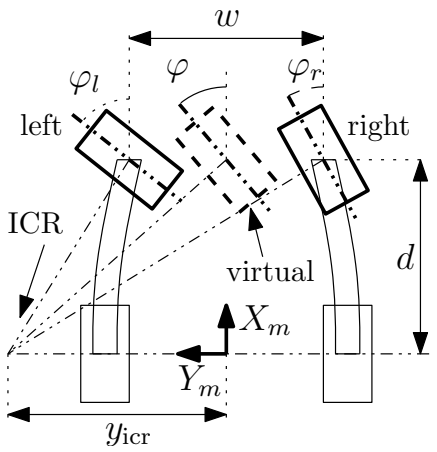

Figure 3.3: *FriWalk* car–like modelling

The model is then the differential kinematics of a front-steering rear-driven bicycle [70]

$$\begin{cases} \dot{x} &= v\cos(\theta), \\ \dot{y} &= v\sin(\theta), \\ \dot{\theta} &= \dfrac{v}{d}\tan(\varphi), \\ \dot{\varphi} &= u_v, \end{cases} \tag{3.4}$$

where the state becomes $\chi = [x, y, \theta, \varphi]^T$. With respect to Figure 3.3, the coordinates $[x, y]$ denote the position of the vehicle reference point, i.e. the mid point O_m of the rear wheel axle, with respect to the ground reference frame $\{O_w, X_w, Y_w, Z_w\}$, θ is the vehicle yaw, i.e. the orientation of the vehicle-fixed reference frame $\{O_m, X_m, Y_m, Z_m\}$ with respect to ground, $v \geq 0$ is the forward velocity, d is the distance between O_m and the contact point of the virtual front wheel, φ is the steering angle of the virtual

front wheel, and u_v is the rotational velocity of the virtual front wheel. Since the vehicle is not rear propelled, it means that it is passive, so the forward velocity v is an exogenous control input determined by the user's thrust, while the steering velocity u_v is a control input. If the vehicle has two steering wheels, like the *FriWalk*, the virtual steering angle φ is related to the left and right wheel angles φ_l and φ_r to ensure that the instantaneous rotation centre (ICR) of the vehicle is properly positioned (see Figure 3.3). This problem is well known as the Ackerman steering problem. Let y_{icr} be the Y coordinate of the vehicle ICR in the vehicle frame $\{O_m, X_m, Y_m, Z_m\}$. By applying standard geometrical relations to the triangles in Figure 3.3, we get

$$\begin{aligned} y_{\text{icr}} &= \frac{d}{\tan(\varphi)}, \\ \varphi_l &= \arctan\left(\frac{d}{y_{\text{icr}} - \frac{w}{2}}\right), \\ \varphi_r &= \arctan\left(\frac{d}{y_{\text{icr}} + \frac{w}{2}}\right), \end{aligned} \tag{3.5}$$

where $w > 0$ is the distance between the contact points of the front steering wheels. Therefore, the desired steering velocities are

$$\begin{aligned} \dot{\varphi}_l &= \frac{d^2 \csc^2(\varphi)\dot{\varphi}}{(d\cot(\varphi) - \frac{w}{2})^2 \left(\frac{d^2}{(d\cot(\varphi) - \frac{w}{2})^2} + 1\right)}, \\ \dot{\varphi}_r &= \frac{d^2 \csc^2(\varphi)\dot{\varphi}}{(d\cot(\varphi) + \frac{w}{2})^2 \left(\frac{d^2}{(d\cot(\varphi) + \frac{w}{2})^2} + 1\right)}. \end{aligned} \tag{3.6}$$

3.1.2 Dynamic model of the *FriWalk*

In order to perform a more sophisticated analysis of the actuation effects and develop a system where the inertia is an important feature, as will be clearer in Chapter 10, the kinematic model (3.1) is no more sufficient.

Dynamic unicycle model

In such case it is necessary to expand the state of the unicycle with $\chi = [x, y, \theta, v, \omega]^T$. The kinematic model (3.1) can be rewritten in a dynamic model as

$$\begin{cases} \dot{x} = \cos(\theta)v, \\ \dot{y} = \sin(\theta)v, \\ \dot{\theta} = \omega, \\ \dot{v} = \frac{F}{M}, \\ \dot{\omega} = \frac{N}{J}, \end{cases} \tag{3.7}$$

where F is the external force acting on the vehicle along the direction of motion, N is the external torque about the Z_w–axis, while m and J are, respectively, the mass and the moment of inertia of the cart, which are assumed to be known.

Dynamic car–like model

Regarding the case of the rear–driven car–like, if we suppose to add the full dynamic imposed by the user (force and momentum), this model (3.4) is no more valid. In fact, let us analyse the third equation, i.e. $\dot{\theta} = \frac{v}{d}\tan(\psi)$: the angular velocity of the rear axis is linearly dependent on the forward velocity imposed to the vehicle and in particular, if $v = 0$, the vehicle is firmly stopped. Let us now suppose that, from this condition, the user imposes a momentum on the cart handles, without applying any force F. In this case, in order to let the vehicle rotate around the middle–point of the rear axis (which is actually feasible), the front wheels have to be caster to reach an angle $\psi = \pm\frac{\pi}{2}$. This is evidently in contrast with $\dot{\theta} = \frac{v}{d}\tan(\psi)$, which has a singularity in $\psi = \pm\frac{\pi}{2}$. In practice, to avoid the singular point a violation of the pure rolling without slipping hypothesis is necessary. As a consequence, the car-like robot works fine if the user only imposes the forward (pushing) force F, while the unicycle model has to be used if the full human dynamic is of interest. So under the assumption that the user pushes only the vehicle with a force F, we get

$$\begin{bmatrix} \dot{x} \\ \dot{y} \\ \dot{\theta} \\ \dot{\psi} \\ \dot{v} \end{bmatrix} = \begin{bmatrix} v\cos(\theta) \\ v\sin(\theta) \\ \frac{v}{d}\tan(\psi) \\ u \\ \frac{F}{m} \end{bmatrix}. \tag{3.8}$$

3.2 Path following problem definition

The path is a curve in the plane that the vehicle has to follow in order to reach a desired target. In particular, it describes the sequence of values $[x_d, y_d, \theta_d]$ that the vehicle has to replicate in order to satisfy the task. Usually, for simplicity, a curvilinear abscissa s moving along the path is introduced in order that, each desired configuration, can be parametrized with it. This lead to define that a path Γ is a function that associates for each value of the curvilinear abscissa a desired state $\chi_d(s) = \begin{bmatrix} x_d(s) & y_d(s) & \theta_d(s) \end{bmatrix}^T$ that the vehicle has to track properly. To fully describe the path following problem, let us denote by t the standard time. Given a path Γ and an unicycle or car–like robot, the problem consist in finding the evolution of the control inputs $v(t)$ and $\omega(t)$ such that

$$\lim_{t\to\infty} \chi(t) = \chi_d(s(t)) \quad \Rightarrow \quad \begin{cases} \lim_{t\to\infty} x(t) = x_d(s(t)), \\ \lim_{t\to\infty} y(t) = y_d(s(t)), \\ \lim_{t\to\infty} \theta(t) = \theta_d(s(t)). \end{cases} \tag{3.9}$$

3.2.1 Curvilinear coordinates: the Frenet Frame

Let us now consider an infinitesimal portion of a generic path Γ. By looking at Figure 3.4, introducing a generic point $P = [x_P(s), y_P(s)]$ we can derive the following set of equations:

$$\begin{cases} \frac{dx_P(s)}{ds} & = \cos(\theta_d(s)) \\ \frac{dy_P(s)}{ds} & = \sin(\theta_d(s)) \\ \frac{d\theta_d(s)}{ds} & = c(s) \end{cases} \tag{3.10}$$

in which $c(s)$ represents the curvature of the path (in the case of circular arcs it is equal to $1/R$, where R is the radius of curvature of the path).

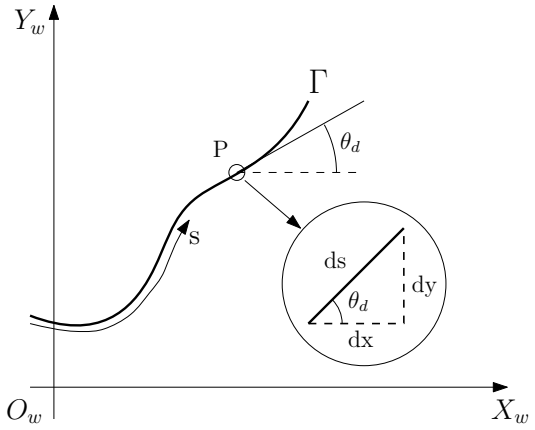

Figure 3.4: Infinitesimal portion of a generic path Γ.

Since in term of Cartesian coordinates the path following problem can be very complex, it is a common practice to introduce a reference frame $\{O_f, X_f, Y_f, Z_f\}$, called Frenet frame [70], moving along the path and following the vehicle motion. The simplest way to place such frame is by locating its origin O_f on the orthogonal projection of the vehicle position on the path, i.e. in the point of the path closest to the vehicle, as shown in Figure 3.5. The X-axis X_f of the Frenet frame will be oriented according to the tangent of the path at the point corresponding to O_f. The angle between X_f and X_w is then identified as the desired angle $\theta_d(s)$ that the vehicle has to assume in order to properly follow the given path. In this way it is possible to introduce the error $\tilde{\theta} := \theta - \theta_d$ representing the difference between the vehicle yaw θ and the path orientation θ_d. Moreover, let us denote by l the distance of the vehicle from the path along the Y_f axis, which assumes positive values whenever the vehicle is above the path, while negative values when it is under it. Thanks to this new set of generalized coordinates it is possible to rewrite the position of the unicycle with respect to the global reference frame as

$$\begin{bmatrix} x(t) \\ y(t) \end{bmatrix} = \begin{bmatrix} x_P(s) \\ y_P(s) \end{bmatrix} + \begin{bmatrix} \cos(\theta_d(s)) & -\sin(\theta(s)) \\ \sin(\theta_d(s)) & \cos(\theta(s)) \end{bmatrix} \begin{bmatrix} 0 \\ l \end{bmatrix}. \tag{3.11}$$

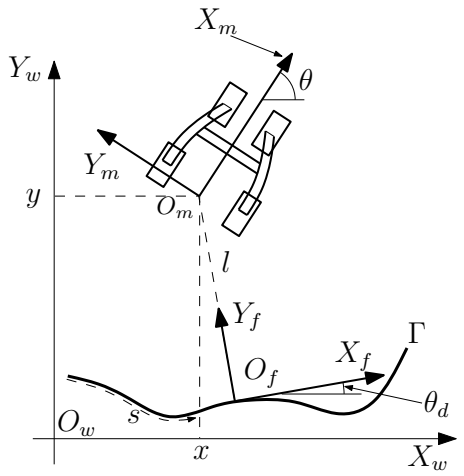

Figure 3.5: Positioning of the Frenet frame on the orthogonal projection of the vehicle on a generic path Γ.

Let us now compute the time derivative of equation (3.11), what we get is

$$\begin{cases} \dot{x}(t) &= \cos(\theta_d(s))\dot{s} - \dot{l}\sin(\theta_d(s)) - l\cos(\theta_d(s))c(s)\dot{s}, \\ \dot{y}(t) &= \sin(\theta_d(s))\dot{s} + \dot{l}\cos(\theta_d(s)) - l\sin(\theta_d(s))c(s)\dot{s}, \\ \dot{\theta}(t) &= c(s)\dot{s} + \dot{\tilde{\theta}}. \end{cases}$$

By collecting the cosine and sine functions we can simplify a little bit this equation and get

$$\begin{cases} \dot{x}(t) &= \cos(\theta_d(s))\dot{s}(1 - lc(s)) - \dot{l}\sin(\theta_d(s),) \\ \dot{y}(t) &= \sin(\theta_d(s))\dot{s}(1 - lc(s)) + \dot{l}\cos(\theta_d(s)), \\ \dot{\theta}(t) &= c(s)\dot{s} + \dot{\tilde{\theta}}. \end{cases}$$

Now by using the kinematic unicycle model expressed in equation (3.1), it is possible to rewrite the expression above as

$$\begin{cases} v\cos(\theta) &= \cos(\theta_d(s))\dot{s}(1 - lc(s)) - \dot{l}\sin(\theta_d(s)), \\ v\sin(\theta) &= \sin(\theta_d(s))\dot{s}(1 - lc(s)) + \dot{l}\cos(\theta_d(s)), \\ \omega &= c(s)\dot{s} + \dot{\tilde{\theta}}. \end{cases}$$

For the first two equations, recalling that $\tilde{\theta} := \theta - \theta_d$, we can rewrite

$$\begin{bmatrix} \cos(\theta_d + \tilde{\theta}) & -\sin(\theta_d + \tilde{\theta}) \\ \sin(\theta_d + \tilde{\theta}) & \cos(\theta_d + \tilde{\theta}) \end{bmatrix} \begin{bmatrix} v \\ 0 \end{bmatrix} = \begin{bmatrix} \cos(\theta_d) & -\sin(\theta_d) \\ \sin(\theta_d) & \cos(\theta_d) \end{bmatrix} \begin{bmatrix} \dot{s}(1 - lc(s)) \\ \dot{l} \end{bmatrix}.$$

$$\begin{bmatrix} \cos(\tilde{\theta}) & -\sin(\tilde{\theta}) \\ \sin(\tilde{\theta}) & \cos(\tilde{\theta}) \end{bmatrix} \begin{bmatrix} v \\ 0 \end{bmatrix} = \begin{bmatrix} \dot{s}(1 - lc(s)) \\ \dot{l} \end{bmatrix}$$

Therefore, we finally have found the coordinate transformation

$$\begin{cases} v\cos(\tilde{\theta}) & = \dot{s}(1 - lc(s)), \\ v\sin(\tilde{\theta}) & = \dot{l}, \\ \omega & = c(s)\dot{s} + \dot{\tilde{\theta}}, \end{cases}$$

which, solved with respect to $\dot{s}$, $\dot{l}$ and $\dot{\tilde{\theta}}$, allow us to solve the path following problem by replacing the vehicle state $[x, y, \theta]^T$ with the coordinates $[s, l, \tilde{\theta}]^T$, having the following dynamics:

$$\begin{cases} \dot{s} & = v\dfrac{\cos(\tilde{\theta})}{1 - c(s)l}, \\ \dot{l} & = v\sin(\tilde{\theta}), \\ \dot{\tilde{\theta}} & = \tilde{\omega}, \end{cases} \tag{3.12}$$

where $\tilde{\omega} = \omega - c(s)\dot{s}$ is the auxiliary control input related to the angular speed of the vehicle and the curvature of the path. Using the equation (3.12), the path following conditions (3.9) can be rewritten as the new following asymptotic stability problem:

$$\begin{aligned} \lim_{t\to+\infty} |l(t)| = 0, \\ \lim_{t\to+\infty} |\tilde{\theta}(t)| = 0, \end{aligned} \tag{3.13}$$

which simply means that the distance l between the vehicle and the path and the attitude error $\tilde{\theta}$ of the vehicle with the desired path have to converge to zero to properly track the planned path.
A possible solution to the problem (3.13) relies on the following control law

$$\tilde{\omega} = \tilde{\omega_d} \triangleq -lv\frac{\sin(\tilde{\theta})}{\tilde{\theta}} - k_2\tilde{\theta}, \tag{3.14}$$

with $k_2 > 0$. This control action solves the path following problem provided that the initial robot configuration is not too far from the desired path [24].
Another possible solution is found by recalling that the main objective of the path following control law is to drive l and $\tilde{\theta}$ to zero. In [113] a solution to the trajectory following problem has been proved using Lyapunov technique. In particular the Lyapunov function candidate reported next has been proposed:

$$V_1 = \frac{1}{2}l^2 + \frac{1}{2\gamma}(\tilde{\theta} - \delta(l, v))^2, \tag{3.15}$$

referring to the kinematic model (3.12). The choice of the function $\delta(l, v)$ in (3.15) is instrumental in shaping the transient maneuvers during the path approach phase. The derivative of V_1 in (3.12) can be easily computed to give

$$\dot{V}_1 = l\dot{l} + \frac{1}{\gamma}(\tilde{\theta} - \delta)(\dot{\tilde{\theta}} - \dot{\delta}), \tag{3.16}$$

now if we substitute (3.12) into (3.16) we obtain

$$\dot{V}_1 = lv\sin(\tilde{\theta}) + \frac{1}{\gamma}(\tilde{\theta} - \delta)(\dot{\tilde{\theta}} - \dot{\delta}).$$

Summing and subtracting $lv\sin(\delta)$, we get

$$\dot{V}_1 = lv\sin(\delta) + \frac{1}{\gamma}(\tilde{\theta} - \delta)\left(\dot{\tilde{\theta}} - \dot{\delta} + \gamma lv\frac{\sin(\tilde{\theta}) - \sin(\delta)}{\tilde{\theta} - \delta}\right).$$

By defining the control law $\tilde{\omega} = \dot{\tilde{\theta}}$ as

$$\dot{\tilde{\theta}} = \dot{\delta} - \gamma lv\frac{\sin(\tilde{\theta}) - \sin(\delta)}{\tilde{\theta} - \delta} - k_2(\theta - \delta), \tag{3.17}$$

we get for (3.16)

$$\dot{V}_1 = -\frac{k_2}{\gamma}(\tilde{\theta} - \delta)^2 + lv\sin(\delta). \tag{3.18}$$

Evidently the first term is negative definite with respect to $\tilde{\theta} - \delta$, while, in order to verify that $lv\sin(\delta) \leq 0$, it is necessary to find an expression for $\delta(l, v)$ which makes (3.18) negative defined.

3.2.2 Dynamic Frenet Frame

Let us consider the kinematic equation for the Frenet Frame (3.12). For what concern the curvilinear abscissa s, this variable can be easily found solving a geometrical problem, i.e. finding the closest point of the path with respect to the position of the robot. Once found the corresponding value s, the curvature $c(s)$ of that specific point is determined as well. The velocity $\dot{s}$ of the Frenet frame is then always determined relying on the first equation, but a singularity problem arises whenever $c(s)l = 1$, i.e. whenever the robot is placed exactly in correspondence of the centre of curvature. Intuitively, this happens when the vehicle is on the centre of the path curvature since the closest point on the path is not well defined (more points have the same distance from the vehicle). Theoretically, this singularity could compromise the stability of the controller since $\dot{s}$ could become extremely high, causing undesired and uncomfortable movements of the robot. From a practical point of view, in our experiments performed with the Frenet frame kinematic (3.12) in [10, 11, 7, 12], the singularity issue has kicked in. However, since the main users are elderly people with physical impairments, safety is the most important feature to be guaranteed, and, for this reason, this annoying singularity has to be avoided. The safety issue can be easily overcome relying on a dynamic Frenet frame [113]. According to the authors, the Frenet frame can be located in an arbitrary point as reported in Figure 3.6. For this reason we can denote by l_x the distance between the origin of the Frenet frame and the reference point of the robot along the X_f axis, and by l_y the distance of

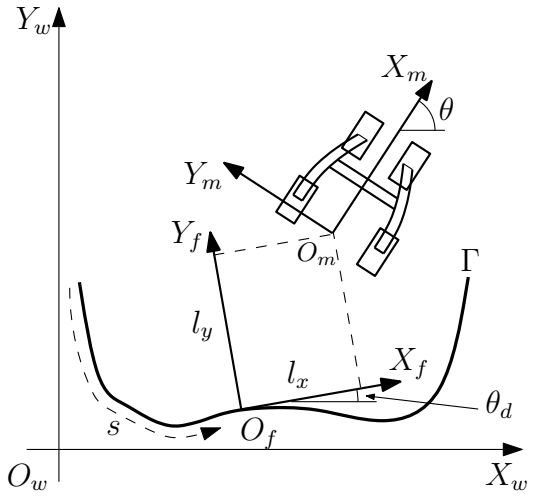

Figure 3.6: Positioning of the dynamic Frenet frame on a generic path Γ.

the robot along the Y_f axis. Using this new state $\chi = [l_x, l_y, \tilde{\theta}]^T$, equation (3.12) becomes

$$\begin{cases} \dot{l_x} &= -\dot{s}(1 - c(s)l_y) + v\cos(\tilde{\theta}), \\ \dot{l_y} &= -c(s)\dot{s}l_x + v\sin(\tilde{\theta}), \\ \dot{\tilde{\theta}} &= \omega - c(s)\dot{s}. \end{cases} \tag{3.19}$$

Thanks to (3.19) the singularity has been evidently removed, but with the consequence that now $\dot{s}$, i.e. the velocity of the Frenet frame, acts as an auxiliary control input and, then, needs to be properly designed in order to synthesize the control law. Similarly to equation (3.13), it is possible to rewrite the path–following problem (3.9) with respect to the new state $\chi = [l_x, l_y, \tilde{\theta}]^T$ as:

$$\begin{aligned} \lim_{t\to+\infty} |l_x(t)| &= 0, \\ \lim_{t\to+\infty} |l_y(t)| &= 0, \\ \lim_{t\to+\infty} |\tilde{\theta}(t)| &= 0, \end{aligned} \tag{3.20}$$

which means that the main objective of the control law is to drive l_x, l_y and $\tilde{\theta}$ to zero. In [113] a possible solution to solve the problem (3.20) has been proposed relying on Lyapunov technique. The authors propose the following Lyapunov candidate:

$$V_1 = \frac{1}{2}(l_x^2 + l_y^2) + \frac{1}{2\gamma}(\tilde{\theta} - \delta(l, v))^2, \tag{3.21}$$

The time derivative of V_1 of (3.21) can be easily computed obtaining

$$\dot{V_1} = (l_x\dot{l_x} + l_y\dot{l_y}) + \frac{1}{\gamma}(\tilde{\theta} - \delta)(\dot{\tilde{\theta}} - \dot{\delta}), \tag{3.22}$$

now, substituting (3.20) into (3.22), the following expression is obtained:

$$\begin{aligned}\dot{V}_1 &= l_x\left(-\dot{s}(1-c(s)l_y)+v\cos(\tilde{\theta})\right)+l_y\left(-c(s)\dot{s}l_x+v\sin(\tilde{\theta})\right)+\frac{1}{\gamma}(\tilde{\theta}-\delta)(\dot{\tilde{\theta}}-\dot{\delta})\\ &= -l_x(\dot{s}-v\cos(\tilde{\theta}))+l_y v\sin(\tilde{\theta})+\frac{1}{\gamma}(\tilde{\theta}-\delta)(\dot{\tilde{\theta}}-\dot{\delta}).\end{aligned}$$

Again, summing and subtracting $lv\sin(\delta)$, we get

$$\dot{V}_1 = -l_x(\dot{s}-v\cos(\tilde{\theta}))+l_y v\sin(\delta)+\frac{1}{\gamma}(\tilde{\theta}-\delta)\left(\dot{\tilde{\theta}}-\dot{\delta}+\gamma l_y v\frac{\sin(\tilde{\theta})-\sin(\delta)}{\tilde{\theta}-\delta}\right). \quad (3.23)$$

By defining

$$\begin{cases}\dot{s} &= v\cos(\tilde{\theta})+k_1 l_x,\\ \dot{\tilde{\theta}} &= \dot{\delta}-\gamma l_y v\dfrac{\sin(\tilde{\theta})-\sin(\delta)}{\tilde{\theta}-\delta}-k_2(\theta-\delta),\end{cases} \quad (3.24)$$

we get

$$\dot{V}_1 = -k_1 l_x^2-\frac{k_2}{\gamma}(\tilde{\theta}-\delta)^2+l_y v\sin(\delta). \quad (3.25)$$

Evidently the first and the second terms are negative definite, while in order to verify that $l_y v\sin(\delta)\leq 0$, it is necessary to find an expression for $\delta(l_y, v)$ which makes (3.25) be negative definite.

3.2.3 A solution for the approach angle

As seen in the previous sections, both equation (3.25) for the dynamic Frenet frame and equation (3.18) require the definition of a function $\delta(\cdot)$ which makes the Lyapunov function derivative be negative definite. In the literature it is a common practice to define such function as an approaching function $\delta(\cdot)$ defining the manoeuvre that the vehicle has to take to approach and follow the path as a function of the distance, like in [84, 113, 119]. It is possible to note that l for the Frenet frame (Figure 3.5) is totally equivalent to l_y for the dynamic Frenet frame (Figure 3.6) so the condition that needs to be respected is

$$lv\sin(\delta) < 0. \quad (3.26)$$

Since we are dealing with Smart Walkers used by elderly people, it is completely reasonable to perform path–following only if $v > 0$, i.e. if the user pushes the vehicle forward only. In fact, whenever the user wants to go backwards, a completely different strategy has to be considered in order to preserve users' safety, and the path–following problem has to be relaxed (e.g. let the user be the only element in charge of motion). So, assuming that $v > 0$ and imposing a limit up to $\pi/2$ on the convergence angle, the function $\delta(l)$ needs to be:

1. Continuous and bounded, i.e. $|\delta(l)| \leq \frac{\pi}{2}\ \forall l$;
2. Strictly monotonic;
3. Odd, i.e. $l\delta(l) \leq 0\ \forall l$.

In order to satisfy such constraints, [113] proposes the following two solutions (see Figure 3.7):

$$\begin{aligned} \delta(l) &= \frac{2\theta_a}{\pi}\arctan(l), \\ \delta(l) &= \theta_a \tanh(l), \end{aligned} \tag{3.27}$$

in which $\theta_a > 0$ is a parameter such as

$$\{\phi : \mathbb{R} \to \mathbb{R} | -\theta_a \leq \phi(l) \leq \theta_a\ \forall l \in \mathbb{R}\}, \tag{3.28}$$

identifying the maximum approaching angle.

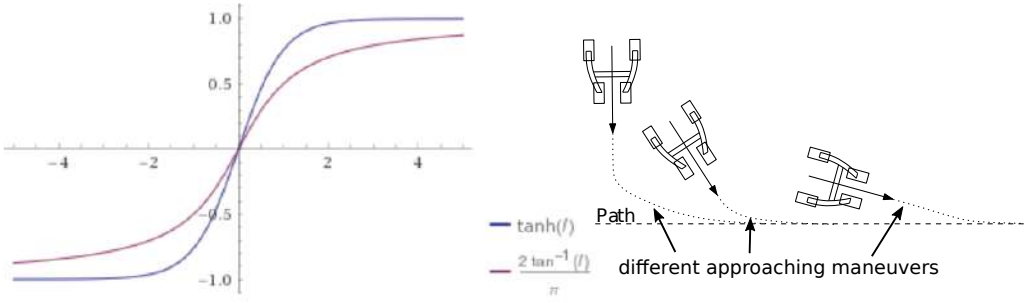

Figure 3.7: Approaching functions $\delta(l)$ of equation (3.27) in which $\theta_a = 1$.

Looking at Figure 3.7 it can be easily notice that the large is the distance of the vehicle from the path, the larger $|\delta(l)|$ is, meaning that the robot needs to approach the path more orthogonally. Contrarily, whenever the distance of the robot from the path is close to 0, then also $\delta(l) \to 0$, meaning that the vehicle is properly oriented. Considering, for simplicity, the path-following problem parametrized by the Frenet frame (3.12), it is possible to prove that exploiting a function $\delta(l)$ which is bounded, strictly monotonic and odd, then the path–following conditions (3.13) hold if

$$e_\theta = \tilde{\theta} - \delta(l) = 0 \Rightarrow \tilde{\theta} = \delta(l), \tag{3.29}$$

where e_θ is the attitude error of the robot. In other words, it is possible to conclude that the path–following problem is then solved if the attitude $\tilde{\theta} = \theta - \theta_d$ of the vehicle tracks properly the reference $\delta(l)$, defined by an approaching function [30].

3.2.4 Path following with humans

Stability and comfort are the two most important features that have to be taken into account whenever a robot has to cooperate with an user. Since one of the main tasks of the *FriWalk* is to perform path–following, we want the robot to be less intrusive as possible. The basic idea is that, whenever the user behaves *well* (so he/she is following or approaching correctly the path), then the robot has bo be completely passive, meaning that the user is totally in control of the device. As soon as the user exits from a safety region, hence he/she departs from the planned path or is no more correctly aligned, then the control action of the *FriWalk* kicks in to properly suggest the correct direction that he/she has to take to realign toward the path.
By looking at equation (3.21) it can be noticed that it is quite impossible to define a value $V^\star$ such that

$$\begin{aligned} V_1 \leq V^\star \quad &\Rightarrow \quad \text{user in control,} \\ V_1 > V^\star \quad &\Rightarrow \quad \text{robot in control.} \end{aligned}$$

For instance, suppose that the user is far away from the path such that $l_x^2 + l_y^2 > V^\star$, but $e_\theta = \tilde{\theta} - \delta(l_y) = 0$ (meaning that the user is correctly aligned toward the approaching direction). This condition lead to $V_1 > V^\star$, so that the robot is in control even if the user is correctly oriented, producing an annoying intervention of the robot since its control action results to be useless. To intuitively understand the importance of measuring the distance via e_θ, consider the following examples:

- The vehicle is very far from the path (huge value of $|l_y|$) but is it properly oriented to approach it, i.e. $e_\theta = 0$. In this case the control authority can be left to the user since he/she is properly approaching the path;
- The vehicle is located on the path (i.e. $|l_y| = 0$) but it is oriented in the opposite direction, i.e. $\delta(l_y) = 0$ and $e_\theta = \tilde{\theta} - 0 \approx \pi$. In this case the controller needs the authority to reorient the vehicle and then the error cannot be considered zero.

To reduce the path following errors $|l_x|$, $|l_y|$ and $\tilde{\theta}$, it is sufficient limiting the value of $|e_\theta|$. In fact, modifying the Lyapuonv candidate (3.21) to

$$V = \frac{1}{2} e_\theta^2, \tag{3.30}$$

whose time derivative is

$$\dot{V} = e_\theta \dot{e}_\theta = e_\theta \left(\omega - c(s)\dot{s} - \dot{l}_y \frac{\mathrm{d}\delta}{\mathrm{d}l_y}(l_y) \right) = e_\theta \left(\omega - v\gamma(\chi) \right). \tag{3.31}$$

The control law

$$\omega = \omega^\star(\chi) = v \left(\gamma(\chi) - \kappa \left(\tilde{\theta} - \delta(l_y) \right) \right), \tag{3.32}$$

where κ is a constant gain such that $v\kappa > 0$ and

$$\begin{aligned} \gamma(\chi) &= c(s)\dot{\xi} + \left(-c(s)\,\dot{\xi}\,l_x + \sin\tilde{\theta}\right)\frac{\mathrm{d}\delta}{\mathrm{d}l_y}(l_y), \\ \dot{s} &= v\dot{\xi}, \\ \dot{\xi} &= \cos(\tilde{\theta}) + \kappa_x l_x, \end{aligned} \tag{3.33}$$

with $\kappa_x > 0$, ensures that the attitude error $e_\theta = \tilde{\theta} - \delta(l_y)$ converges to zero.
To maximize the user comfort the path–following problem (3.20) can be rewritten in a more relaxed form as

$$\begin{aligned} \lim_{t\to+\infty} |l_x(t)| &\leq l_\infty, \\ \lim_{t\to+\infty} |l_y(t)| &\leq l_\infty, \\ \lim_{t\to+\infty} |\tilde{\theta}(t)| &\leq \tilde{\theta}_\infty, \end{aligned} \tag{3.34}$$

where t denotes the time, and $l_\infty > 0$ and $\tilde{\theta}_\infty > 0$ are positive arbitrary constants.
In the rest of the thesis, especially in the chapters of Part II, all the guidance strategies developed will deal with the problem (3.34) and each strategy will solve this problem in a different way, according to the available actuation and to the user needs.

Chapter 4

Smart Walker in Acanto

From the model-based analysis previously carried out, it is evident how the walker can act as a navigation aid using the path-following approach previously presented. The role of this chapter is then to describe the robot architecture that enables such features and endows the commercial frame with autonomous capabilities. The project ACANTO covers many aspect on different layers, ranging from the mechanical components to the high level electronic units. The cognitive support and the interaction with the *FriWalk* will contribute to maintain high levels of mobility. The requirements at the basis of the *FriWalk* are summarized in Table 4.1.

In this thesis, we have mainly focused on R1, R2, R5 and R6. In particular this chapter deals with R1 and R5, providing the mechanical and software solution adopted for the *FriWalk* to satisfy the corresponding requirements. Then Part II focuses on R2 developing different guidance strategies that can adapt differently according to the user needs. At the end Part III deals with R6 and R1 focusing on the benefits of the *FriWalk* used as a rehabilitation device.

Table 4.1: Requirements table of the *FriWalk*.

Requirement 1 (R1)	*Flexibility and versatility*: develop a flexible and versatile robot that can adapt to the user needs, able to modify its inertia according to the situation.
Requirement 2 (R2)	*Navigational aid*: develop different guidance strategy on the basis of the nature of the *FriWalk* (unicycle active, passive or car–like) with a compliant behaviour according to the user impairments;
Requirement 3 (R3)	*Cognitive aid*: develop a fine localization and sensing system to localize itself inside an environment and detect moving obstacles.
Requirement 4 (R4)	*Reactive aid*: develop real–time planning strategy, connecting the actual robot position with a point of interest required by the assisted person, avoiding moving obstacles.
Requirement 5 (R5)	*Modular*: develop a software architecture connecting all the modules, ensuring safety, security, robustness and easiness of learning (simple GUI).
Requirement 6 (R6)	*Rehabilitation aid*: develop a rehabilitation version of the *FriWalk* to work with real patients (at the University Hospital of Getafe–Madrid).

4.1 The DaLi Smart Walker

The preliminary investigations have been performed with the prototype reported in Figure 4.1 which was developed for the European Project Dali [1]. This robot is simply derived from a commercial walker, mounting two electromechanical brakes on the rear wheels and two independent stepper motors on the front forks. The choice of this configuration is due to have a completely passive robot (i.e. no power can be injected by motors to allow autonomous navigation), so that the user has to push the vehicle to move forward or backward, while the brakes or the steering system intervene to guide the user through a planned path. In order to solve the localization problem, the rear wheels host incremental encoders, which are used in combination to an extended Kalman filter with a camera system to reconstruct the position and the attitude of the robot [92], [93]. Furthermore, the robot exploits vision technologies to detect information on the surrounding environment about the presence of dangers and unexpected obstacles in order to let the planner decide the most convenient path to preserve the user's safety [28].
For what concern the path–following problem, we have developed passive guidance

Figure 4.1: DaLi Smart Walker.

algorithms to ensure that the user is gently and securely guided toward a desired path, exploiting both the brakes [5, 11] and the front steering wheels [12]. Although several interesting results have been obtained, thanks to these preliminary analyses we understood that:

- Relying on a braking system which is not able to tune the braking force and without any knowledge about the human thrust (i.e. without any force sensors), the performances with the rear configuration only are very limited. The controller proposed in [11] and [5], according to the user, is abrupt and not intuitive at all. In fact, in order to completely exploit its potentiality, training is required to better understand the robot behaviour;
- Using the steppers motors on the front steering wheels, the path–following problem is solved with exceptional precision [12]. However, due to the nature of stepper motors, the human–robot interaction is very limited since the torque imposed by these actuators is much higher than the one provided by the user. These types of motors have also an high inertia, which means that, whenever they are disengaged, the user has to win their resistance to let them freely rotate, causing a very annoying and tiring effect on the user.

4.2 The *FriWalk* Smart Walker

The analysis briefly reported in section 4.1 about the robot realized for the DaLi project led us to the development from scratch of a new smart walker visible in

Figure 4.2.

Figure 4.2: The *FriWalk* Smart Walker.

To achieve the requirement R1 of Table 4.1, a completely passive robot is not sufficient. Therefore we have decided to radically change the mechatronic nature of the device, but keeping a low–cost architecture, by mounting motors on the rear wheels too. It has been therefore developed and analysed the possibility to equip the robot with brushless motors and study a configuration comfortable for the user. This means that, whenever the user pushes and steers the vehicle, he/she doesn't perceive any resistance of the motor, which is mandatory to preserve manoeuvrability and comfort, even without the presence of any clutch (that would increase costs and complexity dramatically). The reason of relying on brushless motor instead of stepper is to guarantee the smart control of the actuators in velocity or current (i.e. torque), hence allowing more degrees of freedom in the control strategy. Moreover, we opted for brushless instead of brushed because:

- Brushed motors: have the main advantage that are very economical, but they have several drawbacks. In fact they are noisy due to the presence of brushes, they have a low efficiency (0.7–0.8), their rotation causes inner sparks and they cannot be used to keep the wheel halted for long periods;
- Brushless motors: have the main disadvantage that are expensive aggravated by the fact that they need an inverter to be controlled (since they need alternating current), but they have a long lifetime, they have an high efficiency

(0.8–0.9), they can reach high speeds and they can be used as brakes to keep the wheel halted for longer periods than the brushed motors.

In addition to the actuators, the rear wheels host a pair of incremental encoder, meanwhile on the front forks there are mounted two absolute encoders to properly know the position of the steering wheels. Since the robot is equipped both with front and rear motors it means that is overactuated. This configuration has been chosen on purpose in order to guarantee that the *FriWalk* fulfil requirement R2 of Table 4.1 allowing different driving strategies:

- Passive rear driven behaviour: in this configuration the front motors are disengaged, so that the front wheels act as caster wheels, while the rear motors are exploited as brakes only, in order that the user is the only one responsible of the device thrust;
- Active rear driven behaviour: in this configuration the front motors are disengaged, like in the previous one, while the rear motors are exploited to help the user's thrust, in order to let the user perceive the vehicle with less inertia. This configuration can also be exploited to guide the user steering him/her toward a planned path;
- Passive front driven behaviour: in this configuration the rear motors are mainly disengaged, so that the thrust is given by the user only (the brakes intervene to halt the vehicle in emergency situations). At the same time the front motors are involved to properly steer the vehicle toward the desired direction.

Furthermore, all the cabling system has been hidden inside the walker–loom in order to maintain the *FriWalk* as clean as possible. All the electronic parts, like batteries and embedded circuits, have been placed inside a box under the seat. These improvements in the robot appearance are fundamental from the human–robot interaction point of view, especially for this kind of robot which is thought to work with elderly people, who are often frightened and does not feel confident with the technology.

4.2.1 Mechanical design

The power transmission system implemented on the rear wheels of the *FriWalk* has been performed with the introduction of a gear box composed by two stages, and the solution overview is visible in Figure 4.3.
The combination of the gears leads to an overall transmission ratio $\tau = 40$ with an efficiency of the 80%. This transmission, operating at the rated current of the motor (the equipment should be operated in such a way that the rated current shall not exceed at any given time), provides a rated torque of

$$C = K_\tau I_r \tau \eta = 3.85 \text{ Nm},$$

Figure 4.3: *FriWalk* rear transmission overview.

where $K\tau$ is the torque constant of the motor, I_r is the rated current, τ is the transmission ratio of the gearbox and η is the efficiency of the transmission. This C is the torque applied by the motor to the wheel shaft, which means that the force available at the contact point with the ground is equivalent to

$$F = \frac{C}{R} = 25.7\text{N},$$

where R is the radius of the wheel (0.15 m). This is the force that each rear wheel can apply to the ground without overheating the motors. In order to give a better idea of the power of such motor, let us suppose that a typical user weight is 70 kg. Knowing that the weight of the robot $m = 30$ kg, it means that the *FriWalk* is able to carry a user over an up-hill having a maximum slope of

$$\alpha = \arcsin\left(\frac{F}{mg}\right) \simeq 3.5^\circ \simeq 5\%.$$

Furthermore, this coupling system keeps the motion of the *FriWalk* completely reversible without the implementation of expensive and complex clutches, which means that, if the motors are disengaged, the user is still able to move freely the device. Considering instead the peak torque available by the motor, the *FriWalk* is able to carry up an user over a surface with an inclination equal to the $\alpha_{\max} = 20\%$. In addition, the transmission ratio has been chosen equal to 40 in order to have a good compromise between available force and speed. In fact the motor can run up to 4840 rpm, which means that the walker maximum speed is equal to

$$v = \text{rpm}\frac{2\pi}{60} \cdot \frac{1}{\tau} \cdot R \simeq 2 \text{ m/s},$$

which is much higher than the 1.3 m/s defined as the comfortable walking speed for seniors in [22] (over 70 years old without walking impairments).
Since the *FriWalk* has to work in direct contact with people (e.g., in hospitals, museums), a cover system aiming at protecting the user from danger of entanglement with mechanical organs (such as gears) has been designed and mounted as visible in Figure 4.3. The cover also protects actuators, sensors and drivers from dust and preserves the grease. Indeed, lubrication is fundamental in this type of mechanical couplings mainly, to reduce friction and to avoid wearing.

Regarding the front wheels of the *FriWalk*, the actuation is guaranteed by a pulley-belt system, where the original pulley available on the fork of the Trionic walker adopted has been preserved, but a gearbox having a transmission ratio of $\tau = 24$ with an efficiency $\eta = 0.9$ has been coupled with the motor. The overall idea is visible in Figure 4.4.

Figure 4.4: *FriWalk* front transmission overview.

The choice of the transmission ratio for the front has been a big challenge. In fact the power required by the motor to steer the front wheels is quite a bit, due to the weight of the device and the user, so a high transmission ratio is required. But, at the same time, the motion has to be kept reversible, in order that the user is still able to steer the vehicle if the actuator is disengaged. To have a good compromise between available force and speed, a transmission ration $\tau = 24$ gives

$$v = \text{rpm}\frac{1}{60} \cdot \frac{1}{\tau} \simeq 3.3 \text{ rps}.$$

It is important to remind that this feature is very important from an user–robot interaction point of view, (as it will be clearer in Section 7.4). Similarly to the rear actuation system, also for the front the power wires comes from the inside of the

frame, while the connection between the motor and its driver and the pulley–belt system is protected by means of a carter.

4.2.2 Software architecture

To satisfy requirement R5 of Table 4.1 a modular software architecture has to be designed. The *FriWalk* is then composed by four layers shown in Figure 4.5, which operate at different conceptual levels.

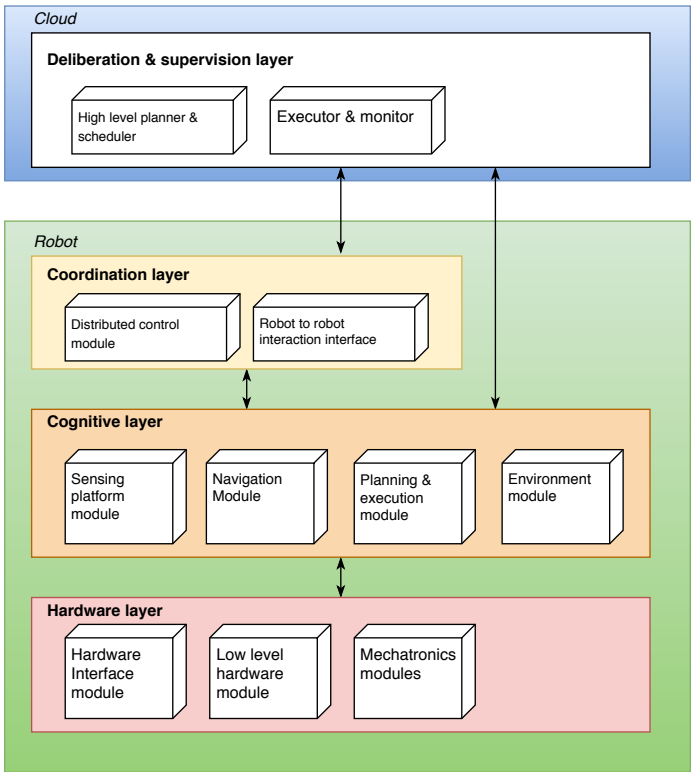

Figure 4.5: Software architecture layer diagram.

For what concerns the lowest level, thus the *hardware layer*, it is defined by many modules that are interfaced and interconnected each other and, all of them, are coordinated by an hardware interface module. Beyond this module, for the *FriWalk*, there are four mechatronics modules designed for the actuators management, one module for the power management and one for the coordination of the low–level sensors (e.g., sonars and IMU). The hardware module manages the periodic information with the status of the wheels and routes the execution of the actuation commands in the physical nodes.
At the second level, hence the *cognitive layer* in Figure 4.5, there are four modules in charge of management of:

- High–level sensors for surrounding environment perception (sensing platform module);
- Algorithms that interpret and elaborate data coming from the perception sensors (environment module);
- Algorithms for navigation, hence guidance and localization algorithms (navigation module);
- Algorithms for low–level path–planning (point to point) and for reactive planning (planning and execution module).

The cognitive subsystem provides a technical interface which includes the options to test the correct functionality of the robot at a mechatronic level. Additionally, a user interface has been designed. This interface includes the possibility of performing tasks and to visualize its execution and results.
At the third level there is the *coordination layer* that allows more robots to have local instances of distributive algorithms for tasks coordination performed by more robots.
These three modules are installed on board of the *FriWalk* and are able to communicate each other thanks to different communication patterns. Moreover the coordination and the cognitive layer are allowed to communicate with outside modules (hosted in the *supervision layer*) by means of wireless technologies.
The coordination and the cloud layers are not yet implemented on the actual version of the *FriWalk*, but their presence has been taken into account.

Once that all the layers composing the software architecture of the *FriWalk* have been defined it is possible to establish all the software components, which are depicted for clarity in Figure 4.6. In the remaining part of this section, we are going to have a deep analysis about hardware and cognitive layers, by defining the interconnections and the data exchange between the single modules.

The cognitive layer

The components on the basis of the cognitive layer are reported in the component diagram represented in Figure 4.6, where we can appreciate 4 modules:

- *Environment module*: collects in a database the map information that can be known a priori or computed by real–time algorithms, e.g. by slam methods;
- *Environment sensing platform*: overall interface structure to link cognitive sensors like cameras and lidar;
- *Low–level planning and execution module*: manages the point–to–point planning described in Section 4.2.5;

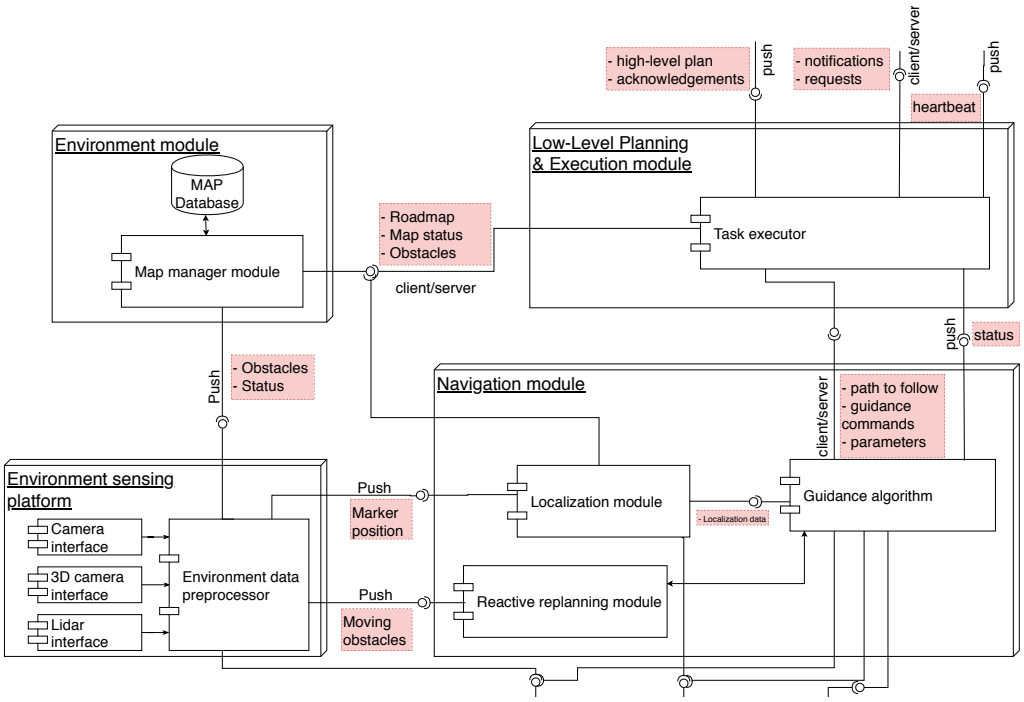

Figure 4.6: Component diagram of the cognitive layer of Figure 4.5.

- *Navigation module*: gathers all the information coming from localization sensors to estimate the position of the robot. These informations, in combination with the reactive planning module data, are sent to the guidance module which aim is to guide the vehicle through a planned path computing the desired inputs.

The hardware layer

At a lower layer there is the hardware layer which is composed by several modules as visible from Figure 4.7:

- *Hardware interface*: this is a gateway which has mainly two scopes:

  1. Collect all the information coming from the peripheral nodes, such as node state and node status, and modifies such data to make them available at an higher level;
  2. Receives high level commands (for instance from the guidance module) and sends the desired commands to the interested node with the appropriate language.

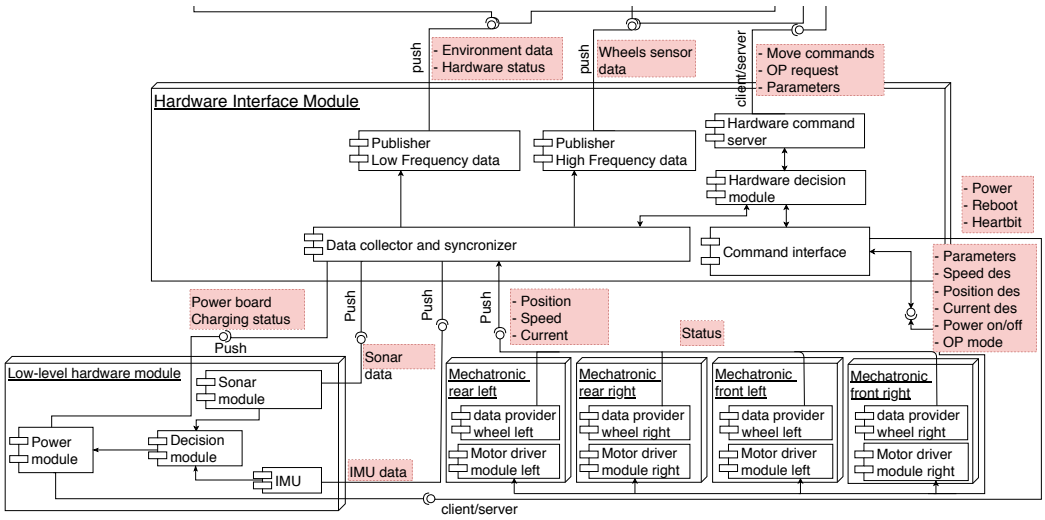

Figure 4.7: Component diagram of the hardware layer of Figure 4.5.

- *Low level hardware module*: manages the low level sensors like sonars, IMU and manages the power of the robot;
- *Mechatronic modules*: are responsible of the management of the actuators mounted on the rear and on the front wheels. They collect basic information of the state and of the status of the motor and properly send desired commands.

The *FriWalk* software deployment

The deployment diagram structure developed for the *FriWalk* has been bio–inspired. This is due to the nature of the sensors installed on the smart walker, since each sensor requires a different bandwidth (due to the data weight) and a different refresh rate. For the *FriWalk*, the sensors exploited for environment perception requires high bandwidth with a low frequency rate, while data coming from the hardware module needs a limited bandwidth but a very high frequency rate. This is exactly what happens in the human body. For instance, the sight requires a very high bandwidth with a low frequency rate, and for this reason it is directly connected with the brain, while the sense of touch or the heat perception are directly managed in the peripheral cells, allowing the muscles to compute movements without receiving any input from the brain.
For this reason, on the *FriWalk*, all the communication at the cognitive layer between all the modules happens via Ethernet, while the management of cameras and lidar happens with high capacity bus, i.e. USB. At the hardware layer it has been chosen to exploit a bus widely used in automotive and industrial applications, called CAN bus. The hardware interface is a software installed on a hardware (*BeagleboneBlack*) able to connect to both bus in order to interpret messages coming from the CAN

and replicate them at Ethernet level, so available to all the high level modules. At the same time it is able to interpret the messages coming from the guidance module and transform them into CAN messages to be sent to the single nodes.

The *FriWalk* hardware infrastructure and communication

For the *FriWalk* we opted for a star configuration to connect all the nodes with the CAN bus to a central embedded board, as shown in Figure 4.8.

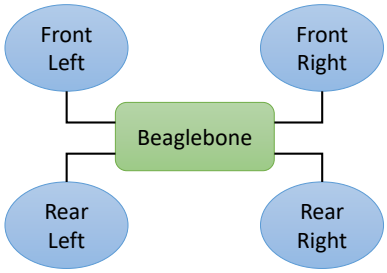

Figure 4.8: CAN star connection over the *FriWalk*.

The embedded board on the *FriWalk*, which is necessary to properly control actuators mounted on the device and manage all the data coming from each node, is a *BeagleboneBlack*, which is a low–cost community–supported development platform. As explained in section 4.2, each node is based on a brushless motor, which requires a specific driver to be controlled since it works in alternating current, i.e. an inverter is mandatory. Furthermore, to rely on a CANOpen communication protocol, we opted to mount four *LitePro E65* drivers, one for each motor. Beyond the implementation of the CANOpen protocol, such driver allow the user to control the motor either in position, velocity and current. At the same time this driver gives the possibility to directly connect a relative encoder. Its information is then fused with the data coming from the hall sensors to better the control performances of the motor. Thanks to the CANOpen–SDO protocol installed on such driver the user can, straightforwardly, send commands to the driver and, at the same time, collect data from it. For instance to set a desired rotational velocity, the requester has to transmit the message (a) reported in Figure 4.9 below the blue arrow. This message starts with 0x60i as COB–ID, where i identifies the node–ID, and continues with 23, since it is a write request, then 00 35 identifying the desired register and finishes with *aa bb cc dd* corresponding to the rotation speed set point. If the transmission has succeeded, then the driver will reply with the message (a) above the orange arrow in Figure 4.9. This logic perfectly fits in the CANOpen write request scheme reported in Figure A.3 in Appendix A.
The main drawback of such driver is that any PDO protocol is available and configurable, moreover the software is completely closed, so that it is impossible to

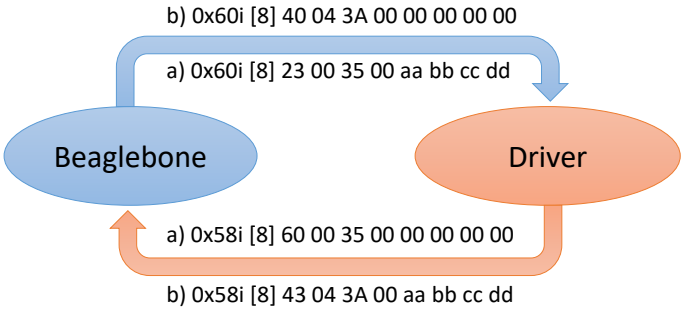

Figure 4.9: Example of messages transmitted between the Beablebone and the driver.

stream any node data in an efficient way. Because of such limitation, any time that the system needs to know the value of a state variable, a CANOpen read request message has to be transmitted (Beaglebone message (b) in Figure 4.9). Whenever the reading procedure has succeeded, then the driver will reply with the message (b) containing the information about the variable requested and stored in the address 04 $3A$. Although this procedure perfectly follows the logic on the basis of a CANOpen read request (Figure A.5 in Appendix A), we can easily understand that it generates a very high information flow over the CANbus, doubling the messages passing through it with respect to the use of a PDO protocol. Since the bandwidth available is limited up to 1 Mbit/s and four nodes are present on the *FriWalk*, relying on a PDO protocol that manages the data stream of each node results to be the most efficient solution.

4.2.3 *FriWalk* node design and definition

Beyond the control strategy available related to the CANOpen–SDO protocol provided by the driver, to have the complete control over the robot it is necessary to gather mandatory information from the four nodes of the *FriWalk*. The rear nodes are responsible of the robot thrust ($[\omega_l, \omega_r] \rightarrow [v, \omega]$, equation (3.2)), the robot odometric localization (Section 4.2.4) and the user thrust estimation (Chapter 10), while the front nodes are mainly exploited to explore different guidance strategies relying on a rear–driven car–like model. The *FriWalk* is then composed by two front nodes and two rear nodes, each of which is composed by a state and a status. The first collects the basic information coming from the driver, which are mandatory to control the robot and to implement the different guidance algorithms, while the latter contains the information about the status of the driver. In particular:

- **Rear node state** is composed by:
  - *Ticks*: information determined by the incremental encoder mounted on

the rear wheels and necessary for the odometric reconstruction (see section 4.2.4)

- *Speed*: rotational velocity of the wheel, necessary to know v and ω that are the control variable of an unicycle (see equation (3.1));
- *Force*: user thrust applied on the wheel to satisfy requirement R1 of Table 4.1. This information is determined thanks to an observer that estimates the user thrust thanks to the current absorbed by the motor coils (section 10.3).

- **front node state** is composed by:
  - *Position*: information determined by the absolute encoder mounted on the front fork and sent via serial interface;
  - *Speed*: rotational speed of the fork $\dot{\varphi}$ that is necessary to control a car–like vehicle (see equation (3.4));
  - *Current*: average current absorbed by the motor. This information is mandatory to implement an advanced cooperative guidance strategy (section 7.4).

- **Node status**: this information is the same for both the front and the rear node. It contains the information about the current control mode of the driver (position, velocity, current), enable status (power enable or disable), error register status (error information if arise) and driver status.

All the nodes state and status, apart from the force of the rear node, are driver available relying on the CANOpen–SDO protocol, hence sending a read request and waiting for a read response. In light of the previous analysis and considering the large amount of messages needed to properly steer the vehicle, it is possible to define the frequency rate of the streamer. As stated before, the CAN bus has 1Mbit/s (125kbyte/s) of bandwidth. Let us suppose that 25kbyte/s are reserved for protocol management for safety and to allow non–periodic data flow exchange (e.g. sending messages to enable/disable the driver, change the current modality). The remaining 100kbyte/s are used to accommodate the data flowing over the bus. It is absolutely reasonable to think that the node state is an high priority data, while the node status is less important. Indeed, a controller is more reliable as the update rate of each node is fast, while the status does not affect the controller performances. So, to limit the traffic flow over the *FriWalk* CAN bus, we decided to update the node status every 25 node state updates, which is still a sufficient frequency to properly manage the *FriWalk* status. Moreover, not only the messages to update the state and the status of the node flows over the bus, in fact also the messages sent by the control algorithm needs to be taken into account. The control kicks in every time that the node state is updated, so two other messages are generated (one for the

request and one for the reply). The *FriWalk* is over–actuated, but the controller manages only either the front nodes or the rear nodes when a guidance is activated, so that only 2 nodes are involved in this messages exchange. So, to summarize, over the CAN bus we have:

- 28 messages flowing with high priority, hence high frequency. In particular:
  - 24 messages are necessary to stream the node status;
  - 4 messages are necessary to properly control the nodes;
- 32 messages containing the node status flow with low frequency rate.

Since we decided that every low priority information are sent every 25 priority data messages, then, in a period T_{low} 25x28+32=732 messages flow over the CAN bus. This means that, to occupy all the bandwidth:

$$T_{\text{low}} = \frac{n \times \text{message size}}{\text{bandwidth}} = \frac{732 \times 16}{100000} \simeq 0.12 \text{ s}$$

which leads to a data stream from each node every

$$T_{\text{high}} = T_{\text{low}}/\text{rep} = 0.12/25 \simeq 5 \text{ ms}$$

Rear node design

One of the most important feature of the *FriWalk* is its ability to estimate the user thrust without relying on expensive force sensors (R1 of Table 4.1). To develop an effective variable inertia approach that exploits the rear motor informations, as we will see in Chapter 10, Section 10.3, it is necessary to implement two observers:

- The first one requires, as input, several information gathered from the motor to estimate the torque load at the wheel shaft. Such data are:
  - Voltage of each motor coil;
  - Current absorbed by each motor coil;
  - Absolute position of the motor rotor, necessary to transform the three–phase model of the motor into a bi–phase equivalent one.
- The second observer uses, as input, the information coming from the first one to estimate the thrust imposed by the user to the walker frame.

To implement such observers it is necessary a frequency rate at least 10 times higher than the dynamic of the motor current, which means that the observer has to run with a frequency of 10kHz. This led to the fact that voltage, current and absolute position of the rotor has to be gathered with such frequency.
To collect the data and implement such observer, a specific embedded board has been

developed (see Appendix B) based on a microcontroller belonging to the STM32F4 series, offering full performance of the ARM 32–bit Cortex–M4 core (with floating point unit) running up to 168MHz. The reason of using an ST is mainly due to the performances provided by the ARM core, which has a floating point unit already included on it, and the low cost. The choice of the F415 is mainly due to:

- Presence of three 12–bits ADC converters multichannel (up to 24) with a very high sampling rate (up to 2.4 MSPS) and 7.2 MSPS in triple interleaved mode;
- High clock rate, which offers the possibility to implement the observers and manages the data coming from the sensors connected as GPIO–input;
- Presence of a double CAN bus interface. This feature can be exploited to maximize the efficiency of the data flowing over the CAN bus, avoiding bus saturation and significantly reducing the cycle time of the algorithms up to 2ms;
- Up to 17 timers: up to twelve 16-bit and two 32-bit timers up to 168 MHz.

The rear node configuration is depicted in Figure 4.10, where we can appreciate the overall interconnection between all the elements, i.e., beaglebone, ST, driver and motor. The double CAN bus interface is exploited as follows:

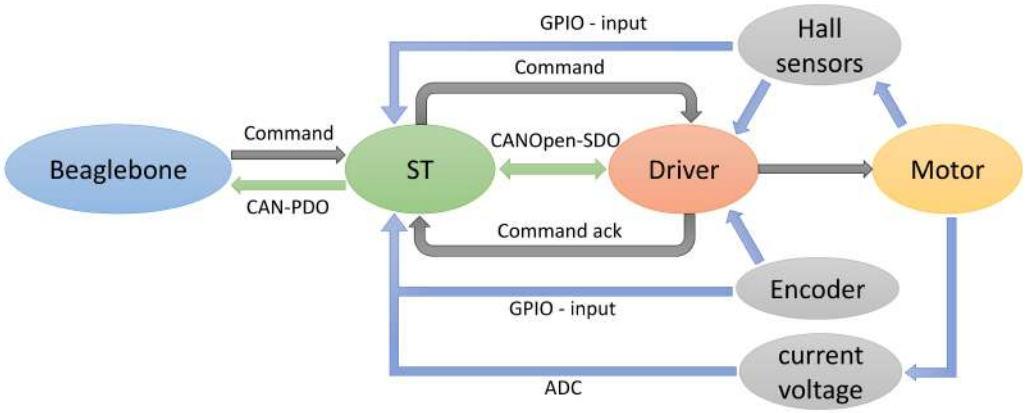

Figure 4.10: Rear node design.

- CAN bus 2 is used to allow the communication between the ST and the driver. Relying on the CANOpen–SDO protocol the ST gathers the information about the node state (every 2 ms) and status (every 50 ms);
- CAN bus 1 is the inner bus connecting the ST with the Beablebone. Implementing over the ST a CAN–PDO protocol it is possible to stream state and

status of the node in a more efficient and compact form, saving a lot of bandwidth. In particular, for the rear node, the following two messages will flow over the CAN bus

a) 0x30i [8] $\underbrace{\text{xx xx}}_{\text{velocity}}\ \underbrace{\text{xx xx}}_{\text{thrust}}\ \underbrace{\text{xx xx xx xx}}_{\text{ticks}}$

b) 0x31i [8] $\underbrace{\text{xx}}_{\text{power enable}}\ \text{00}\ \underbrace{\text{xx}}_{\text{driver status}}\ \text{00}\ \underbrace{\text{xx}}_{\text{device mode}}\ \text{00}\ \underbrace{\text{xx xx}}_{\text{error register}}$

where the message *a* contains all the node state and is sent with high frequency (2 ms), while the message *b* contains the information about the node status with low frequency (50 ms).

For what concerns the commands, the messages are firstly sent by the Beaglebone to the ST over the CAN bus 1, then they are extrapolated and sent by the ST over the CAN bus 1 to the associated driver. This allow us the opportunity to control more motors with only one message. For example, to control the rear motors in velocity, it is possible to send over the CAN bus 1 the following message

$$\text{BB message: 0x715 [8]}\ \underbrace{aa\ bb\ cc\ dd}_{\text{left wheel}}\ \underbrace{ee\ ff\ gg\ hh}_{\text{right wheel}}$$

where 0x715 as COB–ID does not respect the CANOpen specification, but is defined by us for the *FriWalk* to maximize the communication efficiency. Whenever the BB send such message, the left node understand that it has to consider the first four bytes, while the right node takes only to last four bytes. Once the information about the speed set point is extrapolated, the ST sends, over the CAN bus 2, the correct message to its driver, i.e.

$$\text{Left ST message: 0x601 [8] 23 00 35 00 } aa\ bb\ cc\ dd$$
$$\text{Right ST message: 0x601 [8] 23 00 35 00 } ee\ ff\ gg\ hh$$

By looking at Figure 4.10 we can also see that three sensors are installed on the rear node:

- Hall: three hall sensors are mounted on the motor, positioned 120° one from each other. Six possible configurations can be obtained (001, 011, 010, 110, 100, 101) indicating that a the magnetic field belongs to a certain range, e.g. the configuration 001 means that the orientation is within 0 and 60°. The hall sensors are directly connected to the driver, providing the knowledge about the rotational orientation of the motor, and to the ST as GPIO-input to provide a mandatory information to the observer (section 10.3). Since the motor can reach a maximum speed of 4800 rpm (80 rps) and six configuration are possible for each rotation, then 480 signals every seconds are generated by the hall sensors (480Hz signal frequency);

- Encoder: the encoder is mounted on the gear shaft because of space restrictions. The channel A and B of the encoder are directly connected to the driver to increment the control performances and to the ST to better estimate the magnetic field orientation obtained from the hall sensors, passing from a range measure (via hall sensors) to a continuous estimation. The encoder has a resolution of 2048 PPR in quadrature, meaning that 8192 signals are generated for each rotation. By the way, since the encoder is mounted on the gear shaft we have a reduction of 4, causing a downscale to 2048 signals/revolution. Considering the worst case, hence the maximum rotational speed of the motor, we have that the encoder generates a signal having a frequency of 164 kHz. This frequency has to be considered since it is not allowed to miss any tick to correctly estimate the absolute position of the magnetic field;

- Current and voltage: thanks to a pair of current sensors (ACS723) and a resistive divider the current absorbed by two motor coils and the voltage drop of the three motor coils are gathered relying on three 12–bits multichannel ADC available on board of the microcontroller STM32F415. The high frequency is guaranteed exploiting the multichannel mode maximized relying on the Direct Memory Access (DMA) for automatic transfer data from ADC to memory. This informations are used by the observer, so it is required to sample them with a frequency of 10 kHz.

Front node design

The front node, whose scheme is reported in Figure 4.11, has a much simpler design with respect to the rear node, since no observer has to be implemented on it, but an absolute encoder (AEAT–6010) is exploited to measure the position of the front fork to properly control the steering angle of the robot. Since this sensor transmit its data via synchronous serial interface (SSI), to preserve the CAN input/output architecture, a dedicated embedded board has to be installed on the front node. Exploiting the same embedded board used for the rear node it can be easily implemented the same logic for the CAN bus, so that an optimizing of the traffic flow has been performed, highly increasing the performances.

4.2.4 Robot localization

A *Smart Walker* is a device mainly developed to provide cognitive assistance, hence assist the user navigation performing path–following control. To enable such a feature localizing the vehicle inside the environment is mandatory and in the *FriWalk*, to satisfy requirement R3 of Table 4.1, a modular software architecture has to be designed. This is done by the navigation module at the cognitive layer depicted in Figure 4.5. The localization algorithm aims to provide suitable estimates of the vehicle state $\chi = [x, y, \theta]^T$. To provide $\hat{\chi} = [\hat{x}, \hat{y}, \hat{\theta}]^\top$, the localization algorithm

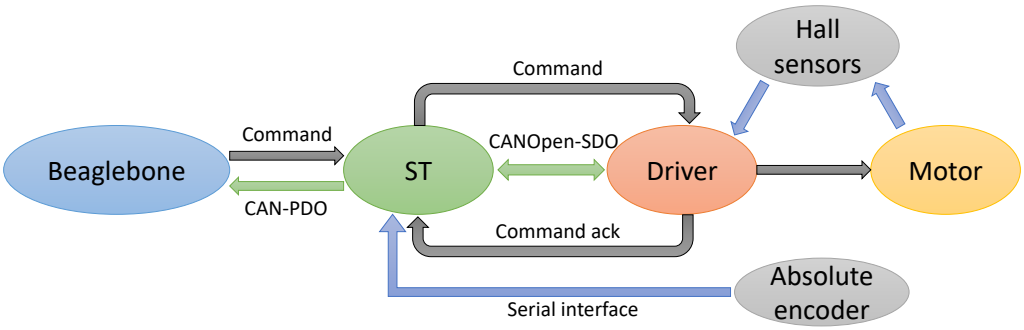

Figure 4.11: Front node design.

fuses the available information from wheel encoders and landmarks placed on the ground with the vehicle model using an extended Kalman filter.

As seen previously, the rear wheels of the vehicle are equipped with encoders, providing the necessary information from odometric reconstruction. Their resolution is 2048 ticks in quadrature, meaning that 8192 ticks correspond to a revolution of the encoder shaft. Since they are mounted on the first gear box the coupling between the wheel and the encoder is equal to 10, with the consequence that for 1 revolution of the wheel we have 10 revolutions of the encoder shaft (as reported in Section 4.2.1). This leads to

$$\Delta\phi = 0.00439 \ \frac{\text{deg}}{\text{tick}},$$

meaning that for each tick of the encoder the wheel has rotated by 0.00439 degrees, ensuring an extremely high accuracy in the odometric reconstruction. The encoders are used to measure the wheel angular rotations $\Delta\phi_R$ and $\Delta\phi_L$ of the right and the left wheel, respectively. During a sampling time interval T_s the forward displacement of the vehicle Δs_k and the yaw rotation $\Delta\theta_k$ are computed as

$$\Delta s_k = \frac{r}{2}\left(\Delta\phi_{R,k} + \Delta\phi_{L,k}\right),$$

$$\Delta\theta_k = \frac{r}{b}\left(\Delta\phi_{R,k} - \Delta\phi_{L,k}\right),$$

where b is the distance between the rear wheels and r is the rear wheel radius. The odometric localization is estimated by discretizing the unicycle kinematics (3.1) obtaining

$$\begin{cases} x_{k+1} &= x_k + \Delta s_k \cos\left(\theta_k + \dfrac{\Delta\theta_k}{2}\right), \\ y_{k+1} &= y_k + \Delta s_k \sin\left(\theta_k + \dfrac{\Delta\theta_k}{2}\right), \\ \theta_{k+1} &= \theta_k + \Delta\theta_k. \end{cases}$$

Despite the high accuracy that we obtain thanks to the high resolution of the encoder, the odometric reconstruction is affected by noise because of the need to know

the wheel radius r and the wheel wheelbase b are needed, which are available with limited accuracy. This is a well known problem that causes drift increasing with the time, i.e. dead reckoning.

Figure 4.12: QR detection by the *FriWalk*.

To compensate the drift effect, the *FriWalk* is also equipped with a camera reading landmarks placed on the floor, whose coordinates in the map are known, providing an absolute measure of the vehicle localization, as visible from Figure 4.12. The *FriWalk* can obtain a measure about its relative position with respect to the landmark once it is detected by the camera. Thanks to a coordinate transformation, it is possible to translate the relative measure into the absolute position of the *FriWalk* in the environment (the absolute position of the landmark is always known). Since the landmark position is available only when it is in the field of view of the camera, the absolute vehicle pose can be estimated intermittently, conversely to the encoders that provide an estimate at each time step.

The measures coming from the encoders and the camera are fused using a Bayesian observer that estimates $\hat{\chi} = [\hat{x}, \hat{y}, \hat{\theta}]^\top$ according to the standard deviation of the measures, hence giving more weight to the one having less uncertainty. The final estimate of $\hat{\chi}$ is then computed by fusing this first estimate with the vehicle model by means of an extended Kalman filter.

4.2.5 Path planner

In order to satisfy requirement R2 and R4 of Table 4.1, hence be a navigational and reactive aid, the *FriWalk* needs to have a path planner able to plan a safe route in a known environment, avoiding obstacles and passing through key–points. At the

same time it has to be able to re–plan, in real–time, the planned path whenever a moving obstacle detected by the robot risks to collide with it.
The path planner exploited by the robot relies on the strategy proposed by [20] and is visible in Figure 4.13. From this figure we can see how it is necessary to define the

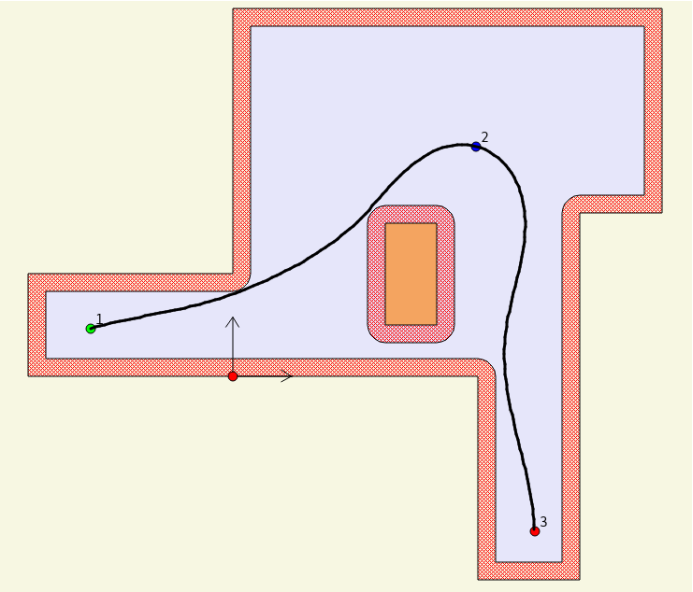

Figure 4.13: Path planner [20] installed on the *FriWalk*.

key–points so that a path computed via clothoids is found passing through them and avoiding fixed obstacles (e.g., walls, tables, pillars). The path is so generated and the guidance algorithms can work to let the *FriWalk* follow it. During the guidance a real–time planner [21] is always running to re–plan a safe route whenever a moving obstacle is on a collision course with the robot as depicted in Figure 4.14.

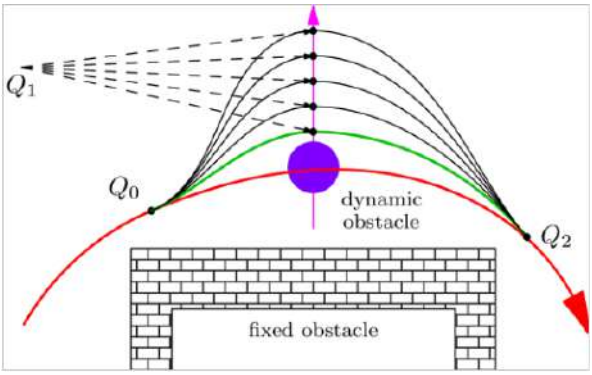

Figure 4.14: Reactive planner [21] running on the *FriWalk*.

Part II

The *FriWalk* as a navigational aid

Summary

One of the requirements reported in Table 4.1 is related to the *FriWalk* ability to assist the user navigation (R2 of Table 4.1), performing path–following control. According to the mechanical configuration adopted on the device we can have mainly three kind of strategies:

- Rear passive: exploiting the rear actuators to steer only the device, while the locomotion is completely in charge of the user;
- Rear active: exploiting the rear actuators both to steer and to propel the robot to assist the user navigation;
- Front passive: exploiting the front actuators to steer the user but not to propel the device, since no thrust can be injected with the configuration adopted on the *FriWalk*.

The reason of developing different strategies is related to understand the benefits and the problems that each solution encounters while dealing with elderly people. In fact, beyond solving the task of path–following, the maneuverability and the comfort perceived by the user while using the *FriWalk* has to be always maximized, in order to don't compromise the user's feeling.
For what concern the rear passive strategies, during the DALi project [1], a mechanical guidance system for older adults, based on a standard walker pushed by the user and controlled through suitable braking actions has been proposed. In DALi the main objective was to develop to a low cost solution that uses embedded hardware and avoids expensive force sensors. The problem of identifying a minimally intrusive braking action that keeps the user close to a planned route has been first formulated in [35]. Successively, in [36], the same authors pushed forward the solution always relying on the robot of Figure 4.1. In particular, in this new solution, rather than forcing the user to move on a predefined trajectory, the purpose of the developed guidance system is to gently "suggest" to the user the optimal direction of motion with a minimal impact on her comfort. This is achieved by defining a safety tunnel around the desired path and imposing corrective actions only when the walker approaches or crosses the tunnel boundaries. Furthermore, in order to achieve a higher level of comfort for the user, the authors proposed a solution of an optimal control

where the objective function is the braking time. This solution is really promising but has the main limitation that user's force has to be estimated with accuracy and the controller has to apply a torque to the brakes.

Since the DAli prototype of Figure 4.1 hosts a pair of electromechanical brakes controlled in current, in order to be sure to apply the desired torque, it is necessary to know the inner model of the actuator. Moreover, a model of the friction between the wheel and the surface has to be formulated. For this reason, to reduce the hardware cost and the mechanical work on the platform, we searched for a solution that does not need at all the measures on the applied torque. Hence, we pushed the idea of passive guidance even further. A useful inspiration come form the work of Ballucchi et al. [15, 114], where the authors propose an all–or–nothing (bang-bang) control action, which guarantees asymptotic tracking of the path. This approach cannot be directly used in a service robot like the *FriWalk*, since it generates a "chattering" behaviour which is annoying and difficult to interpret for the user. To solve such a limitation in [10, 11] we proposed a solution to this problem by relaxing the path following requirements. However, the practical application of the proposed method is impaired by the presence of an unavoidable actuation delay, which stems from the limited dynamic of the electromechanical actuation presented on the robot. In preparation of a large experimental round with senior adults, we have collected quantitative and qualitative data on a number of PhD students and of staff members and made preliminary tests with a small group of elderly users. In the tests with the seniors, a tablet acting as visual aid is integrated on the robot to better simulate the real working conditions. After a relatively short learning time, all the subjects were able to successfully execute their navigation task despite the simplicity of the actuation here proposed. In [5] we designed a solution that solved most of the problem of [10, 11], hence:

1. We implemented a method to compensate the actuation delay due to the nature of the electromechanical brakes of the robot;

2. We implemented a simple tuning parameter based on the attitude error e_θ that enables the execution of the controller according to a threshold.

Despite the inherent safety, the small set of manoeuvrers produced enables a relatively accurate tracking of the path, although with a questionable user comfort [5].

An evident advantage of the passive solutions is that brakes are often mounted on a walker for safety reasons and the dual use of an actuator is always desirable to reduce costs and simplify the system design. Even if these solutions are very robust and efficient to make emergency manoeuvres, they inevitably generate high jerk (in case of frequent corrections), which could adversely affect the user's comfort. Another possibility is given by modulated actions which are smoother, but they require a complex sensing to estimate the torques applied by the user to the cart [106]. In a few words, we could say that steering by brakes is a viable solution when the user

is cooperative and the control actions are not so frequent to be "disturbing". When the user is less autonomous, the guidance mechanism needs to be in control of the motion almost all the time. In this case, a guidance solution using rear actuators is promising but still present some limitations from the user's comfort due to the jerk introduced by the actuators intervention. The solution for the *FriWalk* based on active guidance, hence exploiting only the rear actuators (front caster wheels), seeks a difficult balance between three contrasting goals:

1. Preserving the advantages of passive guidance (safety and intuitive behaviour);
2. Avoiding force sensors and expensive actuators;
3. Delivering high levels of comfort.

Another available possibility relies on the use of a front steering vehicle that arguably improves the system quality and the user's comfort at the price of a small increase in the mechanical complexity. This approach presents mainly three advantages:

- The walker remains passive, hence, as in the case of a braking guidance, no accidental motion of the vehicle can be generated since it is completely propelled by the user;
- A front steering actuation increases the localization accuracy since rear wheel slipping is clearly more probable when the velocities of the wheels are controlled by actuators like brakes or motors;
- This positive "feeling" can be further magnified if the path planner generates trajectories with a continuous curvature, in order to optimize the user's comfort while respecting the kinematic and dynamic constraints of the vehicle [19].

Chapter 5

Passive Guidance Solutions

All the passive guidance strategies developed on the *FriWalk* have been presented in [8]. In such work we proposed an hybrid approach whose application allows a controlled blend of haptic (i.e. two haptic bracelets, equipped with vibrating motors) and mechanical actions (i.e. bang–bang braking action), thus reducing the control authority and guaranteeing the performance. The controller is based on the definition of safety regions around the desired path, where corrective actions simply do not occur. The proposed hybrid controller has been successfully applied to the *FriWalk* and its effectiveness has been proved through extensive experiments with older adults. We compared the haptic and mechanical solutions in isolation with the proposed approach to highlight the benefits, in terms of user comfort, of the orchestrated fusion of the two approaches. To summarize, in [8] we compared three guidances strategies:

- **Bang–bang**: guidance that blocks right or left wheels to obligate the user to turn and follow the desired path. The solution is simple (on/off control action) and inexpensive (no need of additional hardware for braking modulation);
- **Haptic**: guidance which provides signals on the direction through vibrating wrists;
- **Combined**: solution that combines the previous two style of guidances.

The common strategy at the basis of each guidance is that the supervisor understands and decides which action the *FriWalk* has to perform according to the attitude error e_θ . Whenever the user is aligned with the path $e_\theta = 0$, then the *FriWalk* is passive, which means that the user is completely in charge of the robot motion. As far as the user departs from the planned route $e_\theta \neq 0$, then the robot intervenes in order to properly steer the user toward the planned path. Furthermore, the navigation system can be supported by a graphical user interface (GUI) represented by a green arrow on a white blanked background which provides indications on the direction to follow. However, since the variability of elder population in capabilities

and deficits (e.g., visual impairments), and the impossibility for the user to be permanently focused on the graphical interface in a real environments, all the kinds of guidance were created with the aim of working even without any visual cues.

5.1 Problem formulation and solution overview

The *FriWalk* prototype used for [8] is reported in Fig. 1.3 while in Figure 5.1 the robot is actually executing a guidance task with one of the seniors participating in the experiments. For the passive guidance solutions the model adopted for the *FriWalk* is the unicycle–like robot kinematic model (3.1). Since the robot is propelled by the user, the forward velocity v is completely determined by the assisted person, hence it is not a control variable. The angular velocity ω is, instead, the control input that should be generated by the actuators. For the work presented in [8], the *FriWalk* is equipped with two front caster wheel, while the motors mounted on the rear wheels are exploited as brakes capable of blocking the wheels only, i.e. no modulation of the braking action is possible because of hardware limitations. This way, the vehicle rotates around the blocked wheel with angular velocity $|\omega| = v/R$, while it moves forward if the wheels are free to rotate, i.e. $\omega = 0$. This means that the control input ω generated by the braking system can assume only three values

$$\omega \in \left\{-\frac{v}{R}, 0, \frac{v}{R}\right\}. \tag{5.1}$$

Notice that when $\omega = -\frac{v}{R}$ and $\omega = +\frac{v}{R}$ the vehicle turns right and left, respectively, with fixed curvature radius R, while when $\omega = 0$ the vehicle can move freely. Notice that the set of control actions (5.1) describe the vehicle behaviour generated by the braking system. When the brakes are not active the vehicle is totally passive, as a standard rollator. Nevertheless, using the vibrating bracelets, it is possible to adjust the heading by providing haptic stimuli. To limit the use of the tactile channel and the recognition time, the haptic system is used to provide the user with three simple indications, resembling (5.1):

1. *Turn left*: the user is suggested to turn left, i.e. to apply an angular velocity $\omega > 0$, by activating the left bracelet;

2. *Turn right*: the user is suggested to turn right, i.e. to apply an angular velocity $\omega < 0$, by activating the right bracelet;

3. *Go straight*: no haptic stimuli are provided to the user, who is then is suggested to go straight, i.e. to apply and angular velocity $\omega \approx 0$.

As seen in chapter 3, to properly represent the path following problem it is adopted a moving Frenet frame collocated along the planned path. The work [8] solves a path–following problem, i.e. ensures that the vehicle approaches and follows a given path by considering the actuator limitations (recall that the brakes are capable of

Figure 5.1: Picture of the *FriWalk* prototype with one of the older adults participating in the experimental trials [8].

only blocking the wheels). Using the coordinates introduced in (3.20), the problem can be formalised as follows: find the control law $\omega(\chi)$ satisfying the actuation constraints (5.1) ensuring (3.34), hence

$$\lim_{t\to+\infty} |l_x(t)| \leq l_\infty, \lim_{t\to+\infty} |l_y(t)| \leq l_\infty, \lim_{t\to+\infty} |\tilde{\theta}(t)| \leq \tilde{\theta}_\infty.$$

Notice that this path following problem is *passive* and constrained since we are using passive actuators (i.e. brakes) without modulations (i.e. either blocking or non blocking the wheels) and the forward velocity v is determined by the assisted person. It is worthwhile to note that the haptic bracelets can not be considered as actuators in the control design, since, even when they vibrate, the behaviour of the system is still entirely determined by the user behaviour.

5.2 The Bang–Bang steering controller

Due to the braking actuation constraints (5.1), the controlled trajectories are Dubins's like paths. The control of a unicycle following a Dubins' trajectory of minimal length towards a generic path with known maximum curvature is solved in [16] using a hybrid automaton by moving the vehicle along the direction that is locally perpendicular to the path. In [16] the input angular velocity $\omega \in \left\{-\frac{v}{R}, 0, \frac{v}{R}\right\}$ that solves the classical path following problem (3.13) is selected on the basis of the actual path coordinates l, $\tilde{\theta}$. In particular, the state space $(l, \tilde{\theta})$ is partitioned into a set of non-overlapping regions, each one corresponding to a value of the input ω in the

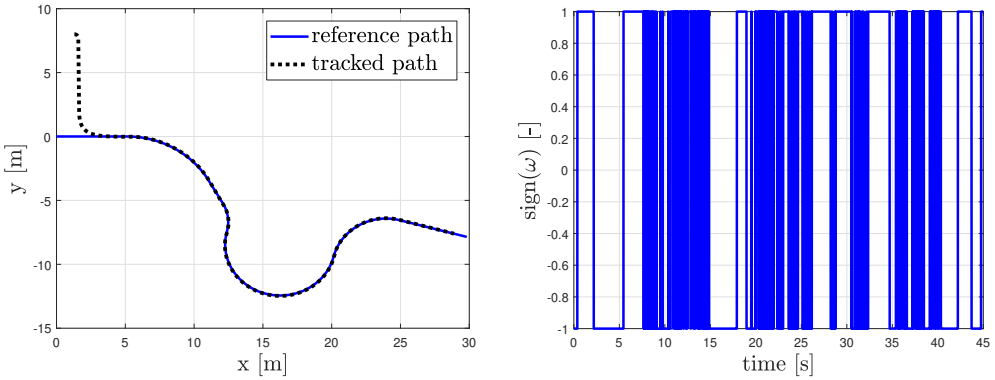

(a) *Path following accuracy.* (b) *Chattering for control action.*

Figure 5.2: Path following performance solving the problem (5.2).

set $\left\{-\frac{v}{R}, 0, \frac{v}{R}\right\}$. This solution has been generalised in our work [10] introducing the approaching angle $\delta(l)$ (on the basis of the assumptions reported in section 3.2.3), which defines the way in which the path is approached, and solves the path-following problem with zero steady state error, i.e.:

$$\begin{aligned} \lim_{t \to +\infty} |l(t)| &= 0, \\ \lim_{t \to +\infty} |\tilde{\theta}(t)| &= 0. \end{aligned} \tag{5.2}$$

To limit the number of braking actions, the steering angle δ should have a varying rate smaller than the maximum angular velocity of the vehicle [10], i.e.,

$$|\dot{\delta}(l)| \leq \frac{v}{R}.$$

Although our solution proposed in [10] is of relevance from a theoretical point of view, it is unavoidably based on the chattering of the braking actions (phenomenon depicted in Figure 5.2–(b)) , i.e., the controller requires infinite switches between the control action $\{-\frac{v}{R}, 0, +\frac{v}{R}\}$ to accurately follow the planned path as visible in Figure 5.2–(a). The chattering phenomenon is characterized by a continuous switch between -1 to 1 of the sign of the angular velocity (Figure 5.2–(b)), meaning that ω switches from $-\frac{v}{R}$ to $\frac{v}{R}$ in a time interval equal to the simulation time step. It is obvious to understand that this chattering actuation cannot be obtained with a real actuation system and highly penalizes the user's comfort. Indeed, besides the practical limits of generating a number of infinite switches in finite time subject to the brakes limited dynamics, the human perceives a system that persistently brakes and release the back wheels, thus generating a sort of mechanical Pulse Width Modulation, which generates discomfort.

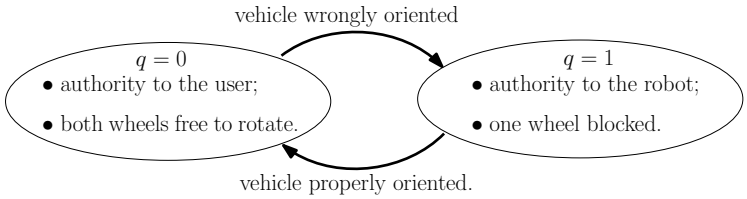

Figure 5.3: Schematic representation of the hybrid system [8].

5.2.1 The hybrid controller: a solution for the chattering

To get rid of the chattering phenomenon, a hysteresis-based behaviour, which limits the number of braking system interventions along the trajectory, is defined to the point. This idea is quite close to the user loose path following natural behaviour: when someone is asked to follow a path in an environment, the path is usually followed "approximately". In other words, we do not want the user to accurately follow the approaching path, but just to move in the correct direction, i.e. towards the desired direction. This means that the path–following problem (5.2) can be relaxed and, exploiting the dynamic Frenet frame (3.19), can be rewritten as in (3.34), i.e.:

$$\lim_{t\to+\infty} |l_x(t)| \leq l_\infty, \lim_{t\to+\infty} |l_y(t)| \leq l_\infty, \lim_{t\to+\infty} |\tilde{\theta}(t)| \leq \tilde{\theta}_\infty.$$

This way, the controller we are aiming at provides "most of the time" the *Go Straight* manoeuvre, in which the user is in complete control of the motion. To pursue this idea, a hybrid controller switching among three different modalities, depending on four hysteresis thresholds have been defined and presented in [11]. The solution was very complex from a human–robot interaction point of view, since it was missing a parameter linked to the user's comfort. In [8] a solution based on the attitude error e_θ has been formalized, enabling the possibility to tune the user's comfort with only one variable. The hysteresis mechanism of [8] is depicted in Figure 5.3 and avoids the chattering phenomenon on the basis of four ingredients:

- Orientation error $e_\theta = \tilde{\theta} - \delta(l_y)$, o.e. the angular error of the vehicle. This variable is used as metric to define the distance from the path;
- $g(e_\theta, \epsilon_q) : \mathbb{R} \times \mathbb{R}_{\geq 0} \mapsto \{-1, 0, 1\}$ defined as the function

$$g(e_\theta, \epsilon_q) := \begin{cases} \text{sign}(e_\theta), & \text{if } |e_\theta| \geq \epsilon_q, \\ 0, & \text{if } |e_\theta| < \epsilon_q. \end{cases} \tag{5.3}$$

  In practice, function $g(e_\theta, \epsilon_q)$ is the sign function of e_θ with a dead zone defined by $\epsilon_q > 0$ (see Figure 5.4);
- $q \in \{0, 1\}$ as the hybrid controller logic variable. Condition $q = 0$ who be used to state that $|e_\theta|$ is negligible and the controller does not need to kick in to

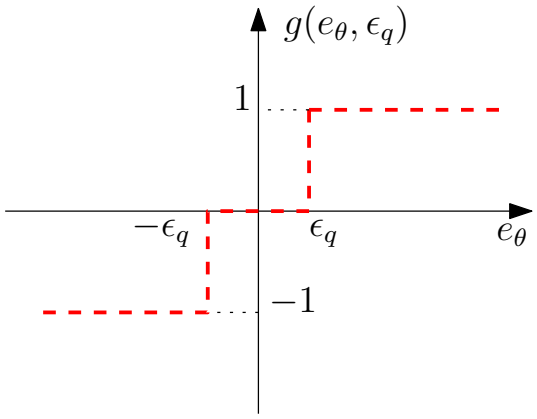

Figure 5.4: Function $g(e_\theta, \epsilon_q)$ in (5.3) [8].

ensure that conditions (3.34) hold. On the oher hand, condition $q = 1$ will indicate that the attitude error $|e_\theta|$ has to be reduced buy the controller to properly follow the path. This automaton is depicted in Figure 5.3;

- $\Theta \triangleq [\chi^T, q, \omega, s]^T$ the extended state of the hybrid system, introduced for convenience of notation.

The hybrid controller is then defined as follows:

$$\begin{cases} \dot{\chi} &= f(\Theta, v), \\ \dot{q} &= 0, \\ \dot{\omega} &= 0, \\ \dot{s} &= v\cos(\tilde{\theta}) + kl_x, \end{cases} \quad \Theta \in \mathcal{C},$$
$$\begin{cases} \chi^+ &= \chi, \\ q^+ &= 1 - q, \\ \omega^+ &= -g(e_\theta, \epsilon_q)\dfrac{v}{R}, \\ s^+ &= s, \end{cases} \quad \Theta \in \mathcal{D}, \tag{5.4}$$

where function $f(\cdot)$ describes the nonlinear unicycle kinematic (3.1), $k > 0$ is a tunable gain, the flow set is $\mathcal{C} = \mathcal{C}_0 \cup \mathcal{C}_1$ and the jump set $\mathcal{D} = \mathcal{D}_0 \cup \mathcal{D}_1$, where

$$\begin{aligned} \mathcal{C}_0 &= \left\{\Theta \in \mathbb{R}^6, |e_\theta| \leq \theta_{q_2} \ \wedge \ q = 0\right\}, \\ \mathcal{C}_1 &= \left\{\Theta \in \mathbb{R}^6, |e_\theta| \geq \theta_{q_1} \ \wedge \ q = 1\right\}, \\ \mathcal{D}_0 &= \left\{\Theta \in \mathbb{R}^6, |e_\theta| \geq \theta_{q_2} \ \wedge \ q = 0\right\}, \\ \mathcal{D}_1 &= \left\{\Theta \in \mathbb{R}^6, |e_\theta| \leq \theta_{q_1} \ \wedge \ q = 1\right\}, \end{aligned} \tag{5.5}$$

where $\theta_{q_2} > \theta_{q_1}$ are two positive constants defining the hysteresis mechanism. The constant ϵ_q used in function $g(e_\theta, \epsilon_q)$ satisfies $\epsilon_q \in (\theta_{q_1}, \theta_{q_2})$. With this choice of

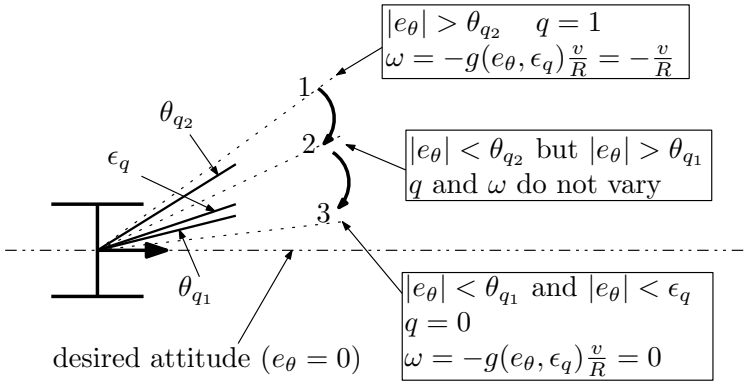

Figure 5.5: Angular hysteresis mechanism [8].

θ_{q_1}, θ_{q_2} and ϵ_q, the hysteresis is well defined and the control system never brakes when the orientation error is smaller than the lower threshold θ_{q_1}. A graphical representation is depicted in Figure 5.5: the vehicle starts oriented as the dotted line, labelled with a 1. Since $|e_\theta| > \theta_{q_2}$ the control system is activated ($q = 1$) and the vehicle turns right to reduce the orientation error ($\omega = -\frac{v}{R}$). $|e_\theta|$ is reduced below the threshold θ_{q_2} (dotted line labelled with a 2) until it becomes smaller than the lower threshold θ_{q_1} (dotted line labelled 3). Only at this point, the discrete dynamics of the hybrid controller in (5.4) is activated, turning $q = 0$ and stopping the braking action on the vehicle ($\omega = -g(e_\theta, \epsilon_m)\frac{v}{R} = 0$ since $|e_\theta| \leq \theta_{q_1} < \epsilon_q$). The path–following problem is the solved for any $\epsilon_q \in (\theta_{q_1}, \theta_{q_2})$, that can then be chosen arbitrarily in the set.

5.3 The Haptic strategy

To keep safety features on this inexpensive system and simultaneously increase the user experience, we tested vibrotactile interfaces, since tactile devices are generally portable, not encumbering and have a wider range of action [73].
Tactile vibratory sensitivity is influenced by the spatial location on the body, the distance between the stimulators, the frequency of stimulation and the age of the user. Studies have demonstrated that vibration is better sensed on hairy skin due to its thickness and nerve depth, and that vibrotactile stimuli are best detected in bony areas [41]. In particular, wrists and spine are generally preferred for detecting vibrations, with arms and ankles next in line [62]. Due to the aforementioned considerations and since our aim is to design an intuitive and non-obtrusive device which could be easily worn, we concentrated on the development of vibrotactile bracelets. Results presented by Scheggi et al. in [108], we decided to use the bilateral configuration, that required two bracelets, one for each arm.

Regarding the *Haptic* strategy adopted for the *FriWalk*, since it is designed to

work with elderly with possible disabilities (like cognitive), we decided to rely on the simplest stimulation in order to don't confuse the user with different patterns that change the frequency and the amplitude according to environmental situation. Moreover we tried to design a solution that vibrates the bracelets as less as possible, in order to don't saturate the user with the stimulus. It is known that, under a prolonged vibrating action, the user tends to become less and less sensitive to the stimulus, a phenomenon known with the term inurement.
So, for this strategy, the basic idea is the same as for the *BangBang* presented in section 5.2, but this time the *FriWalk* intervenes vibrating the left or the right bracelets whenever it is necessary to advertise the user that he/she has to steer leftward or rightward to maintain the planned path. Contrary to the *BangBang*, this strategy maximise the comfort for the user, but, at the same time, can be also potentially dangerous for her/his safety. In fact, since no actuation is directly performed on the robot, the user can very simply ignore the stimulus coming from the bracelets and override the robot suggestions. So, if the user is distracted, he could collide against obstacles.
This strategy is very simple and can be definitely improved, understanding which pattern fits better with elderly, and can also be very personal according to the user disabilities.

5.4 Combining Haptic with Bang–Bang

In order to achieve a good balance between comfort and safety, but maintaining a low device cost, the *Combined* strategy, which fuses both the techniques described previously, can be adopted.
The haptic guidance is used to suggest the user to steer the vehicle towards the path. In principle, if the user is cooperative, i.e. he/she properly steers the vehicle when the haptic system is active, the path following requirements (3.34) may be satisfied without using the brakes, then improving the user's comfort.
To design the activation policy of the bracelets, recall that we have shown that controller (5.4) solves the path following problem by maintaining the angular error $|e_\theta|$ small via a hysteresis mechanism. The same logic is also used to activate the haptic system. To improve the user comfort, we require that:

- If the user is leaving the path, the bracelets vibrate before the vehicle brakes. This way, the user is allowed to follow the path without braking interventions;
- The bracelets are deactivated at a smaller angular error e_θ, i.e. the lower threshold of the bracelets hysteresis is smaller than the lower threshold of the brakes hysteresis. This way, the undesired situation where the haptic system does not provide suggestions to the user and the vehicle brakes is avoided.

Therefore, if we denote with $\theta^h_{q_2} > \theta^h_{q_1}$ the hysteresis thresholds of the haptic system (the superscript h stands for "haptic"), we impose $\theta_{q_2} > \theta^h_{q_2}$, $\theta_{q_1} \geq \theta^h_{q_1}$ and $\theta^h_{q_2} > \theta_{q_1}$.

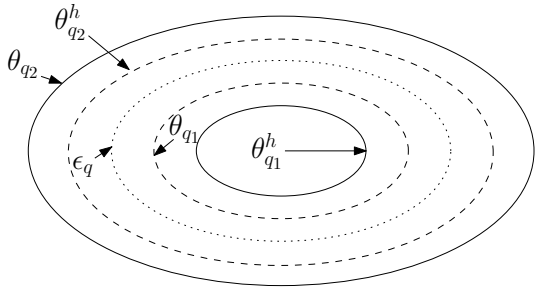

Figure 5.6: Graphical representation of the hysteresis thresholds [8].

Moreover, we pick $\epsilon_q \in (\theta_{q_1}, \theta^h_{q_2})$, as depicted in Figure 5.6.
Then, let $\psi \in \{-1, 0, 1\}$ be the working mode of the bracelets. We have $\psi = 1$ when the left bracelet vibrates (i.e. the user is suggested to turn left), $\psi = -1$ when the right bracelet vibrates (i.e. the user is suggested to turn right) and $\psi = 0$ when the haptic system is not active (i.e. no vibrations, than no indications are provided to the user). To describe the haptic system with an hybrid dynamic similar to (5.4), we introduce a logic state p having discrete dynamic only. Its meaning is similar to the meaning of q in (5.4). When $p = 1$, the bracelets vibrate since the attitude error $|e_\theta|$ is large, while when $p = 0$ the bracelets do not vibrate since the attitude error $|e_\theta|$ is small. The hybrid dynamic system managing the haptic bracelets is designed as follows:

$$\begin{cases} \dot{\psi} &= 0, \\ \dot{p} &= 0, \end{cases} \Xi \in \mathcal{C}^h, \quad \begin{cases} \psi^+ = -g(e_\theta, \epsilon_q), \\ p^+ = 1 - p, \end{cases} \quad \Xi \in \mathcal{D}^h, \tag{5.6}$$

where $\Xi = [\psi, e_\theta, p]^T$, the flow set is $\mathcal{C}^h = \mathcal{C}^h_0 \cup \mathcal{C}^h_1$ and the jump set $\mathcal{D}^h = \mathcal{D}^h_0 \cup \mathcal{D}^h_1$, where

$$\begin{aligned} \mathcal{C}^h_0 &= \left\{ \Xi \in \mathbb{R}^3, |e_\theta| \leq \theta^h_{q_2} \ \wedge \ p = 0 \right\}, \\ \mathcal{C}^h_1 &= \left\{ \Xi \in \mathbb{R}^3, |e_\theta| \geq \theta^h_{q_1} \ \wedge \ p = 1 \right\}, \\ \mathcal{D}^h_0 &= \left\{ \Xi \in \mathbb{R}^3, |e_\theta| \geq \theta^h_{q_2} \ \wedge \ p = 0 \right\}, \\ \mathcal{D}^h_1 &= \left\{ \Xi \in \mathbb{R}^3, |e_\theta| \leq \theta^h_{q_1} \ \wedge \ p = 1 \right\}. \end{aligned} \tag{5.7}$$

Notice that the correctness of the haptic controller (5.6) is proved once $\epsilon_q \in (\theta_{q_1}, \theta^h_{q_2})$ as for the mechanical system in Section 5.2, hence it is chosen for simplicity as $\epsilon_q = (\theta^h_{q_2} + \theta_{q_1})/2$.

5.5 Experimental results

The three types of guidance were used during the human-robot interaction task which consisted in completing a path with the *FriWalk* within the rectangular open

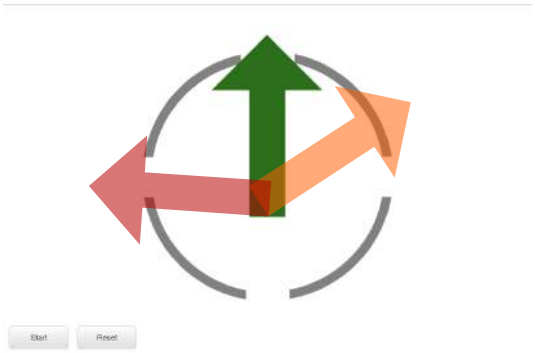

Figure 5.7: An example of the GUI used for the test. The color of the arrow goes from green to red proportionally with the attitude error e_θ [8].

space. An experimental design with 3 within-subjects conditions (Type of guidance: *BangBang* vs. *Haptic* vs. *Combined*) × 2 between- subject conditions (GUI vs. No GUI) was developed (an example of the GUI is depicted in Figure 5.7). All participants completed the path task three times, one for each different kind of guide. The order of the guides was randomized between participants, apart from the *Combined* guidance which was always performed as last. Since the *Combined* guidance was in fact the combination of the *BangBang* and the *Haptic*, we wanted to avoid participants had the perception that *BangBang* or *Haptic* guides were "incomplete". In No GUI condition participants could rely uniquely on the signals provided by the *FriWalk* (i.e., the intervention on wheels and the vibration of the wrists), whereas in GUI condition they could be supported by the visual indications of the graphical user interface to better understand the route to follow. Except for participants with serious visual impairment, who were all assigned to the condition without graphical interface to avoid they felt frustrated for the impossibility to use the visual feedback, all the other participants were randomly assigned to the GUI or No GUI condition, counterbalancing the gender.
39 participants came to the BIC of Pergine Valsugana to participate to the study. Participants were contacted through the Municipality of Pergine Valsugana and the senior centre "Sempreverde" of Mattarello (both in the Trento province) and invited to participate. They were informed that data collection and that all information provided are covered by the ethical rules conceived for the ACANTO project [2] and that they could quit the experiment at anytime. Once consent was obtained they were invited to perform the tasks with the *FriWalk*. However, as some of them decided to at the last moment to not participate or they interrupted the experiment after they completed just one path task with the *FriWalk* (for the present study we considered only those participants who completed the path task in two different guidance conditions), the final sample consisted of 30 participants (11 males and 18 females), ranging from 66 to 96 years old (Mage = 84.14, SD = 7.64). 28 partic-

ipants reported to daily use a support device for walking, and specifically 23 used a walker (76.7%), 3 participants used a walking or tripod stick (10.0%) and other 2 declared to move with a wheelchair (6.7%). 8 participants (26.6% of the sample) had a serious visual impairment and they were assigned to the No GUI condition.
Before the path task started, every participant received the description of the *FriWalk*'s guidance style and, accompanied by an experimenter, carried out a first trial to take confidence with the machine. After that, participants were randomly assigned to one of the experimental paths, which were different from the first trial path. They were invited to complete autonomously the path with the *FriWalk*, but it was specified that they could stop and interrupt the task and/or ask the support of the experimenter at any moment.
As the guidance function of the robotic walker demonstrates its real usefulness when the user must move in unfamiliar spaces, and he/she does not know (or recall) the way to reach a specific goal, we did not provide to the participants any information about the experimental path they had to complete. This forced them to rely completely on the robotic walker cues, to the signals given by the different kinds of guidance and on the information of its graphical interface (only in GUI condition).

5.5.1 Quantitative analysis

The controller hysteresis threshold are set to $\theta_{q_2} = 40°$, $\theta^h_{q_2} = 30°$ and $\theta_{q_1} = \theta^h_{q_1} = 20°$. Four sample trajectories along a randomly selected path are reported in Figure 5.8, Figure 5.9 and Figure 5.10 for the *BangBang*, *Haptic* and *Combined* strategies respectively. The localisation is provided with an EKF [93] fusing the encoder data and the QR codes (see section 4.2.4), positioned on the floor using the deployment [90, 78] and read by the available front camera pointing downwards.

Bang–bang braking system

In this experiment, we asked the user to follow a desired path (blue solid line in Figure 5.8–(a)) while the *FriWalk* is controlled by the bang-bang braking strategy reported in Section 5.2. In Figure 5.8–(a) the dash–dotted red line (Exp_1) reports an example of trajectory followed with the presence of the GUI, while the others are in No GUI condition.
It is important to recall that the user is always in control when the attitude error e_θ is below the inner threshold (see Figure 5.8–(b)), while the robot is always in control when e_θ is greater than the outer threshold. Within the two values, the control authority depends on the history of e_θ due to the hysteresis nature of the controller. Moreover, from Figure 5.8–(b) it is worthwhile to note that as soon as $e_\theta > \theta_{q_2}$, the controller kicks in and e_θ does not increase anymore, thus showing that the controller is able to steer the user towards the desired path.

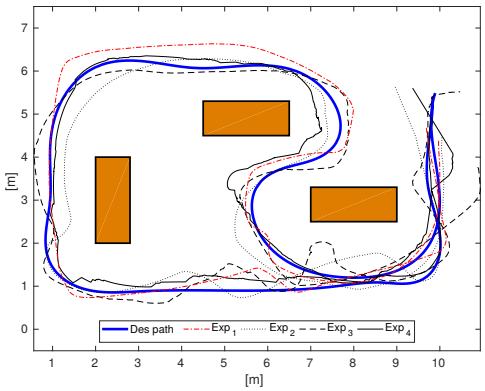

(a) *Experimental trajectories for four participants along a randomly selected path (solid thick line) followed with the bang-bang strategy. The rectangles represent the obstacles (i.e. tables) in the environment.*

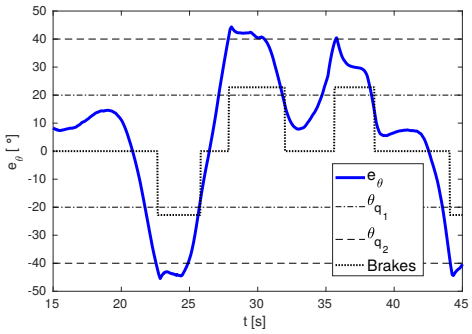

(b) *30 seconds of the time evolution of the error e_θ for the* Exp_1 *in Figure 5.8–(a). The evolution of the discrete hybrid variable brakes (scaled for visibility) and the controller thresholds θ_{q_1} and θ_{q_2} are also reported.*

Figure 5.8: Path following performance relying on the *BangBang* strategy [8].

Haptic guidance

When the haptic guidance described in Section 5.4 is used, the results look like Figure 5.9–(a). In Figure 5.9–(a) the dash–dotted red line (Exp_1) reports an example

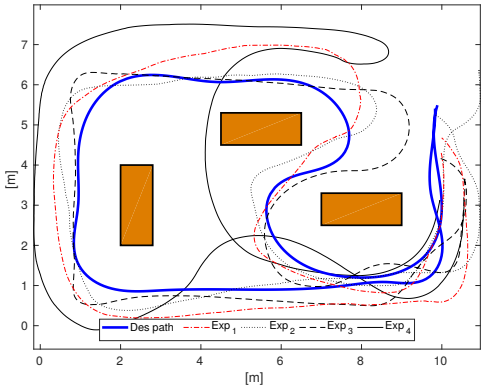

(a) *Experimental trajectories for four participants along a randomly selected path (solid thick line) followed with the haptic strategy. The rectangles represent the obstacles (i.e. tables) in the environment.*

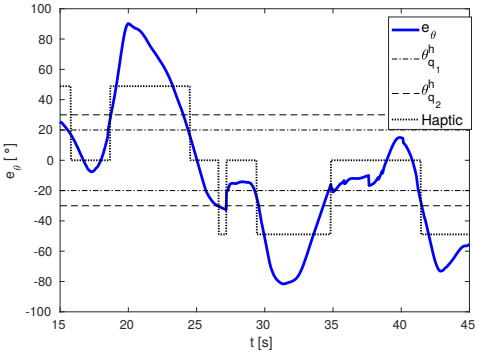

(b) *30 seconds of the time evolution of the error e_θ for the* Exp_1 *in Figure 5.9–(a). The evolution of the discrete hybrid variable haptic (scaled for visibility) and the controller thresholds $\theta^h_{q_1}$ and $\theta^h_{q_2}$ are also reported.*

Figure 5.9: Path following performance relying on the *Haptic* strategy [8].

of trajectory followed with the presence of the GUI, while the others are in No GUI condition.

For this approach, the user is always in control, independently from the value of e_θ, while steering suggestions are given with the haptic interfaces. The user can follow the suggestion of the bracelets and then be steered to the desired path, or ignore the stimuli. It could happen, also, that the user interprets wrongly the information coming from the bracelets, as in Exp_4 of Figure 5.9–(a), where it is possible to appreciate how the user steers right, since he receive a stimulus from the right bracelets, but not enough to follow the desired path. As consequence the user follows a wrong path, leaving the middle table on his right instead of his left. Similarly, in the bottom part of the plot Figure 5.9–(a), another wrong path is followed in the Exp_4. This misbehaving users are not so uncommon in the target class of this work. The time evolution of e_θ for the haptic guidance is reported in Figure 5.9–(b). From this graph, once compared with Figure 5.8–(b), the higher deviation can be easily appreciated, even for Exp_1. Furthermore, whenever e_θ exits from the outer threshold, it takes some time before the user follows the control signal, with the unavoidable consequence that the error increases largely before decreasing.

Combined controller

The trajectories obtained with the integrated controller detailed in Section 5.4 are reported in Figure 5.10–(a).

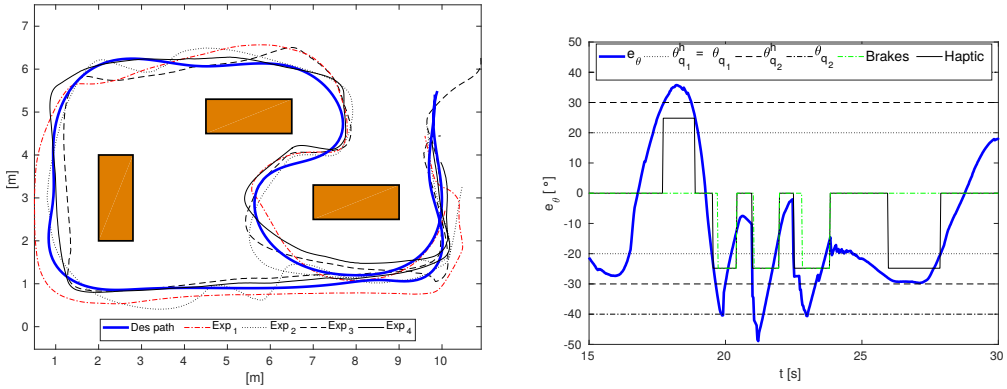

(a) *Experimental trajectories for four participants along a randomly selected path (solid thick line). The rectangles represent the obstacles (i.e. tables) in the environment.*

(b) *15 seconds of the time evolution of the error e_θ for the* Exp_1 *in Figure 5.10–(a). The evolution of the discrete hybrid variable haptic and brakes (scaled for visibility) are also reported.*

Figure 5.10: Path following performance relying on the *Combined* strategy [8].

In Figure 5.9–(a) the dash–dotted red line (Exp_1) reports an example of trajectory followed with the presence of the GUI, while the others are in No GUI condition. In this plot it is possible to appreciate how the two strategies can be either both activated or only the haptic strategy kicks in. In particular, at the beginning of the plot in Figure 5.10–(a), the nature of the integrated strategy is easily recognisable:

Table 5.1: Summary of the controllers performance of the three different passive strategies in GUI (G) and No GUI (N) conditions.

Feature	**Bang–Bang**		**Haptic**		**Integrated**			
	N	G	N	G	N		G	
Average $\|l_y\|$ [m]	0.24	0.15	0.59	0.57	0.25		0.24	
std $\|l_y\|$ [m]	0.10	0.10	0.27	0.25	0.06		0.05	
					Brakes		Haptic	
					N	G	N	G
n° of interventions	20.3	15.5	7	6	10.6	9	8.3	8
std n° of interventions	12.5	8.3	2	2	3.24	3.12	2.8	2.5
time perc. active controller	21.2	10.4	45.9	43.5	12.5	11.7	24.7	22.4
std perc. active controller	10.4	7.8	18.6	15.7	10.5	8.8	19.4	7.6

as soon as $e_\theta > \theta^h_{q_2}$, the bracelets actuation is activated. At this point, if the user is cooperative and follows the suggestion, the error e_θ remains below θ_{q_2}, with the consequence that the braking system is never actuated. Whereas if $e_\theta > \theta_{q_2}$, the brakes intervene to steer the user towards the correct orientation, with the positive effect that the error never reaches the high values observed in Figure 5.10–(b).

5.5.2 Performance analysis

The overall controller performance are reported in Table 5.1, where we report the average path-following error $|l_y|$ of the user for the different strategies and its standard deviation, the number of interventions of the controller and the percentage of time that the controller is active during the guidance.
For what concerns the path-following error $|l_y|$, the haptic guidance poorly perform due to the high level of freedom given to the user. This outcome is totally expected since the bracelets provides only a feedback that doesn't actively intervene on the *FriWalk*, so that both the locomotion and the steer are in charge of the user. This lead us to conclude that a rough on/off haptic feedback for elderly with disabilities in not sufficient to complete the path–following task.
Using the braking system, either in isolation or combined, the overall mean error $|l_y|$ is reduced significantly, since the *FriWalk* is allowed to actively intervene when the path following error overcomes a certain threshold, steering the user towards the desired path.
On the other hand, regarding the number of interventions in Table 5.1 (also reported in Figure 5.11-(a)) we can see how the number of times that the controller is activate is maximum in the *Bang-Bang* strategy, meaning that the guidance solution is not very clear for the user (due to the abrupt nature of the solution). The difficulties in understanding the control suggestions is visible also from the standard deviation, leading us to conclude that for some user the guidance solution is clear and intuitive,

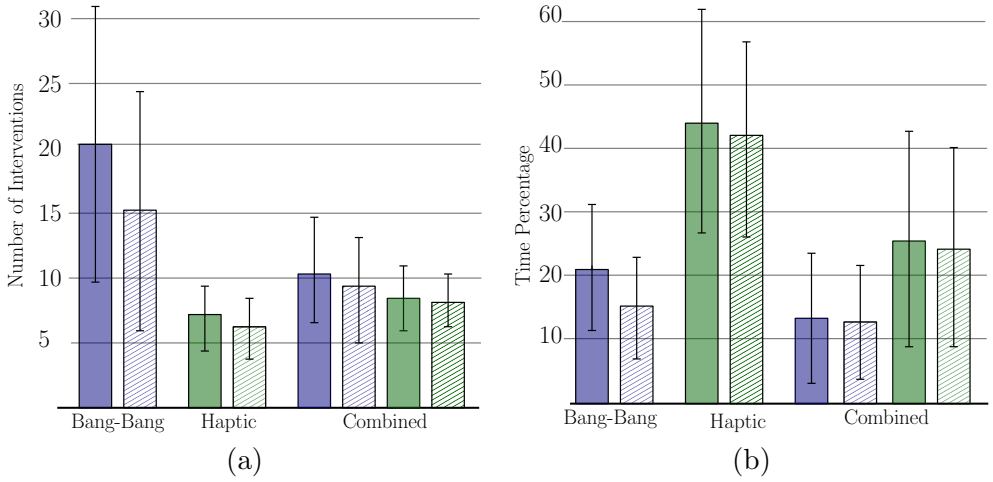

Figure 5.11: Comparison between strategy performance: (a) number of controller interventions, (b) percentage of time for which the controller is active [8]. The solid patter represents the experiments performed with the GUI, while the rising tiling patter is for the No GUI.

while for others is very difficult to handle. Nevertheless, from Figure 5.11-(b), we notice that, even if the number of interventions is high, the controller remains active only for 20% of the time, meaning that the corrections are frequent but very short. The haptic guidance is instead characterised by an opposite behaviour, which means that the controller acts infrequently, but the overall activation time is around 45% of the overall experiment. In other words, the user does not clearly interpret the stimulus coming from the bracelets and it takes some time to properly react. These results justify the proposed approach of fusing these two opposite behaviours in a trade-off. Indeed, combining the two solutions in a integrated controller, the number of interventions of the braking system Figure 5.11-(a) and the activation time of the bracelets Figure 5.11-(b) is halved, highly increasing the comfort perceived by the user and simultaneously achieve good performance in terms of the path following error $|l_y|$. Also for the *Haptic* and for the *Combined* strategies the standard deviation is quite large, meaning that the performance of the solutions highly depends on the user's skill in understanding the *FriWalk* suggestions. It is worthwhile to point out that user's disabilities were pretty different among the group and the amount of training was very limited for each person. This lead us to conclude that all the passive strategies performances are strictly dependent on the user's skill to correctly interpret the suggestion deriving from the *FriWalk*, even if the system can actively intervene on the braking system. So the *Bang–Bang* strategy can be exploited as a last resort in case of dangerous situation, but cannot be used to solve path–following tasks since it is abrupt, uncomfortable and quite difficult to be understood from all the possible user's.

Concerning the presence of the GUI, we found that providing visual signals to participants affected mostly participants in *BangBang* condition reducing their time in completing the task. Surprisingly, we found a significant effect of the GUI in completing correctly the path in *Combined* but not in *Haptic* condition, suggesting that a strong intervention of the walker (blocking of the wheels) is needed to properly guide elders when they have to reach a goal without knowing the correct path, while a suggestion about the direction is not sufficient. The presence of the graphical interface however affected the requests of help to experimenter since, suggesting that providing clear indications on the direction to follow lead participants to autonomously try to complete the path without the support of other people.

5.5.3 Users' evaluation

In the present study [8], we used a questionnaire to conduct a structured interview in order to collect the impressions and opinions of people who participated in the studies. After the tests with the robotic walker, participants were invited to sit next to an experimenter who conducted the structured interview reading the items of the questionnaire. The aim of the structured interview was to collect the impressions of people on the proposed control approach. To this end, we included different questions (open ended and closed ended). Participants were asked to answer using yes or no and/or a 5 point Likert scale reported in Table 5.2.

Table 5.2: Likert scale used for user's evaluation about the guidance strategy [8]

Likert Scale	grade
1	not at all
2	a little but
3	moderately
4	very much
5	extremely

The questions concerned different features of the interaction with the robotic walker (i.e., if they felt vibration during the use, if it was clear if and when *FriWalk* decided the path and if they felt pushed or blocked: in the affirmative case, they were requested to indicate how much unpleasant or annoying was that specific feeling), followed by items on the pleasantness of usage (i.e., if the experience was pleasant or frustrating and if they feel satisfied about the job they did with the walker) and the ease of learning (i.e., if it is easy to learn the interaction, if they were able to control it in short time). For the control over the robot, three items were conceived: if they were sure that the *FriWalk* would always respond to her/his commands and if they had the impression of suddenly miss the control or not. Items used for the structured interview are shown in Table 5.3.
The percentage of affirmative responses, with their relative mean **M** and standard

Table 5.3: Items of the questionnaire for the users' evaluation [8].

Characteristics of the interaction
Vibration: Have you felt vibrations?
Path: Was it evident that was the walker to decide the path to follow?
Blocked: Have you felt to be pulled, pushed, pulled, or stuck?
Pleasantness (in using the *FriWalk*) - P
P.1: The experience with the walker was pleasant.
P.2: It was frustrating to carry out the task with the walker. *
P.3: You are satisfied with how he did the job with the walker.
Ease of learning - L
L.1: It was easy to learn to use the walker.
L.2: You could use the walker properly in a short time.
L.3: You had trouble understanding how to move around. *
Control over the *FriWalk* - C
C.1: You were sure the walker would always respond.
C.2: You had the impression you could suddenly miss the control. *
C.3: You had the impression you did not have full control. *
Adaptability of the walker - A
A.1: The walker fits well with your movements.
A.2: You had to adjust to the movements decided by the walker. *
A.3: The walker hindered/prevented your usual way of walking. *
* = Reversed

deviations **SD** on how much annoying/disturbing were the different features of the interaction on the Likert scale for all the strategies *BangBang*, *Haptic* and *Combined* is reported in Figure 5.12. The results of the questionnaire is summarized in the following with support by Figure 5.12:

- Characteristics of the interaction: in all the guidance strategies the participants declared they felt vibrations during the interaction but they were not at all disturbing;

- Pleasantness: we found that participants reported that the experience was moderately pleasant (P1) and they felt satisfied with their performance (P2), especially in the case of the *Combined* strategy. Moreover, they reported they did not fell frustrated for the interaction (P3);

- Ease of learning: we found that for participants it was easy to learn to use the walker (L1) and they could use it properly in a short time (L2). Especially for

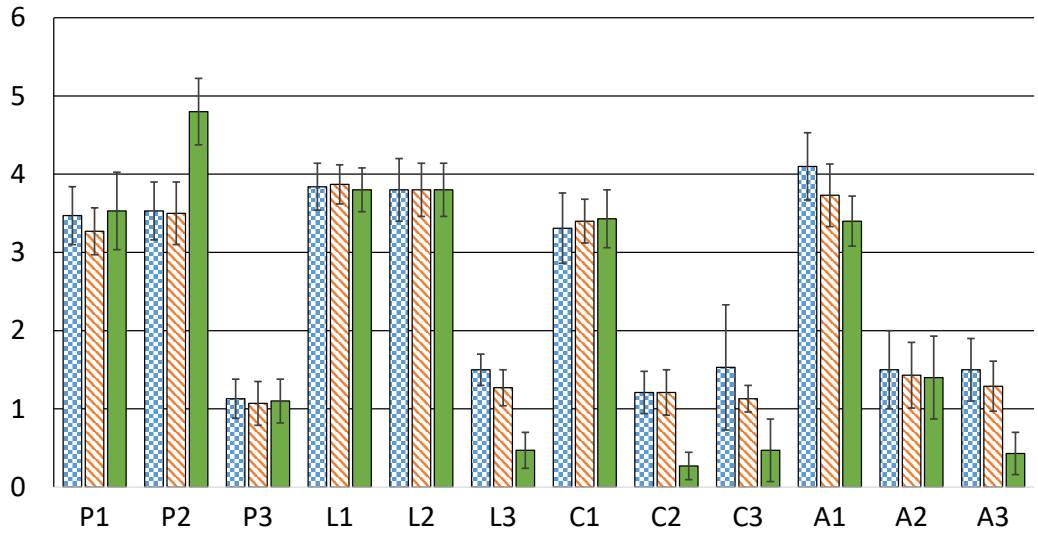

Figure 5.12: Means and standard deviations for the items on pleasantness (P1, P2, P3), ease of learning (L1, L2, L3), control perception (C1, C2, C3) and adaptability (A1, A2, A3) of the *FriWalk* for the *BangBang* (squared s bars), *Haptic* (raising tiling patterns bar) and *Combined* (solid filled bars).

the *Combined* guidance they did not have problems of movement, while they had majority of such problems with the *BangBang* solution as expected;

- Control: participants reported they felt the *FriWalk* responded well to their or commands (C1) and, especially for the *Combined* strategy, they did not have the sensation they could lose the control over it suddenly (C2) nor they did not control it completely (C3);

- Adaptability: participants reported they felt the *FriWalk* adapted well to their walking speed (A1), but they had the sensation they had to adapt a little bit to its motion (A2). The *Combined* strategy, in comparison to the *Haptic* and to the *BangBang* did not represent an obstacle to their movements.

Video analysis

During the experiments several videos have been recorder in order to perform an objective analysis and analyse the performances of the guidances. Such videos of the interaction between the elder participants and the *FriWalk* were analysed using the video analysis software BORIS [40] which allowed observing the frequencies and the length of a series of events occurred during the experiment with the robotic walker. Between all the events considered for the analysis of the interaction, those

that showed interesting results for the present study are described in Table 5.4.

Table 5.4: Elements analyzed to evaluate the guidance performance of [8].

Element 1 (E1)	*Total length and correct completion of the path following task*: we observed if the participants followed correctly the indications provided by the *FriWalk* and completed correctly the path and how much time required.
Element 2 (E2)	*Stop and braking*: we considered the number and length of participants' stop and braking during the task. An high number of of stop and braking is, of course, considered negative in the human–robot interaction.
Element 3 (E3)	*Help requests to the experimenter*: we measured the number and length of participant's requests to be assisted by the experimenter.
Element 4 (E4)	*Potential collision with an obstacle*: we observed how much and how long each participant moved in the close proximity of one obstacles and risked the collision.

Flexible interview

Beyond the quantitative approach given by the video analysis and the performance analysis given by the questionnaire, we relied also on a qualitative approach. To collect the impressions on the *FriWalk* and the interaction with it, the approach suggested by Minocha et. al [86] in conducting research with elders was used. We developed the protocol for informal flexible interviews establishing the main areas of interests for our study (flexible interview reported in Table 5.5.
Except for the first question on the general impressions of the participant toward the *FriWalk* and the interaction with it, the informal interview of Table 5.5 was characterised by the absence of a pre-determined order in the questions and by the possibility to adapt the conversation to the issues raised by the participant during the interview. In this way, the discussion with the participants had a flexible strategy and focused on what each participant believed more important.

Table 5.5: Flexible interview analyzed to evaluate the *FriWalk* in [8].

Question 1 (Q1)	*General impression*: first question to understand the general impressions of the participants on the *FriWalk* quality.
Question 2 (Q2)	*Control*: to investigate possible problems of control over the robot;
Question 3 (Q3)	*Intuitiveness*: the ease in using the *FriWalk* was investigate through two different question. First, the participants were asked directly if they had some difficulties in understanding the use of the *FriWalk*. The second type of questions were focused on the suggestion provided by the device to follow the path, hence if they were clear or not.
Question 4 (Q4)	*Motion*: a series of question were developed to investigate the impressions on the *FriWalk* motion, e.g. if it was abrupt.
Question 5 (Q5)	*Adaptability*: we perform three question to investigate the adaptability of the robot. The first one regarded if the users had the impression to adapt to the *FriWalk* motion or vice versa. The second type of questions aimed at investigating the participant's feeling to be blocked, pushed or pulled during the task. Finally, participants were asked if they felt that the robotic walker was an effort to them.

5.6 Discussions about the guidance strategies

In the present study, we aimed to observe the impact on elder participants of the *FriWalk* which one of the main purposes was to guide them in completing an unknown path. We tested three different kinds of guidance, *BangBang*, *Haptic* and *Combined*, considering the presence or absence of a graphical user interface to provide signals on the direction to follow. Participants were asked to complete a path following the signals of the robotic walker (with or without GUI) and they were interviewed to collect their impressions.
Results showed that *Combined* guidance worked more properly than *Haptic* and *BangBang*. Even if in *Haptic* participants needed less time to complete the path task, a lot of them finished the task wrongly, whereas this did not happen in *Combined* where almost all participants completed correctly the programmed path. As we expected, since in the *Haptic* the *FriWalk* did not block the wheels to guide the user on the correct path and we did not provide feedback to the participants about the correctness of their route, participants using the *FriWalk* in this kind of guidance stopped and slowed their speed at a lower extent than in *Combined* and *BangBang*. More importantly, we found that in *Combined* participants stopped and

braked significantly less than in *BangBang*. Moreover, we found that participants required the help of the experimenter at a lower extent in *Combined* in comparison to other kinds of guide, showing the indications provided by the *FriWalk* were clearer. Another important element is the strong reduction of zigzagging motion from *BangBang* to *Combined*. All these results suggest that the combination of the two signals (block of the wheels and vibrating wheels) worked properly in reducing the different problematics of *Haptic* and *BangBang* guidance styles. *Combined* guidance indeed reduced all the *BangBang*'s problems related to motion like stopping and zigzagging, but at the same time guaranteed a significant higher success in driving correctly the user in comparison to *Haptic*.
However, if the outcomes concerning the human-robot interaction indicated that *Combined* guidance was the best system to properly guide an elder user, the results of flexible interviews showed a different depiction. Except for answers concerning the perception of adaptability of the *FriWalk* to the participant, all the other variables we considered, i.e. perception of control, clear indications, smooth motion and feeling blocked, showed the same results: *Haptic* was perceived as the best guidance followed by the *Combined* and finally by *BangBang* (even if concerning clear indications *Combined* was judged as the worst). These results are not surprising since in *Haptic* the walker did not intervene but only suggested the route to follow, however they evidenced a series of issues (both social and ethical) in forcing a person to follow a determined path. Even if the percentages of participants who reported problems in controlling the walker were low and most of them were enthusiastic about the development of the robotic walker, elders who used the *FriWalk* were particularly critics toward the blocking wheel technique of *BangBang* and *Combined* guidance styles. They spontaneously defined the events of blocking as "frustrating", "annoying", and when the blocking repeated several times leading to the zigzag motion the interaction with the *FriWalk* was described even as "going with a spoiled child who does not know where he wants to go". Probably the effect of the type of guidance, and in particular of blocking or not blocking wheels, was so strong to nullify the presence of the GUI, as it affected uniquely the impressions of the adaptability of the robotic walker in *BangBang* and *Combined* conditions (not in *Haptic*), but not the intuitiveness of the indications even if we found that the GUI reduced the requests of help to the experimenter.

5.7 Conclusions

To summarise, we observed the human-robot interaction (HRI) between older adult users and the robotic walker *FriWalk*, developed to guide elders with walking problematics using different kinds of guidance (*BangBang*, *Haptic* and *Combined*) and the (possible) support of a graphical user interface (GUI), and we collect the impressions toward it. Results showed that participants interacted more properly with the robotic walker in *Combined* condition, but they reported better impressions toward

the *FriWalk* in *Haptic* guidance. Moreover, the outcomes evidenced very slow effect of the GUI which did not improve significantly nor the HRI neither the impressions toward the robot, indicating possible problematics related to a specific feature of *Combined* and *BangBang* guidance styles (i.e., blocking wheels).

Chapter 6

Active Guidance Solutions

At the heart of our active strategies there is the concept of *simulated passivity*, meaning that the vehicle moves as much as possible at the forward speed desired by the user, which is estimated by the robot during the walking with the rollator. In our works [9, 37] this is done by alternating phases when the user is in control with phases in which the robot is in control. When the user is in control, his/her desired forward speed is estimated. When the robot is in control the forward velocity remains consistent with the one estimated. This way, the user does not have the impression that the robot is actually governing the motion because he/she keeps moving at his/her pace (hence the name *simulated passivity* introduced in [9]). Moreover, the robot in control mode is never activated if the user's motion is compliant with the (safe) planned path. Therefore, the action of the motors is perceived by the user in form of a gentle rotational torque only when he/she has to turn toward the path.
The main goal of the analysis performed in [37] is to test the interaction with the acceptance of the *FriWalk* and its guidance system to a population of heterogeneous seniors, some having an almost intact eyesight and some with severe visual impairments. To this end, a human robot interaction (HRI) experiment was conducted in [37] to observe the relation between the elder users and the *FriWalk* in completing a path with obstacle avoidance. After the HRI task, participants were interviewed to collect their impressions of the *FriWalk* and the experienced interaction.
The *simulated passivity* [9, 37] strategy is a particular solution for path–following problem that, to ensure convergence, assumes that en exact localization of the robot in the environment is provided. This means that whenever the controller kicks in the *FriWalk* steers toward the desired path with absolute reliability. By the way, if the localization is not enough accurate the control action performed by the robot could be counterproductive. The main goal of the solution performed in [77] is to design a control algorithm that intervenes only if the controller is enough "sure" that its correction is going to help the user in following the planned path, hence if the control action is enough reliable.

6.1 Problem formulation and solution overview

For the active guidance solutions the model adopted for the *FriWalk* is the unicycle–like robot kinematic model (3.1). For a standard passive walker, the forward and angular velocities v and ω are imposed by the user's thrust. However, if the vehicle is actuated with the two controlled rear motors, the vehicle velocities v and ω are determined by the rotational velocities ω_L and ω_R of the left and right motors, by means of

$$v = \frac{r(\omega_R + \omega_L)}{2}, \quad \omega = \frac{r(\omega_R - \omega_L)}{d}, \tag{6.1}$$

where r is the wheel radius and d is the length of the rear interaxle. As seen in chapter 3, to properly represent the path following problem it is a common practice to introduce a Frenet reference frame moving along the path (see Figure 6.1).

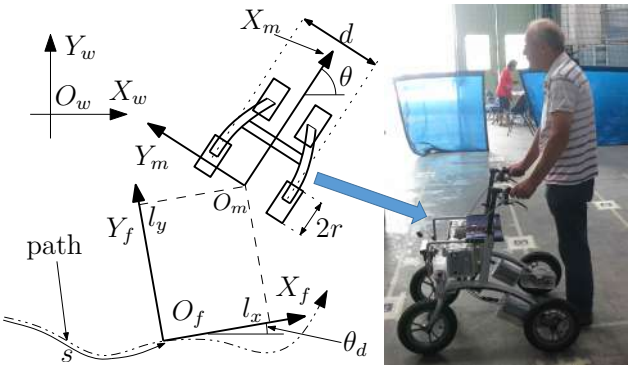

Figure 6.1: Adopted reference frames and coordinates [9].

Using the set of coordinates (3.19), we aim at solving the path following problem as expressed in (3.20), i.e.

$$\lim_{t\to+\infty} |l_x(t)| \leq l_\infty, \lim_{t\to+\infty} |l_y(t)| \leq l_\infty, \lim_{t\to+\infty} |\tilde{\theta}(t)| \leq \tilde{\theta}_\infty,$$

If the vehicle is a unicycle robot equipped with rear motors controlled in velocity, the solution to the passive path following problem (3.20) is theoretically impossible. In fact, whenever the vehicle is actuated (i.e. the motors impose the velocity ω_R and ω_L in (6.1) to command an angular velocity ω the forward velocity v is imposed as well and can not be modified by the user. Conversely, if the motors are not active, the user is in full control of the vehicle, hence the path following requirement satisfaction (3.20) depends on the assisted person's accuracy only. By the way it is very important to remember that in assistive robotics, for safety issues and comfort reasons, the vehicle angular velocity ω can be chosen to control the yaw θ to approach and follow the path, while the forward velocity v must be chosen by the user. In fact it is extremely important that the vehicle does not pull the assisted person. A

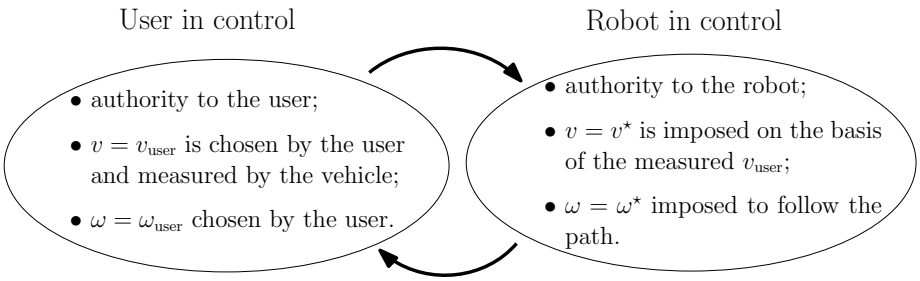

Figure 6.2: Simulation of passivity via authority-sharing [9].

possible way to face this issue is the use of *passive* robots that, by definition, do not have the authority on the vehicle forward velocity v [11, 12, 5]. In our case, instead, the robot is *active*, hence the motor velocities in (6.1) are used as input, therefore, as in [11], we propose to *simulate* the passivity of the vehicle by sharing the control authority between the user and the robot by alternating the following two working modes as shown in Figure 6.2:

- **Robot in control**: The control authority is given to the robot. The wheel velocities ω_R and ω_L are controlled and the forward velocity $v = v^\star$ and the angular velocity $\omega = \omega^\star$ are imposed to the vehicle as in (6.1);

- **User in control**: The control authority is given to the user. The motors are not activated, hence the vehicle is totally passive. Consequently, the vehicle velocities $v = v_{\text{user}}$ and $\omega = \omega_{\text{user}}$ are completely determined by the user and measured by the vehicle sensors, e.g. wheel encoders.

The passive behaviour in *Robot in control* mode is here simulated by imposing a controlled velocity $v^\star$ close (or even equal) to v_{user}, estimated in the *User in control* mode. This way, the user feels in control of the vehicle forward motion as if the robot were passive. As a consequence, to ensure that the path following requirements (3.20) are satisfied, in the *Robot in control* mode only the angular velocity $\omega^\star$ can be freely determined.

6.2 Simulating passivity strategy

The overall controller developed in [9] implementing simulated passivity via authority-sharing is then composed by two ingredients:

1. A path following control law ensuring (3.20) and simulating a passive robot, i.e. suitably computing the forward velocity $v^\star$ given the desired user velocity v_{user}, to be applied in the *Robot in control* mode;

2. A switching strategy between the two modes based on the user behaviour and implementing the simulated passivity via authority-sharing paradigm.

The path following problem (3.20) is decoupled in two subproblems in [9]. In order to simulate passivity and to improve the user balance, the robot should not pull the assisted person, that is the vehicle should not increase the speed v_{user}. To this end, we design two alternative strategies to compute $v^\star$, whose on-line selection is determined as described in Section 6.2.1. Then, we design a control law $\omega = \omega^\star(\chi)$, where χ is the vehicle state in the dynamic Frenet reference frame (3.19), that correctly steers the vehicle regardless of the forward velocity v of the vehicle. For this purpose we exploit the control law $\omega^\star(\chi)$ defined in (3.32) that perfectly fits the path–following problem with humans.

6.2.1 Forward velocity selection to simulate passivity

Velocity projection

Whenever the angular velocity $\omega \neq 0$, one of the two wheels has a larger velocity than the vehicle reference point velocity v (according to Equation (6.1)). For instance, if the vehicle turns right, the left wheel is faster than both the right wheel and v. Therefore, since the walker handles are approximately located above the rear wheels and even if the applied controlled velocity $v^\star \leq v_{\text{user}}$, the user may feel to be pulled by the fastest wheel. Hence, we impose that the fastest point of the vehicle has a forward velocity equal to v_{user}. In particular, if the requested angular velocity is positive, i.e. $\omega^\star > 0$, the vehicle turns left and the right wheel, the fastest one, is set to $\omega_R = v_{\text{user}}/r$. According to (6.1), we finally get

$$v^\star = v_{\text{user}} - \omega^\star \frac{d}{2}, \quad \omega_L = \frac{v_{\text{user}}}{r} - \omega^\star \frac{d}{r}.$$

The case of $\omega^\star < 0$ is homologous. A compact formula to describe this strategy is $v^\star = v_{\text{user}} - |\omega^\star|\frac{d}{2}$. An example of the proposed algorithm is in Figure 6.3.

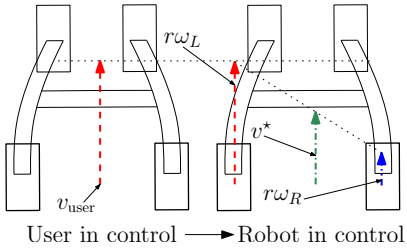

Figure 6.3: Computation of the vehicle velocities when the *Robot in control* mode is enabled and the vehicle has to turn right [9].

Braking actuation

Since the motors directly command the wheel velocities, projecting the user's velocity v_{user} on the fastest wheel might still generate discomfort if the correction that the robot has to apply is relevant. Consider for example Figure 6.4. In the *User*

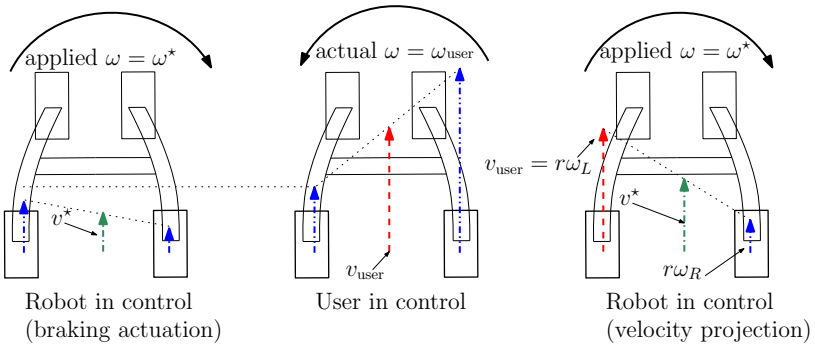

Figure 6.4: Difference between velocity projection and braking actuation for uncooperative users [9].

in control mode (centre of the figure) the user is steering the vehicle left. Suppose that, when the *Robot in control* mode is enabled, the vehicle has to turn right. If the velocity projection strategy is applied, the velocity of the left wheel may increment and still compromise the user's balance if the difference between angular the velocities is relevant (right part of Figure 6.4). To avoid such a condition, the vehicle is braked by setting $v^\star = \alpha v_{\text{user}}$, where $\alpha < 1$ in order to ensure a braking action and avoid that the user is pulled by the left handle (left part of Figure 6.4).

Choice of the forward velocity

The rationale of the forward velocity $v^\star$ choice in the *Robot in control* mode is the following. If the robot intervention considerably varies the vehicle angular velocity ω, the braking actuation method is applied to guarantee the user's safety. Conversely, if the robot can apply a small correction only (i.e. the required angular velocity $\omega^\star$ is close to the actual ω), the velocity projection method is applied to improve the user's comfort. Overall, the forward velocity simulating passivity applied in the *Robot in control* mode is

$$v^\star = \begin{cases} v_{\text{user}} - |\omega^\star|\dfrac{d}{2}, & \text{when } |\omega - \omega^\star| \leq \Omega, \\ \alpha v_{\text{user}}, & \text{when } |\omega - \omega^\star| > \Omega, \end{cases} \tag{6.2}$$

where $\Omega > 0$ and α are two comfort parameters to be tailored on the specific user's requirements.

6.2.2 Basic idea of the controller

The overall vehicle passive behaviour is simulated by switching the control between the user and the robot, hence a switching logic between the *User in control* mode and the *Robot in control*, as depicted in Figure 6.2, has necessarily to be defined.
The switching strategy of [9] is synthesised with a synergistic use of two different ideas:

- Time based approach: in the *User in control* mode the vehicle behaves passively and estimates the user's velocity v_{user} for a time window T_U. While, in the *Robot in control* mode, the motors impose the velocities $v = v^\star$ and $\omega = \omega^\star(\chi)$ for a maximum time window of T_R;
- Behavioural based approach: whenever the *Robot in control mode* is active according to the time based approach, but the user is autonomously following the path, i.e. the path following error e_θ is limited, then the control authority is given back to the user ($e_\theta < \theta_1$ in Figure 6.5). This means that the controller kicks in only whenever the error e_θ overcomes a certain threshold (θ_2 in Figure 6.5). To better the comfort of the user in [9] we designed an hysteresis mechanism to manage the control law $\omega^\star(\chi)$ according to the value of e_θ and two thresholds θ_1 and θ_2.

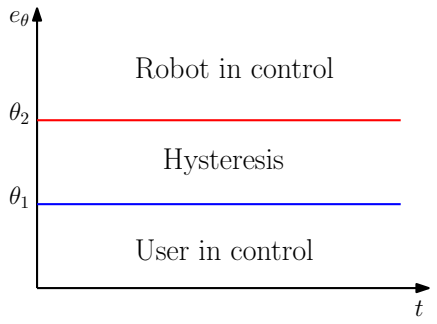

Figure 6.5: Switching strategy between *User in control* and *Robot in control* according to the value of e_θ.

The complex switching strategy exploiting hysteresis utilized in [9] has been formalised using hybrid system theory [43] and its behavior has been depicted in Figure 6.6 for simplicity.
Form Figure 6.6 it is possible to distinguish different sub–paths:

- **Sub–path A**: the user is in control of the robot and pushes freely the vehicle. Since $e_\theta < \theta_2$, then the path–following error is small with the consequence that the *Robot in control* mode never kicks in. Anyway the estimation phase of the forward velocity v_{user} last T_U so, after this time, if the error e_θ is still below θ_2, another estimation phase starts for a time T_U;

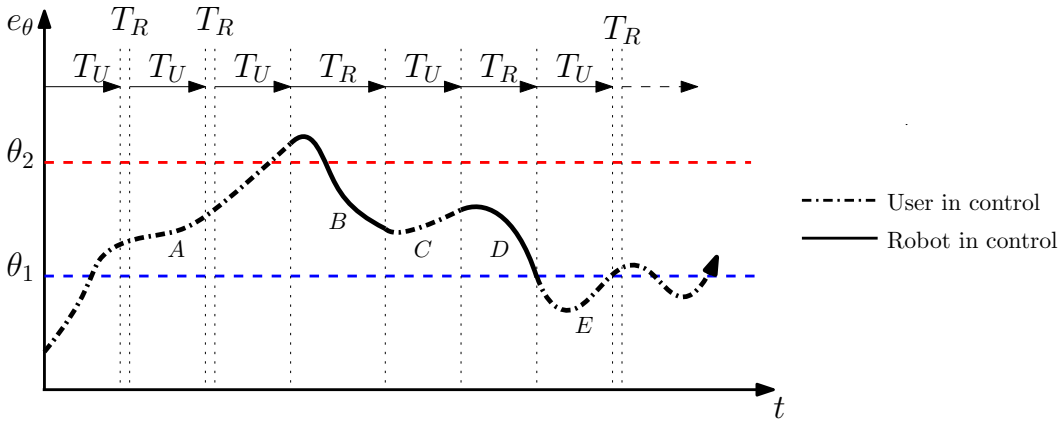

Figure 6.6: Switching strategy between *User in control* and *Robot in control* according to the value of e_θ.

- **Sub–path B**: as soon as the error e_θ overcomes the threshold θ_2 and the estimation phase T_U elapses, then the *Robot in control* mode kicks in, giving the control authority to the robot. During this phase the velocity imposed by the robot is $v = v_{\text{user}}$, while $\omega = \omega^\star$ defined in (3.32). This input steers the vehicle toward the desired path so that e_θ decreases;
- **Sub–path C**: the *Robot in control* mode last for a maximum time $T_R^{\max}$ even if the error e_θ is still larger then θ_1. After this phase the *User in control* mode kicks in to renew the estimation of v_{user} for a time T_U;
- **Sub–path D**: in this sub–path we can appreciate the hysteresis behaviour of the controller that, contrary to what happened in the sub–path A, gives back the authority to the robot since $e_\theta > \theta_1$. The robot intervenes and steers the user toward the desired path, decreasing e_θ;
- **Sub–path E**: as soon as $e_\theta < \theta_1$ the *Robot in control* mode elapses even if $T_R < T_R^{\max}$ giving back the control to the user.

6.2.3 Experimental results

In this section we present the experimental results of the proposed approach. Two studies were conducted in which the older adult participants completed different paths using the *FriWalk* in one laboratory of the University of Trento. In the first study (with 4 males, 10 females, ageing between 65 and 75 years old and 4 of them with walking problems (29%), the participants were asked just to travel along a couple of paths, while in the second study (with 6 males, 9 females, ageing between 64 and 100 years old and 7 of them (44%) with walking problems) a more extensive study, with more than eight paths for each participants were considered. Some of

the participants usually use walking aids, such as crutches and/or a walker (28.6% of *Study 1* and 43.8% of *Study 2*). Participants were contacted through the Municipality of Pergine Valsugana and the senior centre "Sempreverde" of Mattarello (both in the Trento province) and invited to participate. They were informed that data collection and that all information provided are covered by the ethical rules conceived for the ACANTO project [2] and that they could quit the experiment at anytime. Once consent was obtained they were invited to perform the tasks with the *FriWalk*. Before starting, an experimenter showed to the participant the path to follow and explained the features of the robotic walker and its motion mode. All participants completed a first trial (which was common for everybody) to take confidence with the robot walker and its movements. More than ten different paths, starting and ending in the same home position, were randomly chosen for each participant, that completed at least one of them. In the laboratory arena, three tables were placed to emulate an actual indoor environment (see the rectangular obstacles in Figure 6.7). The controller parameters adopted in the experiments are reported in [9]. Four

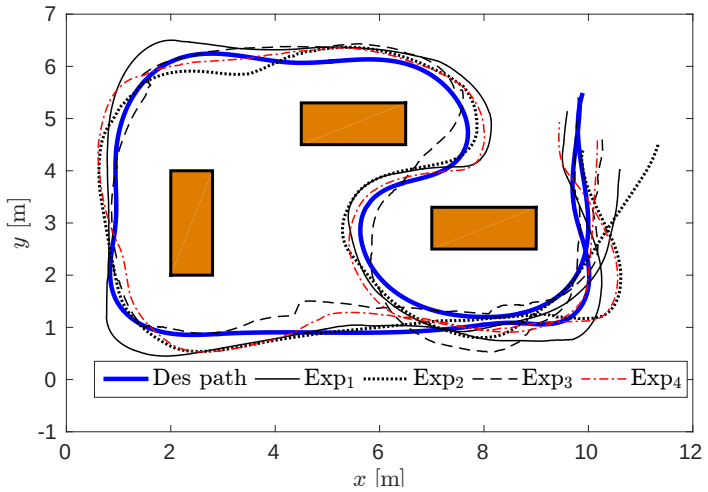

Figure 6.7: Experimental trajectories for four participants along a randomly selected path (solid thick line). The rectangles represent the obstacles (i.e., tables) in the environment [9].

sample trajectories along a randomly selected path are reported in Figure 6.7. The localization is provided with an extended Kalman filter [93] fusing the encoder data and the QR codes, positioned on the floor using the deployment [90] and read by the available front camera pointing downwards (see section 4.2.4). It may happens that a QR code reading is missed, hence a localization jump can be detected in the estimated trajectory (see the dashed trajectory of Exp_3 in Figure 6.7). Nonetheless, the controller is able to correctly steer the user towards the desired path.

Table 6.1: Summary of the controllers performance of the *Simulated passivity* strategy.

Feature	**Simulated Passivity**
Average $\|l_y\|$ [m]	0.16
std $\|l_y\|$ [m]	0.08
n° of interventions	10.3
std n° of interventions	2.5
time perc. active controller	11.2
std perc. active controller	3.4

6.2.4 Performance analysis

The overall controller performance are reported in Table 6.1, where we report the average path-following error $|l_y|$ of the user while relying on the *Simulated Passivity* strategy, the number of interventions of the controller and the percentage of time that the controller is active during the guidance. Comparing the results reported in Table 6.1 with the ones collected in Table 5.1, we can appreciate how the *Simulated Passivity* strategy has definitely better path–following performances. This is due to the fact that such guidance highly limits the freedom of user's movement, directly intervening on the rear actuators to steer him/her towards the desired path. Moreover, such actuation is much more intuitive (limited standard deviation) than the one provided by the *Bang-Bang* solution, since it's behavior is more smooth and natural. For this reason the amount of time for which the controller is engaged is reduced, and also the overall amount of interventions are limited.

6.2.5 User's evaluation

In both studies, we used a questionnaire to conduct a structured interview to collect the impressions and opinions of people who participated in the studies. After the session with the robotic walker, participants were invited to sit next to an experimenter who conducted the structured interview reading the items of the questionnaire. The aim of the structured interview was to collect the impressions of people on the proposed control approach. To this end, we included different questions (open ended and closed ended). In [9] we present the analysis of closed ended questions. Participants were asked to answer using yes or no and/or a 5 point Likert scale reported in Table 6.2.
The questions concerned different features of the interaction with the robotic walker, followed by items on the pleasantness of usage, the ease of learning, the control over the robot and its adaptability. Items used for the structured interview are shown in Table 6.3.
We first report the results of the characteristics of interaction in Table 6.4. The percentage of affirmative responses, with their relative mean **M** and standard de-

Table 6.2: Likert scale used for user's evaluation about the guidance strategy [9]

Likert Scale	grade
1	not at all
2	a little but
3	moderately
4	very much
5	extremely

Table 6.3: Items of the questionnaire for the users' evaluation [9].

Characteristics of the interaction
Vibration: Have you felt vibrations?
Path: Was it evident that was the walker to decide the path to follow?
Blocked: Have you felt to be pulled, pushed, pulled, or stuck?
If yes, "How much unpleasant/annoying...?" was each feature.
Pleasantness (in using the *FriWalk*) - P
P.1: The experience with the walker was pleasant.
P.2: It was frustrating to carry out the task with the walker. *
P.3: You are satisfied with how he did the job with the walker.
Ease of learning - L
L.1: It was easy to learn to use the walker.
L.2: You could use the walker properly in a short time.
L.3: You had trouble understanding how to move around. *
Control over the *FriWalk* - C
C.1: You were sure the walker would always respond.
C.2: You had the impression you could suddenly miss the control. *
C.3: You had the impression you did not have full control. *
Adaptability of the walker - A
A.1: The walker fits well with your movements.
A.2: You had to adjust to the movements decided by the walker. *
A.3: The walker hindered/prevented your usual way of walking. *
* = Reversed

viations **SD** on how much annoying/disturbing were the different features of the interaction on the Likert scale, are reported.
For the other items, the results, with mean and standard deviation, are summarized in tables 6.5 and Figure 6.8.

Table 6.4: Answers on the characteristics of the interaction [9].

	Study 1		***Study 2***	
Item	**Yes**	**M (SD)**	**Yes**	**M (SD)**
Vibration	33.3%	1.75 (0.50)	53.3%	2.00 (0.76)
Path	91.7%	1.82 (0.98)	93.3%	1.31 (0.63)
Blocked	25%	2.00 (0.00)	66.7%	1.80 (0.79)

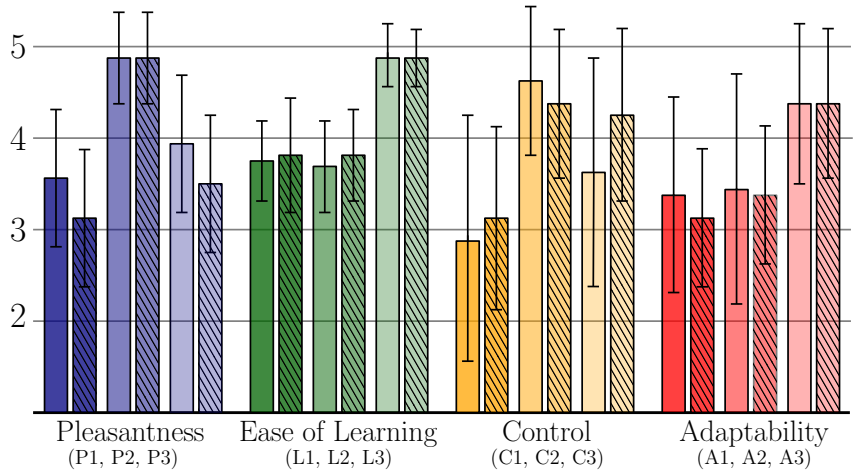

Figure 6.8: Means and standard deviations for the items on pleasantness (P1, P2, P3), ease of learning (L1, L2, L3), control perception (C1, C2, C3) and adaptability (A1, A2, A3) of the *FriWalk* in *Study 1* (solid fill bars) and *Study 2* (falling tiling pattern).

Discussions

The results of the studies showed an overall positive impression of the *FriWalk*. Concerning the characteristics of interaction that in both studies most of the participants were aware that the *FriWalk* decided the path to follow, whereas a low percentage of them reported they felt the vibration and had the sensation of being blocked or pushed. In any case, we observed that participants did not perceive these features as disturbing or annoying, thus validating our definition of comfort. The results also showed that participants evaluated the experience as moderately pleasant and that they felt happy with their performance with the robot. Moreover, they reported they did not feel frustrated by the interaction with the walker. Importantly, from a user experience point of view, the participants reported they had the feeling they could always easily control the *FriWalk*. Finally, we found that participants

Table 6.5: Means and standard deviation (in parenthesis) for the questionnaire described in Table 6.3.

Study 1			
P - M (SD)	**L - M (SD)**	**C - M (SD)**	**A - M (SD)**
P1: 3.58 (0.79)	L1: 3.75 (0.45)	C1: 2.83 (1.34)	A1: 3.33 (1.07)
P2: 4.83 (0.58)	L2: 3.67 (0.49)	C2: 4.67 (0.89)	A2: 3.42 (1.24)
P3: 3.83 (0.72)	L3: 4.83 (0.39)	C3: 3.67 (1.23)	A3: 4.33 (0.89)
Study 2			
P - M (SD)	**L - M (SD)**	**C - M (SD)**	**A - M (SD)**
P1: 3.13 (0.74)	L1: 3.80 (0.68)	C1: 3.13 (0.92)	A1: 3.13 (0.74)
P2: 4.80 (0.56)	L2: 3.80 (0.56)	C2: 4.33 (0.82)	A2: 3.36 (0.74)
P3: 3.47 (0.74)	L3: 4.87 (0.35)	C3: 4.23 (0.93)	A3: 4.33 (0.82)

had the feeling that the *FriWalk* well adapted to their speed and natural pace, so that the walker was not an obstacle to their usual way of walking.
Furthermore, it has been noted that participants showed good confidence in interpreting the walker suggestions with low path following errors. The fact that the *FriWalk* corrected the users by slightly slowing down was considered fundamental in this respect. Notice that in a few minutes participants understood the functioning of the robot and that with a clear explanation of its features and capabilities they did feel they were in control of the system.

6.2.6 Comments about the simulated passivity strategy

The *simulated passivity* solution is based on alternating intervals in which the system is not engaged and the user is in control with other intervals in which the system comes into play to execute turns. The impression is that of a passive system in which the user is never "pulled" even if the turns are imposed using the motorized rear wheels. The system has been validated with a large base of senior users.
From a technical perspective, future works will concentrate in changing dynamically the thresholds $\theta_{q_2} > \theta_{q_1} > 0$ according to the actual free space in front of the robot and still preserving the convergence properties. Moreover, future studies will focus on comparing different mechanical solutions and longer interactions with the robot walker using an ecological approach, and the possibility of orchestrating them with a visual feedback. Furthermore, learning algorithms to improve the user experience (i.e., tunable parameters or forward velocity adaptation) will be developed and tested.

6.3 Introduction of a GUI

The navigational system seen so far and used in [9] can be complemented by a graphical user interface (GUI), which provides indications on the direction to follow to the user [37]. The orchestration of the *Simulated Passivity* mechanical guidance and the visual GUI in the navigation support is specifically conceived to address the great variability of the elder population in capabilities and deficits. Very autonomous user could anticipate the interventions of the mechanical system by looking at the GUI in the proximity of the path selection points (e.g., intersections between different roads), whilst the user more reliant on the system could use the GUI to better understand how the system actually behaves.
To provide visual indications on the direction to follow to the participants, a Samsung Galaxy Tab S2[1] was positioned at the right part of the walker seat place. The tablet showed a GUI with a green arrow of 8 cm height and 3 thick on a white background, shown in Figure 6.9.

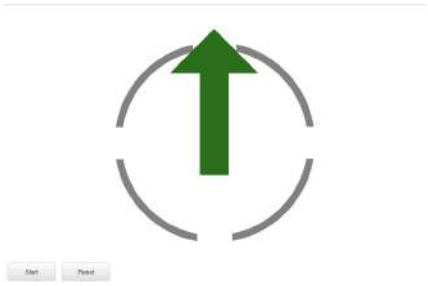

Figure 6.9: An example of the GUI used for the test.

The arrow that rotates 360° to indicate the direction to follow on the planned path has been chosen to represent the direction to take because it was a very simple, quick and intuitive feedback to give to the user. The direction to follow was computed according to the distance and the orientation that the user has with respect to the path, hence the attitude error e_θ.

6.3.1 Experimental Design and Hypotheses

A between-subjects experimental design with 2 conditions (*Tablet* vs. *No Tablet*) was developed. Participants in *Tablet* condition could rely on the support of a graphical user interface to understand the path to follow, whereas participants in *No Tablet* condition referred uniquely on the simulated passivity guidance to complete the task with the robot. Moreover, participants with visual impairments were observed as a separate group in order to understand possible differences in interacting with the *FriWalk* due to vision deficits. As simulated passivity was developed with the aim

[1] https://www.samsung.com/global/galaxy/galaxy-tab-s2/

of adapting and guiding elders with different problems and characteristics, we drew the hypothesis reported in Table 6.6.

Table 6.6: Hypothesis on the basis of the study performed in [37].

Hypothesis 1 (H1)	Most of the participants can complete correctly the path following task.
Hypothesis 2 (H2)	There should be no significant difference between participants in *Tablet* vs. *No Tablet* condition.
Hypothesis 3 (H3)	Presence or absence of visual impairment could play any role in completing the path with the *FriWalk*.
Hypothesis 4 (H4)	As the user interface helped in understanding the expected direction of motion of the *FriWalk*, we hypothesised that participants with intact eyesight in *Tablet* condition would show a better impression toward the *FriWalk* and a higher interaction acceptance in comparison with the *No Tablet* condition.

Before starting the path following, each participant received a description of the *FriWalk* guidance style and, accompanied by an experimenter, carried out a first trial to be acquainted with the guidance style of the machine. After that, participants were randomly assigned to one of the two experimental paths which were different from the first trial path. They were invited to complete autonomously the path with the *FriWalk*, although they could stop and interrupt the task and/or ask for the experimenter support at any time. Since the guidance function of the *FriWalk* shows its real utility when the user has to move in unfamiliar environments or when he/she does not know (or remember) the route to reach a specific goal, participants did not receive any upfront information about the experimental path they had to complete. This obliged them to totally rely on the robotic walker *Simulated Passivity* guidance and, when in *Tablet* condition, on the information provided by the GUI.

Participants

39 participants came to the BIC of Pergine Valsugana to participate to the study. However, since some of them decided at the last moment to not participate or they interrupted the experiment before completion, the final sample consisted of 29 participants (11 males and 18 females), ranging from 66 to 96 years old ($M = 84.27, SD = 7.35$). 27 participants reported to daily use a support device for walking, and specifically 24 used a walker (82.8%), 2 participants used a walking or tripod stick (6.9%) and other 2 declared to move with a wheelchair (6.9%). 8 participants (27.6% of the sample) reported to have a serious visual impairment and they all completed the experiment in *No Tablet* condition only.

Procedure

The videos of the interaction between the elder participants and the *FriWalk* were analysed using the video analysis software BORIS [40] which allowed observing the frequencies and the length of a series of events occurred during the experiment with the robotic walker. Between all the events considered for the analysis of the interaction, those that showed interesting results for the present study are described in Table 6.7.

Table 6.7: Elements analysed to evaluate the guidance performance of [37].

Element 1 (E1)	*Total length and correct completion of the path following task*: we observed if the participants followed correctly the indications provided by the *FriWalk* and completed correctly the path and how much time required.
Element 2 (E2)	*Stop and braking*: we considered the number and length of participants' stop and braking during the task. An high number of of stop and braking is, of course, considered negative in the human–robot interaction.
Element 3 (E3)	*Help requests to the experimenter*: we measured the number and length of participant's requests to be assisted by the experimenter.
Element 4 (E4)	*Potential collision with an obstacle*: we observed how much and how long each participant moved in the close proximity of one obstacles and risked the collision.

Beyond this quantitative approach we relied also on a qualitative approach. To collect the impressions on the *FriWalk* and the interaction with it, the approach suggested by Minocha et. al [86] in conducting research with elders was used. In place of questionnaires and structured or semi-structured interviews, we developed the protocol for informal interviews establishing the main areas of interests for our study (flexible interview reported in Table 6.8.
Except for the first question on the general impressions of the participant toward the *FriWalk* and the interaction with it, the informal interview of Table 6.8 was characterised by the absence of a pre-determined order in the questions and by the possibility to adapt the conversation to the issues raised by the participant during the interview. In this way, the discussion with the participants had a flexible strategy and focused on what each participant believed more important.

Table 6.8: Flexible interview analyzed to evaluate the *FriWalk* in [37].

Question 1 (Q1)	*General impression*: first question to understand the general impressions of the participants on the *FriWalk* quality.
Question 2 (Q2)	*Control*: to investigate possible problems of control over the robot;
Question 3 (Q3)	*Intuitiveness*: the ease in using the *FriWalk* was investigate through two different question. First, the participants were asked directly if they had some difficulties in understanding the use of the *FriWalk*. The second type of questions were focused on the suggestion provided by the device to follow the path, hence if they were clear or not.
Question 4 (Q4)	*Motion*: a series of question were developed to investigate the impressions on the *FriWalk* motion, e.g. if it was abrupt.
Question 5 (Q5)	*Adaptability*: we perform three question to investigate the adaptability of the robot. The first one regarded if the users had the impression to adapt to the *FriWalk* motion or vice versa. The second type of questions aimed at investigating the participant's feeling to be blocked, pushed or pulled during the task. Finally, participants were asked if they felt that the robotic walker was an effort to them.

6.3.2 Results

The results of the video analysis to analyse the events of Table 6.7 during the experiments is reported in Table 6.9. In particular E1 expresses the total length travelled by the user during the experiments. While E2, E3 and E4 report, respectively, the number of the participants that stopped, asked for experimenter help and risked to collide against an obstacle. The video analysis of the interaction with the *FriWalk* revealed that all participants completed the path correctly, meaning that the interaction was clear. After that, we run two ways ANOVA with condition *Tablet* vs *No Tablet* and visual impairment as fixed factors, and the total length of the path–following task as dependent variable. We found that the time to complete the task and the length travelled were affected neither by the experimental conditions nor by the visual conditions of the participants. No significant difference regarding E1, E2, E3 and E4 has arisen between the condition *Tablet* vs *No Tablet* and visual impairment.

The content of flexible interviews was analysed through the approach of direct content analysis described by [55]. Responses were examined in relation to the areas of interest created (control, intuitiveness, motion, and adaptability) in order to

Table 6.9: Quantitative analysis results of events reported in Table 6.7 with 29 participants with visual impairments (V.I.) and without visual impairments (N.V.I.).

	Tablet	***No Tablet***	
Label	**N.V.I** $N = 15$	**N.V.I** $N = 6$	**V.I.** $N = 8$
E1 [m]	49.36 ± 10.99	49.93 ± 10.05	48.73 ± 11.74
E2 [#]	4	1	1
E3 [#]	1	1	3
E4 [#]	1	–	2

summarise their content within specific categories. We considered both the valence (positive or negative) of each response and the explanation provided by the participant to better understand their impression on the *FriWalk*. In particular, for the question on the general impression, we observed the frequencies of each area of interest mentioned in participants' responses in order to understand what were the priorities for them in interacting with the *FriWalk* and completing the path with it.

6.4 Discussions

Results of video analysis on human-robot interaction showed that all participants completed correctly the path following task (confirming hypothesis H1) irrespective of the presence of the visual GUI (confirming hypothesis H2). Similarly, the task completion was not affected by the visual impairments of the participants (confirming hypothesis H3). Only a small percentage of participants stopped or braked during the path following task, requested the support of the experimenter during the interaction with the *FriWalk* and showed problems related to potential collisions with the obstacles. Thus, the outcomes confirmed that the *FriWalk* and the *Simulated Passivity* are quite effective and adaptable to elder individuals with different types and measures of deficits. The analysis of the content of the flexible interview showed an overall participants' appreciation of the *FriWalk*. Nevertheless, the questionnaire on the *FriWalk* general impressions highlighted that the most relevant issues, in order of importance, are the intuitiveness (and in particular the indications on its direction), the control over the robot, its motion and its adaptability.
We also found no significant differences related to the presence or the absence of the GUI and visual impairments for the intuitiveness and the motion of the *FriWalk*, with most of the participants reporting it was easy to learn to use the robotic device and half of them declaring the indications on the direction were clear. However, most of the participants reported they perceived the *FriWalk* movements as "jerky".

For adaptability, most of the participants reported the sensation they had to adapt to the robotic walker, although the most of them declared it was not tiring walking with the *FriWalk*. These results highlighted that the weight of the robotic walker is not perceived as excessive by the users, but that it is necessary to improve the adaptability to the user's walking style avoiding abrupt changing of speed especially in the changing of the user in control and robot in control phases. Finally, concerning the question on the sensation of feeling blocked, pushed or pulled by the robotic walker, we did not find an effect of participants' visual impairments, but results were affected by the experimental condition: a higher number of participants in *Tablet* condition than those in *No Tablet* condition reported they felt to be blocked by the *FriWalk* during the completion of the path.

About the flexible interview

The results of content analysis of flexible interviews evidenced that participants in *No Tablet* condition (and especially those with visual impairments) had a better impression of the *FriWalk* and the interaction with it, thus disconfirming H4. As a consequence, the results of the present study highlighted that the *FriWalk*, with its *Simulated Passivity* mechanical guidance system, represents a trustworthy device for assisting seniors in walking. Moreover, they showed reliability in guiding both people with or without visual impairments, showing the good adaptability of the assistive device to users with different physical deficits. Furthermore, the general impression is that the *FriWalk* was more appreciated by people with visual difficulties, thus without the possibility of using the GUI. A possible explanation of these differences in perceiving the robotic walker could be related to the additional information provided by the GUI. In fact, participants in *Tablet* condition reported that the direction was already clearly shown by the GUI, so the intervention of the mechanical guidance was perceived as unnecessary and disturbing. Follow these information, we may argue that the *Simulated Passivity* corrections should be milder in presence of the GUI. Nonetheless, we want to highlight two important elements concerning the results of the present study. First, the answer's of participants were recoded through a severe approach (e.g., replies indicating a minimum issue in controlling the *FriWalk* were coded as having problems in controlling the robotic walker). Second, the differences concerning the several areas of interests were only marginally significant, indicating that *Simulated Passivity* can work properly also without the GUI.

6.5 Conclusions

The results showed that the robotic device worked properly with or without a GUI which provided indications on the direction to follow, as well as for people with and without visual impairments. The interviews evidenced overall positive impressions

of participants, with visually impaired users evaluating slightly better the robot than individuals who could rely also on the graphical user interface to complete the path.
Of course, the present research has some limitations. First, we developed the path following task has been carried out within a university lab. Clearly, a controlled environment have effects on the interaction between the elder participants and the *FriWalk*. A more ecological approach, despite methodological limitations, certainly allows the collection of more comprehensive information on the interaction [39, 104]. Second, the possibility of observing the interaction in a longitudinal way may open to information gathering on possibly unobservable features that are not at disposal in laboratory tests [47, 26]. Finally, in the present study, all participants showed no cognitive problems: future studies should include older adults with cognitive problems, as they can show different issues in relating to assistive technological devices [122], with the aim of enlarge the user group that can benefit of the proposed technological solutions.

Chapter 7

Front steering actuations

A front–steering passive walker, pushed forward by a user, has the dynamics of a rear–driven bicycle. Different solutions exist to solve the path following problem for vehicles of this kind. One of the most famous is the chained form coordinate transformation proposed by Samson et al. [107]. When applied to our context, such standard solutions have to face two big problems. First, the control can be saturated by the limiting turning angle of the wheels. Second, the controller makes an explicit use of the forward velocity as a control input, which is not possible for the problem at hand where the robot is propelled by the user. The general problem of actuator saturation has been extensively studied in the context of path following for unicycle vehicles when the forward velocity is available [57, 60].
One promising approach for passive path following that applies also to robots without control on the forward velocity, but still making the relaxed hypothesis that the vehicle is persistently in motion, is presented in [113], inspired by the work in [85] in which a vehicle with two independent steering wheels is considered. The common idea is to steer the front wheels to generate the desired vehicle angular velocity. However, this solution is singular at null forward velocity, phenomenon that obviously does not appear for differentially driven robots. Despite the condition of non-zero velocity is clearly necessary for convergence to the path, an undesired behaviour of the controller in singular configurations can not be neglected in assistive robotics, where the user often stops or slows down. In order to solve the path following problem and guarantee a proper behaviour even when the singularity is triggered, in [12] we presented a control law where the angular velocity is generated by steering commands that are *independent* from the forward motion. Our theoretical analysis reveals that this law secures convergence to the path. Moreover, experimental trials on the *FriWalk* clearly show the improved user's comfort with a preserved effective path tracking performance.

7.1 Problem formulation

The analysis performed in [12] has been performed with the DaLi prototype reported in Figure 4.1 that, since it is a rear–driver car–like, follows the kinematic reported in equations (3.4). In this case the angular velocity ω of the vehicle, hence its yaw rate, becomes

$$\omega = \frac{v}{d}\tan(\varphi). \tag{7.1}$$

As done for the other guidances strategies described in chapter 5 and chapter 6, also in this case, to solve the path–following problem, a Frenet frame moving along the desired path has been introduced ruled by equations (3.12). In such work it has been chosen a static Frenet frame only for simplicity. With the model (3.12), the path–following can be represented as a stability problem, where the conditions (3.13) ensure that the path is correctly followed, and are reported in the following for completeness:

$$\lim_{t\to+\infty} |l(t)| = 0,$$
$$\lim_{t\to+\infty} |\tilde{\theta}(t)| = 0,$$

Since the *FriWalk* is a passive vehicle, φ of model (3.4) is the only available control input for the robot, a few considerations are necessary:

- In order to avoid discomfort and increase manoeuvrability, the steering angle φ is saturated to a value $\varphi_{\max} \in (0°, 90°)$. This way ω of (7.1) becomes

$$\omega = \frac{v}{d}\tan\left(\text{sat}_{\varphi_{\max}}(\varphi)\right), \tag{7.2}$$

  where $\text{sat}_L(\cdot)$ denotes the symmetric saturation function with saturation limits $\pm L$. Notice that this value is an additional tuning parameter that can be tailored on the user's perceived comfort;

- By means of (7.2), φ acts on the system in a strong non–linear way;

- If the saturation constraint is not considered, by plugging ω in (7.1) in the vehicle model (3.4), the unicycle–like dynamic is readily retrieved. Suppose that a feedback controller $\omega(\chi)$ solving the path following problem as stated in (3.13) is available (e.g. [113]). By selecting

$$\varphi(\chi) = \arctan\left(\frac{d}{v}\omega(\chi)\right), \tag{7.3}$$

  where $\chi = [s, l, \tilde{\theta}]^T$ is the state of the vehicle, the controlled steering action is computed. However, (7.3) turns to be singular for $v = 0$. In a real scenario, this situation will surely take place whenever the walker starts or when the user

stops for any reason. In such a case, the commanded control steering angle is the maximum admissible value, which generates a large deviation and, hence, worsens the comfort. In the limit, if the saturation is neglected, φ gets to 90° and then the user cannot move any further without forcing the wheels to slip.

As a consequence, in [12] we designed a control law $\varphi(\chi)$ that solves the path following problem and:

1. Explicitly considers the presence of the saturation limit $\varphi_{\max}$;
2. Avoids the singularity in (7.3). Ideally the function $\varphi(\chi)$ should be independent from v.

7.2 Solution overview

As done for the other guidance strategies of chapter 6 and chapter 5 we make use of the approaching angle $\delta(l)$ selected within (3.27). Since the vehicle (3.4) with the saturated control action (7.2) has a limited steering angle and a limited curvature radius depending on the geometrical parameter d (rear wheelbase), the path to be followed cannot be arbitrary. So, we require an *admissible path*, hence a path that can be followed considering the robot constraints. Let M, $\gamma(\chi)$ be

$$\begin{aligned} M :=& \frac{1}{d}\tan(\varphi_{\max}), \\ \gamma(\chi) :=& \frac{c(s)\cos(\tilde{\theta})}{1-c(s)l} + \sin(\tilde{\theta})\frac{\mathrm{d}\delta}{\mathrm{d}l}(l). \end{aligned} \tag{7.4}$$

We require that the condition $M > |\gamma(\chi)|$ always holds. Suppose, for instance, that the vehicle is located on a circular path, i.e. $l = 0$ and $\tilde{\theta} = 0$, with curvature radius $R > 0$. Take for simplicity $\varphi_{\max} = 45°$. Since $\gamma(\chi) = 1/R$, the condition $M > |\gamma(\chi)|$ becomes

$$\frac{1}{d} > \frac{1}{R} \implies R > d.$$

In practice the assumption made in (7.4) states that the maximum steering angle $\varphi_{\max}$ guarantees the angular velocity needed to reach the path in the case of zero angular error, i.e. when $\tilde{\theta} = \delta$, which is a very loose constraint in a realistic situation.

7.2.1 Control law

In order to have $\varphi(\chi)$ independent from v, we may take $\omega(\chi)$ in (7.3) linear with respect to v.
Considering the system (3.4) with constraint (7.2) and supposing that the path is admissible, then the path following problem (3.13) is solved by the control action

$$\varphi(\chi) = \arctan\left(d\left(\gamma(\chi) - \mathrm{sat}_{\bar{\beta}(\chi)}(ke_\theta)\right)\right), \tag{7.5}$$

where $k > 0$ is a gain and $\bar{\beta}(\chi) = M - |\gamma(\chi)|$ is a variable saturation limit. Moreover the control action $\varphi(\chi)$ in (7.5) never exceeds the saturation limit $\varphi_{\max}$ in (7.2). The proof of the path–following convergence of this control law is reported in [12].

7.3 Experimental results

The experimental results have been collected using the DaLi robot depicted in Figure 4.1, which is equipped with two independent front steering wheels actuated by stepper motors implementing the Ackerman's steering (ruled by equation (3.5)). The users have been required to push the vehicle forward to follow different paths passing around several obstacles and synthesised by means of the path planner defined in Section 4.2.5. In the tests, the user did not receive prior information on the path, hence forcing her/him to completely rely on the guidance system. Nevertheless, to improve safety and comfort, in the actual deployment the user uses also the *FirTab* as a visual navigator running. The experiments have been carried out in the facilities of the University of Trento, where 14 cameras Optitrack Prime are installed. Again, having the localisation noise negligible and users with no knowledge of the path highlights the path tracking accuracy of the controller. Finally, the saturation $\varphi_{\max} = 60^\circ$ and the approaching angle $\delta = -\frac{\pi}{2}\tanh(l)$.

7.3.1 Comparison for singularity handling

In the first set of results, the ability of the proposed controller to deal with singularities is firstly tested. To this end, the users were requested to push forward the vehicle on a straight path, and after few seconds, they were requested to stop in a marked position, i.e. $v = 0$. After 5 seconds, the users were asked to complete the path. An example of results obtained with the presented controller is given with the thin dashed line of Figure 7.1, marked with φ: in such a case the user smoothly follows the straight path avoiding the singular configuration.
To better clarify the benefits of the proposed controller in handling the singularity for an improved user comfort, a comparison with straightforward controllers is now discussed. At first, the control input $\omega^\star(\chi)$ solving the path following (3.34) for a unicycle vehicle by means of the control law computed in [113] is considered, with no limit on the steering angle. The steering angle is then computed via (7.3), that is $\varphi_1(\chi) = \arctan\left(\frac{d}{v}\omega^\star(\chi)\right)$. Notice that the limits of the steering angle are not explicitly considered. When the singularity is triggered, the controller φ_1 steers the wheels at the maximum admissible angle (see (7.3)). When the user starts over, since the steering wheels cannot be instantaneously turned (i.e. intrinsic dynamic of the stepper motors), the vehicle moves in the non-straight direction imposed by the steering system, as reported by the dotted trajectory in Figure 7.1 and dubbed φ_1. Notice that the vehicle slightly comes back (i.e. its curvilinear abscissa s decreases) since, to reproduce a virtual steering angle of 90°, the differential steering strategy requires

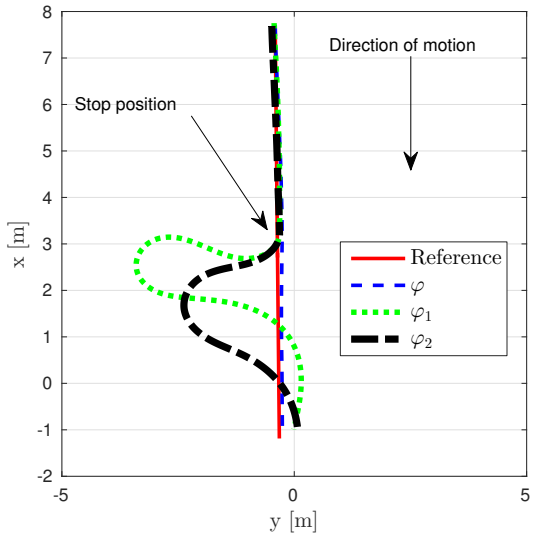

Figure 7.1: Experimental effects of singular velocities. The proposed algorithm (φ) lets the vehicle remain in the path when the singularity happens, which instead is not the case for the compared controllers (φ_1 and φ_2) [12].

a wheel (the right wheel in the experiment in Figure 7.1) to steer at 90°. Then, when the user pushes the vehicle forward, the right steering wheel is turned to an angle $\varphi_r > 90°$ because of the friction with the ground. To overcome this nuisance, a saturation is imposed to the control law $\varphi_1(\chi)$, i.e. $\varphi_2(\chi) = \text{sat}_{\varphi_{\max}}\left(\arctan\left(\frac{d}{v}\omega^\star(\chi)\right)\right)$. Albeit the trajectories obtained are better than in the previous case (see the thick dashed line in Figure 7.1 named φ_2), the perceived comfort and the following performance are clearly worsened with respect to the proposed solution.

7.3.2 Path–following performance

An extensive campaign of experiments has been conducted with 14 individuals of both sexes aged 19 to 47. Figure 7.2–(a) shows some sampled trajectories with the desired planned path (solid line) synthesised using the path planner in [19].
Notice that the experiments are very repetitive. The path following errors are mainly due to the actuation delay of the stepper motors. Nonetheless, the tracking error (measured by means of the distance from the path l) is larger in the presence of important steering manoeuvrers (at the end of the approaching phase and in the second curve in Figure 7.2–(a)). Nonetheless, the mean error is 2 cm, the mean absolute error is 8 cm and the maximum absolute error is 26 cm (see Figure 7.2–(b) for the histogram of $|l|$). The results are independent from the user velocity and the path followed. Finally, Figure 7.3 shows the commanded and the actual steering angles for the front wheels for Test 4 in Figure 7.2–(a). The actuation delay is visible only between 20 and 23 seconds, in the proximity of the second corner, i.e.

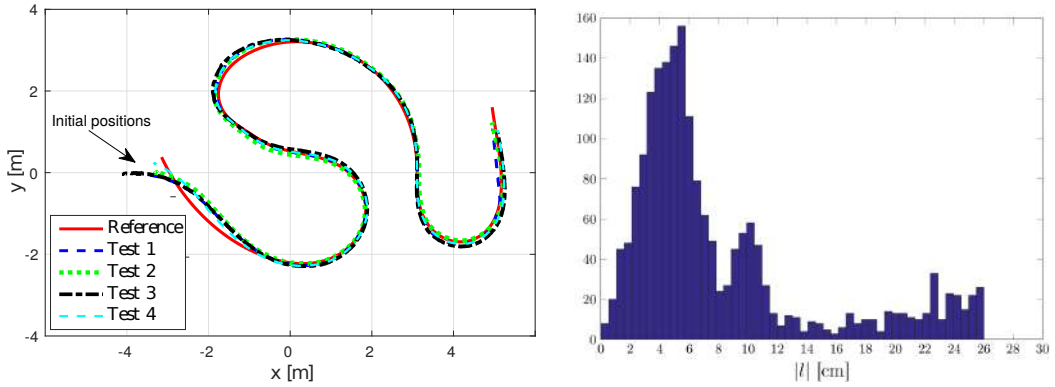

(a) *Experimental path following tests [12].*

(b) *Histogram of the path following absolute errors $|l|$ for the experiments executed with the reference path [12].*

Figure 7.2: Path following performance relying on the front steering strategy [12].

aggressive right turn. Notice how the Ackerman's steering induces differences in the two steering angles φ_l and φ_r. Since the actual steering angles are overlapped to the desired ones almost everywhere and the vehicle is equipped with front stepper motors, the validity of the kinematic model (3.4) considering the steering angle φ as control input, instead of $\dot{\varphi}$, is confirmed.

7.3.3 Considerations about the guidance

In [12] we presented a control algorithm for a passive robotic vehicle equipped with front steering wheels. The algorithm allows the designer to specify limits on the steering angles and is completely insensitive to the singularity arising for zero velocity, that otherwise considerably worsens the performance in a real vehicle having steering wheels with non-infinitely fast dynamics.

The front steering system [12] is very efficient to follow the path since it completely force the user to move in the direction imposed by the front wheels without allowing any freedom to the user. The comfort of such guidance system is very high, since no abrupt interventions occur, but the feeling is like walking on a railway track, which is quite annoying. This is not the case of the braking guidance [8] of chapter 5, where freedom is needed to avoid chattering and implemented by safety tunnels in which the user is completely in charge of the motion. Also in the case of the simulated passivity approach [9] described in chapter 6, where the control must be periodically given to the user to estimate his/her desired forward speed, users feel more freedom during the walking and the comfort is increased.

To better the comfort of the user with the front steering wheels, we may apply a control logic that ensures intervention according to the path following error, hence giving the authority to the robot only far from the path, while leaving the total

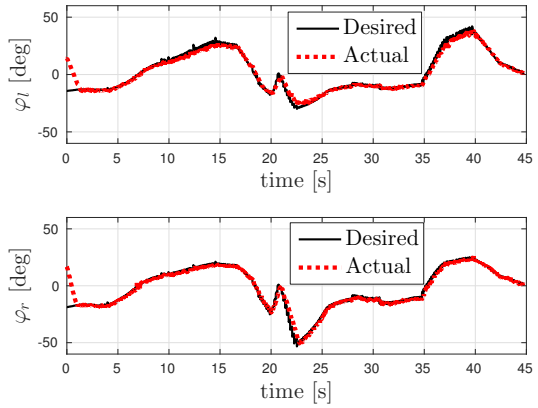

Figure 7.3: Experimental steering angles along Test 4 in Figure 7.2 [12].

control of the motion to the user when the tracking error is bounded. Unfortunately, if the front actuation were activated only for large deviations, a sudden reorientation of the front wheels would stiffly happen whenever the robot takes the control, hence mining the comfort advantage of the car-like kinematics, which ensures a smooth control action. To avoid this nuisance and guarantee a coexistence between the user and its *FriWalk*, a more compliant actuation of the front wheels is then required.

7.4 The variable stiffness approach (confidential)

The basic idea at the basis of the variable stiffness approach is a gain varying controller. In fact, normally:

- High gain control offers good tracking performance but, at the same time, produces a stiffer action of the robot;
- Low gain control increases the user freedom, since he/she can overrule the system actuation, but with the price that the working precision is obviously compromised (in case of non–cooperative users or if the path to follow is unknown).

Since the actuators available on the *FriWalk* are brushless motors such effect can be obtained by controlling them in current to reach a desired position. To mimic an high gain, we inject an high current, so that the control action will result stiff. Conversely, to have a low gain a limited current is necessary, so that a limited torque is applied by the motor, enabling the possibility to the user to overrule the motor action. Implementing a gradual transition between a low and an high gain, the human–robot interaction is arguably highly increased. This effect is viewed as a virtual spring-damper system acting on the steering wheels, where the spring stiffness (hence the term “stiff” vehicle) and the damping coefficient vary with a

suitable measure of the distance from the path, considering both geometric distance and relative orientation (hence the attitude error e_θ). Whenever the user is close to the path a low gain controller is applied so that he/she perceives the vehicle as compliant, having the impression than it is not actuated and he/she is completely in charge of the *FriWalk* motion. Conversely, the larger the distance, the stiffer becomes the control action, reducing the possibility of the user to overrule the motor actuation and preventing the possibility to deviate from the path. It is also possible to exploit an increasing stiffness to guarantee safety since it ensures that the user doesn't deviate from the path. So, whenever the path is critical (e.g. in proximity of obstacles), the action becomes so stiff that it is completely impossible for the user to depart from the path as experiments performed in [12] confirms. On the other hand, whenever the planned path goes through safe environments (e.g. corridors), the action becomes so light that the user feels in completely charge of the *FriWalk* motion.

Notice that the classical car-like model (3.4) is based on a first order dynamics $\dot{\varphi} = u_v$, i.e., it is supposed that the velocity is commanded by the motor with negligible settling time. This working mode of the motor is denoted as *velocity-tracking*. Although this hypothesis is reasonable and widely accepted [111], we need to consider a second order dynamics to implement the variable stiffness paradigm. This requires to use the motors in *torque-tacking* mode. The motor dynamics and the corresponding working modes of its controller are described in the following section.

7.4.1 Motor control

Each wheel of the *FriWalk* in Figure 3.1 is coupled with a permanent magnet synchronous motor (PMSM) via a gear box having a gear ratio $n_g = 24$ (see section 4.2.1). A PMSM can be used both to command the steering velocity u_v (velocity-tracking mode) and to apply a torque to the steering wheels (torque-tracking mode), as explained in the following.
The dynamic model of a PMSM in the dq-rotor reference frame can be expressed as in [66]. The wheel is considered as a passive rotating system. The dynamic model of each wheel-motor system is expressed as

$$\begin{cases} \dfrac{\mathrm{d}i_d}{\mathrm{d}t} &= \dfrac{1}{L_d}\left(-R_s i_d + n_g n_p L_q i_q v_w + \nu_d\right), \\ \dfrac{\mathrm{d}i_q}{\mathrm{d}t} &= \dfrac{1}{L_q}\left(-R_s i_q - n_g n_p L_d i_d v_w - n_g n_p K_e v_w + \nu_q\right), \\ \dfrac{\mathrm{d}v_w}{\mathrm{d}t} &= \dfrac{3 n_g n_p}{2 J_{eq}}\left(K_e i_q + (L_d - L_q) i_d i_q\right), \end{cases} \tag{7.6}$$

where i_d and i_q are the direct and quadrature current components, ν_d and ν_q are the direct and quadrature input voltage components, v_w is the steering velocity, R_s is the phase resistance, L_d and L_q are the phase inductances along the direct and

quadrature axes respectively, n_p is the number of permanent magnet pole pairs, K_e is the back electromotive force (EMF), and $J_{eq} = J_w + n_g^2 J_m$ is the equivalent inertia moment of the motor-wheel system, where J_m and J_w are the inertia moments of motor and of the wheel (around the steering axis), respectively.
At this point it is possible to adopt the field oriented control strategy [118, 72] for system (7.6). In particular it is possible to design the two control inputs ν_d and ν_q, by means of a state feedback, as

$$\nu_d = -n_g n_p L_q i_q v_w + \nu'_d, \tag{7.7}$$
$$\nu_q = n_g n_p L_d i_d v_w + n_g n_p K_e v_w + \nu'_q, \tag{7.8}$$

where ν'_d and ν'_q are two auxiliary control input designed in order to assign the desired behavior to the system

$$\begin{cases} \dfrac{\mathrm{d}i_d}{\mathrm{d}t} &= \dfrac{1}{L_d}\left(-R_s i_d + \nu'_d\right), \\ \dfrac{\mathrm{d}i_q}{\mathrm{d}t} &= \dfrac{1}{L_q}\left(-R_s i_q + \nu'_q\right), \\ \dfrac{\mathrm{d}v_w}{\mathrm{d}t} &= \dfrac{3n_g n_p}{2J_{eq}}\left(K_e i_q + (L_d - L_q) i_d i_q\right). \end{cases} \tag{7.9}$$

By means of the state-feedback (7.7) and (7.8) the dynamics of the stator currents are made linear and decoupled between each other: a variation of ν'_d produces only a variation of i_d and a variation of ν'_q produces only a variation of i_q. Now we can act on the input ν'_d to force the current i_d to zero by means of a PI controller. In such a case, after a transient in which the i_d goes to zero, the non–linear term $i_d i_q$ in the speed equation is also zero and the system can be viewed as a linear system, in which the speed, depends only on the current i_q which can be controlled by the input ν'_q.
In other words, it is possible to design the speed controller (motor in velocity-tracking mode) or the torque controller (motor in torque-tracking mode) by the dynamics

$$\begin{cases} \dfrac{\mathrm{d}i_q}{\mathrm{d}t} &= \dfrac{1}{L_q}\left(-R_s i_q + \nu'_q\right), \\ \dfrac{\mathrm{d}v_w}{\mathrm{d}t} &= \dfrac{3n_g n_p}{2J_{eq}} K_e i_q, \end{cases} \tag{7.10}$$

and by recalling that the torque τ_w applied by the motor on the steering wheel is given by

$$\tau_w = \frac{3}{2} n_g n_p K_e i_q. \tag{7.11}$$

Summarizing, the two working modes are obtained as follows.

- ***Torque–tracking***: the motor controller tracks the desired torque $\tau_{w,d}$ via the control scheme in Figure 7.4. The desired torque is transformed in a desired

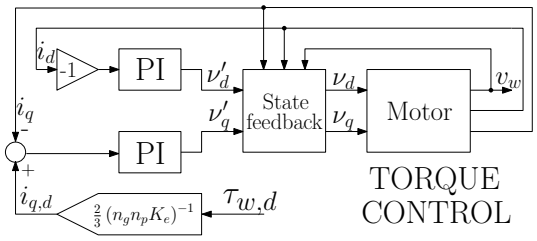

Figure 7.4: Block diagram of the torque control [13].

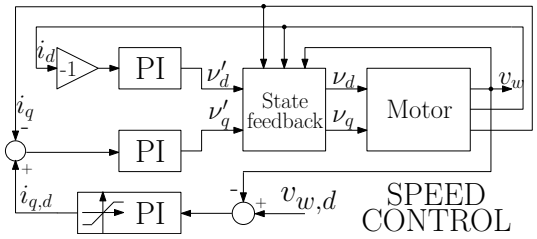

Figure 7.5: Block diagram of the speed control [13].

quadrature current $i_{q,d}$ by inverting relation (7.11). The auxiliary control input ν'_d acts as a PI controller based on the quadrature current error $i_{q,d} - i_q$ in the quadrature current dynamics $\frac{\mathrm{d}i_q}{\mathrm{d}t}$ in (7.10);

- ***Velocity-tracking***: The motor controller tracks the desired velocity $v_{w,d}$ via the control scheme in Figure 7.5 acting on dynamics (7.10). the velocity error $v_{w,d} - v_w$ is fed to a saturated PI controller (endowed with anti-wind up scheme), whose output is interpreted as desired quadrature current $i_{q,d}$, to be tracked by means of the control input ν'_d as in the torque-tracking mode.

It is a well-know result that, since the currents have a first order dynamics forced by a PI controller, the settling-time of the current loop can be made arbitrarily small by proper tuning the PI controller accordingly with the upper bound on the source voltage. In other words, the current dynamics is negligible with respect to the other mechanical variable dynamics (i.e., steering velocity and steering position). Moreover for a standard car-like robot (3.4), also the steering velocity dynamics is negligible with respect to the dynamics of the steering angle φ (and indeed with respect to the vehicle position $[x, y, \theta]$), hence the choice to model the steering velocity u_v as a control input.

7.4.2 Solution overview

The variable stiffness paradigm aims to gradually share the control authority between user and vehicle on the basis of the distance from the path. If the vehicle is far

from the path, the controller is supposed to have the control authority to reduce the path following errors $|l_x|$, $|l_y|$ and $|\tilde{\theta}|$, hence satisfying equation (3.20). Conversely, if the vehicle is close to the path, it gradually releases the control authority to the user. To implement this effect, we use the two working modes of the motor as shown in Figure 7.6.

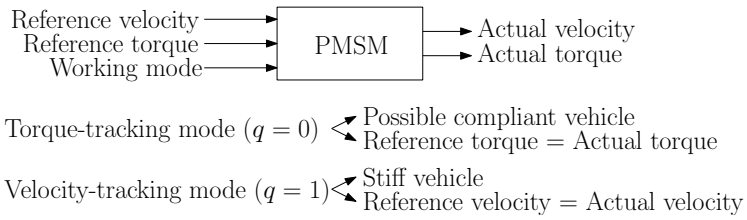

Figure 7.6: Motor schematic behavior [13].

Stiff velocity–tracking

The controller in Figure 7.5 ensures that the actual motor velocity approximately coincides with the velocity reference. In the classical robotic literature, this working mode is considered in the car-like model (3.4) by equation $\dot{\varphi} = u_v$. Obviously, the velocity command u_v (related to the virtual wheel) is reproduced by imposing the actual velocity of the motors via (3.6) as described in section 3.1.1 by means of equation (3.6). When this mode is enabled, the driver commands up to the maximum available current to reproduce any velocity reference, therefore the user perceives a stiff vehicle since any attempt to modify the vehicle motion is rejected as a disturbance. This "stiff" mode will be use to override the user's command in dangerous situations (e.g., whenever an obstacle is detected or in dangerous environment where the path has to be followed with extreme accuracy to guarantee safety).

Compliant torque–tracking

The controller in Figure 7.4 ensures that the actual torque produced by the motor approximately coincides with a torque reference. When this mode is enabled, the dynamic equation $\dot{\varphi} = u_v$ is replaced by the augmented model

$$\begin{cases} \dot{\varphi} & = v_\varphi, \\ \dot{v}_\varphi & = \dfrac{u_\tau}{J_{eq}}, \end{cases} \tag{7.12}$$

where state φ is the position of the steering angle of the virtual wheel, the state v_φ is the steering velocity (that is no more control input) and the actual control input u_τ is the torque provided to the virtual wheel. It is remarked that, when the torque-tracking mode of the motor is enabled, the control input acts on the

second derivative of the steering angle $\ddot{\varphi}$. This model is even more precise than the previous $\dot{\varphi} = u_v$, since the current dynamics is indeed negligible. If the commanded torque is small, the user perceives a soft vehicle since the driver commands limited currents. This mode is then used to vary the vehicle stiffness, i.e., to implement the spring-damper variable stiffness system.
In other words, a motor is supposed to reproduce either a velocity reference u_v or a torque reference u_τ on the basis of the working mode (see Figure 7.6). The working modes are labelled with a logic variable $q \in \{0, 1\}$. In particular, $q = 1$ indicates that the velocity-tracking mode is enabled, while $q = 0$ indicates that the torque-tracking mode is enabled.
To implement the overall variable stiffness path following controller, we have to design:

1. A feedback control law $u_v(\chi, v)$ solving the path following problem (3.34) when the vehicle has full control authority;

2. A feedback control law $u_\tau(\chi, v)$ to implement the spring-damper variable stiffness system to share the control authority. The stiffness of this spring-damper system will vary with respect to the distance from the path, measured as the attitude error e_θ defined by (3.29);

3. The switching law between the two modes, i.e., the conditions under which q jumps from 0 to 1 and vice versa. We will use hybrid system theory [43] to represent the switching behavior of the model between the dynamics $\dot{\varphi} = u_v$ and $\dot{\varphi} = u_\tau$.

In the proposed control scheme the control synthesis of $u_v(\chi, v)$ (i.e., the control input when the velocity-tracking mode is enabled) is based on a backstepping approach, where the steering velocity u_v is designed to ensure that the steering angle φ converges to a desired steering angle φ_d: this desired value φ_d (and its derivative $\dot{\varphi}_d$) will be used to define the equilibrium position of the spring-damper variable stiffness system acting in the torque-tracking mode.

Control requirements

The controller $u_v(\chi, v)$ acts when the motor is the (rigid) velocity-tracking mode. However, it defines also the equilibrium position of the spring-damper variable stiffness system by means of the desired steering angle φ_d and the desired steering velocity $\dot{\varphi}_d$. It is fundamental that:

1. The steering command φ_d avoids the singularity of zero velocity by means of equation (7.5) [12];

2. The path following controller relies on a common strategy seen for all the guidances that exploits an approaching angle $\delta(\cdot)$ satisfying the requirements reported in section 3.2.3;

3. Gradually gives more authority to the robot by means of the attitude error $e_\theta = \tilde{\theta} - \delta(l_y)$ as seen in section 3.2.4.

7.4.3 Rigid path following controller

The stiff path–following controller is designed using the motor in the velocity–tracking mode ($q = 1$), i.e. the classical car–like model (3.4) with dynamics $\dot{\varphi} = u_v$.

Consider the vehicle kinematic model (3.4) rewritten in the dynamic Frenet frame (3.19), then assuming that $v \geq 0$ the passive path following problem (3.34) is solved with $l_\infty = \tilde{\theta}_\infty = 0$ by the control actions

$$\begin{aligned} u_v &= \dot{\varphi}_d - \kappa_\varphi \sin\left(\frac{e_\varphi}{2}\right) - v\,\eta, \\ \dot{s} &= v\,\dot{\xi}, \end{aligned} \tag{7.13}$$

where

$$\begin{aligned}
\dot{\xi} &= \cos\tilde{\theta} + \kappa_x l_x, \\
\ddot{\xi} &= -\sin\tilde{\theta}\left(\frac{v}{d}\tan\varphi - c(s)v\,\dot{\xi}\right) - \kappa_x v\,\dot{\xi}(1 - c(s)l_y) + v\cos\tilde{\theta}, \\
\gamma &= \dot{\xi}c(s) + \frac{\mathrm{d}\,\delta}{\mathrm{d}\,l_y}(l_y)\,\left(-c(s)\dot{\xi}l_x + \sin\tilde{\theta}\right), \\
\varphi_d &= \arctan\left(d\,(\gamma - \kappa_\theta e_\theta)\right), \\
\dot{\varphi}_d &= \frac{d}{1 + \left(d\,(\gamma - \kappa_\theta e_\theta)\right)^2}\left\{c(s)\ddot{\xi} + \frac{\mathrm{d}\,c}{\mathrm{d}\,s}(s)v\dot{\xi}^2 + + \frac{\mathrm{d}^2\,\delta}{\mathrm{d}\,l_y^2}(l_y)\,v\,\left(-c(s)\,\dot{\xi}\,l_x + \sin\tilde{\theta}\right)\right)^2 + \\
&\quad - \frac{\mathrm{d}\,\delta}{\mathrm{d}\,l_y}(l_y)(\ddot{\xi}\,c(s)\,l_x + \dot{\xi}\,\left[\frac{\mathrm{d}\,c}{\mathrm{d}\,s}(s)\,v\dot{\xi}\,l_x + \,c(s)\,\dot{l}_x\right] - \dot{\tilde{\theta}}\cos\tilde{\theta}) - \kappa_\theta\left(\dot{\tilde{\theta}} - \frac{\mathrm{d}\,\delta}{\mathrm{d}\,l_y}(l_y)\dot{l}_y\right)\Bigg\}, \\
e_\theta &= \tilde{\theta} - \delta(l_y), \\
e_\varphi &= \varphi - \varphi_d, \\
\eta &= \frac{4e_\theta\cos\left(\frac{e_\varphi}{2}\right)}{d\cos(\varphi_d)\cos(\varphi)},
\end{aligned}$$

and $\kappa_\theta > 0$, $\kappa_\varphi > 0$, and $\kappa_x > 0$ are constants. Such controller is still independent from the forward velocity v, which means that the solution is completely insensitive to the singularity problem (7.3) as in [12].

7.4.4 Variable–stiffness controller

Controller (7.13) ensures that the vehicle follows the path by overriding the user's command. So this ensures that the front wheels of the *FriWalk* are steered toward the desired orientation independently from the torque applied by the user on the grips. For this reason, whenever a dangerous situation is detected by the *FriWalk*,

the robot can exploit the controller (7.13) to force the user to stay exactly on the path. While, if the environment is safe, this controller is engaged any time that the error $|e_\theta| > \Theta$, where Θ indicates the maximum tolerated error. If the vehicle is close to the path and in a safe region, a different controller is used to maximize the user comfort via a variable stiffness paradigm.

Vehicle compliance

The vehicle compliance is reproduced by enabling the torque-tracking mode of the motor, by introducing in dynamics (7.12) a virtual spring-damper system having stiffness and damping coefficient depending on the vehicle position. The closer the vehicle to the path, the more compliant the spring-damper (i.e., smaller stiffness and damping coefficient). The distance between vehicle and path is measured via the attitude error $|e_\theta|$, then the vehicle is close to the path if $|e_\theta| \leq \Theta \in \left[0, \frac{\pi}{2}\right]$. The equilibrium position of the mass-spring damper is defined by the desired steering angle φ_d and the desired steering velocity $\dot{\varphi}_d$ computed by the "rigid" controller. Hence, the final torque applied by the motor is

$$u_\tau = -\kappa_p \ (\varphi - \varphi_d) - \kappa_v \ (v_\varphi - \dot{\varphi}_d), \tag{7.14}$$

where the positive gains κ_p and κ_v vary on the basis of the distance between vehicle and path. The gains are computed as cycloidal functions of the attitude error, i.e.,

$$\begin{aligned} \kappa_p(e_\theta, \Theta, \bar{\kappa}_p) &= \bar{\kappa}_p \left(\frac{|e_\theta|}{\Theta} - \frac{1}{2\pi} \sin\left(\frac{2\pi |e_\theta|}{\Theta} \right) \right), \\ \kappa_v(e_\theta, \Theta, \bar{\kappa}_v) &= \bar{\kappa}_v \left(\frac{|e_\theta|}{\Theta} - \frac{1}{2\pi} \sin\left(\frac{2\pi |e_\theta|}{\Theta} \right) \right), \end{aligned} \tag{7.15}$$

where the constants $\bar{\kappa}_p > 0$ and $\bar{\kappa}_v > 0$ are the maxima values for the gains κ_p and κ_v. An example of cycloidal profile is reported in Figure 7.7.
Notice that, because of the non–linear behaviour (7.15), for small attitude errors we have $\kappa_p \approx 0$ and $\kappa_v \approx 0$, i.e $u_\tau \approx 0$ in (7.14). In other words, where the vehicle is close to the path, the controller has a limited intensity since the commanded torque is very small. Conversely, if the attitude error $|e_\theta|$ increases, the controller strength increases as well since the gains κ_p and κ_v become large.

The overall controller can be modelled by an hybrid controller whose scheme is reported in Figure 7.8. The switching logic between the two states $q = 0$ and $q = 1$ is ruled by the attitude error $|e_\theta|$ via hysteresis mechanism.

7.4.5 Experiments

The proposed controller has been tested with extensive tests performed with more than 30 users, but not with elderly. In the experiments, the controller gains are $\kappa_x = 1$, $\kappa_\theta = 2$, $\kappa_\varphi = 10$, and $m_\varphi = 2$. The variable stiffness parameter are $\bar{\kappa}_p = 2.5$,

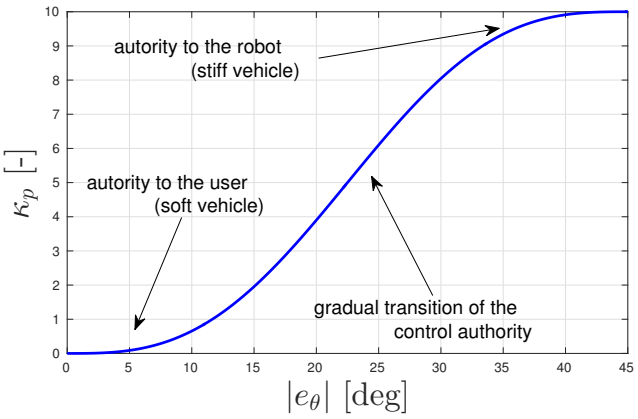

Figure 7.7: Example of cycloidal stiffness with $\bar{\kappa}_p = 10$ and $\Theta = 45°$ [13].

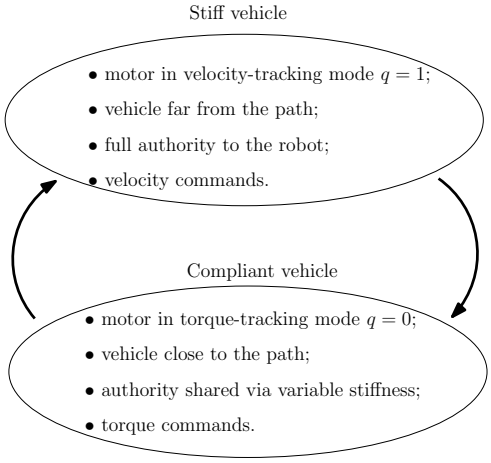

Figure 7.8: Final hybrid controller [13].

$\bar{\kappa}_v = 0.1$ and $\Theta = 70°$. The hysteresis thresholds are set to $V_{\text{out}} = \frac{1}{2}\Theta^2 = 0.75$ and $V_{\text{in}} = 0.14$.

We performed two different kind of test, on in *Tablet* condition, and the other in *No Tablet*. The user was asked to follow a predefined path without having any priori knowledge about it, so he was simply pushing forward the robot fully trusting the guidance system. The GUI exploited for tests in *Tablet* condition is depicted in Figure 7.9, where, with respect to the one used for the other guidance strategies with elderly (represented in Figure 5.7), is more complex and filled by extra information. In fact, in the bottom, a top view representation of the *FriWalk* is shown, in order to give to the user always a vision of the map from it's point of view (like in standard navigators). The orange rectangles represents fixed obstacles (e.g., walls and pillars), the black filled circle represents the QR code attached on the ground to localize the

robot (as explained in section 4.2.4). Moreover the path to follow is depicted with a solid thick black line, that becomes green as the *FriWalk* moves forward on the path. Furthermore, at the top of the GUI, an arrow that is orientated according to e_θ is used to show to the user the correct direction that he/she has to take. Such arrow goes from green to red according to $|e_\theta|$.

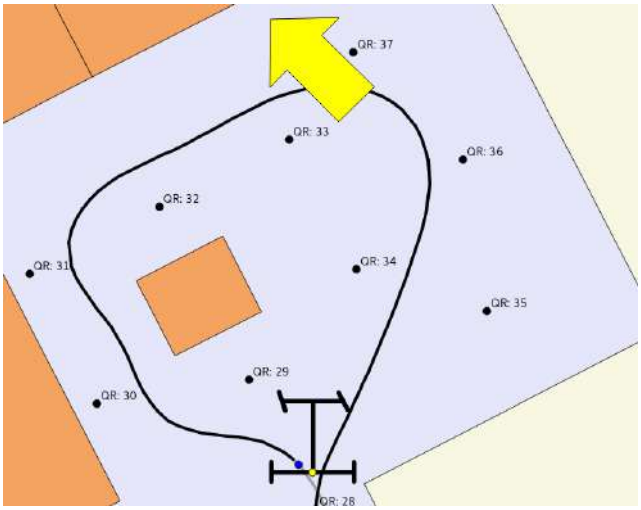

Figure 7.9: GUI used for the experiments in *Tablet* conditions. The orange rectangle represents the obstacles, while the filled black circle the position of the QR codes used for localizing the robot (a). [13].

The experimental results are depicted in Figure 7.10, where the trajectory followed in four different experiments is reported with the reference path. From both figures it is possible to appreciate the efficiency of such controller that, either in *Tablet* (a) and in *No Tablet* condition (b) is able to let the user follow the path with good accuracy. From Figure 7.10–(b), hence in *No Tablet* condition, we can notice how each turn is performed with a certain delay, causing a path–following error. This behaviour is completely expected since the user was asked to push forward the *FriWalk* since the path was unknown. However, the resultant path–following error is larger than the one obtained with the stiff controller proposed in [12] and reported in Figure 7.2. This is due to the nature of the variable controller (7.14) [13] that is characterized by a smooth behavior in the narrow of the path. By looking at Figure 7.11–(b) we can see the time evolution of the controller. At the beginning, the user lies in the proximity of the path so the current requested by the controller is very limited. Around 5s of the experiment the user is requested to steer left (first turn of the reference path Figure 7.10) so that the desired currents i_r^{des} and i_l^{des} gradually increase as the *FriWalk* departs from the path (larger e_θ). At the beginning the current is low so that the user overrides it, with the consequence that he/she goes straight on. As the error e_θ gradually grows, the current i^{des} grows as

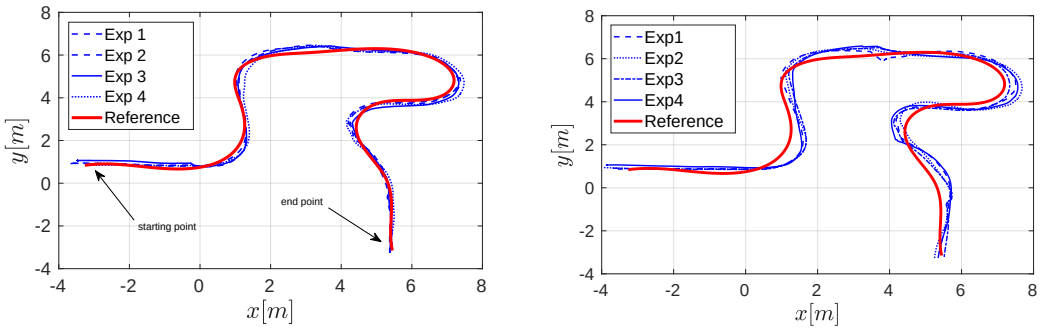

(a) Tablet. (b) No Tablet.

Figure 7.10: Trajectory followed with and without tablet [13].

well, stiffening the steer. If the user proceeds overriding the controller, as soon as the attitude error $e_\theta = \Theta$, the stiff controller (7.13) kicks in ($q = 1$) so that it is impossible for the user to override the control action. This effect can be noticed in Figure 7.11–(a) where, as soon as $q = 1$ we get the effect that $\varphi(t) = \varphi^{\text{des}}(t)$. As soon as the error $|e_\theta|$ goes below the threshold, then the current control is again engaged ($q = 0$).

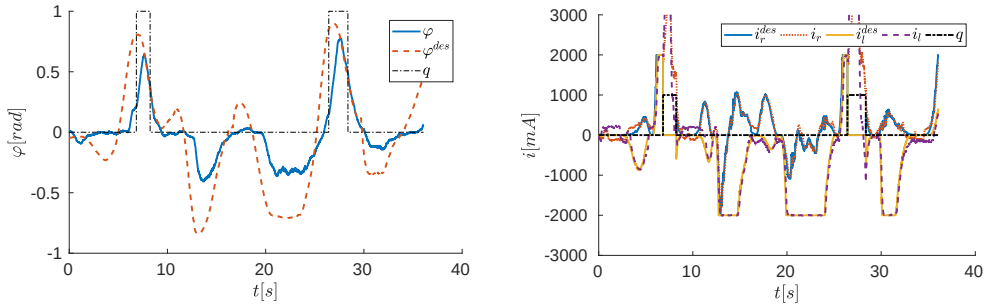

(a) *Virtual steering angle.* (b) *Desired and absorbed left and right current.*

Figure 7.11: Time evolution during Exp4 with *No Tablet* of Figure 7.10–(b) [13].

Conversely, in *Tablet* condition we have that the user is able to follow the path with high accuracy (Figure 7.10–(a)) without the request that the stiff controller kicks in, as visible from Figure 7.12.

7.4.6 Conclusions

In [13] we presented a compliant control algorithm for a passive robotic vehicle equipped with front steering wheels. The algorithm is completely insensitive to the

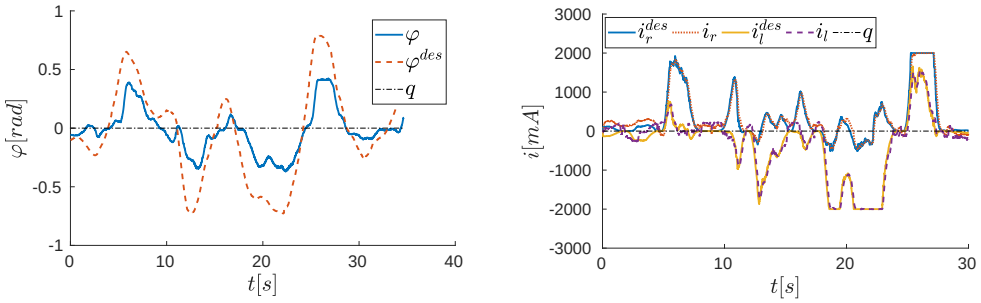

(a) *Virtual steering angle.*

(b) *Desired and absorbed left and right current.*

Figure 7.12: Time evolution during Exp4 with *Tablet* of Figure 7.10–(a) [13].

singularity arising for zero velocity, that otherwise considerably worsens the performance in a real vehicle. Moreover, such controller gives to the user a certain degree of freedom in the movement, highly increasing the human–robot interaction. Thanks to the nature of the variable stiffness controller the user is able to follow a predefined path without having any knowledge about it, with and without a GUI. The comfort of such guidance system is very high, since no abrupt interventions occur, and the feeling of the control action is very pleasant, since it gradually intervenes to steer the vehicle toward the desired path.
To better the comfort of the user with such strategy, we may apply a control logic that varies the intervention of the "stiff" controller according to the dangerousness of the surrounding environment.

Chapter 8

Probabilistic controller

All the guidance strategies presented in the previous chapters (*BangBang*, *Haptic*, *Combined*, *Simulated Passivity* and front–steering strategy) are particular solution for path–following problem using a robotic walking assistant. One of the requirements to ensure that this algorithm actually works is that en exact localization of the robot in the environment is provided. An accurate localisation is obtained either with a heavy infrastructure (e.g., an active sensing system deployed in the environment or deploying landmarks in known positions) or using SLAM approaches with a massive data collection.
The solution to general path–following problem is typically designed by supposing that the localisation algorithm is "accurate enough" to produce a negligible error in the estimate of the vehicle state [70]. Assuming a good localisation accuracy is fairly acceptable for robots relying on exogenous sensor readings (absolute measures) always or most of the times. Indeed, endogenous sensors (relative measures) are affected by the well known dead-reckoning effect that produces an unbounded growth of the position uncertainty [17, 91]. Several ways have been proposed to improve the accuracy of the robot localisation, such as optimal deployment of landmarks to meet a desired target accuracy [25, 90, 123], or using active sensors [83, 61, 88] or mapping detected landmarks [109, 74]. Whatever the strategy used to deploy and use markers in the environment, a certain fact with this type of solution is that the absolute position measures come intermittently. It is well known [112, 93] that closing a control loop with intermittent observation can lead to a poor performance (possibly even to instability) if the average rate is not sufficient to compensate for the system dynamics. On the other hand a massive deployment of landmarks is inconceivable in realistic environments (e.g., a museum, or a shopping mall). Authority sharing offers an elegant and unexpected escape from this quandary. The key observation is that even a user with mild cognitive impairments is able to maintain a direction of motion when the environment does not require choices (e.g., a corridor). Only in presence of decision points (e.g., bifurcations, cross-roads, doors) is a constant intervention of the system required. We can translate this simple idea

into a design principle: use a heavy infrastructure (dense landmarks) when a close support is required for the user and a light infrastructure (i.e., sparse landmarks) when we can shift the authority to the user. This natural strategy has to be complemented by a control algorithm that decides the balance of the authority according to the accuracy of the information on the system state, which is the most important contribution of the paper. Specifically, we propose a hybrid control scheme with two states: robot in control and human in control [77]. The control scheme is Lyapunov based and gives the authority to one of the two states according to the available localisation precision or when the deviation from the path becomes relevant. The performance on the path following maximum error are experimentally characterised as a function of the uncertainty growth due to dead-reckoning. This could allow us to offer performance guarantees for known hardware and the environment are known. To the best of the Author's knowledge, this is the first work that directly considers data uncertainties to rule the controller behaviour, being most of the literature devoted to the compensation of parametric model uncertainties (e.g., [4]) or to the disturbance rejection (e.g., [27]).

8.1 Localization issues

Of course, when intermittent observations are adopted, as in the localisation system running on the *FriWalk* and reported in [93], the effect of the feedback control can be highly wrong and, hence, the control should be given to the user. To implement this authority-sharing, how the localisation accuracy is derived and a description of the controller implemented is needed.
Let us denote $\hat{a}$ the estimate of the quantity a and σ_a the corresponding standard deviation. With localisation algorithm we intend the execution of an estimator that provides "suitable estimates" of $\hat{x}, \hat{y}$ and $\hat{\theta}$ of the vehicle states of (3.1). As seen in section 4.2.4, for the *FriWalk* the available sensors are encoders mounted on the rear wheels (odometry-based localisation) and a camera reading landmarks (QR codes placed on the floor, the ceiling or on the walls) whose positions in the map are known. The odometry data are always available but affected by drift. The measures of vehicle position and attitude obtained by the landmarks are absolute but available only when a landmark is in the field of view of the camera. The two measures are fused using a Bayesian estimator, such as an Extended Kalman filter [17]. The estimator returns minimum variance estimates $\hat{x}, \hat{y}$ and $\hat{\theta}$ of the vehicle state and the corresponding estimation error covariance matrix

$$P = \mathrm{E}\left\{[x - \hat{x}, y - \hat{y}, \theta - \hat{\theta}]^T [x - \hat{x}, y - \hat{y}, \theta - \hat{\theta}]\right\}, \tag{8.1}$$

where $\mathrm{E}\{\cdot\}$ is the expected value operator.

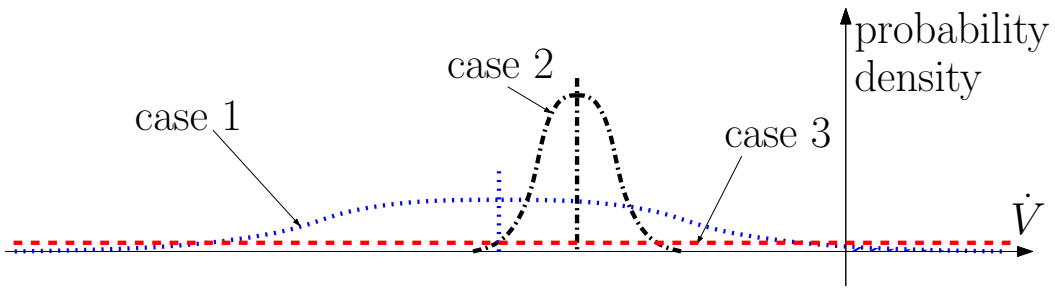

Figure 8.1: Examples of distributions of Lyapunov function derivatives [77].

8.2 Probabilistic controller idea and design

The controller (3.32) ensures asymptotic tracking of the path in ideal conditions (i.e. the estimation error of χ is zero). Intuitively, if the estimation error is limited, controller (3.32) is expected to ensure that the path is followed with an error due to (3.31). However, if no landmark is detected, hence no absolute measure is available, the localisation is affected by dead-reckoning of odometry and hence the estimation error grows potentially unbounded. Hence, the path following error grows as well. In [77] we proposed a solution that manages the shift of the control authority between the robot and the user and how this authority-sharing idea can be formally modelled using tools from hybrid systems [43]. First of all in [77] the *controller reliability* has been defined, hence the probability that the controller action $\omega^\star(\chi)$ ensured convergence, therefore that $\dot{V} < 0$.

Definition 1 (Controller reliability)**.** *Given $\Gamma \leq 0$, the reliability $p_\Gamma(\hat{\chi})$ of a control action $\omega(\hat{\chi})$ is given by probability*

$$p_\Gamma(\hat{\chi}) = \Pr \dot{V} < v\Gamma, \tag{8.2}$$

where $\Pr \dot{V} < v\Gamma$ denotes the probability that the event $\dot{V} < v\Gamma$ takes place.

The constant $\Gamma \leq 0$ is a minimum convergence speed that the controller is required to guarantee. Roughly speaking, the reliability $p_\Gamma(\hat{\chi})$ is the probability that the controller ensures at least such convergence speed. Scaling Γ by v is not strictly necessary but it comes handy since $\dot{V}$ is linear with respect to v as well. In fact, if the controller were deterministic as in (3.31), we would get $\dot{V} < v\Gamma \iff -v\kappa e_\theta^2 < v\Gamma \iff -\kappa e_\theta^2 < \Gamma$.
The idea proposed in [77] is to allocate the control authority on the basis of the controller reliability (8.2). To intuitively describe this approach, we compare `case 1` and `case 2` in Figure 8.1. Suppose for simplicity that $\Gamma = 0$ in the definition of controller reliability (8.2). The mean value of $\dot{V}$ in `case 1` is smaller (i.e. larger convergence rate) than `case 2`, while its covariance is much larger than the covariance of `case 2`. This implies that the reliability of the controller is larger in `case`

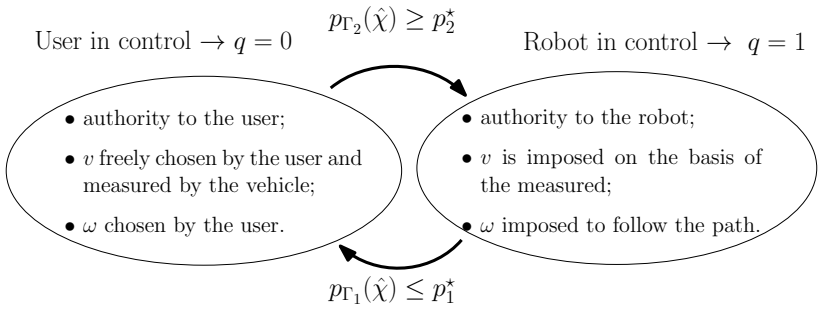

Figure 8.2: Control authority sharing of the hybrid controller (8.4) [77].

2, since the probability to get $\dot{V} < 0$ is larger than `case 1`. Consider also `case 3`, where the covariance tends to infinity, i.e. absence of information. Since the controller reliability is in this case 0.5, any action the robot performs has 50% chance of reducing the attitude error e_θ.
The control authority is then shared between the robot and the user on the basis of the controller reliability, and the idea of the switching rule of [77] is depicted in Figure 8.2. To properly implement a smooth transition, we define a hysteresis mechanism by formulating the control law as a hybrid system [43]. More in depth, let $q \in \{0, 1\}$ be a logic variable defining who retains the control authority. If $q = 0$ the controller reliability is small and then the user is in control of the vehicle, i.e. the vehicle actuators are not active (*user in control* state in Figure 8.2). While if $q = 1$ the controller reliability is large and hence the robot is in control (*robot in control* state in Figure 8.2 and the control action (3.32) is applied to steer the vehicle towards the path). The hysteresis is defined on the basis of two constants $\Gamma_2 > \Gamma_1 \geq 0$ representing convergence speed thresholds. Let $p_1^\star \in (0, 1)$ and $p_2^\star \in (0, 1)$, $p_1^\star \leq p_2^\star$, be the minimum tolerated reliabilities that, respectively, activate and disengage the controller. The overall controller is formalised as the following hybrid system having state $[e_\theta, q]^T$.

$$\begin{cases} \dot{q} &= 0, & [e_\theta, q]^T \in \mathcal{C}, \\ q^+ &= 1 - q, & [e_\theta, q]^T \in \mathcal{D}, \end{cases} \tag{8.3}$$

where $\mathcal{C} := \mathcal{C}_0 \cup \mathcal{C}_1$ and $\mathcal{D} := \mathcal{D}_0 \cup \mathcal{D}_1$ are the flow and the jump set respectively, where

$$\begin{aligned} \mathcal{C}_0 &= \{p_{\Gamma_2}(\hat{\chi}) \leq p_2^\star \ \wedge \ q = 0\}, \\ \mathcal{C}_1 &= \{p_{\Gamma_1}(\hat{\chi}) \geq p_1^\star \ \wedge \ q = 1\}, \\ \mathcal{D}_0 &= \{p_{\Gamma_2}(\hat{\chi}) \geq p_2^\star \ \wedge \ q = 0\}, \\ \mathcal{D}_1 &= \{p_{\Gamma_1}(\hat{\chi}) \leq p_1^\star \ \wedge \ q = 1\}. \end{aligned} \tag{8.4}$$

This way, the angular velocity of the vehicle is

$$\omega = qv\left(\gamma(\hat{\chi}) - \kappa\hat{e}_\theta\right) + (1 - q)\omega_{\text{user}}, \tag{8.5}$$

where ω_{user} is the angular velocity that the user imposes when he/she has the control authority and $v(\gamma(\hat{\chi}) - \kappa\hat{e}_\theta)$ is the angular velocity that the robot applies to ensure convergence, hence $\omega^\star(\chi)$ of equation (3.32).

8.3 Experiments

The experimental results have been collected using the *FriWalk* (Figure 4.2). The controller parameters adopted in the experiments are: $\kappa_x = 1$, $\kappa = 0.5$, $p_1^\star = 0.7$, $p_2^\star = 0.9$, $\Gamma_1 = -0.004$ and $\Gamma_2 = -0.137$. To maximize the user comfort, the probability $p_1^\star$ has been reduced to give more authority to the controller. Similarly, both the mean tolerant attitude errors Γ_1 and Γ_2 have been set to 5° and 30°, respectively.
The experimental scenario is the Dept. of Information Engineering and Computer Science of the university of Trento, comprising corridors and rooms Figure 8.3. The starting point, of the *FriWalk* is inside one room, represented with a blue circle in Figure 8.3. Following the idea reported at the beginning of section 8.2, the landmarks are placed only in proximity of difficult decision points, i.e. landmark #1 is in the starting room in the vicinity of the exit door, landmark #2 has been collocated at the beginning of the corridor, while landmark #3 is deployed before two intersecting corridors. In the corridor, due to the particular desired path considered (dash-dotted black line of Figure 8.3), has no landmark since the only available choice is to maintain on the course. The depicted yellow solid triangle pointing forward represents the field of view of the camera attached to the vehicle and used to detect the landmarks, while the dotted blue ellipses represent the localisation error covariance P_{xy} (upper 2×2 matrix of (8.1)) in selected positions. To better analyse the experiments, the path is divided in the following parts:
Sub-path A: the user is in control of the robot ($q = 0$ in (8.3)) and pushes the *FriWalk* outside from the room since the localisation error is very high (i.e. kidnapped robot problem, dashed green line in Figure 8.3).
Sub-path B: when the vehicle detects a landmark in position $B^\star$, $p_{\Gamma_2}(\hat{\chi}) > p_2^\star$ and the controller (8.4) enters in the jump set $\mathcal{D}_1$ so that $q \to 1$. The robot is hence in control ($q = 1$ in Figure 8.2). The Gaussian probability density function (pdf) of $\dot{V}$ in point $B^\star$ is reported with dash-dotted black line in Figure 8.4. During the *robot in control* state ω is imposed by the control law and steers the walker toward the desired path (red solid line in Figure 8.3). At point $B^\dagger$, $p_{\Gamma_1}(\hat{\chi}) < p_1^\star$ and the authority is given back to the user since $q \to 0$ (the solid green Gaussian pdf in Figure 8.4).
Sub-path C: in this section the user is in control and the covariance P_{xy} grows (no landmark detected), hence the pdf flattens, so that it is more difficult for the controller to kick in. Nonetheless, at the end of sub-path **C**, the orientation error becomes so large that $p_{\Gamma_2}(\hat{\chi}) \geq p_2^\star$ and the controller intervenes to align the user toward the path.

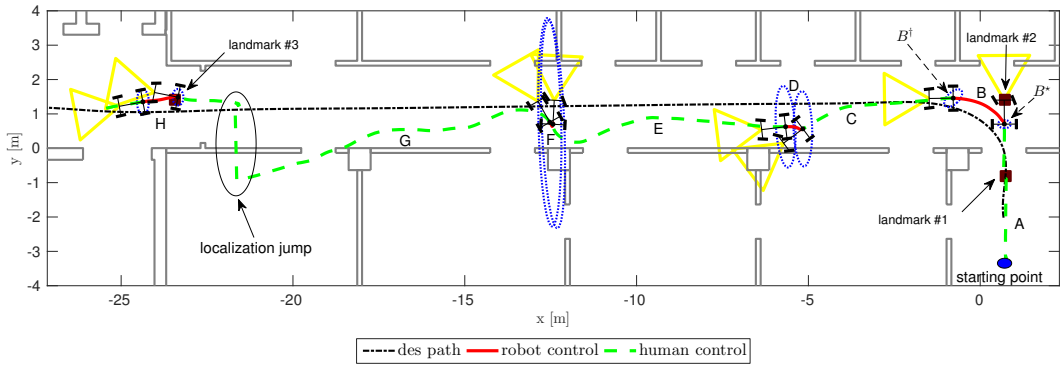

Figure 8.3: A sample trajectory of the experimental trial with localisation covariance depicted in selected points. The picture reports the desired path (dash-dotted line) and the estimated trajectory obtained by the localisation algorithm (dashed line). This trajectory is divided into sub-paths for reading easiness.

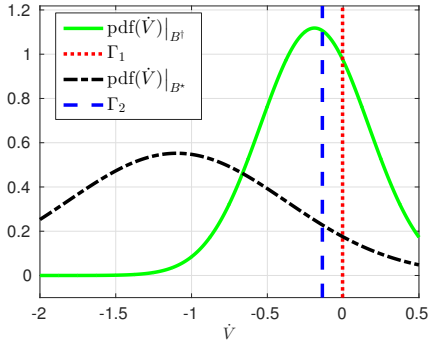

Figure 8.4: Distribution of $\dot{V}$ at the beginning of section $B \rightarrow B^\star$ (dash–dotted black line) and at the end of section $B \rightarrow B^\dagger$ (solid green line).

Sub-path D: due to the shape of the Gaussian, which is more flat than in sub-path **B**, it takes a smaller time to reach the condition $p_{\Gamma_1}(\hat{\chi}) < p_1^\star$. However, the user receives the input to realign towards the desired path.
Sub-path E: the user has the possibility to move freely since the covariance of the localisation error is very high. At the end of this sub-path the user tried to perform an U-turn, but the controller do not allow this manoeuvre as at the end of Sub-path **C**.
Sub-path F: the same of sub-path **D**, but even shorter.
Sub-path G: from the beginning of this sub-path, no landmark is in view for 12.5 meters, so that the uncertainty grows unbounded. Notice that the walker wrongly localises through a wall, which is obviously not true: however, if the *robot in control* was active, the vehicle would be guided over the desired path and hence, aligning the green dashed line over the dash-dotted desired path, the *FriWalk* would be steered

towards the wall on the other side of the corridor. Instead, after landmark #3 is detected and the uncertainty drops, it can be seen that the vehicle was correctly very close to the path, guided by the user.
Sub-path H: finally, the controller takes the control of the robot since $p_{\Gamma_2}(\hat{\chi}) \geq p_2^\star$.

8.4 Conclusions

In [77] we have presented a control strategy for shifting control authority between a human user and a controller for robotic navigation assistance. In this context, the problem of assisting a person can be seen as an instance of path–following problems, for which most of the available solutions currently require an accurate localisation of the vehicle in the environment. This requirement comes along with the need for deploying a heavy infrastructure of landmarks in the environment, which is not always feasible in such spaces as museums or large shopping malls. Our idea to solve the problem is to use a precise localisation only when needed (i.e., in proximity of complex decision points) and leave the guidance responsibility to the user when the task is relatively easy to do (i.e., just keep going along a direction). This strategy requires an effective way to shift the control authority to the user when the localisation precision is low, and give it back to the controller when it increases (i.e., when more landmarks are in sight) or when the user is compromising the control goals (i.e., turning backwards). This idea has been formalised with a hybrid control design.
There are several open problems that deserve future investigation. From the theoretical point of view, the most interesting problem that needs to be addressed is to offer "certifiable" performance guarantees based on the knowledge of the vehicle and the environment. Another important goal is to test the idea with a number of actual users and carry out a quantitative and qualitative study on their performance and impressions.

Part III

The *FriWalk* as a rehabilitation device

Chapter 9

The rehabilitation device (confidential)

In the context of the ACANTO [2] project, a pilot study have been carried out to evaluate the clinical validity of the *FriWalk* used as a rehabilitation tool in a clinical environment [102]. In fact, it is largely known that hospitalization adversely affects the functional outcomes of older adults due to patient's inactivity, even in people with non–disabling conditions and with a relatively good baseline function [58, 125]. Studies have demonstrated significant decreases in muscle mass, which is a major risk factor in the hospitalized older person for functional deterioration [79]. For example, 50% of patients who suffer a hip fracture cannot recover their previous functional status experiencing a loss of independence. This occur even in elders with good functional status. There is considerable evidence to support the hospitalization with prevention programs like multicomponent physical exercise, rehabilitation and education to avoid functional decline, falls and frailty. Maintaining the autonomy and independence of the elderly should be a priority in health care services.

To this purpose the ACANTO project proposes the use of a rehabilitation version of the *FriWalk* to supports the execution of controlled physical activities during hospitalization, aiming the following clinical objectives:

1. mitigate functional deterioration whilst hospitalization;
2. recover functional performance earlier after hospitalization.

9.1 The *FriWalk* rehabilitation platform

In our clinical pilot [102] the *FriWalk* has been exploited as a therapeutic tool, endowed with a series of technological components allowing patients to perform five physical stimulation activities:

1. Walking to foster early mobilization;

2. Standing on one leg to work on balance;
3. Standing on the tip–toes to strengthen the lower limbs' muscles and to work on balance;
4. Isometric exercises;
5. Standing–up from a chair to strengthen the lower limbs' muscles

The shape of the rehabilitation version of the *FriWalk* is reported in Figure 9.1, which has been obtained by the removal of the front actuators since they are useless for rehabilitation purposes. Beyond the maintenance of the rear mechatronic components, the robot has been equipped with extra sensors, i.e.:

- A stereocamera looking forward exploited for skeleton pose estimation;
- A stereocamera looking backward and downward for gait analysis;
- Grip pressure sensors to understand if the user is holding the grips or not.

Figure 9.1: Rehabilitation version of the *FriWalk* exploited for pilot study [102].

The user can directly interact with the *FriWalk* by means of a tablet, which shows in real–time the exercises evolution. Moreover the *FriWalk* is also accompanied with a telemedic platform for the clinical professionals to prescribe functional decline prevention programs tailored to the patients' needs and to assess their evolution by watching a reproduction on how the patients performed their exercises.

Interaction systems for both patients and clinical professionals have been iteratively designed through a co–creation process. A first approach was first designed taking into consideration the needs of the final users. This initial design was taken to a trial session in which potential final users participated to collect their input. The insights collected were finally used to refine the prototypes before the implementation.

The rehabilitation version of the *FriWalk* permits then to record and estimate the performance of the user performing different exercises. The description of such activities is listed in the following sections.

9.1.1 Isometric/isotonic exercise

The goal of the isometric/isotonic exercise is to strengthen the leg muscles of the patient. This type of exercise is typically prescribed by physicians for patients that live in nursing homes or are recovering in a clinic. The patient is expected to perform a number of knee-bending repetitions while seated. Each repetition is timed. The patient is required to hold the leg extended with the knee at above a minimum angle for a number of seconds. With *FriWalk* the exercise is automated enabling the parallel collection of body posture information. The walker is tasked to remind the patient with audio and visual alerts that he must perform the exercise prescribed by the physician and invites him/her to complete it in preset intervals. As soon as the patient accepts the invitation, the caregiver moves the walker to the optimal position for the measurement. To achieve that, the system guides the caregiver to the proper position with on-screen visual indicators. The isometric/isotonic exercise is initiated and the *FriWalk* gives audible and written instructions to the patient. The patient is instructed to lift and hold each leg up a preset number of times alternating left and right. During each repetition, the patient is required to hold the left up for a given number of seconds.

9.1.2 Tip–toe stand exercise

This exercise aims at strengthening calf muscles and the stability, which are fundamental for maintaining the patient's autonomy and preventing falls. The patient is expected to perform a number of repetitions on the tip-toes stand. Each repetition is timed. The patient is required to hold the position, keeping the heels off the floor, for a number of seconds. During this holding stage, the patient breaths regularly. After each repetition, the patient places the heels back on the floor delicately so as to avoid any impact on the back. With the support of the *FriWalk*, the automatic collection of feet posture information is achieved. Similar to the previously described exercises, the walker provides audio and visual information to the patient in order to perform the exercise prescribed by the physician.

9.1.3 Single–leg stand exercise

This exercise is mainly performed to enhance balance, as it requires the ability to keep the centre of gravity over the ankles while standing. It will also strengthen the ankles and hips for improved stability. The patient is requested to perform a series of timed repetitions per leg. At each repetition, the patient is required to hold the position, keeping the foot off the floor, for a limited amount of seconds. The physician may prescribe the duration and amount of repetitions individually for each leg, according to the specific patient physical conditions. Additionally, the use of handlers can be prescribed, for balance support. The *FriWalk* automatically collects information from the standing pose of the patient. As previously described, the walker assists the patient providing audio and visual information along the exercise execution.

9.1.4 SPPB test

The Short Physical Performance Battery (SPPB), whose phases are depicted in Figure 9.2, is a group of measures that combines the results of the gait speed, chair stand and balance tests. It has been used as a predictive tool for possible disability and can aid in the monitoring of function in older people. The SPPB has been shown to have predictive validity showing a gradient of risk for mortality, nursing home admission, and disability. Such test is characterized by three steps:

1. In the first test (*Balance Test* – phase (1) of Figure 9.2) the *FriWalk* is positioned in front of the user to take measurement and offer support in case of balance loss. The task is required to keep the feet in a well specified position without holding the grips of the FriWalk. The gait sensor gather the information about the feet posture and analyses the test performance. If the feet have moved or the user touches the grips, then the test fails. If the tests for all the positions are satisfied, then the balance test is passed; The tablet and onboard speakers of the walker are used to interact with the patient and provide instructions;

2. The second test (*Gait Speed Test* – phase (2) of Figure 9.2) measures the time required to walk 4 meters at a normal pace. Similar to the first test the *FriWalk* monitors the patient through its onboard cameras and provides audible and visual instructions. In case that the patient succeed in the first test, then the user has to walk autonomously, while the *FriWalk* follows him/her at a certain distance gathering walking parameters. Conversely, if the user not succeed the first test, then he/she has to walk exploiting the walker that gathers gaits parameter;

3. The last test (*Chair Stand Test* – phase (3) of Figure 9.2) measures the time required to perform five rises from a chair to an upright position as fast as possible without the use of the arms. This test is based on the automatic human

body model analysis capabilities of the platform. The *FriWalk* is placed opposite to the patient who is sitting on a chair. The patient is being monitored by the *FriWalk*'s front facing camera and he/she receives audible instructions from the walker's speakers. After the execution of the exercise, the physician can review the specific patient performance, which is replicated from the skeleton information recorded.

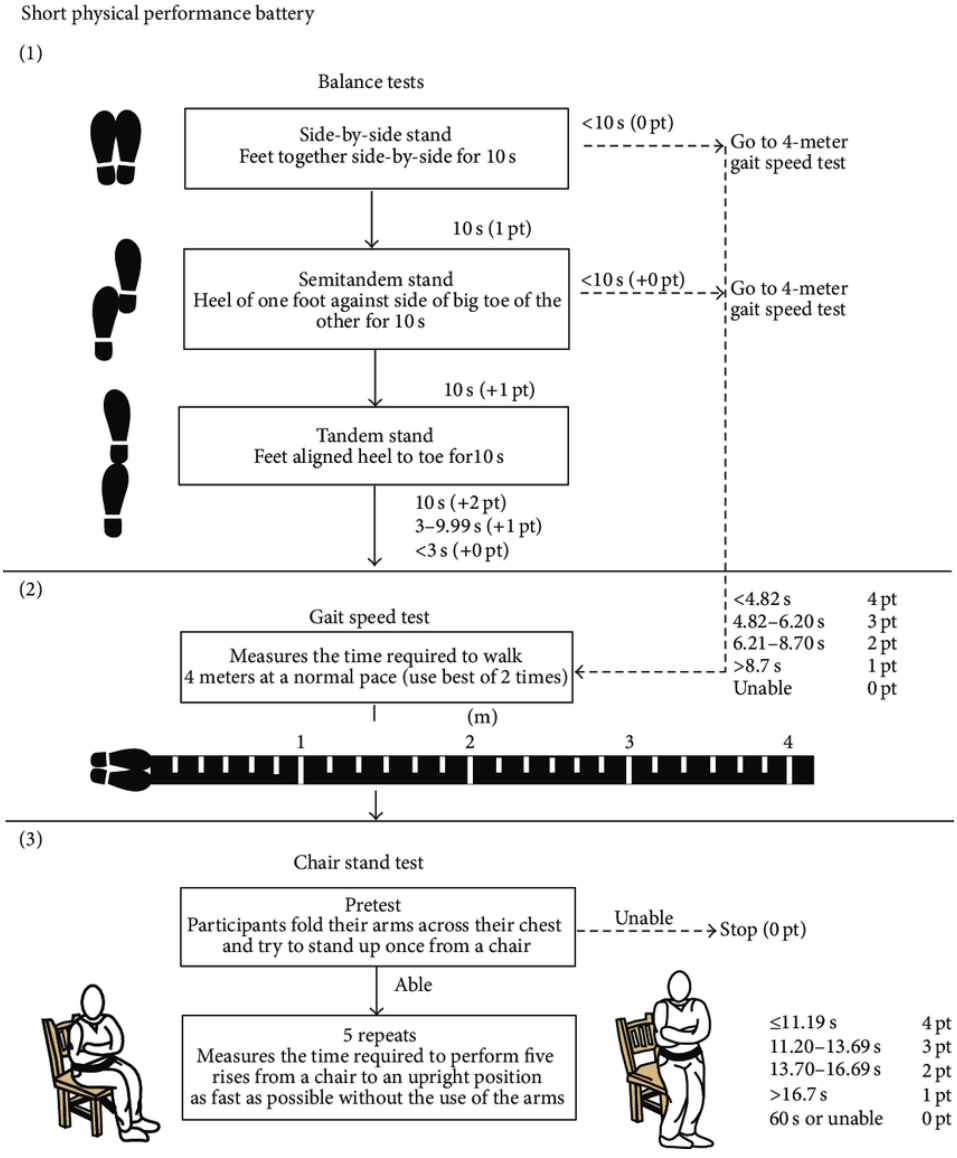

Figure 9.2: The different phases of the SPBB test.

9.2 Therapeutic activities

During the pilot [102] many activities have been carried out with patients. Such therapeutic activities are of two types: orthogeriatric activities and therapeutic activities.

9.2.1 Orthogeriatric activities

Orthogeriatric activities are executed in the hospital (e.g., while the patient is healing from a trauma). For all orthogeriatric activities, the patient receives an invitation on the tablet, which can be accepted only if a caregiver is available for a direct supervision (the caregiver can be a paramedic, a relative or a close friend of the patient). If a caregiver is not available, either the exercise is simply skipped or it is prohibited to execute the exercise alone because being too dangerous. In the latter case, a mechanism of authorization/confirmation by the caregiver is adopted. The orthogeriatric activities supported by the *FriWalk* are the following:

- Walk x minutes / one hour: in this scenario the walker reminds and invites the user to take a walk. The user exploits the robot as a standard walker to move wherever he wants, meanwhile sensors gather information about the distance covered by the user and the time of the walk;
- Isometric/isotonic exercise: the walker is positioned in the environment for the correct detection of the user. The user is required to perform specific isometric exercises while the skeleton sense his/her performance.

9.2.2 Therapeutic activities

Therapeutic activities are executed in a protected residence. In this case the user is allowed to make a personal use of the walker (at least for some time), without the constant supervision of a caregiver (although one should always be in easy reach). The activities designed for the *FriWalk* are the following:

- Walk certain X metres/day at a velocity v: the robot, periodically, reminds the user about the distance and the velocity that the user has to walk today. The user exploits the robot as a standard walker while the sensors gather the desired information. Meanwhile, the graphical user interface shows the total distance to be walked, the travelled and pending distance and a speedometer. Whist the user walks the *FriWalk* activates environment monitoring and obstacle avoidance.
- Standing on one leg: the robot, periodically, reminds the user about the exercise that he/she has to perform. So that, the user performs the test, meanwhile the skeleton sensor gather information about the user performance; this information is consolidated within the user's profile and periodically reviewed by the physicians;

- Standing on the tiptoes: the robot, periodically, reminds the user about the exercise that he/she has to perform. In this case the gait components analyses the user during its exercise and evaluate the user performances.

9.3 Overview of the experimental validation

The clinical evaluation of the *FriWalk* took place for 17 months. The pilot study started with the recruitment process that was performed by clinical researchers and physicians who applied screening tests following inclusion and exclusion selection criteria. During such period, a total of 42 patients with an average age of 88 were recruited. All patients were assessed at admission, at the first, third and sixth month and after discharge to evaluate the impact of the intervention at medium–term.
The *FriWalk* enables the automation of a number of geriatric tests and exercises that are traditionally performed by the patients with the help of physicians or other trained hospital personnel.

The *FriWalk* has been deeply assessed by the patients and the clinical professional in terms of:

- **Usability**: using the System Usability Scale (SUS) [23], which consists in 10 items, that can be evaluated from 1 (fully disagree) to 5 (fully agree), providing a total score up to 100;

- **User experience** (UX): evaluated with a questionnaire that does not provide an overall score but a score per 6 different categories: attractiveness, perspicuity, efficiency, dependability, stimulation and novelty. The score for each category is calculated by averaging the different items within it; each item's value ranges from -3 to 3, where extreme values represent two opposite concepts (e.g. attractive vs. unattractive);

- **Acceptance**: evaluated using the Technology Acceptance Model (TAM) and a customized short qualitative interview for the clinical professionals and patients respectively. Final scores are calculated by averaging. The acceptance interview to evaluate patients' acceptance consisted in the following open questions to assess perceived ease of use, usefulness and emotions respectively:

  - Which were the main problems you faced when using the walker?
  - What is your general opinion of the walker?
  - How did you feel when you used the walker?

9.4 Results and discussions

9.4.1 Usability

Patients

The results of the usability test (SUS) performed with the patients scored an average of 52.86/100 (SD 14.37). This result, that can be considered below average since it is lower then 68/100[1]. This relatively low scoring can be mainly associated to the fact that the *FriWalk* was still at a prototype stage brought in a real scenario. Several technical problems associated to hardware limitations influenced the assessment of the robot, e.g.:

- The *FriWalk* needed to be charged for the whole night. It happened many times that the caregiver forget to charge it, causing the impossibility to let the patient perform the exercises the next day;
- Due to a problem of the tablet, it was necessary to recharge it independently, which caused some unavailability issues;
- One of the computer installed within the *FriWalk* used for experimentation entered by default in hibernation if the system was not used for 2–3 hours, causing it to be unavailable to patients. This issue was detected and solved very close to the end of the experimentation.

In any case, the mean SUS score indicates that although the usability of the *FriWalk* is not yet above average, it is still usable. Patients, with the help of their caregivers, were able to use the *FriWalk* despite the technical problems that arose. The items that have been evaluated as most negative are related to the perception of the user about the ease of use, the need of technical support and the amount of learning needed to use the system. These three negative evaluations seem to be inevitably associated to the instability of the *FriWalk*, which was at a prototype stage (especially at the beginning of the clinical evaluation).

Clinical professional

The SUS score evolution along the clinical trials provided by the clinical professional about the *FriWalk* is depicted in Figure 9.3.
At the beginning of the clinical validation the SUS score was 62, close to the 68/100 to be considered above average, but at the end the assessment highly increased. This growing trend is really promising and shows that the perceived usability increases with the time of use of the *FriWalk*. Furthermore the score has also been influenced by many technical issues solved during the clinical validation with patients.

[1] https://www.usability.gov

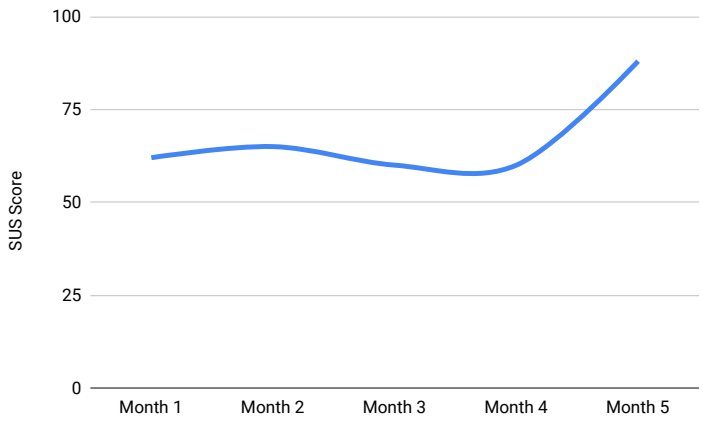

Figure 9.3: Evolution of the SUS score provided by the professional during the experimental phase [102].

9.4.2 User experience

The user experience (UX) was only assessed by the clinical professional in charge of delivering care to the patients using the *FriWalk*. Patients were not evaluating the device from this perspective to avoid overloading. As done for the usability evaluation, the assessment tool was administered monthly. The results showed that almost all individual items were positively evaluated, while only 5 items over 26 have been catalogued as neutral. In particular any item has been assessed as negative, that leaves a good opinion about the *FriWalk*.

9.4.3 Acceptance

Patients

To assess patient's acceptance, an interview consisting in a set of three question reported in section 9.3 was administered.

From the answers provided to the first question, that evaluated ease of use, it can be extracted that the charging mode of the prototype caused problems, whose consequences restrained from performing the exercises. Additionally, the interaction through a tablet device caused some problems for the older people, which could be explained by their low IT literacy. Furthermore, the size and weight of the device was considered as problematic since patients had to handle it inside a relatively small hospital room shared with another patient.

Regarding the second question, that assessed usefulness, participants stated that, despite the performance problems, they liked the device because they see it as beneficial for themselves. The general appreciation is that an old person would be

able to use it alone.

Finally from the last question, that evaluated the emotions elicited by the *FriWalk*, the feelings about using the walker were mostly positive, although patients stopped sometimes using it due to technical issues or device's size. Besides, in general, participants showed a positive mood to be immersed in this research study.

Clinical professional

The acceptance from the professional perspective has been assessed using the Technology Acceptance Model (TAM). A mean TAM of 46.6/60 has been obtained and depicted in Figure 9.4, showing a high acceptance by the professional that used the system during the experimental phase. Furthermore, the TAM score, as for the SUS score, showed a growing trend during the clinical validation. If acceptance results are analysed by perceived usefulness and ease of use, mean values of 23/30 and 23.6/30 are obtained respectively, which means that the clinician was highly satisfied with the system from both points of view.

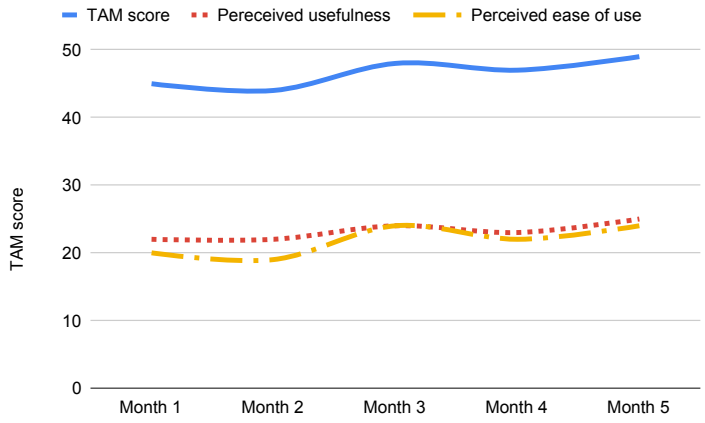

Figure 9.4: Evolution of the TAM score provided by the professional during the experimental phase [102].

9.5 Conclusions

The main objective of the work [102] is to evaluate the usability and acceptance of the *FriWalk* from the perspectives of the patients, and the usability, user experience and acceptance from the clinical professionals' point of view. Obtained results are satisfactory.

Regarding usability, although results obtained from the SUS given by patients do

not qualify *FriWalk* as above average, the reasons explaining this have been identified and clearly point out to the prototypical stage of the hardware. For this reason reaching the desired usability score is feasible. Regarding the usability reported by the clinical professional, they showed a growing trend with the experience, which is really promising.
Since UX analysis is an overloading task for the person answering the questionnaire, this aspect was only assessed by the clinical professional. Obtained results indicate an above average qualification for category (attractiveness, perspicuity, efficiency, dependability, stimulation and novelty).
In terms of acceptance, in general, patients positively value the *FriWalk*. However, the same than in the evaluation of the usability, the hardware flaws negatively biased their perception. On the other hand, the clinical professional showed a high acceptance in terms of TAM. In any case, the acceptance evaluation has helped the research team to propose a new organizational model to provide a functional decline prevention therapy using the *FriWalk* for a future incorporation in the clinical routine of the Hospital. Walkers will not be delivered individually for each patient but shared and kept in an exercising room; charging and technical maintenance will be carried out by the staff.
Finally, future work will mainly address upgrading the *FriWalk* to the next development stage. This will help not only obtaining the desired values in terms of patients' usability but also reaching the "good" or "excellent" categories in the UX benchmarking. Besides, more clinicians will be involved during the second clinical validation of the *FriWalk* system, which will allow reaching to more solid conclusions related to professionals' usability, UX and acceptance.

Chapter 10

Towards variable inertia

In this chapter we present the novel solution we are aiming at to estimate the human applied torque and force *without* additional expensive sensors but, instead, making the most of the walker dynamics and motor drive measurements. First, we present a design of an effective identification procedure to determine the system dynamic parameters and, hence, having a suitable motor–wheel model [6]. We will focus on the particular system under study, which is the brushless direct current (BLDC) motors mounted on the *FriWalk*, and we will synthesise on purpose a time–based identification algorithm. Since the long–term goal is to design an estimation algorithm for the human applied thrust, the validation tests will be focused on the effectiveness of the identification procedure for such a context. After the modelling of the motor, we present an observer implemented to estimate the user thrust based on the absorbed currents and on the voltage drop on the motor coils. The big limitation of such approach is that a knowledge about the mass of the vehicle, on the inertia and on the friction is required.
For this reason, at the end, a different and simpler approach, still able to modify the perceived inertia by the user without relying on the motor model and on the others information, is presented.

10.1 Model

To properly develop a device with a variable inertia, the kinematic model (3.1) is no more sufficient, hence we need to exploit the dynamic model of the unicycle (3.7). The forward velocity is supposed to be applied on the mid-point of the rear wheel axle, while the angular velocity on the axis perpendicular to the plane of motion. Starting from (3.7), the dynamics of the vehicle is given by the Newton-Euler equa-

tions

$$\begin{cases} \dot{v} = \dfrac{1}{m}\left(F_w^r + F_w^l + F_h\right), \\ \dot{\Omega} = \dfrac{1}{J_v}\left(d\dfrac{F_w^r - F_w^l}{2} + \tau_h\right), \end{cases} \tag{10.1}$$

where the parameters m, J_v and d are the mass, the central moment of inertia with respect to the perpendicular axis, and the length of the rear axle of the vehicle. In this chapter, the angular velocity of the vehicle is denoted with Ω, instead of ω, to avoid confusions with the other quantities adopted. F_w^r and F_w^l are the forces applied on the vehicle chassis by the rear right wheel and the rear left wheel, respectively. F_h and τ_h are the unknown force and the torque applied by the human on the vehicle chassis, respectively. These two quantities represent the human thrust, which has to be estimated to properly control the rear wheels motor and, hence, gently guide the *FriWalk* user towards its desired destination.
To this end, under the hypothesis of pure rolling motion, the vehicle accelerations $\dot{v}$ and $\dot{\Omega}$ are linked to the angular velocities ω_w^r and ω_w^l of the right and the left wheel, respectively, by

$$\begin{cases} \dot{v} &= \dfrac{\dot{\omega}_w^r + \dot{\omega}_w^l}{2} r, \\ \dot{\Omega} &= \dfrac{\dot{\omega}_w^r - \dot{\omega}_w^l}{d} r, \end{cases} \tag{10.2}$$

where r is the wheel radius. Then, by substituting (10.2) in (10.1), we get the explicit formulae of the human thrust

$$\begin{cases} F_h &= m\dfrac{\dot{\omega}_w^r + \dot{\omega}_w^l}{2} r - \left(F_w^r + F_w^l\right), \\ \tau_h &= J_v\dfrac{\dot{\omega}_w^r - \dot{\omega}_w^l}{d} r - \left(d\dfrac{F_w^r - F_w^l}{2}\right). \end{cases} \tag{10.3}$$

A sketch of the estimation algorithm, based on Equations (10.3), is depicted in Figure 10.1. The basic pillar upon which the algorithm builds on is the motor

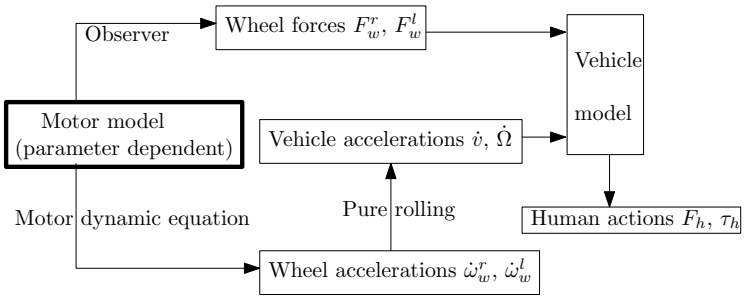

Figure 10.1: Flowchart of the human thrust estimation algorithm.

model (bolded in Figure 10.1), which is used to generate the input to the observer that estimates the wheel forces F_w^r and F_w^l, and whose motor dynamic equation is used to generate the wheel accelerations $\dot{\omega}_w^r$ and $\dot{\omega}_w^l$. The vehicle parameters m, d and r can be easily measured, while J_v has to be estimated. First of all, it is necessary to find a solution for the motor model parameters identification, which is the initial step for the human thrust estimation algorithm.

10.2 Parameter identification of the motor-wheel mechanical model

The continuous-time mechanical model of the brushless direct current (BLDC) motor available on the *FriWalk* is given from the equilibrium equation of the torques

$$\dot{\omega}_r(t) = \frac{1}{J_r}\big(T_e'(t) - T_l'(t) - \mu_{v_r}\omega_r(t) - \mu_{c_r}\mathrm{sgn}(\omega_r(t))\big), \tag{10.4}$$

where ω_r is the angular velocity of the rotor, T_e' is the electromagnetic torque generated by the motor, T_l' is the load torque, J_r is the inertia moment of the rotor, μ_{v_r} is the viscous coefficient and μ_{c_r} is the equivalent Coulomb's friction torque acting on the motor shaft. The expression of the electromagnetic torque, generated by the motor, can be written as

$$T_e'(t) = K_e I(t), \tag{10.5}$$

where K_e is the torque constant, expressed in Nm/A, and given as a nominal parameter in the data-sheet, while $I(t)$ is the module of the space-vector of the stator current.
Equations (10.4)-(10.5) represent the mechanical dynamic model of the considered BLDC motor. Now this model have to be coupled with the model of the wheel, which can be considered as a passive rotating model. In particular, for such a system, the following equation can be written

$$\dot{\omega}_w(t) = \frac{1}{J_w}(T_e(t) - T_l(t) - \mu_{v_w}\omega_w(t) - \mu_{c_w}\mathrm{sgn}(\omega_w(t))), \tag{10.6}$$

where J_w is the inertia moment of the wheel, μ_{v_w} is the viscous coefficient and μ_{c_w} is the equivalent Coulomb's friction torque acting on the wheel shaft, T_e is the torque applied to the wheel by means of the motor, and T_l is the load torque on the wheel due to the wheel-floor contact. It is worthwhile to note that (10.6) is the motor equation used to infer the wheel accelerations in the algorithm depicted in Figure 10.1 and, hence, that should be plugged into (10.3).
Remembering that the wheel is coupled to the motor by means of a gear-box. Since

the gear ratio is equal to n_g, the following relations hold

$$T_e = n_g T'_e, \tag{10.7}$$
$$T_l = n_g T'_l, \tag{10.8}$$
$$\omega_w = \frac{1}{n_g}\omega_r. \tag{10.9}$$

Note that T_l is related to the the forces applied on the vehicle chassis F_w^r and F_w^l, introduced in equation (10.1), by $T_l = r\,F_w$, where F_w is either F_w^r or F_w^l depending on the considered wheel.
By coupling equations (10.4)-(10.6) by means of equations (10.7)-(10.9), the complete model of the motor-wheel system is derived

$$\dot{\omega}_w(t) = \frac{1}{J}(T_e(t) - T_l(t) - \mu_v\omega_w(t) - \mu_c \mathrm{sgn}(\omega_w(t))), \tag{10.10}$$

where

$$J = J_w + n_g^2 J_r, \tag{10.11}$$
$$\mu_v = \mu_{v_w} + n_g^2\mu_{v_r}, \tag{10.12}$$
$$\mu_c = \mu_{c_w} + n_g\mu_{c_r}, \tag{10.13}$$

are the equivalent inertia moment, the viscous friction coefficient and the Coulomb's friction torque of the motor-wheel system, while

$$T_e = n_g K_e I(t). \tag{10.14}$$

The parameters J, μ_v and μ_c are unknown upfront and, hence, they have to be properly identified. Nevertheless, it is very hard to estimate these parameters with conventional methods due to the complexity of the geometry of the system, hence an alternative procedure is needed. To this end, let us consider the discrete-time model of (10.10). Using the step response invariance, the following discrete equation can be written

$$\omega_{k+1} = \alpha\omega_k + \beta\mathrm{sgn}(\omega_k) + \gamma(T_{ek} - T_{lk}) \tag{10.15}$$

where subscript k is the discrete time instant, i.e. being δ_t the sampling time, $k\delta_t$ is the actual time, and

$$\alpha = \mathrm{e}^{-\delta_t\frac{\mu_v}{J}},\ \beta = \frac{\mu_c}{\mu_v}(\alpha - 1),\ \gamma = -\frac{1}{\mu_v}(\alpha - 1).$$

It is then trivial that model (10.15) can be used in the algorithm in Figure 10.1 providing that the model parameters α, β and γ are correctly identified. In order to simplify the identification procedure, we impose $T_{lk} = 0$, $\forall k$, i.e. we assume that the parameter identification is carried out with the wheel disconnected from the floor.

Let $\{T_{ek}\}_{k=0}^{N}$ and $\{\omega_k\}_{k=0}^{N}$ be two input-output sequences of measured data during suitable velocity transient. Then, the use of model (10.15) is to generate a simulated output sequence $\{\hat{\omega}_k\}_{k=0}^{N}$ that matches the measured sequence $\{\omega_k\}_{k=0}^{N}$ under the same input sequence $\{T_{ek}\}_{k=0}^{N}$. More precisely, let us define the following objective function

$$V(q) = \frac{1}{N}\sum_{k=0}^{N}\left(\omega_k - \hat{\omega}_k(T_{ek}, q)\right)^2, \tag{10.16}$$

where N is the number of measures collected with a sampling period δ_t, and $q = [\alpha, \beta, \gamma]^T$ the vector of the unknowns. The solution of the identification problem is the parameter vector q^* that minimises the objective function (10.16), i.e.

$$q^* = \arg\min_{q} V(q). \tag{10.17}$$

10.2.1 Problem solution

Problem (10.17) is a non–linear problem, whose convexity is hard to be inferred. Therefore, the choice of the optimisation algorithm and the selection of the initial conditions are crucial. Besides the mathematical aspects of the optimisation, the main issue for the problem at hand is its structural identifiability: there is the only equation (10.15) to identify the three parameters vector $q = [\alpha, \beta, \gamma]^T$, which yields to a solution that is not unique [75, Chapter 8.4]. In other words, there exist different parameter sets that can reproduce the same experimental data for the given input T_e. To overcome this problem, the original problem is divided in two feasible subproblems: at first, the motor is operated at constant and high velocity, then it is turned off and the free motion transient is measured. The main idea here is to have $T_e = 0$ along the transient, that together with the fact that the wheel is disconnected from the floor ($T_{lk} = 0$), yields to the following model

$$\omega_{k+1} = \alpha\omega_k + \beta\mathrm{sgn}(\omega_k). \tag{10.18}$$

Equation (10.18) can be rewritten, as

$$b_k = A_k\theta, \tag{10.19}$$

where

$$b_k = \omega_{k+1},\ A_k = \begin{bmatrix}\omega_k & \mathrm{sgn}(\omega_k)\end{bmatrix},\ \theta = \begin{bmatrix}\alpha & \beta\end{bmatrix}^T.$$

The Equation (10.19) is solved by the Ordinary Least Squares (OLS) method, which returns the two parameters α and β. Using the same cost function in (10.16) with $q = \theta$ and $T_e = 0$, the solution of the OLS problem is

$$\theta^*_{LS} = \left(\bar{A}^T\bar{A}\right)^{-1}\bar{A}^T\bar{b}, \tag{10.20}$$

where

$$\bar{A} = \begin{bmatrix} \omega_0 & \operatorname{sgn}(\omega_0) \\ \omega_1 & \operatorname{sgn}(\omega_1) \\ \vdots & \vdots \\ \omega_{N-1} & \operatorname{sgn}(\omega_{N-1}) \end{bmatrix}, \ \bar{b} = \begin{bmatrix} \omega_1 \\ \omega_2 \\ \vdots \\ \omega_N \end{bmatrix}.$$

Notice that the noise of the measurements of the output sequence $\{\omega_k\}_{k=0}^{N}$ can be filtered out easily, since pre-filtering the input and the output data through the same filter will not change the input-output relation for a linear system as shown in [75, Chapter 14.4].
Once the two parameters α and β are derived, the parameter γ is obtained by solving the original problem but with fixed α and β, i.e. we have to solve the optimisation problem (10.17) with $q = \gamma$. Two aspects are of paramount importance for a successful identification: the first is the choice of the experiment and the second is the choice of the identification criterion. For the former, to ensure a rich dataset, a piece-wise sequence of different amplitude steps is selected for the input. The latter choice is a little bit more involved. One solution is to solve a non-linear least squares problem by means of the damped least-squares (DLS) method [42], and the second is the use of the a genetic algorithm (GA) [31]. For the DLS, the choice of the initial condition is not trivial; actually the DLS algorithm searches only for local minima, and in case of multiple minima (that is for non-convex problems), the algorithm generally converges only if the initial guess is in a neighbourhood of the final solution. This problem is instead not present for the GA, since they are evolutionary optimisation algorithms, hence robust with respect to the initial conditions. In order to avoid that the algorithm generates parameters without a physical meaning, the search domain has been reduced by defining an upper and a lower bound for the parameters.

Notice that once the parameters α, β and γ are estimated, the original model parameters of the system (10.3) are obtained by means of the following relations

$$J = \delta_t \frac{\alpha - 1}{\gamma \ln(1/\alpha)}, \ \mu_c = \frac{\beta}{\gamma}, \ \mu_v = \frac{\alpha - 1}{\gamma}. \tag{10.21}$$

10.2.2 Experimental results

The experimental results are obtained on the current configuration of the *FriWalk*, having on each of the rear wheels a controlled three-phase brushless motor, model Nanotec DF45L024048-A. The motor is mechanically coupled to the wheel by means of a gear box with gear ratio equal to $n_g = 40$. The velocity is measured by means of a 2048 ticks per revolution incremental encoder per quadrature.
As stated in the previous section, two tests have been carried out

1. the first test the motor is operated at constant velocity, then it is turned off and the free motion transient is registered. The data have been acquired with a sampling frequency of 1 kHz;

2. the motor has been operated is controlled with a sequence of step velocity references. Also in this case the sampling frequency is 1 kHz.

For both tests the wheel is disconnected from the floor, so that $T_l = 0$.
Moreover, since the acquired wheel angular velocities are very noisy (they are obtained with numerical derivation of the encoder data), a lowpass 4-th order Butterworth filter has been used, with cut-off frequency equal to 110 Hz, whose discrete transfer function is

$$G_f(z) = 10^{-3} \frac{0.589z^4 + 2.36z^3 + 3.53z^2 + 2.36z + 0.589}{z^4 - 3.10z^3 + 3.68z^2 - 1.98z + 0.403}. \tag{10.22}$$

The filter has been applied to both the reconstructed angular velocity and the measured motor current.

The first test is carried out in order to estimate the parameters α and β by means of the equation (10.20). The results of the first test are shown in Fig. 10.2 where it is shown the turn off transient of the velocity and the error $e_\omega = \omega_w - \hat{\omega}_w$ between the measured output velocity $\{\omega_k\}_{k=0}^N$ and the simulated velocity $\{\hat{\omega}_k\}_{k=0}^N$ given by (10.18) using the estimated α and β.

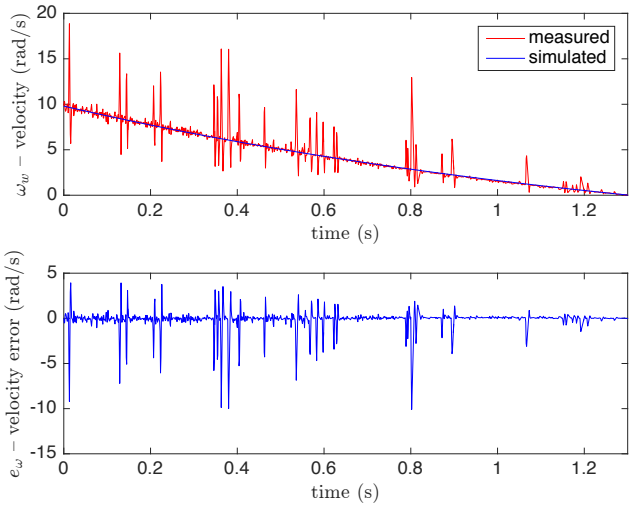

Figure 10.2: Measured and simulated free motion transient of the velocity (upper plot). Estimation error between the measured and the simulated velocity (lower plot).

A total of $N = 1500$ samples have been collected. The following values have been obtained

$$\alpha = 0.9997; \quad \beta = -0.009531.$$

Moreover, to validate these parameters, a further transient has been acquired and it has been compared with the simulated velocity using the parameters estimated

with the previous test. The result of this validation procedure has been shown in Fig. 10.3. From these graphs it is evident that the simulated velocity tracks very

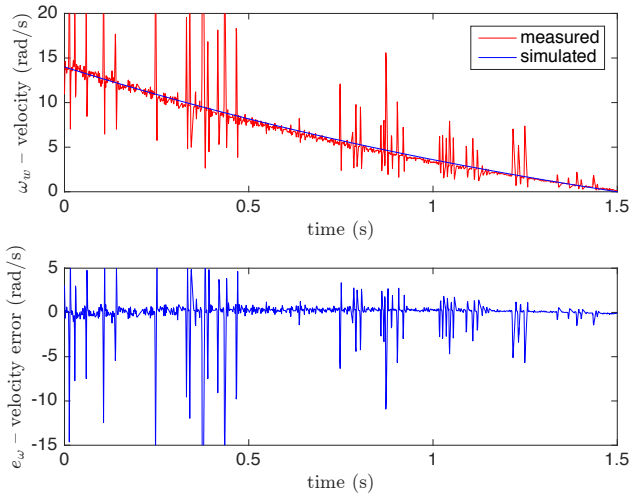

Figure 10.3: Measured and simulated free motion transient of the velocity (upper plot). Estimation error between the measured and the simulated velocity (lower plot).

well the experimental one. This means that the model (10.18), with parameters estimated as explained above, can accurately recover the dynamics of the turn off transient of the motor-wheel system. Finally for the tests in Fig. 10.2 and Fig. 10.3 the following values of the objective function (10.16) have been obtained respectively

$$V = 0.0866; \quad V = 0.255.$$

As a second test the motor has been operated by controlling the angular velocity, and a sequence of velocity references has been given. The waveforms of velocity and current acquired in this test are shown in Fig.10.4. As it is evident from the figure, the last two steps are highly affected by the noise, hence they have been disregarded in the identification procedure. The identification of the last parameter γ has been carried out by means of the genetic algorithm toolbox of Matlab, tuned with the following options: a) population size: 50; b) mutation function: constraint dependent; b) crossover function: scattered; c) selection function: stochastic uniform; d) elite count: 2; e) crossover fraction: 0.8. Note that the use of the GA has been considered in order to avoid the problem of the local minima, as explained in the previous section. Moreover a lower and an upper bound have been considered in order to avoid numerical instability, that are $\underline{\gamma} = 0$ and $\bar{\gamma} = 1$. The choice of these constraints is obvious since γ cannot be negative, and the inertia moment cannot be, in our case, bigger than 1. The outcome of the identification procedure is

$$\gamma = 0.02209.$$

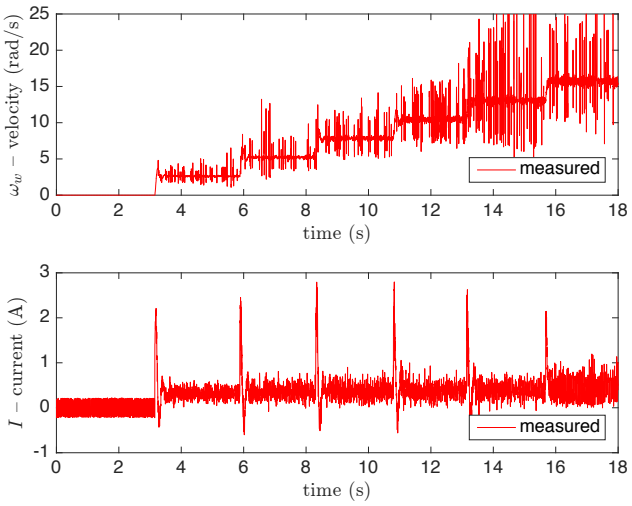

Figure 10.4: Measured velocity (upper plot) and current (lower plot).

Using this value of γ and the precedent values of α and β the equation (10.15) has been used for computing the simulated velocity, where the value of the torque T_e has been computed by means of the measured current and of the equation (10.14). The result is shown in Fig. 10.5 and Fig. 10.6 and the corresponding value of the objective function is

$$V = 0.602.$$

Again, the simulated velocity tracks very well the experimental one. So the obtained model represents a very good approximation of the actual motor. Finally the parameters μ_c, μ_v and J have been obtained by means of the relations (10.21)

$$\mu_c = 0.4315,\ \mu_v = 0.01303,\ J = 0.04526.$$

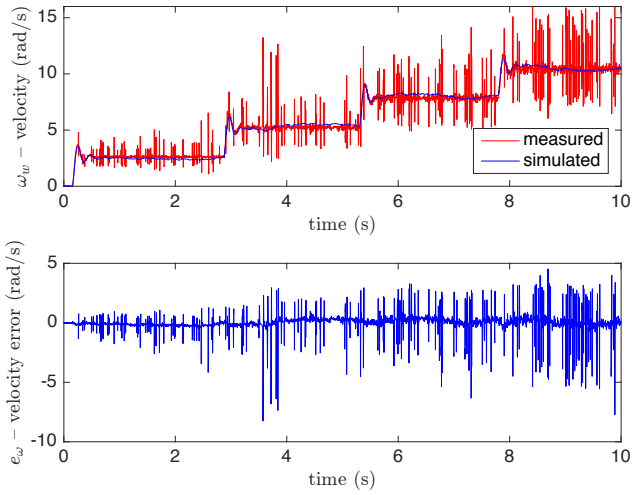

Figure 10.5: Measured and simulated velocity related to the test in Fig.10.4 (upper plot). Estimation error between the measured and the simulated velocity (lower plot).

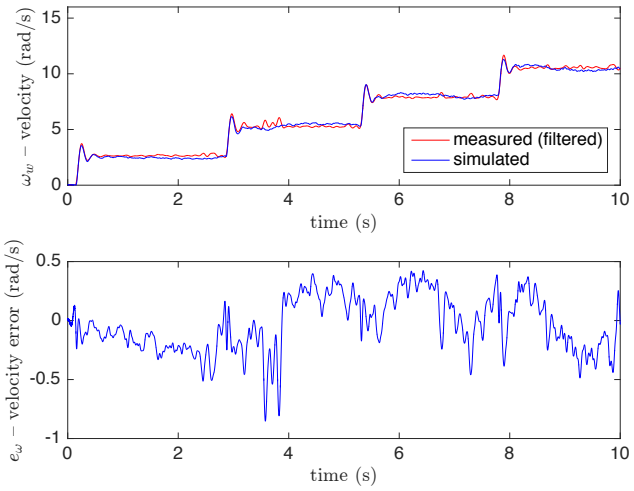

Figure 10.6: Measured filtered and simulated velocity related to the test in Fig.10.4 (upper plot). Estimation error between the measured filtered and the simulated velocity (lower plot).

10.3 Observer

In Section 10.2 we estimated the motor model, which is depicted in the left box of Figure 10.7. In this section, we are going to design an estimator for the external torque applied to the wheel (top box of Figure 10.7) in order to estimate if the user

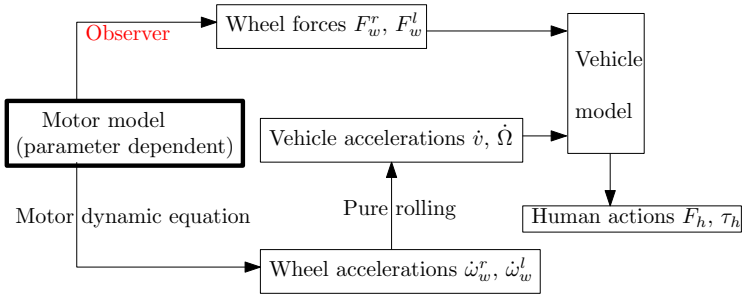

Figure 10.7: Flowchart of the human thrust estimation algorithm.

pushes or pulls the *FriWalk*. Once F_w^r and F_w^l are known it is possible to rely on (10.3) to determine the user thrust.
Given a linear system model

$$\begin{cases} \dot{x} &= Ax + Bu, \\ \dot{y} &= Cx, \end{cases} \tag{10.23}$$

it is possible to define a Luenberger observer

$$\dot{\hat{x}} = A\hat{x} + Bu + K(y - \hat{y}), \tag{10.24}$$

where $\hat{y} = C\hat{x}$ estimates the state variables.
Of course to have a good estimate $\hat{x}$ of the state we need that the estimation error converges to zero, i.e.:

$$e(t) = x(t) - \hat{x}(t) \to 0. \tag{10.25}$$

Computing the time derivative of (10.25) and substituting equations (10.24) and (10.23), we get

$$\begin{aligned} \dot{e} &= \dot{x} - \dot{\hat{x}} \\ &= Ax + Bu - A\hat{x} + Bu + KC(x - \hat{x}) \\ &= A(x - \hat{x}) - KC(x - \hat{x}) \\ &= (A - KC)e(t) \quad \Rightarrow \quad e(t) = e(0) + \exp(-(A - KC)t) \end{aligned}$$

using an appropriate K to make $e(t) \to 0$.

10.3.1 The observer on the *FriWalk*

Each rear wheel of the *FriWalk* is coupled with a brushless motor (permanent magnet synchronous motor PMSM) via a gear box having a gear ratio $n_g = 40$ (see Section 4.2.1). As discussed previously in Section 7.4.1, it is possible to define

the dynamic model of each wheel–motor system as (7.9) which is reported here for completeness

$$\begin{cases} \dfrac{\mathrm{d}i_d}{\mathrm{d}t} &= \dfrac{1}{L_d}\left(-R_s i_d + \nu'_d\right), \\ \dfrac{\mathrm{d}i_q}{\mathrm{d}t} &= \dfrac{1}{L_q}\left(-R_s i_q + \nu'_q\right), \\ \dfrac{\mathrm{d}\omega_m}{\mathrm{d}t} &= \dfrac{3n_g n_p}{2J_{eq}}\left(K_e i_q + (L_d - L_q) i_d i_q\right), \\ \dfrac{\mathrm{d}T_l}{\mathrm{d}t} &= 0, \end{cases}$$

where i_d and i_q are the direct and quadrature current components, ν_d and ν_q are the direct and quadrature input voltage components that are linked to ν'_d and ν'_q by means of (7.7), ω_m is the angular velocity of the motor, R_s is the phase resistance, L_d and L_q are the phase inductances along the direct and quadrature axes respectively, n_p is the number of permanent magnet pole pairs, K_e is the back electromotive force (EMF), and $J_{eq} = J_w + n_g^2 J_m$ is the equivalent inertia moment of the motor-wheel system, where J_m and J_w are the inertia moments of the motor and of the wheel, respectively, and have been estimated in Section 10.2.2.
For the PMSM motor $x = [i_d, i_q, \omega_m, T_l]$ with the following non–linear dynamics:

$$\underbrace{\begin{bmatrix} \dfrac{\mathrm{d}i_d}{\mathrm{d}t} \\ \dfrac{\mathrm{d}i_q}{\mathrm{d}t} \\ \dfrac{\mathrm{d}\omega_m}{\mathrm{d}t} \\ \dfrac{\mathrm{d}T_l}{\mathrm{d}t} \end{bmatrix}}_{\dot{x}} = \underbrace{\begin{bmatrix} -\dfrac{R_s}{L_d} i_d + p n_g \dfrac{L_q}{L_d} \omega_m i_q \\ -\dfrac{R_s}{L_q} i_q - p n_g \dfrac{L_d}{L_q} \omega_m i_d - \dfrac{p n_g K_e}{L_q} \omega_m \\ \dfrac{3}{2}\dfrac{p}{J_{eq}} n_g (K_e i_q + (L_d - L_q) i_d i_q) - \dfrac{F_{eq}}{J_{eq}} \omega_m - \dfrac{1}{J_{eq}} T_l \\ 0 \end{bmatrix}}_{f(x)} + \underbrace{\begin{bmatrix} \dfrac{1}{L_d} & 0 \\ 0 & \dfrac{1}{L_q} \\ 0 & 0 \\ 0 & 0 \end{bmatrix}}_{B} \underbrace{\begin{bmatrix} \nu_d \\ \nu_q \end{bmatrix}}_{u} \tag{10.26}$$

Linearising (10.26), the Luenberg observer can be designed. The observer gain K will be a 4x3 matrix, since the state is of four variables and T_l (the last one) cannot

be directly measured, hence:

$$K = \begin{bmatrix} -k_{11} - \dfrac{R_s}{L_d} & pn_g\dfrac{L_q}{L_d}\omega_m & p\dfrac{L_q}{L_d}i_q \\ -pn_g\dfrac{L_d}{L_q}\omega_m & -k_{22} - \dfrac{R_s}{L_q} & -p\left(\dfrac{K_e}{L_q} + \dfrac{L_d}{L_q}i_d\right) \\ \dfrac{3}{2}\dfrac{p}{J_{eq}}n_g(L_d - L_q)i_q & \dfrac{3}{2}\dfrac{p}{J_{eq}}n_g((L_d - L_q)i_d + K_e) & -\dfrac{1}{n_g}\left(\dfrac{F_{eq}}{J_e q} + k_{33}\right) \\ 0 & 0 & -k_{43}\dfrac{1}{n_g} \end{bmatrix}$$

where $k_{11} = k_{22} = k_{33} = 50$ and $k_{43} = -300$ to have convergent estimates. Now that all the ingredients of (10.24) have been defined it is possible to estimate T_l, which is the external force applied to the wheel.
An estimate of $\hat{x}$ is based on $\dot{\hat{x}} = f(\hat{x}) + Bu + KC(x - \hat{x})$, so a measure of ω_m (motor speed), i_d, i_q, ν_d and ν_q has to be guaranteed. As discussed in Section 4.2.3, the rear node hosts an electronic board (whose electronic scheme is visible in appendix B), which is able to measure the currents absorbed by each motor coil and the voltage drop at each motor coil. Thanks to a well known transformation, it is possible to convert the three phase model of the brushless motor into an equivalent bi–phase model relying on the following transformation matrix

$$\begin{bmatrix} i_\alpha \\ i_\beta \end{bmatrix} = \frac{2}{3}\begin{bmatrix} 1 & -\dfrac{1}{2} & -\dfrac{1}{2} \\ 0 & \dfrac{\sqrt{3}}{2} & -\dfrac{\sqrt{3}}{2} \end{bmatrix}\begin{bmatrix} i_1 \\ i_2 \\ i_3 \end{bmatrix}, \tag{10.27}$$

where i_1, i_2, i_3 are the currents absorbed by the three motor coils. Equation (10.27) is expressed as a function of the currents, but the same expression is exploited to determine the voltages ν_α and ν_β as a function of ν_1, ν_2, ν_3. After this first transformation it is necessary to convert the equivalent fixed–frame bi–phase model into a rotating frame. Using the rotation matrix

$$x_{\alpha,\beta} = \begin{bmatrix} \cos(\theta) & -\sin(\theta) \\ \sin(\theta) & \cos(\theta) \end{bmatrix} x_{dq} \tag{10.28}$$

where θ represents the absolute position of the rotor magnetic field of the motor, it is possible to determine the direct and quadrature current of the brushless motor. The variable θ of equation (10.28) can be estimated thanks to the Hall sensors and the encoder information gathered by the ST electronic board (appendix B) described in Section 4.2.3 thanks to the following method represented by Figure 10.8:

- The brushless motor is equipped with three Hall sensors, providing a range estimation of θ. For instance if the state of the sensors is 001 $\theta \in [0, 60]$ (vector b in Figure 10.8);

- As soon as a switching of the hall state occurs it is possible to calibrate the value of θ. For instance, by looking at Figure 10.8, if the hall state passes from 011 to 010 it means that $\theta = 120°$ (vector c_0);

- After this calibration it is possible to rely on the encoder data to estimate the value of θ (vector c_1, c_2), since the magnetic field rotation is coupled with the rotor rotation by means of a multiplicative factor p, where p corresponds to the number of poles (8 in our case). Therefore, for each revolution of the rotor the magnetic field has computed 8 revolutions. Since the encoder is in quadrature, but it is mounted after the first gear box, we have that θ can be estimated with a resolution of 1.40°, which is the encoder tick resolution.

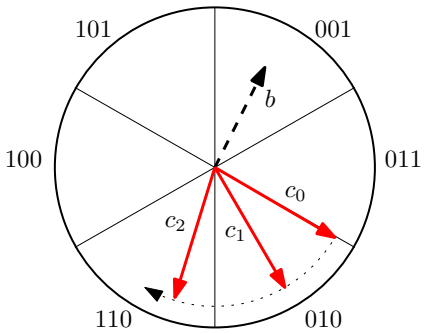

Figure 10.8: Estimation of the rotor magnetic field θ.

The estimation algorithm of θ is an high priority task for the ST, since no encoder ticks can be lost to determine θ. Hence, a very high priority is assigned to the interrupts of the ST that manage the Hall sensors and the encoder. A lower priority is assigned to the ADC converters responsible of the gathering of the currents i_1, i_2, i_3 and the voltages v_1, v_2, v_3, in order that their value is updated with a frequency of 100kHz. The lowest priority is assigned to the observer, which runs with a frequency rate of 10kHz. Every 0.1ms, and assuming that neither interrupts nor ADC conversions are occurring, the state observer is executed according to the following procedure:

1. The interrupts are disabled, so the value of θ cannot change during this phase;

2. The ADC are disabled, so the value of the currents and of the voltages cannot change as well;

3. The currents and the voltages are converted in the equivalent bi–phase model relying on equations (10.27) and (10.28);

4. $f(\hat{x})$ of equation (10.26) is computed;

5. The state error vector is determined, i.e.,

$$e = \begin{bmatrix} i_d - \hat{i_d} \\ i_q - \hat{i_q} \\ \omega_m - \hat{\omega}_m \end{bmatrix}$$

6. Equation (10.24) is computed, so that

$$\dot{\hat{x}} = f(\hat{x}) + Ke;$$

7. $\hat{x}$ is determined on the basis of $\dot{\hat{x}}$ thanks to an Euler integration;

8. The interrupts and the ADC are re–enabled, so that the initial condition is reset.

This logic has been implemented on the ST embedded board and, at the moment, we are obtaining good estimates of $\hat{\omega}_m$, while $\hat{i}_d$, $\hat{i}_q$ and $\hat{T}_l$ are not correctly estimated. This problem is currently under investigation and can be related to the fact that the inductance L and the resistance R of the motor, provided by the data-sheet, could not be correct. For this reason separate estimation of these parameters have to be performed to investigate the nature of the problem that we are encountering.

10.4 A solution to modify the *FriWalk* perceived inertia

As reported in Section 10.1 by equation (10.3), even if the force applied to the wheels F_w^r and F_w^l are correctly estimated by means of the observer described in Section 10.3, we still have the problem that the mass of the vehicle m and especially its inertia J_v are undefined. Moreover these quantities can vary in real–time according to the situation, in fact:

- The user can lean more or less on the *FriWalk* handlebars, highly modifying the mass and the inertia of the robot;
- The user can load the *FriWalk* box with groceries modifying the mass and the inertia of the robot.

The variability of m and J_v can highly compromise the performances of the system. By looking at the dynamic equations of the system are recalled:

$$\begin{cases} F_h &= m\dfrac{\dot{\omega}_w^r + \dot{\omega}_w^l}{2} r - \left(F_w^r + F_w^l\right), \\ \tau_h &= J_v \dfrac{\dot{\omega}_w^r - \dot{\omega}_w^l}{d} r - \left(d\dfrac{F_w^r - F_w^l}{2}\right), \end{cases}$$

we can easily notice how a variation of the mass can modify the sign of F_h, causing the system to wrongly estimate a pulling action while the user is pushing the device.

To avoid this problem an adaptive observer able to estimate the mass and the inertia of the system in real–time, should be developed. Although such solution can be implemented, it requires the actuators to continuously stimulate the *FriWalk*, causing an annoying behaviour that, inevitably, disrupt the user comfort.
To overcome such issue, let us consider the longitudinal dynamics only for easiness, and let us write the dynamics of the system

$$F = ma = F_h + F_m + F_a, \tag{10.29}$$

where F_a is the viscous friction force and it is absolutely reasonable to approximate it as $F_a = \xi v$, where ξ is the damping coefficient. Let us now introduce m_d and ξ_d as, respectively, the desired mass and the desired damping coefficient that we want that the user perceives. If the motors propels the system with a force

$$F_m = (m - m_d)a + (\xi - \xi_d)v = \Delta m a + \Delta \xi v, \tag{10.30}$$

and we substitute equation (10.30) into equation (10.29) we get that

$$F_h = m_d a + \xi_d v, \tag{10.31}$$

which is the only remaining force acting on the *FriWalk*. This means that the user is the only responsible of the *FriWalk* motion and pushes the device feeling a certain desired mass m_d and a certain desired damping coefficient ξ_d. In this way, acting on Δm and on $\Delta \xi$ it is possible to modify the perceived mass and inertia of the *FriWalk* felt by the user. To summarize we can state that:

- If $\Delta m > 0$ and $\Delta \xi > 0$ we get $F_m > 0$. Therefore, to move the vehicle at a certain velocity v, the force required by the user F_h decreases as F_m increases;
- If $\Delta m < 0$ and $\Delta \xi < 0$ we get $F_m < 0$. This is the opposite behaviour, constraining the user to apply more and more force to move the device at a certain desired speed v.

Equation (10.30) is simple but has the big issue that, if the velocity v overcomes a certain threshold $v^\star$, we have that $F_m > F_m^\star$. $F_m^\star$ is the threshold force over which the force applied by the motors is greater than the friction force, causing the system to continuously accelerate. In order to overcome such a problem, equation (10.30) has been modified with

$$F_m = \Delta m a + \Delta \xi \left(\frac{2}{\pi} \arctan(3v) \right) \tag{10.32}$$

in order that the velocity force component saturated and, once defined the maximum damping coefficient $\Delta \xi^\star$, it is impossible to have that $F_m > F_m^\star$.

10.4.1 Experimental results

In order to evaluate the performance of the solution proposed with equation (10.32), several tests have been performed, changing the value of Δm and $\Delta\xi$. Since the feeling of a varying inertia is quite difficult to be determined, we decided to conduct an experiments where the user was not involved. For this reason, since the *FriWalk* needs to be pushed with the same force to appreciate the effect of the variation of the parameters, we set the robot to reach a target speed of 1m/s. As soon as 4 seconds are reached, the *FriWalk* is let to move freely so that F_m is the only applied force, and F_a is the only resistive force. Experimental results are reported in Figure 10.9.

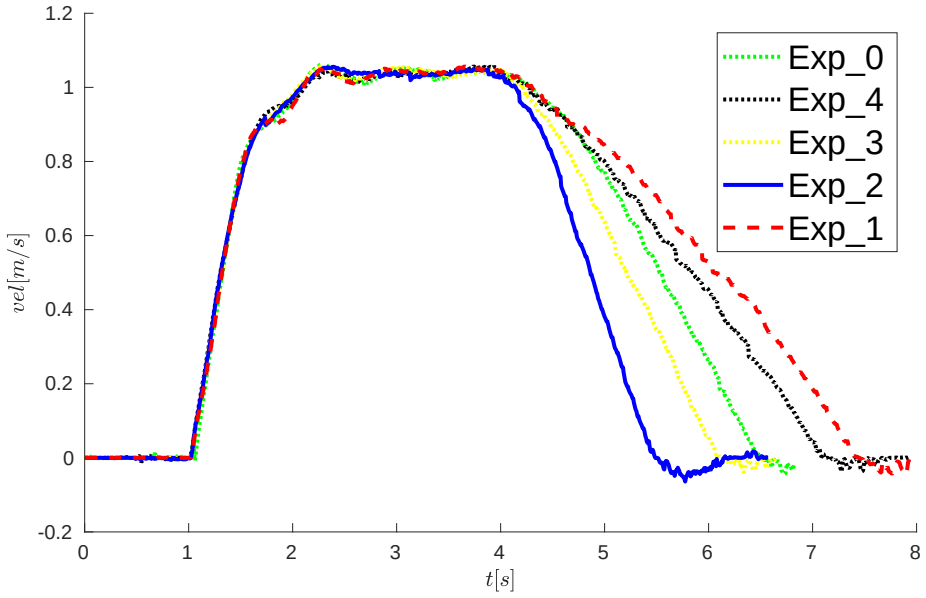

Figure 10.9: Different deceleration profiles of the *FriWalk* varying the value of Δm and $\Delta\xi$.

By looking at Figure 10.9 we have that:

- *Exp_0* is the default experiments, hence with $\Delta_m = \Delta\xi = 0$. This is the natural deceleration profile of the *FriWalk*;
- *Exp_4* and *Exp_3* have been performed, respectively, with $\Delta\xi = 12$ and $\Delta\xi = -12$, while $\Delta m = 0$ for both experiments. This result lead us to notice that for bigger $\Delta\xi$ we have a lower deceleration profile, while for lower $\Delta\xi$ we have the opposite behaviour;
- *Exp_1* has been performed with $\Delta m = 20$ and $\Delta\xi = 12$, so that the combination of the two parameters highly decreases the deceleration profile;

- *Exp_2* has been performed with $\Delta m = -20$ and $\Delta \xi = -12$, highly increasing the deceleration profile.

These experiments allow us to conclude that, increasing the value of Δm and $\Delta \xi$, the friction action and the overall inertia of the robot is perceived lower that in normal conditions, since a lower force is required to be applied by the user to move the *FriWalk* at a constant velocity. At the same time, decreasing the value of Δm and $\Delta \xi$, we get the opposite behaviour, so that the user is required to apply more force to the handlebars to move the *FriWalk* at a constant velocity.
Even if the idea is very simple, the results obtained are really satisfactory since a varying inertia effect is obtained without the implementation of complex observers, current sensors or expensive force sensors.
Another set of experiments have been performed to evaluate the behaviour of the assistance controller under the application of the same impulsive force F at $t = 0$, and the results are shown in Figure 10.10. Also in this case the experiments have been performed with the same parameters Δm and $\Delta \xi$.

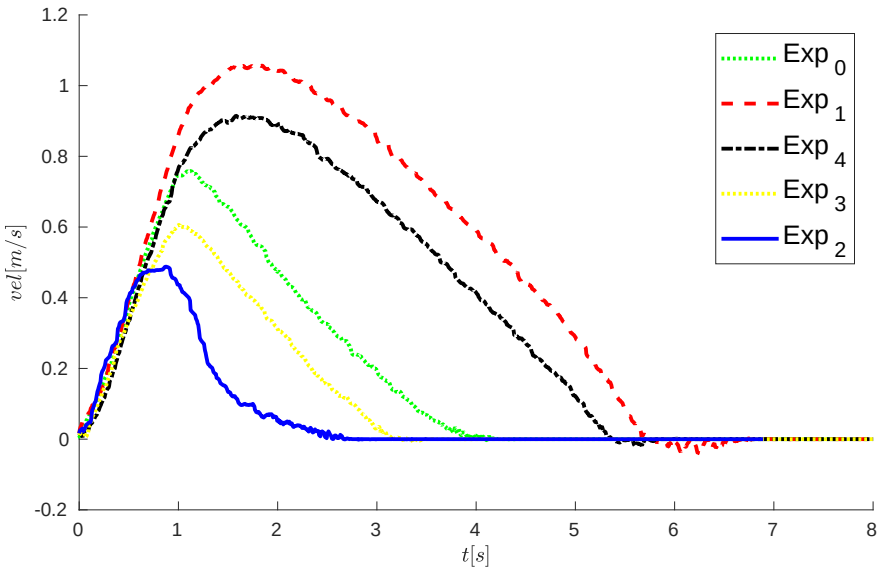

Figure 10.10: Different velocity profiles of the *FriWalk* varying the value of Δm and $\Delta \xi$ under the application of the same impulsive force at $t = 0$.

In Figure 10.10, *Exp_0* reports the behaviour of the *FriWalk* in normal condition, hence without any help provided by the motors. As we can see, by increasing Δm and $\Delta \xi$ (*Exp_1* and *Exp_4*) the device reaches higher velocities and it takes more time to decelerate, meaning that the perceived inertia and friction is highly reduced. Conversely, by decreasing Δm and $\Delta \xi$ (*Exp_2* and *Exp_3*), we have the opposite behavior, as expected.

Chapter 11

Conclusions

11.1 Research evaluation

The thesis proposes the conception, development and implementation of a service robot for navigational assistance and physical rehabilitation of seniors. Regarding the first topic, several strategies to control an assistive robotic walker have been proposed, ranging from complete passive solutions, in which the user is the only responsible of the robot thrust, to active strategies in which the system is propelled by means of a cooperation between the robot and the user. Those strategies have been extensively tested with seniors with different kind of impairments to investigate the human–robot interaction and to understand the comfort perceived by the user. The common logic at the basis of each strategy relies on safety tunnels. If the user is safely performing the task, then he/she is completely in control of the *FriWalk*, so that the feeling of autonomy is enhanced and the comfort is maximised. Conversely, if the user is not capable of safely solving the task (for instance if he/she is going to collide with an obstacle or if he/she is departing too much from the planned path), then the robot intervenes by taking the control of the robot. Acting on the steering system only, the robot is able to help the user to realign towards the desired direction, ensuring his/her safety. In particular in the thesis we focused on:

- Braking guidance solution: due to the hardware limitations the user is guided by blocking either the rear right or the rear left wheel. Although the offered comfort is definitely less than the other guidance systems that exploits rear brakes able to modulate their action, the cheap solution presented in the thesis has been appreciated by the user, feeling the intervention not too abrupt;

- Haptic guidance solution: the user is guided to follow the path relying on vibrating bracelets. This strategy is definitely the most comfortable since it is totally passive and no actuation occurs from the actuators. For this reason the motion of the vehicle is totally provided by the user, hence safety cannot be guaranteed;

- Combined haptic and braking guidance solution: the haptic approach has the mainly advantage that it can be integrated with other guidance strategies. In this thesis we studied the integration of the haptic system with the braking strategy, in order to try to maximise the user comfort (thanks to the bracelets), but at the same time guarantee safety (thanks to the braking system). The user reported an overall great experience with such strategy, pointing out the benefits coming from each independent actuation;

- Simulated passivity: the user is guided using actuated rear wheels. The robot alternates phases in which the user is in complete control of the motion and the sensing system estimates the desired user's velocity, with phases in which the robot takes the control authority and realigns the user towards the path at the estimated user's speed. Although this system is active, the user has the impression to feel the system adapting perfectly to his/her velocity, highly increasing the comfort. The users reported that the system intervention are very smooth even if, sometimes, they felt to be pulled by the *FriWalk*, disrupting the overall comfort;

- Front steering strategies: the user is guided relying on the front steering wheel, while the thrust is provided only by himself. This strategy has been proved to be the most promising, since the intervention are in practice not perceived by the user at all. The only complaint concerned the actuation stiffness as it greatly limited the freedom of movement of the user. To overcome such limitation a variable stiffness approach has been proposed so that the vehicle exhibits a variable strength according to the distance from the path. The larger the distance, the stiffer the front steering system. Thanks to this improvement this strategy is definitely the most promising in terms of comfort and safety.

At the end it is possible to conclude that the best solution cannot be uniquely defined, but it depends on the impairments of the user. The passive strategy solutions fits perfectly for people who suffer limited disabilities, and needs sporadic interventions only in case of dangerous events, while for the rest of the time can follow the predefined path without any hint from the device (or at least from the bracelets that does not disrupt the user's comfort). Every time something unexpected and potentially dangerous happens, the best solution is the use the bang–bang strategy to steer the user faraway from the danger.
If the *FriWalk* is used by users who suffer cognitive disabilities, like eyesight or hearing problems, the best way is to exploit the active strategies to guide the user towards the desired path, since the passive solutions will definitely compromise his/her comfort. The use of the front-steering system is preferable since it maximize the comfort perceived by the user, but the presence of the front actuation limits the maneuverability of the *FriWalk* whenever the motors are disengaged. Moreover the cost of the device increases since it requires extra actuators, while the rear ones are always mandatory. Thanks to the experiments performed we can conclude that

the best strategy relies on exploiting the front steering system with the variable stiffness approach, since comfort and freedom of movement are maximized. The rear active strategy is a good substitute to the front steering system to reduce the cost and the complexity of the *FriWalk*, maximizing also the maneuverability of the robot but sacrificing the user's comfort. For what concert the passive solutions, the main problem is that their performance highly depends on the user accuracy, hence they perfectly fits for people who suffer very limited disabilities. In such case the combined strategy is the most preferable, since the user can rely on the bracelets to correct his/her trajectory and the *FriWalk* actuator's never intervenes, definitely maximizing the comfort of the user. At the same time the rear actuators, exploited as brakes, are user as last resort in case of dangerous situation to preserve user's safety.

The thesis also proposes another further study on the use of the *FriWalk* as a rehabilitation tool. An extensive pilot study, with real patients and physiotherapist have been performed in Spain, at the Universitary Hospital of Getafe (Madrid). The benefits of relying on such device to increase the hospitalization efficacy has been proved and the acceptance rate of the *FriWalk* by patients and the clinical staff has been very high.
At the same time, a solution to modify in real–time the perceived inertia of the *FriWalk* has been proposed so that, acting on two parameters only, the user can feel the device lighter or heavier. This feature can be exploited from a rehabilitation point of view letting the user to exercise more or less force to move the robot.

11.2 Future work

A first possible improvement of the proposed guidance strategies is an adaptive threshold system, meaning that the robot is able to modify in real–time the safety tunnels according to the detected situation. In this thesis, these thresholds have been fixed to a certain values as a trade–off between user's comfort and safety. In a real scenario a real–time adaptation of these parameters, according to the situation detected by the robot, is expected. For instance, whenever the user is walking in a corridor, the thresholds can be left high so that the system never intervenes. As soon as a dangerous situation is detected by the *FriWalk*, e.g. wall collision or a moving obstacle is detected and it could collide with the user, then the thresholds are narrowed to shift the control action to the robot and guarantee the user's safety. At the same time, inside a big room the thresholds can be relaxed and can be limited only in proximity of crosses or decision points.
Another possible improvement on the topic of the *FriWalk* as a navigational aid can be performed in the haptic guidance strategy. In this thesis a rough an simple on–off controller has been proposed, since it can be simply understood by seniors with disabilities. By the way a deeper analysis understanding which vibrating pattern fits better for seniors, depending also on their disabilities, can be studied, analyzed

and developed in future works.
In this thesis, we did not performed a study with seniors exploiting the front actuation system. Future developments will focus on performing a guidance strategy comparison with elderly to better understand the benefits and the limitations of each strategy. In such a way, a common protocol for each guidance solution can be followed to make the comparison simpler.
For what concerns the use of the *FriWalk* as a rehabilitation device, a more extensive pilot study involving more patients have to be performed to gather more data. At the same time, all the exercise algorithms have to be strengthened to work independently from the light condition of the room or from the dress of the patient.
As a final remark, the *FriWalk* developed in the ACANTO project context is still a prototype, so that the robot autonomy and the hardware quality is limited and needs to be increased for a commercial purpose, especially for clinical applications.

Appendix A

The CAN bus and the CANOpen protocol

The CAN bus

Regarding the bus, we decided to rely on the Controlled Area Network (CAN bus), which is a robust vehicle bus standard designed to allow micro–controllers and devices to communicate with each other, without a host computer, and with many communication protocol which are defined (e.g. CANopen). Furthermore, the CAN bus can be physically implemented with two wires, which is a very economical solution, it can reach up to 1Mbit/s of bandwidth and supports different topologies (e.g. line/bus topology, ring topology, star topology). In the same field, also RS485 serial is increasing popularity, but it is currently not used in automotive and has the limitation that any transport protocol layer is defined. The Ethernet communication is another possibility, but it has the main drawback that each node requires its own cable to be connected to a central host computer.
Regarding the Open System Interconnection model (OSI model), the standard CAN implementation defines the lowest two layers, i.e. level–1 (physical layer) and level–2 (data link layer). While high level CAN protocols, like CANopen, operate at level–7 (application layer) and partially implement solution for level–3 (network layer), level–4 (transport layer), level–5 (session layer) and level–6 (presentation layer) as reported in Figure A.1.
Most of the applications rely on the CANopen, that is a communication protocol specification for embedded systems used in automation. The basic CANopen device and communication profiles are given in the CiA 301 (CAN in Automation). Profiles for more specialized devices are build on top of this basic profile, and are specified in numerous other standards such as CiA 401 for I/O modules and CiA 402 for motion control.
In order to understand the transmission frequency to exploit the whole bandwidth of the CAN bus, the message frame dimension is the most important feature. In a

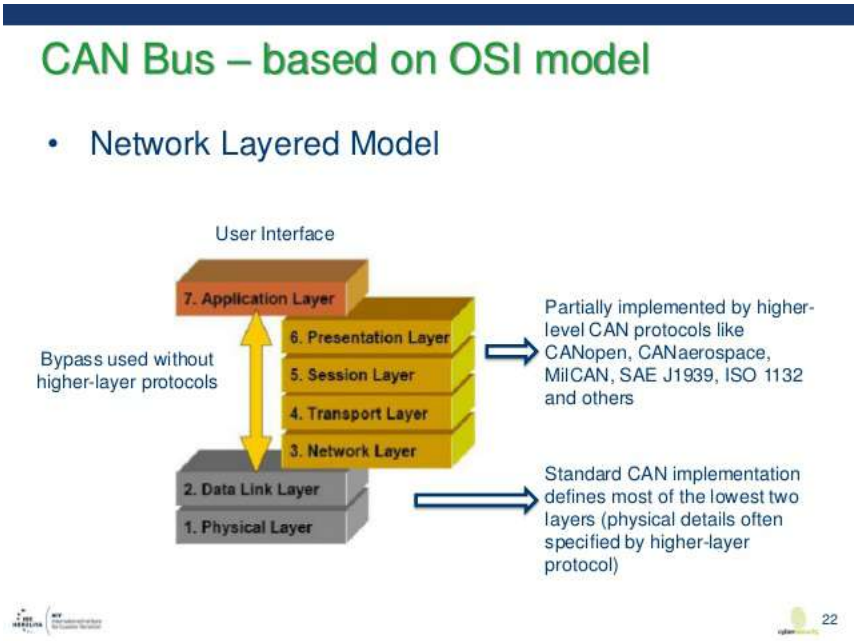

Figure A.1: CAN bus Operating System Interconnection specifications.

CAN message frame, 6 bytes are used by the data link layer to guarantee the correct communication (CRC, ACK, EOF end of frame, INT inter–frame spacing) as visible in Figure A.2, while the user can manage only short packages with a partially fixed structure up to 10 bytes where:

- 11 bits for the COB–ID (CAN object identifier), where the first 4 bits defines the function code and the last 7 the node ID;
- 1 bit for remote transmission request;
- 4 bits for the data length;
- up to 8 bytes for data.

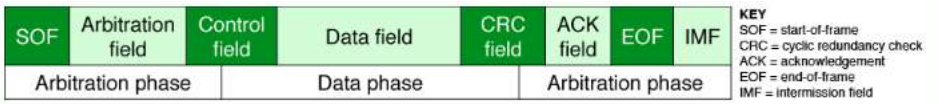

Figure A.2: CAN message structure.

This means that the overall dimension of a single frame is up to 16 bytes. By the way, to ensure enough transitions to maintain synchronization, a bit of opposite polarity is inserted after five consecutive bits of the same polarity. This practice is

called bit stuffing and is necessary due to the non-return to zero (NRZ) coding used with CAN. The stuffed data frames are destuffed automatically by the receiver. So, in the worst case this implies an additional byte to be added to the overall dimension. The last thing that we need to take into account is that, before sending a message through the bus, the hardware senses if the bus is in idle state and starts an arbitration phase (first arbitration phase in Figure A.2) in which the hardware senses the channel to understand if it is free or not.
Ignoring the time required by the arbitration phases to succeed, which is quite impossible to be correctly estimated, in the best case a CAN frame is 16 bytes.

The CANopen protocol

CANOpen supports different communication models, such as master/slave, client/server and producer/consumer, and up to 127 nodes can be connected simultaneously. Furthermore, it implements several protocols among which there are:

- Network Management (NMT): used to issue state machine change commands, like start and stop the single devices. For example setting COB–ID = 0x01 means go to operational, while COB–ID = 0x02 means go to stopped;
- Hearthbeat: used to monitor the nodes in the network and verify if they are alive. This message is identified by a COB–ID = 0x700 + node ID, while the data part frame contains the information indicating the node status (e.g. 0x04 stopped, 0x05 operational).
- Service Data Object (SDO): exploited to implement client/server logic, so it is used for setting and reading values from a desired node. The request message recipient is specified with the COB–ID = 0x580 + node ID, while the reply message is identified with the COB–ID = 0x600 + nodeID;
- Process Data Object (PDO): used to process real time data among various node. This protocol is used to implement the producer/consumer logic according to the user specifications.

Regarding the SDO protocol (used for writing and reading), CiA 301 defines a semantic ruling the request message and the corresponding reply. For what concern the writing procedure, the client starts a write request by transmitting index, subindex, data length and data. If the data have been correctly processed, the server sends a write response. The response contains the same index and subindex as the write request but not data. Figure A.3 shows the idea of such implementation:

- write request:
  - byte 1 and 2 are used to specify the index, hence understand the semantic of the data;

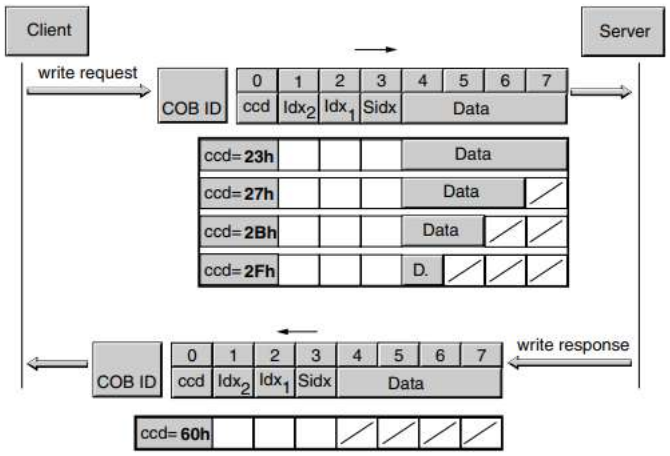

Figure A.3: SDO protocol for a CAN write request.

  - byte 0 can assume four values, according to the length of the data transmitted. In particular: 0x23, 0x27, 0x2B, 0x2F are used to transmit 4, 3, 2 and 1 bytes.

- write response:
  - byte 1, byte 2 and byte 3 corresponds to the one used in the write request;
  - byte 0 is equal to 0x60 whenever the transmission succeed, while is equal to 0x80 is an error has occurred, as visible in Figure A.4. The are many different causes that can lead to an error, e.g. if the parameter value is outside from the possible range, if the index or the subindex is unknown, if the index has no write access.

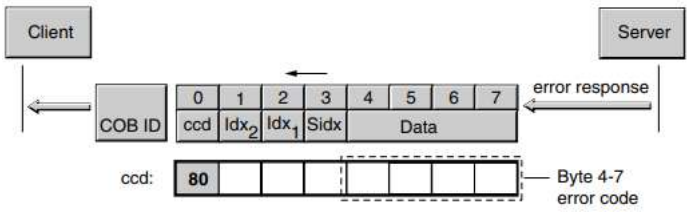

Figure A.4: SDO CAN write error response.

Regarding the reading procedure, the client starts a read request by transmitting index and subindex that point to the register where the client wants to read. The server responds to the request with the desired data. Figure A.5 reports such logic, where the client needs to send a message with the byte 0 equal to 0x40, byte 1 and

byte 2 equal to the index where the reading has to be performed, while the server replies with different values for byte 0 (0x43, 0x47, 0x4B, 0x4F) according to the data length. Also in this case, like for the write procedure, the server can reply with the error logic reported in Figure A.4.

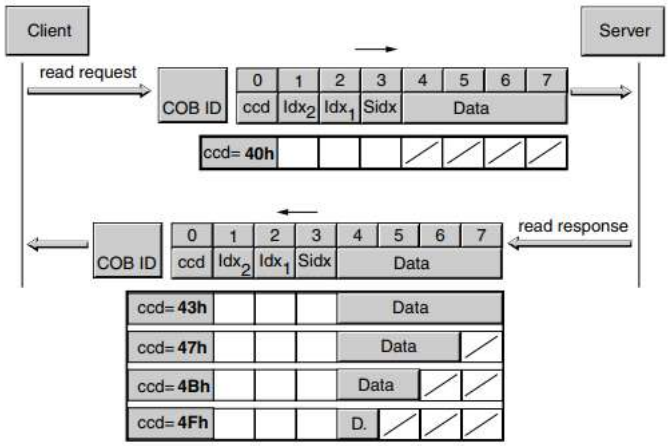

Figure A.5: SDO protocol for a CAN read request.

Appendix B

ST schematic circuit

The configuration of the pins of the ST has been performed through STM32CubeMX program. This software has a graphical interface which can be exploited to easily chose each pin, and decide its specifics as depicted in Figure B.1.

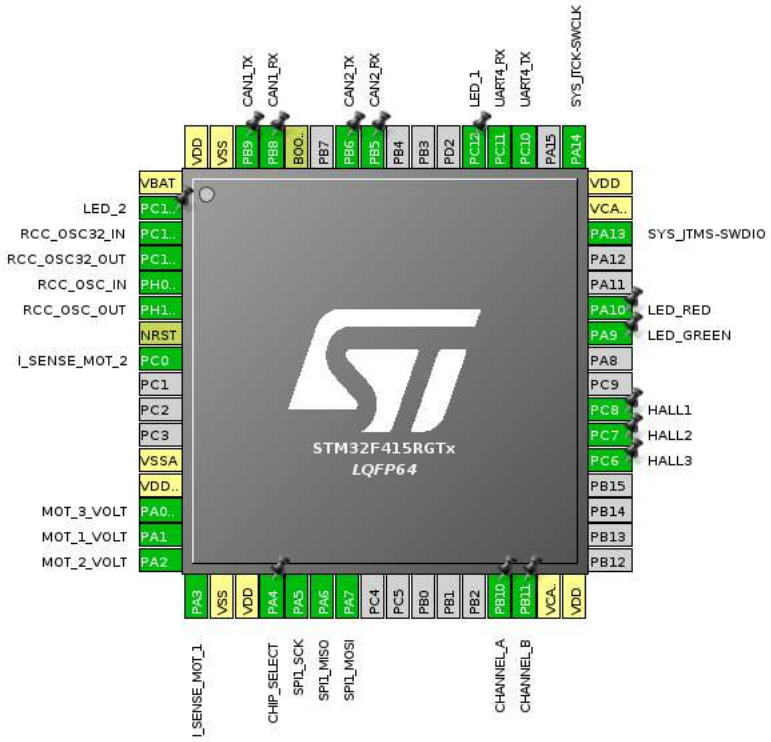

Figure B.1: ST pin configuration.

In particular:

- since we have an external crystal resonator (for the clock purposes), we selected pins *RCC_OSC32_IN*, *RCC_OSC32_OUT*. *RCC_OSC_IN* and *RCC_OSC_OUT*;
- to get the current absorbed by the motor and gather the coil drop voltage (as explained in Section 4.2.3) we need to rely on 5 ADC converters to exploit the full bandwidth of the microcontroller;
- *CHIP_SELECT*, *SPI1_SCK*, *SPI1_MISO* and *SPI1_MOSI* are depicted to the absolute rotative encoder to gather the position of the front fork;
- *HALL_IN1*, *HALL_IN2* and *HALL_IN3* are used to gather the information coming from the hall sensors of the motor;
- *UART4_RX* and *UART4_TX* are for debug purposes;
- *CAN1_TX*, *CAN1_RX* and *CAN2_TX*, *CAN2_RX* are exploited, respectively, to communicate via CAN bus with driver and the Beaglebone;
- *CHANNEL_A* and *CHANNEL_B* are used to connect the relative encoder for the rear wheels.

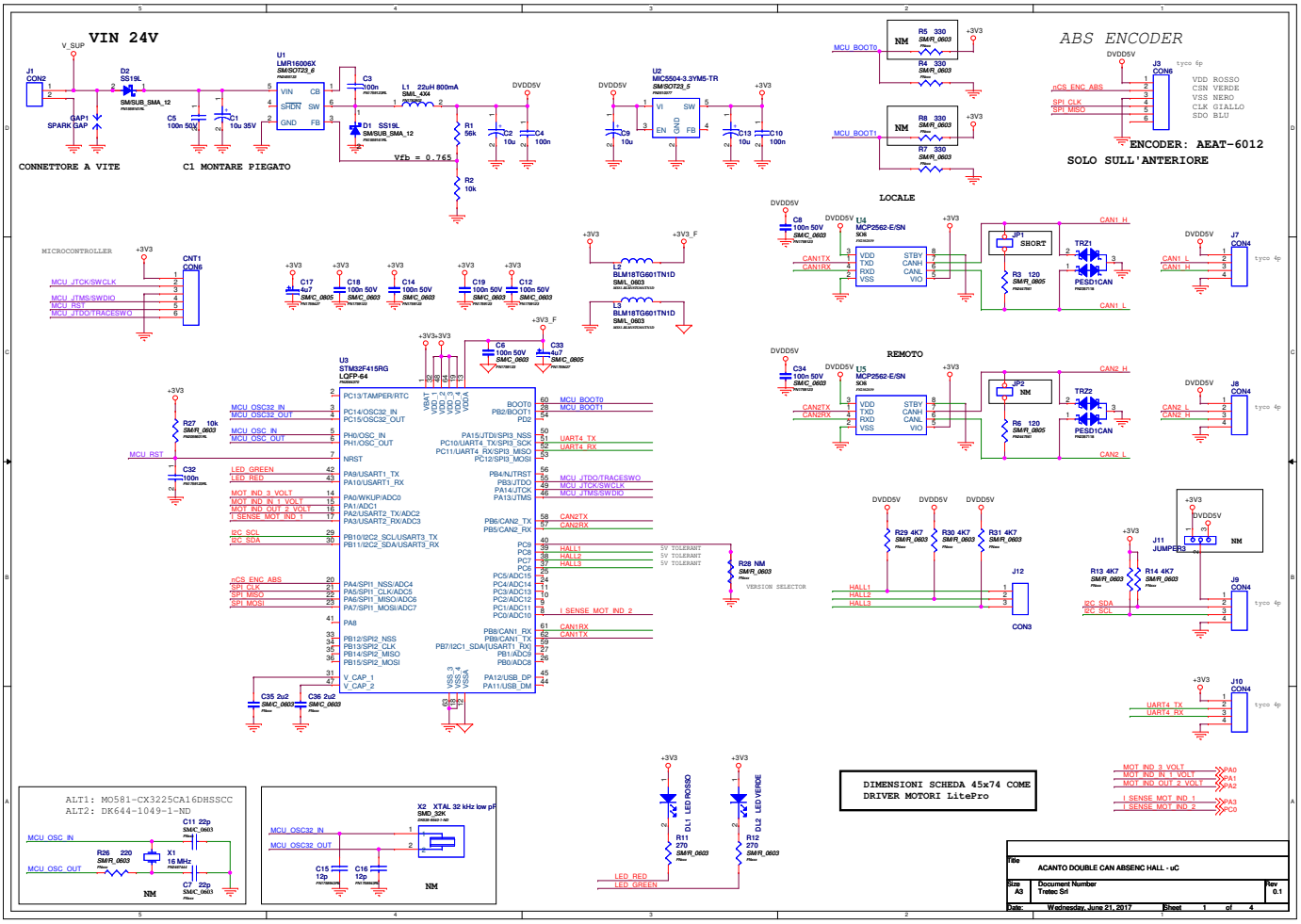
VIN 24V
ABS ENCODER
ENCODER: AEAT-6012
SOLO SULL'ANTERIORE
CONNETTORE A VITE
C1 MONTARE PIEGATO
LOCALE
REMOTO
MICROCONTROLLER
DIMENSIONI SCHEDA 45x74 COME
DRIVER MOTORI LitePro
ACANTO DOUBLE CAN ABSENC HALL - uC

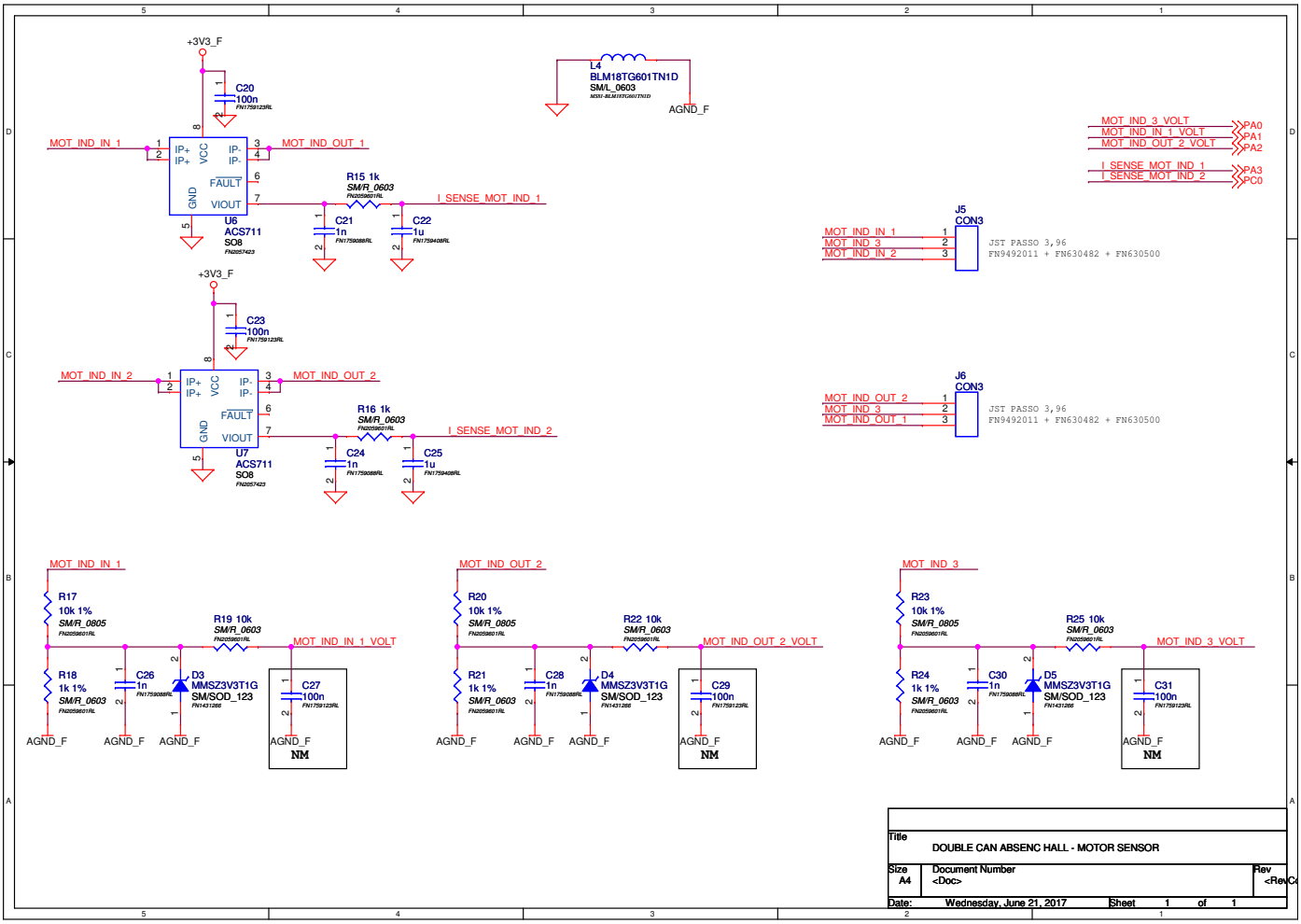
+3V3_F
C20
100n
L4
BLM18TG601TN1D
SM/L_0603
AGND_F
MOT_IND_3_VOLT
MOT_IND_1_VOLT
MOT_IND_OUT_2_VOLT
I_SENSE_MOT_IND_1
I_SENSE_MOT_IND_2
PA0
PA1
PA2
PA3
PC0
MOT_IND_IN_1
MOT_IND_OUT_1
R15 1k
SM/R_0603
C21
1n
C22
1u
U6
ACS711
SO8
I_SENSE_MOT_IND_1
J5
CON3
MOT_IND_IN_1
MOT_IND_3
MOT_IND_IN_2
JST PASSO 3,96
FN9492011 + FN630482 + FN630500
C23
100n
MOT_IND_IN_2
MOT_IND_OUT_2
R16 1k
SM/R_0603
C24
1n
C25
1u
U7
ACS711
SO8
I_SENSE_MOT_IND_2
J6
CON3
MOT_IND_OUT_2
MOT_IND_3
MOT_IND_OUT_1
JST PASSO 3,96
FN9492011 + FN630482 + FN630500
MOT_IND_IN_1
R17
10k 1%
SM/R_0805
R19 10k
SM/R_0603
MOT_IND_IN_1_VOLT
R18
1k 1%
SM/R_0603
C26
1n
D3
MMSZ3V3T1G
SM/SOD_123
C27
100n
NM
AGND_F
MOT_IND_OUT_2
R20
10k 1%
SM/R_0805
R22 10k
SM/R_0603
MOT_IND_OUT_2_VOLT
R21
1k 1%
SM/R_0603
C28
1n
D4
MMSZ3V3T1G
SM/SOD_123
C29
100n
NM
AGND_F
MOT_IND_3
R23
10k 1%
SM/R_0805
R25 10k
SM/R_0603
MOT_IND_3_VOLT
R24
1k 1%
SM/R_0603
C30
1n
D5
MMSZ3V3T1G
SM/SOD_123
C31
100n
NM
AGND_F
Title
DOUBLE CAN ABSENC HALL - MOTOR SENSOR
Size
A4
Document Number
<Doc>
Rev
<Rev.Co
Date:
Wednesday, June 21, 2017
Sheet
1
of
1

References

[1] Dali: Devices for assisted living. http://www.ict-dali.eu/dali, November 2011. EU Project.

[2] ACANTO: A CyberphysicAl social NeTwOrk using robot friends. EU Project, February 2015.

[3] J.L. Pons A. Abellanas R. Raya A. Frizera, R. Ceres. The smart walkers as geriatric assistive device. the simbiosis purpose. *Gerontechnology*, 7:108–115, 2008.

[4] A. P. Aguiar and J. P. Hespanha. Trajectory-Tracking and Path-Following of Underactuated Autonomous Vehicles With Parametric Modeling Uncertainty. *IEEE Transactions on Automatic Control*, 52(8):1362–1379, Aug 2007.

[5] M. Andreetto, S. Divan, D. Fontanelli, and L. Palopoli. Path following with authority sharing between humans and passive robotic walkers equipped with low-cost actuators. *IEEE Robotics and Automation Letters*, 2(4):2271–2278, 2017.

[6] M. Andreetto, S. Divan, D. Fontanelli, L. Palopoli, and A. Sferlazza. Assistive robotic walker parameter identification for estimation of human thrust without force sensors. In *2017 IEEE 3rd International Forum on Research and Technologies for Society and Industry (RTSI)*, pages 1–6, Sept 2017.

[7] M. Andreetto, S. Divan, D. Fontanelli, L. Palopoli, and F. Zenatti. Path following for robotic rollators via simulated passivity. In *2017 IEEE/RSJ International Conference on Intelligent Robots and Systems (IROS)*, pages 6915–6922, Sept 2017.

[8] Marco Andreetto, Stefano Divan, Francesco Ferrari, Daniele Fontanelli, Luigi Palopoli, and Domenico Prattichizzo. Combining Haptic and Bang-Bang Braking Actions for Passive Robotic Walker Path Following. *Transaction on Haptics*, 2018.

[9] Marco Andreetto, Stefano Divan, Francesco Ferrari, Daniele Fontanelli, Luigi Palopoli, and Fabiano Zenatti. Simulating passivity for robotic walkers via

authority-sharing. *IEEE Robotics and Automation Letters*, 3(2):1306–1313, 2018.

[10] Marco Andreetto, Stefano Divan, Daniele Fontanelli, and Luigi Palopoli. Hybrid Feedback Path Following for Robotic Walkers via Bang-Bang Control Actions. In *Proc. IEEE Int. Conf. on Decision and Control (CDC)*, pages 4855–4860, Las Vegas, Nevada, US, Dec. 2016. IEEE.

[11] Marco Andreetto, Stefano Divan, Daniele Fontanelli, and Luigi Palopoli. Passive robotic walker path following with bang-bang hybrid control paradigm. In *Intelligent Robots and Systems (IROS), 2016 IEEE/RSJ International Conference on*, pages 1054–1060. IEEE, 2016.

[12] Marco Andreetto, Stefano Divan, Daniele Fontanelli, and Luigi Palopoli. Harnessing steering singularities in passive path following for robotic walkers. In *Robotics and Automation (ICRA), 2017 IEEE International Conference on*, pages 2426–2432. IEEE, 2017.

[13] Marco Andreetto, Stefano Divan, Daniele Fontanelli, Luigi Palopoli, and Antonino Sferlazza. Variable Stiffness. 2018. To appear.

[14] H. Arai and S. Tachi. Position control of manipulator with passive joints using dynamic coupling. *IEEE Transactions on Robotics and Automation*, 7(4):528–534, Aug 1991.

[15] A. Balluchi, A. Bicchi, A. Balestrino, and G. Casalino. Path tracking control for dubin's cars. In *Proc. IEEE Conf. on Robotics and Automation (ICRA)*, volume 4, pages 3123–3128, Apr 1996.

[16] Andrea Balluchi, Antonio Bicchi, and Philippe Soueres. Path-following with a bounded-curvature vehicle: a hybrid control approach. *International Journal of Control*, 78(15):1228–1247, 2005.

[17] Y. Bar-Shalom, X.R. Li, X.R. Li, and T. Kirubarajan. *Estimation with applications to tracking and navigation*. Wiley-Interscience, 2001.

[18] P. Bevilacqua, M. Frego, D. Fontanelli, and L. Palopoli. Reactive Planning for Assistive Robots. *IEEE Robotics and Automation Letters*, 3(2):1276–1283, April 2018.

[19] Paolo Bevilacqua, Marco Frego, Enrico Bertolazzi, Daniele Fontanelli, Luigi Palopoli, and Francesco Biral. Path planning maximising human comfort for assistive robots. In *Control Applications (CCA), 2016 IEEE Conference on*, pages 1421–1427. IEEE, 2016.

[20] Paolo Bevilacqua, Marco Frego, Enrico Bertolazzi, Daniele Fontanelli, Luigi Palopoli, and Francesco Biral. Path planning maximising human comfort for assistive robots. In *Control Applications (CCA), 2016 IEEE Conference on*, pages 1421–1427. IEEE, 2016.

[21] Paolo Bevilacqua, Marco Frego, Daniele Fontanelli, and Luigi Palopoli. Reactive planning for assistive robots. *IEEE Robotics and Automation Letters*, 3(2):1276–1283, 2018.

[22] RICHARD W. BOHANNON. Comfortable and maximum walking speed of adults aged 20–79 years: reference values and determinants. *Age and Ageing*, 26(1):15–19, 1997.

[23] John Brooke. Sus: A quick and dirty usability scale, 1996.

[24] C. Samons C. Canudas de Wit, H: Khenneouf and O. Sordalen. Nonlinear control design for mobile robots. *Recent trends in mobile robots*, Y. F. Zhend, Ed. World Scientific, 1993, pp. 121-156.

[25] Alec Cameron and Hugh Durrant-Whyte. A bayesian approach to optimal sensor placement. *The International Journal of Robotics Research*, 9(5):70–88, 1990.

[26] Amedeo Cesta, Gabriella Cortellessa, Andrea Orlandini, and Lorenza Tiberio. Long-term evaluation of a telepresence robot for the elderly: methodology and ecological case study. *International Journal of Social Robotics*, 8(3):421–441, 2016.

[27] P. Coelho and U. Nunes. Path-following control of mobile robots in presence of uncertainties. *IEEE Transactions on Robotics*, 21(2):252–261, April 2005.

[28] Alessio Colombo, Daniele Fontanelli, Axel Legay, Luigi Palopoli, and Sean Sedwards. Motion planning in crowds using statistical model checking to enhance the social force model. In *Decision and Control (CDC), 2013 IEEE 52nd Annual Conference on*, pages 3602–3608. IEEE, 2013.

[29] Sara J Czaja, Neil Charness, Arthur D Fisk, Christopher Hertzog, Sankaran N Nair, Wendy A Rogers, and Joseph Sharit. Factors predicting the use of technology: findings from the center for research and education on aging and technology enhancement (create). *Psychology and aging*, 21(2):333, 2006.

[30] L. Lapierre D. Soetanto and A. Pascoal. Adaptive, non-singular path-following control of dynamic wheeled robots. *IEEE Conf. on Decision and Control*, vol. 2. IEEE 2003, pp. 1765-1770.

[31] Lawrence Davis. *Handbook of genetic algorithms*. Van Nostrand Reinhold, 1991.

[32] Alessandro Di Nuovo, Frank Broz, Filippo Cavallo, and Paolo Dario. New frontiers of service robotics for active and healthy ageing, 2016.

[33] S. Dubowsky, F. Genot, S. Godding, H. Kozono, A. Skwersky, Haoyong Yu, and Long Shen Yu. Pamm - a robotic aid to the elderly for mobility assistance and monitoring: a "helping-hand" for the elderly. In *Proceedings 2000 ICRA. Millennium Conference. IEEE International Conference on Robotics and Automation. Symposia Proceedings (Cat. No.00CH37065)*, volume 1, pages 570–576 vol.1, April 2000.

[34] Daniele Fontanelli, Antonio Giannitrapani, Luigi Palopoli, and Domenico Prattichizzo. Unicycle steering by brakes: a passive guidance support for an assistive cart. In *Decision and Control (CDC), 2013 IEEE 52nd Annual Conference on*, pages 2275–2280. IEEE, 2013.

[35] Daniele Fontanelli, Antonio Giannitrapani, Luigi Palopoli, and Domenico Prattichizzo. Unicycle Steering by Brakes: a Passive Guidance Support for an Assistive Cart. In *Proc. IEEE Int. Conf. on Decision and Control*, pages 2275–2280, Florence, Italy, 10-13 Dec. 2013. IEEE.

[36] Daniele Fontanelli, Antonio Giannitrapani, Luigi Palopoli, and Domenico Prattichizzo. A Passive Guidance System for a Robotic Walking Assistant using Brakes. In *Proc. IEEE Int. Conf. on Decision and Control (CDC)*, pages 829–834, Osaka, Japan, 15-18 Dec. 2015. IEEE.

[37] Cristina Guerrero Fabiano Zenatti Roberta Guidolin Luigi Palopoli Daniele Fontanelli Francesco Ferrari, Stefano Divan. Human Robot Interaction Analysis for a Smart Walker for Elderly. *International Journal of Social Robotics*, 2018. submitted.

[38] Marco Frego, Enrico Bertolazzi, Francesco Biral, Daniele Fontanelli, and Luigi Palopoli. Semi-Analytical Minimum Time Solutions for a Vehicle Following Clothoid-Based Trajectory Subject to Velocity Constraints. In *European Control Conference*, Aalborg, Denmark, July 2016. Accepted.

[39] Susanne Frennert, Håkan Eftring, and Britt Östlund. Case report: Implications of doing research on socially assistive robots in real homes. *International Journal of Social Robotics*, 9(3):401–415, 2017.

[40] Olivier Friard and Marco Gamba. Boris: a free, versatile open-source event-logging software for video/audio coding and live observations. *Methods in Ecology and Evolution*, 7(11):1325–1330, 2016.

[41] F. Gemperle, T. Hirsch, A. Goode, J. Pearce, D. Siewiorek, and A. Smailigic. Wearable vibro-tactile display, 2003. Carnegie Mellon University.

[42] Philip E Gill and Walter Murray. Algorithms for the solution of the nonlinear least-squares problem. *SIAM Journal on Numerical Analysis*, 15(5):977–992, 1978.

[43] Rafal Goebel, Ricardo G Sanfelice, and Andrew R Teel. *Hybrid Dynamical Systems: modeling, stability, and robustness*. Princeton University Press, 2012.

[44] A. Goswami, M.A. Peshkin, and J.E. Colgate. Passive robotics: An exploration of mechanical computation. In *Proceedings of the 1990 American Control Conference*, pages 2791–2796, 1990.

[45] H. Hashimoto, A. Sasaki, Y. Ohyama, and C. Ishii. Walker with hand haptic interface for spatial recognition. In *9th IEEE International Workshop on Advanced Motion Control, 2006.*, pages 311–316, March 2006.

[46] Louise C Hawkley, Ronald A Thisted, and John T Cacioppo. Loneliness predicts reduced physical activity: cross-sectional & longitudinal analyses. *Health Psychology*, 28(3):354, 2009.

[47] Denise Hebesberger, Tobias Koertner, Christoph Gisinger, and Jürgen Pripfl. A long-term autonomous robot at a care hospital: A mixed methods study on social acceptance and experiences of staff and older adults. *International Journal of Social Robotics*, 9(3):417–429, 2017.

[48] Laura Hedley, Nicola Suckley, Lisa Robinson, and Pamela Dawson. Staying steady: A community-based exercise initiative for falls prevention. *Physiotherapy Theory and Practice*, 26(7):425–438, 2010.

[49] Laura Hedley, Nicola Suckley, Lisa Robinson, and Pamela Dawson. Staying steady: a community-based exercise initiative for falls prevention. *Physiotherapy theory and practice*, 26(7):425–438, 2010.

[50] Melinda Heinz, Peter Martin, Jennifer A Margrett, Mary Yearns, Warren Franke, Hen I Yang, Johnny Wong, and Carl K Chang. Perceptions of technology among older adults. *Journal of Gerontological Nursing*, 39(1):42–51, 2013.

[51] Yasuhisa Hirata, Asami Hara, and Kazuhiro Kosuge. Motion control of passive intelligent walker using servo brakes. *IEEE Transactions on Robotics*, 23(5):981–990, 2007.

[52] Yasuhisa Hirata, Shinji Komatsuda, and Kazuhiro Kosuge. Fall prevention control of passive intelligent walker based on human model. In *Intelligent Robots and Systems, 2008. IROS 2008. IEEE/RSJ International Conference on*, pages 1222–1228. IEEE, 2008.

[53] Yasuhisa Hirata, Asami Muraki, and Kazuhiro Kosuge. Motion control of intelligent walker based on renew of estimation parameters for user state. In *Intelligent Robots and Systems, 2006 IEEE/RSJ International Conference on*, pages 1050–1055. IEEE, 2006.

[54] Yasuhisa Hirata, Taghvaei Sajjad, and Kazuhiro Kosuge. Vision-based human state estimation to control an intelligent passive walker. In *International Symposium on System Integration*. IEEE, 2010.

[55] Hsiu-Fang Hsieh and Sarah E Shannon. Three approaches to qualitative content analysis. *Qualitative health research*, 15(9):1277–1288, 2005.

[56] Cunjun Huang, Glenn Wasson, Majd Alwan, Pradip Sheth, and Alexandre Ledoux. Shared navigational control and user intent detection in an intelligent walker. In *AAAI Fall 2005 Symposium*, 2005.

[57] G. Indiveri, A. Nuchter, and K. Lingemann. High Speed Differential Drive Mobile Robot Path Following Control With Bounded Wheel Speed Commands. In *Proc. of IEEE International Conference on Robotics and Automation*, pages 2202–2207, April 2007.

[58] Gianluca Isaia, Barbara Maero, Antonia Gatti, Massimo Neirotti, Nicoletta Aimonino Ricauda, Mario Bo, Claudia Ruatta, Federico Gariglio, Cristina Miceli, Laura Corsinovi, Laura Fissore, Cristina Marchetto, and Mauro Zanocchi. Risk factors of functional decline during hospitalization in the oldest old. *Aging Clinical and Experimental Research*, 21(6):453–457, Dec 2009.

[59] ISTAT. *Anziani: Le condizioni di salute in Italia e nell'Unione Europea*, 2015.

[60] Zhong-Ping Jiang, Erjen Lefeber, and Henk Nijmeijer. Saturated stabilization and tracking of a nonholonomic mobile robot. *Systems & Control Letters*, 42(5):327–332, 2001.

[61] Damien B. Jourdan and Nicholas Roy. Optimal Sensor Placement for Agent Localization. *ACM Trans. Sen. Netw.*, 4(3):13:1–13:40, June 2008.

[62] I. Karuei, K.E. MacLean, Z. Foley-Fisher, R. MacKenzie, S. Koch, and M. El-Zohairy. Detecting vibrations across the body in mobile contexts. In *Proc. ACM Int. Conf. on Human Factors in Computing Systems*, pages 3267–3276, 2011.

[63] Karsten Keller and Martin Engelhardt. Strength and muscle mass loss with aging process. age and strength loss. *Muscles, ligaments and tendons journal*, 3(4):346, 2013.

[64] K.-T. Khaw, N. Wareham, S. Bingham, A. Welch, R. Luben, and N. Day. Combined impact of health behaviours and mortality in men and women: The EPIC-Norfolk prospective population study. *PLOS Medicine*, 5(1):e12, 2008.

[65] Kay-Tee Khaw, Nicholas Wareham, Sheila Bingham, Ailsa Welch, Robert Luben, Nicholas Day, et al. Combined impact of health behaviours and mortality in men and women: the epic-norfolk prospective population study. *Obstetrical and Gynecological Survey*, 63(6):376–377, 2008.

[66] Ramu Krishnan. *Permanent magnet synchronous and brushless DC motor drives*. CRC Press/Taylor & Francis, 2010.

[67] V. Kulyukin, A. Kutiyanawala, E. LoPresti, J. Matthews, and R. Simpson. iwalker: Toward a rollator-mounted wayfinding system for the elderly. In *2008 IEEE International Conference on RFID*, pages 303–311, April 2008.

[68] Gerard Lacey, Shane Mac Namara, and Kenneth M. Dawson-Howe. *Personal adaptive mobility aid for the infirm and elderly blind*, pages 211–220. Springer Berlin Heidelberg, Berlin, Heidelberg, 1998.

[69] Jeanne Langan, Scott Peltier, Jin Bo, Brett W Fling, Robert C Welsh, and Rachael D Seidler. Functional implications of age differences in motor system connectivity. *Frontiers in systems neuroscience*, 4:17, 2010.

[70] Jean-Paul Laumond. *Robot motion planning and control. Lectures Notes in Control and Information Sciences 229*, volume 3. 1998.

[71] Geunho Lee, Takanori Ohnuma, and Nak Young Chong. Design and control of jaist active robotic walker. *Intelligent Service Robotics*, 3(3):125–135, Jul 2010.

[72] Werner Leonhard. *Control of electrical drives*. Springer Science & Business Media, 2012.

[73] R.W. Lindeman, Y. Yanagida, H. Noma, and K. Hosaka. Wearable vibrotactile systems for virtual contact and information display. In *Virtual Reality*, volume 9, pages 203–213. Springer, 2006.

[74] Kai Lingemann, Andreas Nüchter, Joachim Hertzberg, and Hartmut Surmann. High-speed laser localization for mobile robots. *Robotics and Autonomous Systems*, 51(4):275–296, Jun. 2005.

[75] Lennart Ljung. *System identification*. Wiley Online Library, 1999.

[76] Cheng-Kai Lu, Yi-Che Huang, and Cheng-Jung Lee. Adaptive guidance system design for the assistive robotic walker. *Neurocomputing*, 170(Supplement C):152 – 160, 2015. Advances on Biological Rhythmic Pattern Generation: Experiments, Algorithms and Applications Selected Papers from the 2013 International Conference on Intelligence Science and Big Data Engineering (IScIDE 2013) Computational Energy Management in Smart Grids.

[77] V. Magnago, M. Andreetto, S. Divan, D. Fontanelli, and L. Palopoli. Ruling the control authority of a service robot based on information precision. In *2018 IEEE International Conference on Robotics and Automation (ICRA)*, pages 7204–7210, May 2018.

[78] V. Magnago, L. Palopoli, R. Passerone, D. Fontanelli, and D. Macii. A Nearly Optimal Landmark Deployment for Indoor Localisation with Limited Sensing. In *International Conference on Indoor Positioning and Indoor Navigation (IPIN)*, pages 1–8, Sapporo, Japan, Sept. 2017. IEEE.

[79] Nicolás Martínez-Velilla, Alvaro Casas-Herrero, Fabrício Zambom-Ferraresi, Nacho Suárez, Javier Alonso-Renedo, Koldo Cambra Contín, Mikel López-Sáez de Asteasu, Nuria Fernandez Echeverria, María Gonzalo Lázaro, and Mikel Izquierdo. Functional and cognitive impairment prevention through early physical activity for geriatric hospitalized patients: study protocol for a randomized controlled trial. *BMC Geriatrics*, 15(1):112, Sep 2015.

[80] M. Martins, C. Santos, and A. Frizera. Online control of a mobility assistance smart walker. In *2012 IEEE 2nd Portuguese Meeting in Bioengineering (ENBENG)*, pages 1–6, Feb 2012.

[81] M. Martins, C. Santos, E. Seabra, L. Basílio, and A. Frizera. A new integrated device to read user intentions when walking with a smart walker. In *2013 11th IEEE International Conference on Industrial Informatics (INDIN)*, pages 299–304, July 2013.

[82] M. M. Martins, C. P. Santos, A. Frizera-Neto, and R. Ceres. Assistive mobility devices focusing on smart walkers: Classification and review. *Robotics and Autonomous Systems*, 60(4):548–562, 2012.

[83] Sonia Martínez and Francesco Bullo. Optimal sensor placement and motion coordination for target tracking. *Automatica*, 42(4):661 – 668, 2006.

[84] Alain Micaelli and Claude Samson. *Trajectory tracking for unicycle-type and two-steering-wheels mobile robots*. PhD thesis, INRIA, 1993.

[85] Alain Micaelli and Claude Samson. Trajectory tracking for unicycle-type and two-steering-wheels mobile robots. Research Report RR-2097, INRIA, 1993.

[86] Shailey Minocha, Elizabeth Hartnett, Kathryn Dunn, Shirley Evans, Tania Heap, Christopher Paul Middup, Brendan Murphy, and Dave Roberts. Conducting empirical research with older people. 2013.

[87] Jaime Valls Miró, Vivien Osswald, Mitesh Patel, and Gamini Dissanayake. Robotic assistance with attitude: A mobility agent for motor function rehabilitation and ambulation support. In *Rehabilitation Robotics, 2009. ICORR 2009. IEEE International Conference on*, pages 529–534. IEEE, 2009.

[88] David Moreno-Salinas, Antonio M. Pascoal, and Joaquin Aranda. Optimal Sensor Placement for Multiple Target Positioning with Range-Only Measurements in Two-Dimensional Scenarios. *Sensors*, 13(8):10674, 2013.

[89] United Nations. *World Population Ageing*, 2015 (accessed July 12, 2018).

[90] P. Nazemzadeh, D. Fontanelli, and D. Macii. Optimal Placement of Landmarks for Indoor Localization using Sensors with a Limited Range. In *International Conference on Indoor Positioning and Indoor Navigation (IPIN)*, pages 1–8, Madrid, Spain, Oct. 2016. IEEE.

[91] P. Nazemzadeh, D. Fontanelli, D. Macii, and L. Palopoli. Indoor Positioning of Wheeled Devices for Ambient Assisted Living: a Case Study. In *Proc. IEEE Int. Instrumentation and Measurement Technology Conference (I2MTC)*, pages 1421–1426, Montevideo, Uruguay, May 2014. IEEE.

[92] Payam Nazemzadeh, Daniele Fontanelli, David Macii, Tizar Rizano, and Luigi Palopoli. Design and Performance Analysis of an Indoor Position Tracking Technique for Smart Rollators. In *International Conference on Indoor Positioning and Indoor Navigation (IPIN)*, pages 1–10, Montbeliard, France, 28-31 Oct. 2013. IEEE GRSS.

[93] Payam Nazemzadeh, Federico Moro, Daniele Fontanelli, David Macii, and Luigi Palopoli. Indoor Positioning of a Robotic Walking Assistant for Large Public Environments. *IEEE Trans. on Instrumentation and Measurement*, 64(11):2965–2976, Nov 2015.

[94] Dejing Ni, Aiguo Song, Lei Tian, Xiaonong Xu, and Danfeng Chen. A walking assistant robotic system for the visually impaired based on computer vision and tactile perception. *International Journal of Social Robotics*, 7(5):617–628, Nov 2015.

[95] L. Palopoli, A. Argyros, J. Birchbauer, A. Colombo, D. Fontanelli, et al. Navigation Assistance and Guidance of Older Adults across Complex Public Spaces: the DALi Approach. *Intelligent Service Robotics*, 8(2):77–92, 2015.

[96] Huang Peng, Guangming Song, Jian You, Ying Zhang, and Jie Lian. An indoor navigation service robot system based on vibration tactile feedback. *International Journal of Social Robotics*, 9(3):331–341, Jun 2017.

[97] J. M. D. Pereira, O. Postolache, V. Viegas, and P. Silva Girão. A low cost measurement system to extract kinematic parameters from walker devices. In *2015 IEEE International Instrumentation and Measurement Technology Conference (I2MTC) Proceedings*, pages 1991–1996, May 2015.

[98] Michael A Peshkin, J Edward Colgate, Wit Wannasuphoprasit, Carl A Moore, R Brent Gillespie, and Prasad Akella. Cobot architecture. *IEEE Transactions on Robotics and Automation*, 17(4):377–390, 2001.

[99] T. Pilutti, G. Ulsoy, and D. Hrovat. Vehicle steering intervention through differential braking. In *Proceedings of the 1995 American Control Conference*, volume 3, pages 1667–1671, 1995.

[100] Jayant M Pinto, Kristen E Wroblewski, Megan Huisingh-Scheetz, Camil Correia, Kevin J Lopez, Rachel C Chen, David W Kern, Philip L Schumm, William Dale, and Martha K McClintock. Global sensory impairment predicts morbidity and mortality in older us adults. *Journal of the American Geriatrics Society*, 65(12):2587–2595, 2017.

[101] O. Postolache, J. M. Dias Pereira, V. Viegas, L. Pedro, P. S. Girao, R. Oliveira, and G. Postolache. Smart walker solutions for physical rehabilitation. *IEEE Instrumentation Measurement Magazine*, 18(5):21–30, October 2015.

[102] Rodrigo Pérez-Rodríguez, Pedro A. Moreno-Sánchez, Myriam Valdés-Aragonés, Myriam Oviedo-Briones, Stefano Divan, Nuria García-Grossocordón, and Leocadio Rodríguez-Mañas. Friwalk robotic walker: usability, acceptance and ux evaluation after a pilot study in a real environment. *Technology and Health Care*, 27, 2018. To appear.

[103] Andrew J Rentschler, Rory A Cooper, Bruce Blasch, and Michael L Boninger. Intelligent walkers for the elderly: Performance and safety testing of va-pamaid robotic walker. *Journal of rehabilitation research and development*, 40(5):423, 2003.

[104] Hayley Robinson, Bruce MacDonald, and Elizabeth Broadbent. The role of healthcare robots for older people at home: A review. *International Journal of Social Robotics*, 6(4):575–591, 2014.

[105] Masao Saida, Yasuhisa Hirata, and Kazuhiro Kosuge. Development of passive type double wheel caster unit based on analysis of feasible braking force and moment set. In *Intelligent Robots and Systems (IROS), 2011 IEEE/RSJ International Conference on*, pages 311–317. IEEE, 2011.

[106] Masao Saida, Yasuhisa Hirata, and Kazuhiro Kosuge. Motion control of caster-type passive mobile robot with servo brakes. *Advanced Robotics*, 26(11-12):1271–1290, 2012.

[107] Claude Samson. Control of chained systems application to path following and time-varying point-stabilization of mobile robots. *IEEE Trans. on Automatic Control*, 40(1):64–77, 1995.

[108] Stefano Scheggi, Marco Aggravi, and Domenico Prattichizzo. Cooperative navigation for mixed human–robot teams using haptic feedback. *IEEE Transactions on Human-Machine Systems*, 47(4):462–473, 2017.

[109] Stephen Se, David Lowe, and Jim Little. Mobile robot localization and mapping with uncertainty using scale-invariant visual landmarks. *The international Journal of robotics Research*, 21(8):735–758, Aug. 2002.

[110] Fei Shi, Qixin Cao, Chuntao Leng, and Hongbing Tan. Based on force sensing-controlled human-machine interaction system for walking assistant robot. In *2010 8th World Congress on Intelligent Control and Automation*, pages 6528–6533, July 2010.

[111] B. Siciliano, L. Sciavicco, L. Villani, and G. Oriolo. *Robotics. Modelling, Planning and Control*. Springer, 2009.

[112] B. Sinopoli, L. Schenato, M. Franceschetti, K. Poolla, M. I. Jordan, and S. S. Sastry. Kalman filtering with intermittent observations. *IEEE Transactions on Automatic Control*, 49(9):1453–1464, Sept 2004.

[113] D Soetanto, L Lapierre, and A Pascoal. Adaptive, non-singular path-following control of dynamic wheeled robots. In *IEEE Conf. on Decision and Control*, volume 2, pages 1765–1770. IEEE, 2003.

[114] Philippe Soueres, Andrea Balluchi, and Antonio Bicchi. Optimal feedback control for route tracking with a bounded-curvature vehicle. *International Journal of Control*, 74(10):1009–1019, 2001.

[115] S. Taghvaei, Y. Hirata, and K. Kosuge. Control of a passive walker using a depth sensor for user state estimation. In *2011 IEEE International Conference on Robotics and Biomimetics*, pages 1639–1645, Dec 2011.

[116] Dirk Vanhooydonck, Eric Demeester, Marnix Nuttin, and Hendrik Van Brussel. Shared control for intelligent wheelchairs: an implicit estimation of the user intention. In *Proceedings of the 1st international workshop on advances in service robotics (ASER03)*, pages 176–182. Citeseer, 2003.

[117] Eleftheria Vaportzis, Maria Giatsi Clausen, and Alan J Gow. Older adults perceptions of technology and barriers to interacting with tablet computers: A focus group study. *Frontiers in psychology*, 8:1687, 2017.

[118] Peter Vas. *Sensorless vector and direct torque control*. Oxford Univ. Press, 1998.

[119] A. Wachaja, P. Agarwal, M. Zink, M. R. Adame, K. Möller, and W. Burgard. Navigating blind people with a smart walker. In *2015 IEEE/RSJ International Conference on Intelligent Robots and Systems (IROS)*, pages 6014–6019, Sept 2015.

[120] Yina Wang and Shuoyu Wang. A new directional-intent recognition method for walking training using an omnidirectional robot. *Journal of Intelligent & Robotic Systems*, 87(2):231–246, Aug 2017.

[121] W. Wannasuphoprasit, R. B. Gillespie, J. E. Colgate, and M. A. Peshkin. Cobot control. In *Robotics and Automation, 1997. Proceedings., 1997 IEEE International Conference on*, volume 4, pages 3571–3576 vol.4, Apr 1997.

[122] Sally Whelan, Kathy Murphy, Eva Barrett, Cheryl Krusche, Adam Santorelli, and Dympna Casey. Factors affecting the acceptability of social robots by older adults including people with dementia or cognitive impairment: A literature review. *International Journal of Social Robotics*, pages 1–26, 2018.

[123] F. Zenatti, D. Fontanelli, L. Palopoli, D. Macii, and P. Nazemzadeh. Optimal Placement of Passive Sensors for Robot Localisation. In *Proc. IEEE/RSJ International Conference on Intelligent Robots and System (IROS)*, pages 4586–4593, Daejeon, South Korea, Oct. 2016. IEEE/RSJ.

[124] Wuxiao Zhou, Li Xu, and Jie Yang. An intent-based control approach for an intelligent mobility aid. In *2010 2nd International Asia Conference on Informatics in Control, Automation and Robotics (CAR 2010)*, volume 2, pages 54–57, March 2010.

[125] Anna Zisberg, Efrat Shadmi, Gary Sinoff, Nurit Gur-Yaish, Einav Srulovici, and Hanna Admi. Low mobility during hospitalization and functional decline in older adults. *Journal of the American Geriatrics Society*, 59(2):266–273.

DOCTORAL PROGRAM IN
INFORMATION AND COMMUNICATION TECHNOLOGY

Doctoral candidate

Stefano Divan

Cycle	**31**
Thesis	**A Service Robot for Navigation Assistance and Physical Rehabilitations of Seniors**
Advisor	**Luigi Palopoli (University of Trento)**
Co-advisor	**Daniele Fontanelli (University of Trento)**

1. **List of publications**

- [1] M. Andreetto, S. Divan, D. Fontanelli and L. Palopoli, "Hybrid feedback path following for robotic walkers via bang-bang control actions," *2016 IEEE 55th Conference on Decision and Control (CDC)*, Las Vegas, NV, 2016, pp. 4855-4860.
- [2] M. Andreetto, S. Divan, D. Fontanelli and L. Palopoli, "Passive robotic walker path following with bang-bang hybrid control paradigm," *2016 IEEE/RSJ International Conference on Intelligent Robots and Systems (IROS)*, Daejeon, 2016, pp. 1054-1060.
- [3] Marco Andreetto, Stefano Divan, Daniele Fontanelli, Luigi Palopoli, "Path following with authority sharing between humans and passive robotic walkers equipped with low-cost actuators", in *IEEE Robotics and Automation Letters, 2017.*
- [4] M. Andreetto, S. Divan, D. Fontanelli and L. Palopoli, "Harnessing steering singularities in passive path following for robotic walkers," *2017 IEEE International Conference on Robotics and Automation (ICRA)*, Singapore, 2017, pp. 2426-2432.
- [5] M. Andreetto, S. Divan, D. Fontanelli, L. Palopoli and F. Zenatti, "Path following for robotic rollators via simulated passivity," *2017 IEEE/RSJ International Conference on Intelligent Robots and Systems (IROS)*, Vancouver, BC, 2017, pp. 6915-6922.
- [6] M. Andreetto, S. Divan, D. Fontanelli, L. Palopoli and A. Sferlazza, "Assistive robotic walker parameter identification for estimation of human thrust without force sensors," *2017 IEEE 3rd International Forum on Research and Technologies for Society and Industry (RTSI)*, Modena, 2017, pp. 1-6.
- [7] M. Andreetto, S. Divan, F. Ferrari, D. Fontanelli, L. Palopoli and F. Zenatti, "Simulating Passivity for Robotic Walkers via Authority-Sharing," in *IEEE Robotics and Automation Letters*, vol. 3, no. 2, pp. 1306-1313, April 2018.
- [8] V. Magnago, M. Andreetto, S. Divan, D. Fontanelli and L. Palopoli, "Ruling the Control Authority of a Service Robot Based on Information Precision," *2018 IEEE International Conference on Robotics and Automation (ICRA)*, Brisbane, QLD, 2018, pp. 7204-7210.

List of publication uder review

- [9] M. Andreetto, S. Divan, D. Fontanelli, L. Palopoli, F. Ferrari, D. Pratichizzo, “Combining Haptic and Bang-Bang Braking Actions for Passive Robotic Walkers Path Following”, Transaction on Haptics, 2018, submitted.
- [10] C. Guerreto, F. Zenatti, R. Guidolin, L. Palopoli, D. Fontanelli, F. Ferrari, S. Divan, “Human Robot Interaction Analysis for a Smart Walker for Elderly”, International Journal of Social Robotics, 2018, submitted.
- [11] Rodrigo Pérez-Rodríguez, Pedro A. Moreno-Sánchez, Myriam Aragonés, Myriam Oviedo-Briones, Stefano Divan, Nuria Grossocordón, and Leocadio Rodríguez-Mañas. Friwalk robotic usability, acceptance and ux evaluation after a pilot study in environment. Technology and Health Care, 2018, submitted.

2. Research/study activities

Research activity

During my PhD period I focused on the modeling and the realization of a robot for the ACANTO project, starting from scratch. I modeled the overall mechanical system with Solidworks, and I set up all the electromechanical components, ranging from actuators and sensors. Thanks to this period I improved my abilities in both the mechatronic and electronic design. In fact, beyond the mechanical modeling, I focused also in the developlment of several embedded platforms for electronic purposes (sensor, actuators and power-managment) and in the programming of microcontrollers. All these embedded platforms have been designed with Eagle and soldered by myself. Moreover, I developed the software architecture of the robot, which is mainly composed by three modules: hardware, localization and guidance. The first one manages the control and communication with the motors, the second one is responsible of the localization of the device, while the third one is used to properly guide the vehicle along a planned path. To conclude, the robot can be controlled and configured via a GUI, designed entirely by myself in Qt. For the use of the robot as a navigation assistance, the system guides the user securing high levels of safety, a perfect compliance with the social rules and non--intrusive interaction between human and machine. We concucted extensive experiments with elderly and I focused on the human-robot interaction point of view. We developed several guidance strategies, exploiting different actuators, to point out which guidance solution adapts better to elderly, according to their impariments, in terms of plesantness, ease of learning, adaptability and comfort. The second field in which I focused during my PhD consist in the use of the robot as a rehabilitation aid. An extensive pilot study, with real patients and physiotherapist have been performed in Spain, at the Universitary Hospital of Getafe (Madrid). The benefits of relying on such device to increase the hospitalization efficacy has been proved and the acceptance rate of the robot by patients and the clinical staff has been very high. At the same time, a solution to modify in real--time the perceived inertia of the robot has been proposed so that, acting on two parameters only, the user can feel the device lighter or heavier. This feature can be exploited from a rehabilitation point of view letting the user to exercise more or less force to move the robot.

Abroad period

I spent 6 months at the Tohoku University of Sendai, Japan. During this period I worked with a commercial walking assistant robot, named Robotics Assisted Walker RT.2, developing the software and designing control algorithms for path-following tasks and motion control purposes. I developed the

software architecture to communicate with the hardware module, the localization module to localize the robot inside an room and the guidance module to guide the user along a planned path. Such a robot was endowed with force sensors that allowed me to implement a path following motion control controller. The idea of such controller is that the forward velocity is estimated thanks to the force sensors, and the robot motors provide enough thrust to reach such speed. At the same time the path-following controller steers the user towards the desired path, preventing him/her to move away from it.

Conference partecipations
During my PhD I partecipated to two conferences. I partecipated to the CDC 2016 conference held in Las Vegas and I presented [1]. Then, in 2017, I partecipated to IROS conferente held in Vancouver in which I presented [5] and [3].

Research projects
- ACANTO: A Cyberphysical Social Network using robot fiends;
- AWARD: development and implementation of a robot for warehouses.

Teaching activities
During the first year of my PhD I worked as assistant for the course *System and Techniques for Digital Signal Processing*